United States
Environmental Protection
Agency

Municipal Environmental Research
Laboratory
Cincinnati OH 45268

EPA-600/2-80-115
August 1980

Research and Development

Significance of Size Reduction in Solid Waste Mangement

Volume 2

RESEARCH REPORTING SERIES

Research reports of the Office of Research and Development, U.S. Environmental Protection Agency, have been grouped into nine series. These nine broad categories were established to facilitate further development and application of environmental technology. Elimination of traditional grouping was consciously planned to foster technology transfer and a maximum interface in related fields. The nine series are:

1. Environmental Health Effects Research
2. Environmental Protection Technology
3. Ecological Research
4. Environmental Monitoring
5. Socioeconomic Environmental Studies
6. Scientific and Technical Assessment Reports (STAR)
7. Interagency Energy-Environment Research and Development
8. "Special" Reports
9. Miscellaneous Reports

This report has been assigned to the ENVIRONMENTAL PROTECTION TECHNOLOGY series. This series describes research performed to develop and demonstrate instrumentation, equipment, and methodology to repair or prevent environmental degradation from point and non-point sources of pollution. This work provides the new or improved technology required for the control and treatment of pollution sources to meet environmental quality standards.

This document is available to the public through the National Technical Information Service, Springfield, Virginia 22161.

EPA-600/2-80-115
August 1980

SIGNIFICANCE OF SIZE REDUCTION IN SOLID WASTE MANAGEMENT

Volume 2

by

George M. Savage
George J. Trezek
University of California
Berkeley, California 94607

Grant No. R-805414-010

Project Officer

Carlton C. Wiles
Solid and Hazardous Waste Research Division
Municipal Environmental Research Laboratory
Cincinnati, Ohio 45268

MUNICIPAL ENVIRONMENTAL RESEARCH LABORATORY
OFFICE OF RESEARCH AND DEVELOPMENT
U.S. ENVIRONMENTAL PROTECTION AGENCY
CINCINNATI, OHIO 45268

DISCLAIMER

This report has been reviewed by the Municipal Environmental Research Laboratory, U.S. Environmental Protection Agency, and approved for publication. Approval does not signify that the contents necessarily reflect the views and policies of the U.S. Environmental Protection Agency, nor does mention of trade names or commercial products constitute endorsement or recommendation for use.

FOREWORD

The Environmental Protection Agency was created because of increasing public and government concern about the dangers of pollution to the health and welfare of the American people. Noxious air, foul water, and spoiled land are tragic testimony to the deterioration of our natural environment. The complexity of that environment and the interplay between its components require a concentrated and integrated attack on the problem.

Research and development is that necessary first step in problem solution and it involves defining the problem, measuring its impact, and searching for solutions. The Municipal Environmental Research Laboratory develops new and improved technology and systems for the prevention, treatment, and management of wastewater and solid and hazardous waste pollutant discharges from municipal and community sources, for the preservation and treatment of public drinking water supplies, and to minimize the adverse economic, social, health, and aesthetic effects of pollution. This publication is one of the products of that research; a most vital communications link between the researcher and the user community.

This report is the second in a three-volume series of comprehensive studies dealing with the size reduction of solid waste. In this report (Volume 2), raw municipal solid waste, air-classified light fraction, and screened light fraction were used in a number of tests simulating single- and multiple-stage size reduction. The basic test data are generalized so that the characteristic particle size and energy consumption could be predicted. Various hardfacing materials and their ability to perform with the different solid waste materials are also tested.

Francis T. Mayo, Director
Municipal Environmental Research
Laboratory

ABSTRACT

This report is the second in a three-volume series of comprehensive studies dealing with the size reduction of solid waste. Tests dealing with solid waste shredding were conducted at the University of California, Berkeley Solid Waste Processing Laboratory located at the Richmond Field Station in Richmond. The objects of these tests were (1) to gain a better understanding of the factors controlling the interrelated variables of feed rate, power consumption, and hammer wear, and (2) to determine how to produce the final product with a minimum expenditure of energy and machine wear.

Volume 1 identifies and quantifies the variables governing refuse size reduction and then gives a preliminary formulation and evaluation of these relationships. Volume 2 addresses the basic questions that were unanswered in the first report: What size grates, how many hammers, what type of hardfacing, and how many stages of shredding should be used for optimum machine wear and energy consumption.

Volume 3 expands the discussions presented in the first two volumes and incorporates the data obtained in the large-scale shredder tests reported by Cal Recovery Systems, Inc.

In this report (Volume 2), raw municipal solid waste, air-classified light fraction, and screened light fraction were used in a number of tests simulating single- and multiple-stage size reduction. Tests were performed with a nominally rated, 10-ton/hr swing hammermill and a small, high-speed fixed hammer shredder. The basic test data are generalized so that the characteristic particle size and energy consumption could be predicted. Various hardfacing materials and their ability to perform with the different solid waste materials are also tested. Furthermore, a comprehensive, computerized comminution model of a size-discrete, time-continuous nature has been developed to predict size distribution and energy consumption.

This report was submitted in fulfillment of Contract No. R-805414-010 by the University of California, Berkeley, under the sponsorship of the U.S. Environmental Protection Agency.

CONTENTS

Foreword iii
Abstract iv
Figures vii
Tables xi
Abbreviations and Symbols xiii

1. Introduction 1

2. Materials, Equipments and Methods 3
   Characteristics of Raw Municipal Solid Waste 3
   Size Reduction Equipment 3
   Air Classifier and Screen 6
   Moisture Content and Size Distribution Analysis 9
   Measurement of Power and Energy Consumption 11
   Data Collection Procedure 13
   Procedure for Obtaining Residence Time 14

3. Shredding Studies 16

   Municipal Solid Waste (Gruendler Hammermill) Studies 16
   Air-Classified Light Fraction Studies 27
   Screened Light Fraction Studies 38

4. Wear Studies 48

   Hardfacing Materials and Application 48
   Experimental Procedure 49
   Hardness Measurements 53
   Wear Measurements 53
   Results 54
   Conclusions 62

5. Interrelation of the Comminution Parameters 68

   Representative Particle Size 68
   Degree of Size Reduction 70
   Energy 70
   Residence Time 79
   Mill Holdup 81
   Hammer Wear 84

6. Comminution Models 91

Size-discrete, Time-discrete Models 92
Size-discrete, Time-continuous Model 95
Implementation of the Model 100
Residence Time Distribution 106
Simulation Results 109
Concluding Remarks 114

7. Unit Operation and System Design Considerations 121

Grate Spacing Considerations 121
Torque Relations 123
Unit Process Optimization 125
System Optimzation 132

References 137
Appendix. Comminution Computer Model 139

FIGURES

Number		Page
1	Size distribution of raw MSW, Richmond, Calif	4
2	Test facility for the Gruendler swing hammermill shredder . .	5
3	W-W fixed hammermill positioned to shred either air-classified light fraction or screened light fraction	7
4	Rotor and hammers of W-W hammermill	8
5	Grate of W-W hammermill	8
6	Schematic of power monitoring systems	12
7	Energy consumption for size reduction of raw MSW as a function of grate opening size (Gruendler hammermill)	22
8	Energy required to reduce raw MSW to a given characteristic product size with a Gruendler hammermill	23
9	Energy required to reduce raw MSW to a given nominal product size with a Gruendler hammermill	24
10	Relation of shredded raw MSW product size to size of grate openings (Gruendler hammermill)	25
11	Sample of raw MSW shredded in a Gruendler hammermill without grate bars	26
12	Size distribution of raw MSW after multiple shredding with grate openings of 2.5 and 1.8 cm in the Gruendler hammermill	29
13	Size distribution for ACLF feed after primary and secondary shredding in the Gruendler hammermill	32
14	Size distribution of the ACLF after single-stage shredding with the W-W hammermill (Run 1)	34
15	Size distribution of the SLF after progressive shredding with the W-W hammermill	42

16 Size distribution of the SLF after multiple shredding with 2.5-cm (1.0-in.) grate openings in the Gruendler hammermill . 45

17 Size distribution of the SLF after multiple shredding with 1.8-cm (0.7-in.) grate openings in the Gruendler hammermill . 46

18 Bare manganese steel hammers before hardfacing 51

19 Hammers used for shredding raw MSW 51

20 Hammer wear as a function of grate opening: raw MSW, Gruendler hammermill 56

21 Hammer wear as a function of average characteristic product size: raw MSW, Gruendler hammermill 57

22 Hammer wear as a function of average nominal product size: raw MSW, Gruendler hammermill 59

23 Hammer wear as a function of hardness for several different grate openings: raw MSW, Gruendler hammermill 60

24 Evidence of chipping on hammers tipped with hardfacing alloys exceeding R_c 50 61

25 Closeup of hammers showing chipping of hardfacing weld deposits on hammer tips 61

26 Hammer wear as a function of grate opening: screened light fraction, W-W hammermill 64

27 Hammer wear as a function of hardness for several different grate openings: SLF, W-W hammermill 65

28 Hammer wear as a function of average characteristic product size: SLF, W-W hammermill 66

29 Mass fraction representation of the size distribution for raw MSW 69

30 Nominal size as a function of characteristic size for shredded raw MSW, Gruendler hammermill 71

31 Nominal size as a function of characteristic size for shredded ACLF and SLF, W-W hammermill 72

32 Degree of size reduction as a function of the ratio of grate spacing to characteristic feed size for raw MSW, ACLF and SLF 73

33 Specific energy as a function of degree of size reduction for raw MSW, ACLF, and SLF 74

34 Degree of size reduction as a function of the ratio of grate opening to characteristic feed size for raw MSW 76

35 Degree of size reduction as a function of the ratio of grate opening to characteristic feed size for ACLF 77

36 Degree of size reduction as a function of the ratio of grate opening to characteristic feed size for SLF 78

37 Schematic representative of milling process 79

38 Residence time distribution for size reduction of raw MSW . . 80

39 Normalized residence time distribution for size distribution for size reduction of raw MSW 82

40 Flow rate as a function of mill holdup for raw MSW 83

41 Characteristic particle size as a function of flow rate for raw MSW 85

42 Net power as a function of holdup for raw MSW 86

43 Net power as a function of moisture content for raw MSW . . . 87

44 Hammer wear as a function of degree of size reduction for raw MSW and SLF 89

45 Hammer wear as a function of D_0/F_0 for raw MSW and SLF 90

46 Diagram of open circuit milling 99

47 Diagram of closed circuit milling 99

48 Nonlinear optimization flow chart for parameter estimation . . 104

49 Flow chart for mill simulation calculations 105

50 Residence time distribution 107

51 Normalized residence time distribution 108

52 Complementary residence time function 110

53 Characteristic size and variation with mean residence time . . 111

54 Variation of K* flow rate 116

55 Variation of initial selection function with flow rate 117

56 Variation of initial breakage function with flow rate 118

57 Comparison of predicted and actual measured size distributions 119

58 Size reduction of raw MSW extended to several different grate openings 124

59 Degree of size reduction and specific energy requirement for shredding raw MSW as a function of D_o/F_o 127

60 Possible configurations for resource recovery unit operations . 133

61 Energy pathway for hypothetical RDF processing trains 135

TABLES

Number		Page
1	Maximum Mass of Shredded Refuse For Efficient Screening Using Using the Sweco Vibratory Screens (4.8-cm grate openings) . . .	11
2	Feed Rates Used in the Size Reduction of Raw MSW with the Gruendler Hammermill	17
3	Size Reduction of Raw MSW Using 4.8-cm (1.9-in.) Grate Openings with the Gruendler Hammermill	18
4	Size Reduction of Raw MWS using 2.5-cm (1.0-in.) Grate Openings with the Gruendler Hammermill	20
5	Size Reduction of Raw MSW using 1.8-cm (0.7-in.) Grate Openings with the Gruendler Hammermill	21
6	Multiple Shredding of Raw MSW with the Gruendler Hammermill . . .	28
7	Multiple Shredding of ACLF with the Gruendler Hammermill	31
8	Single-Stage Shredding of ACLF with the W-W Hammermill	33
9	Multiple Shredding of the ACLF with the W-W Hammermill	36
10	Progressive Shredding of ACLF with the W-W Hammermill	37
11	Single-Stage Shredding of the SLF for a Given Feed Size and Different Grate Openings with the W-W Hammermill	39
12	Progressive Shredding of SLF with the W-W Hammermill	41
13	Multiple Shredding of SLF with the Gruendler Hammermill	44
14	Comparison of Hammer and Hardfacing Materials Used for Shredding Raw MSW	50
15	Comparison of Hardfacing Materials Used for Shredding SLF	52
16	Wear Data for Various Hardfacing Materials Used for Shredding Raw MSW	55

17 Wear Data for Various Hardfacing Materials Used for Shredding SLF 63

18 Comparison of Degree of Size Reduction and Specific Energy for Different Solid Waste Fractions 75

19 Summary of Optimization Results 115

20 Single- and Double-Stage Shredding of Raw MSW in the Gruendler Hammermill 128

21 Single- and Double-Stage Shredding of ACLF in the W-W Hammermill 130

22 Single- and Double-Stage Shredding of SLF in the W-W Hammermill . 131

23 Mass and Energy Balance on Processing Trains for Recovery of RDF 134

LIST OF ABBREVIATIONS AND SYMBOLS

ABBREVIATIONS

ACLF -- air-classified light fraction
amp -- ampere
cm -- centimeter
fps -- feet per second
ft -- foot
g -- gram
hp -- horsepower
h -- hour
J -- joule
kg -- kilogram
kW -- kilowatt
kWh -- kilowatt-hour
lb -- pound
m -- meter
MC -- moisture content, reported as quotient of the difference of the initial weight minus the dry weight divided by the initial weight
min -- minute
MJ -- megajoules (10^6 joules)
MSW -- municipal solid waste
R_c -- Rockwell C hardness
RDF -- refuse derived fuel
rpm -- revolutions per minute
s -- second
SLF -- screened light fraction
W -- watt
Wh -- watt-hour

SYMBOLS

D_o -- characteristic linear dimension of grate opening or grate spacings; the minimum dimension for rectangular grate openings and the diameter for circular openings
E_o -- specific energy or net energy required for processing, generally reported as megajoules per metric ton or kilowatt hours per ton of material processed on a dry-weight basis
F_o -- characteristic size of the feed material
F_{90} -- nominal size of the feed material
X_o -- characteristic size of the product material
X_{90} -- nominal size of the product material
Z_o -- degree of size reduction

SECTION 1

INTRODUCTION

This report is the second in a three-volume series of comprehensive studies dealing with the size reduction of solid waste. Results are based on shredder testing conducted at the University of California, Berkeley, Solid Waste Processing Laboratory at Richmond, California. The motivation for studying the behavior of shredders began in the early 1970's, when facilities were being considered, and in some cases constructed, to process solid wastes by a number of alternative methods such as volume reduction for landfilling and for material and energy recovery. In each of these process schemes, one or more shredders became an integral part of the system. Typically, machines designed for comminuting homogeneous, brittle materials were being used to reduce the size of refuse that was heterogeneous and approximately 75 percent nonbrittle. From some initial field experience, it became apparent that the factors controlling the interrelated variables of feed rate, power consumption, and wear had to be understood if this equipment was to be successfully operated.

Volume 1 of this report addressed the above issues. Basically, the first results indicated how the variables governing refuse size reduction were initially identified and then quantified. Preliminary relationships governing the behavior of these variables were then formulated and evaluated consistent with available data. However, additional questions still remained unanswered and in effect provided the need for continued study.

The additional needs can be summarized as follows. The initial work could not completely answer certain questions such as why the flow rate affected the product size distribution, why moisture content affects the energy consumption, and how all these variables actually affected size distributions, energy consumption, and wear. Furthermore, though the once-through comminution model could predict the product size distribution, it could not provide an adequate physical distribution of the physical process. Other considerations such as the residence time distribution, mill holdup, and mill geometry needed to be identified, evaluated, and formulated into a working model. Another area of concern was the energy consumption required in the so-called fine-grinding process. Essentially no information was available for design and evaluation of processing that required particle sizes finer than 2.5 cm (1 in.). Some evidence indicated that excessive energy and wear would result if a unit operation producing a fine particle size were used. Also lacking was the ability to extrapolate information to other processing regimes. For example, information obtained for various ranges of flow rates, grate spacings, and power consumptions needed to be generalized to the point that it would be useful to predict the comminution events in a significantly larger unit operation. The controversy involved

in staging various shredder unit operations also needed to be addressed. For example, it was not clear whether it would be more prudent to have a single-stage shredding operation produce the final particle size or to employ two stages to achieve the end result. Furthermore, the problems involved in knowing how to structure each stage needed to be considered -- that is, what size of grates, how many hammers, etc., were needed for each stage in order to produce the final product with the minimum expenditure of energy and machine wear.

The present report addresses all of these basic questions. Raw refuse, air-classified light fraction (ACLF), and screened air-classified light fraction (SLF) were used in a number of tests simulating single- and multiple-stage size reduction. Tests were performed with a nominally rated, 10-ton/hr swing hammermill and a small, high-speed fixed hammer shredder. The basic test data have been arranged and generalized enough to predict the characteristic particle size and energy consumption of other unit operation arrangements. In addition, the wear problem has been treated through the investigation of various hardfacing materials and their ability to perform with the different solid waste materials tested. Furthermore, a comprehensive, computerized comminution model of a size-discrete, time-continuous nature has been developed to predict size distribution and energy consumption.

The information reported here consists mainly of basic data obtained from testing. A discussion of an improved and analytical model is given in Section 6, and Section 7 assembles the data so that predictions can be made. These discussions are expanded in Volume 3 with the incorporation of the data obtained in the large-scale shredder tests reported by Cal Recovery Systems, Inc., Richmond, California.

SECTION 2

MATERIALS, EQUIPMENT, AND METHODS

Scientific studies must be able to modify and control systematically the conditions and variables germane to a particular investigation. Consistent with this requirement, a size-reduction facility capable of operating on a scale resembling a commercial installation and yet able to produce laboratory-quality data was developed to conduct the various comminution studies sponsored by the U.S. Environmental Protection Agency (EPA) since 1972. The waste processing facility is located at the University of California (Berkeley) Richmond Field Station. Although the initial emphasis of the laboratory was on size reduction, the facility was later expanded to include complete front-end dry processing as well as certain types of back-end processing for material and energy recovery. The type of processing equipment and instrumentation contained in this facility, and the characteristics of most of the raw waste processed, are discussed in this section.

CHARACTERISTICS OF RAW MUNICIPAL SOLID WASTE

Most of the solid waste processed is residential packer truck material obtained through the courtesy of the Richmond Sanitary Service. The company delivered municipal solid waste (MSW) and removed unwanted processed materials at no cost. Basic composition of the raw MSW is as follows, as a percent of dry weight:

Fe	7.3
Glass	10.2
Aluminum	0.7
Paper	43.2
Plastic	4.5
Other	33.5

Figure 1 shows the size distribution of the raw MSW. Most of the size distribution curve occupies between 2.5 and 25.4 cm (1.0 and 10.0 in.). The range of characteristic particle sizes extends from 11.7 to 15.2 cm (4.6 to 6.0 in.). The corresponding nominal particle sizes are in the interval between 18.8 and 33 cm (7.4 and 13.0 in.).

SIZE REDUCTION EQUIPMENT

The data reported in the present series of comminution studies were obtained from either the Gruendler swing hammermill shredder (Figure 2) or a W-W Grinder Company, high-speed fixed hammermill shredder (Figures

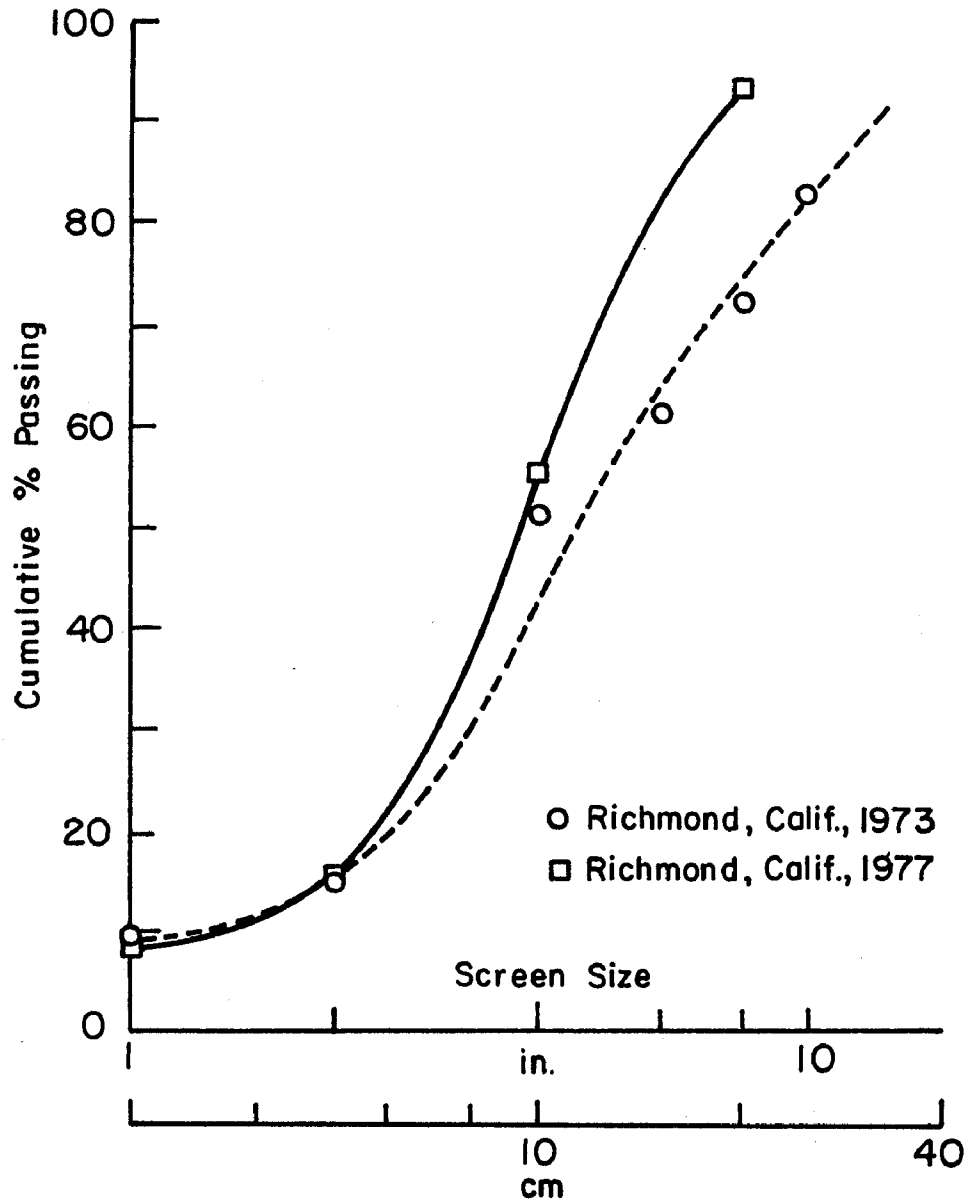

Figure 1. Size distribution of raw MSW, Richmond, Calif.

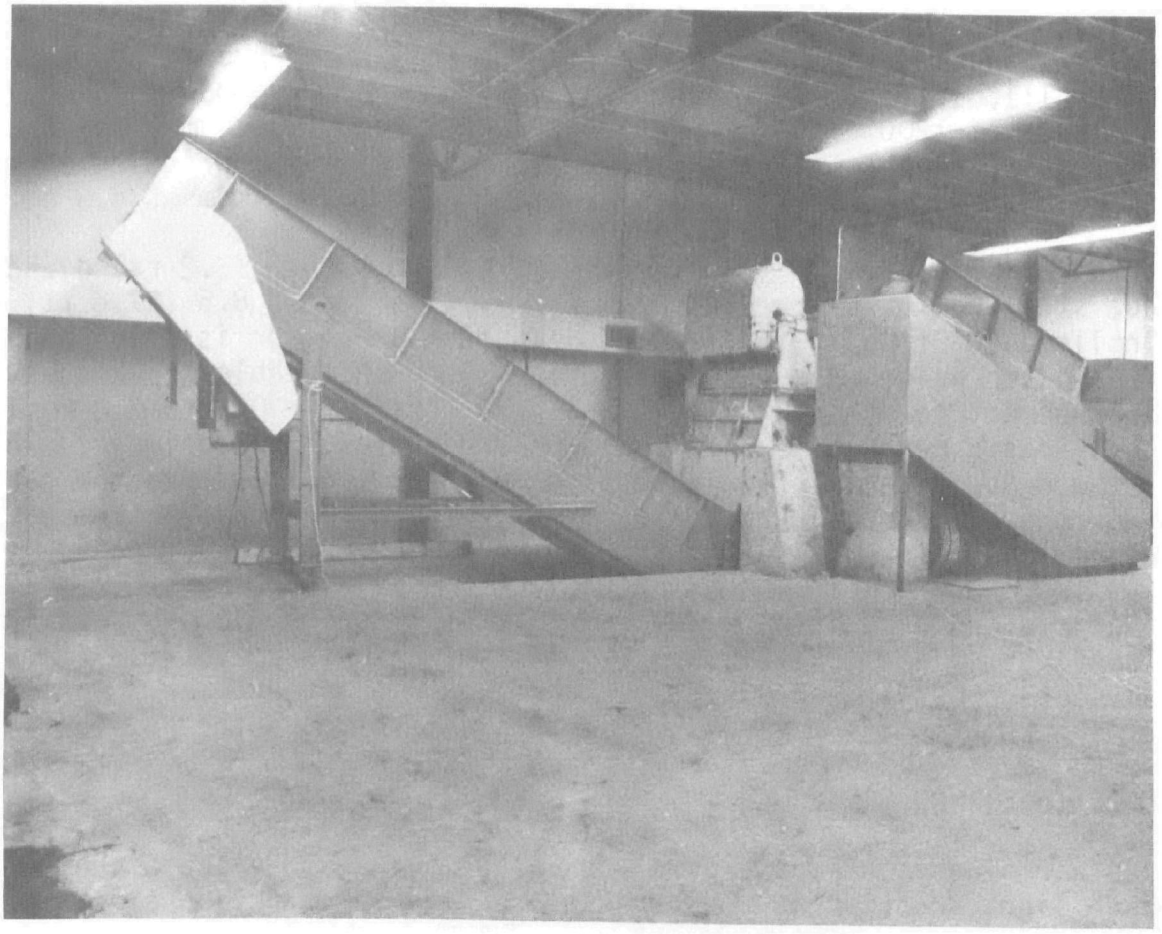

Figure 2. Test facility for the Gruendler swing hammermill shredder.

3, 4 and 5) commonly used for compost size reduction. This machine is driven at 3500 rpm by a 5.6 kW (7.5 hp) motor and has a hammer tip speed of 56 m/s (183 fps). Twenty 0.27-kg (0.59-lb) hammers are attached to the rotor in four rows of five so that approximately 18 to 45 kg/h (40 to 100 lb/h) of light fraction can be processed for the feed size and grate opening conditions investigated.

Most of the shredding was conducted using the Gruendler machine, which is a model 48-4 horizontal hammermill equipped with 44 9-kg, free-swinging manganese steel hammers capable of processing as much as 0.014 mg (15 tons) of refuse per hour. Refuse is introduced into the grinding chamber through the top and removed at the bottom. Power is provided by a 186-kW (250-hp), 480-volt, three-phase, 300-amp motor running at 1200 rpm, and it is transferred to the grinder by way of a variable-speed drive providing discrete ratios of 1:1, 1.22:1, 1.52:1, and 2.16:1, which correspond to shredder rotor speeds of 1200, 985, 790, and 555 rpm. Product size may be controlled by a series of grates placed in the lower portion of the grinding chamber. The range of the grate spacings is from 1.8 cm to a maximum of 4.8 cm.

Raw refuse is fed to the grinder by means of a 1-m (3.2 ft) piano-hinged, steel belt conveyor which is 1.2 m (4 ft) wide, 8.5 (27.8 ft) long, and inclined 20° from the horizontal. The feed conveyor is driven through a variable-pitch drive sheave and one of two interchangeable drive sheaves. The arrangement permits a variation of belt speed from 0.6 to 2.3 m/min and thus provides a means of controlling the feed rate to the grinder. In addition, the drive system is equipped with a sensor that monitors the current drawn by the grinder and automatically stops the feed conveyor in the event of an overload.

The reduced product is removed by way of a second piano-hinged steel belt conveyor. The belt is 0.9 m (3 ft) wide and has a 2.5 (8.2 ft) horizontal section positioned directly under the grinding chamber. The remainder of the belt is 6.8 m long and is inclined at 30 to the horizontal.

AIR CLASSIFIER AND SCREEN

An air classifier and trommel screen were used to prepare the various forms of light fraction that were used in the size reduction experiments.

The air classifier has a capacity of approximately 4 metric tons/h and is of the vertical type consisting of a straight rectangular column. Shredded refuse enters near the top of the column through a gate that acts as an air seal. Lights are moved from the column through a transition piece and pneumatic ducting, which leads to the centrifugal cyclone collector. Heavies fall through the column and are removed by a belt conveyor.

The overall dimensions of the air classifier are 1.1 m (3.6 ft) wide, 0.9 m (3 ft) deep and 4.6 m (15 ft) high. The rectangular cross section of the column has a width of 1.1 m (3.6 ft) and a variable depth of 0.2 to 0.5 m (0.65 to 1.6 ft). Average column air velocities can be controlled within the approximate range of 0.2 to 10 m/s.

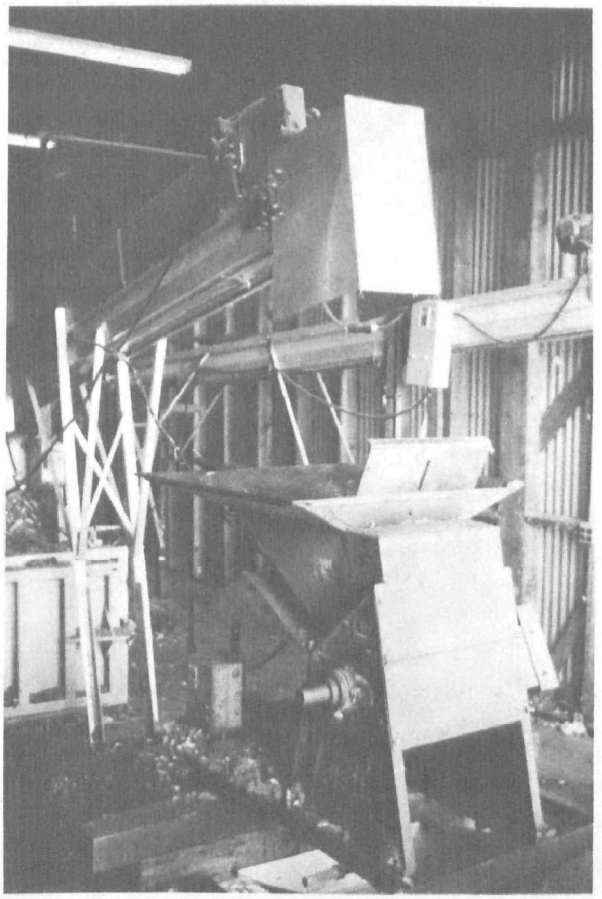

Figure 3. W-W hammermill positioned to shred either air-classified light fraction or screened light fraction.

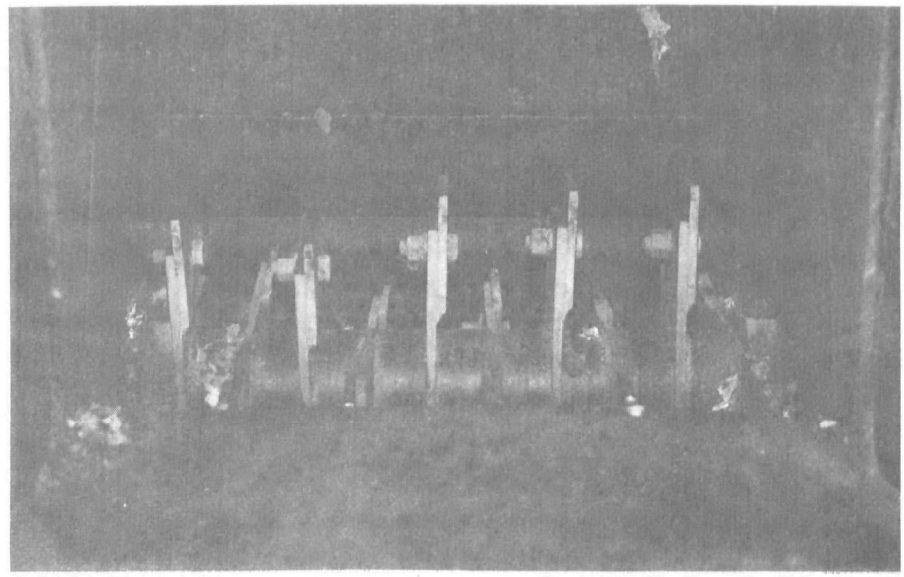

Figure 4. Rotor and hammers of W-W hammermill.

Figure 5. Grate of W-W hammermill.

The light fraction trommel screen has a capacity of 2.8 metric tons/h and consists of a cylindrical screen with 1.3-cm perforations. The screen has a diameter of 0.9 m (3 ft) and an overall length of 4.6 m (15 ft). Inclination of the trommel can be varied within the range of 5° to 20° from the horizontal. In addition, rotational frequency of the trommel can be adjusted within the range of 23 to 38 rpm.

Both undersized and oversized fractions are collected and removed from the trommel screen by belt conveyors. The frictional drive system for the trommel consists of a 1.5 kW motor, speed reducer, chain drive, and rubber drive wheel.

The ACLF used in the experiments was recovered using the Gruendler hammermill for size reduction and the laboratory air classifier. The typical composition of the ACLF on a dry-weight basis was 60.2 percent paper, 5.7 percent plastics, and 34.1 percent other material (namely, organics, dirt, and glass fines).

The SLF was recovered from the ACLF using the trommel screen in our facility. The typical composition of the SLF on a dry weight basis was 78.8 percent paper, 7.8 percent plastics, and 13.4 percent other material, most noticeably organics.

MOISTURE CONTENT AND SIZE DISTRIBUTION ANALYSIS

The characteristic and nominal sizes cited in this study were determined from the size distribution of samples collected during the experimental runs. These samples were dried and subsequently screened in a 46-cm (18-in.) SWECO vibratory screening device for 20 min using various screen sizes. Data were plotted as the cumulative percent passing versus each screen size in order to represent the size distribution of each sample. The characteristic sizes (i.e., 63.2 percent cumulative passing) and the nominal sizes (i.e., 90 percent cumulative passing) for each sample were determined from the graphical size distributions.

The samples of shredded refuse collected from the shredder discharge were dried to constant weight at 22°C (72°F) and 65 percent relative humidity. Consequently, all quantities in the report that use material weights (e.g., specific energy, cumulative weight percent passing, etc.) are based on the above criteria for dry weight, commonly referred to as air-dry moisture content. Moisture content is reported as the quotient of the difference of the initial wet weight minus the air-dry weight divided by the initial wet weight:

$$MC = \frac{\text{(Wet weight)} - \text{(Air dried weight)}}{\text{Wet weight}}$$

The air-dried moisture content of shredded refuse is typically 10 percent less than the bone-dry moisture content.

Samples of shredded refuse for screening analysis were chosen from the air-dried samples after thorough mixing and sectioning. Samples selected for drying ranged in size from 2 kg (4.4 lb) for experimental runs using

4.8-cm (1.9-in.) grate spacings to 0.5 kg (1.1 lb) for experimental runs using 0.64-cm (0.25-in.) grate spacings. The minimum sample size for screening was determined for each grate spacing by successively screening smaller and smaller sample sizes and plotting their size distributions. A sample was deemed too small if its size distribution deviated by more than 10 percent from the average value obtained at each screen size when the aggregate sample was combined and analyzed for an overall size distribution. The trend that was established for sample sizes showed that they could be decreased as the grate spacing decreased.

In this report, the shredded refuse size is described on the basis of characteristic size, X_0 (63.2 percent cumulative passing) and nominal size, X_{90} (90 percent cumulative passing). Each of these values can be determined from the size distribution curve.

Because of the motion of the rotary screen, it is possible for a large piece of material to "move" around the screen without tumbling and thus act as a raft for many smaller particles. For this reason, only one screen at a time was placed on the screen base. Not only did this step have the effect of lowering the total inertia of the system and lead to a more vigorous screening action, but it also allowed the operator to observe the process and to stir the particles occasionally to avoid development of the rafting effect. It was also noted that the efficiency of the screen, that is the rapidity and thoroughness with which all undersized material was passed through a screen, was highly dependent on the mass of material held on the screen at any given time. Therefore careful attention was paid to the amount of material that could initially be placed on a screen before its efficiency was seriously impaired. The maximum amounts shown to be handled efficiently at each screen size are given in Table 1. Each batch of material was screened for 15 min, after which all oversized material was removed and a new batch was placed on the screen. This procedure was repeated until the entire sample had been processed.

Since screening is the most time-consuming of the operations in the experimental program, and since screen time is directly proportional to the weight of the sample, considerable effort was expended to determine the minimum sample size that would be truly representative of the total product. To make this determination, a segment of the refuse stream was removed from the outlet conveyor and was divided into a series of smaller samples in multiples of 500 g. The samples thus obtained were then dried and screened to arrive at a size distribution for each. The segments of the size distribution curve around the 63.2 percent passing mark next were linearized and an equation was found for each. From the equations, corresponding values for X_0 were calculated and the mean and standard variation found. The calculated values of X_0 were compared to the mean, and the absolute value of the errors were converted to percentages and noted. In this manner, it was possible to show that a sample size of roughly 2000 g was all that was required to provide a size distribution whose characteristic size was within a few percentage points of that of parent distribution when 100 percent of the sample was finer than 3 cm.

TABLE 1. MAXIMUM MASS OF SHREDDED REFUSE FOR EFFICIENT SCREENING USING THE SWECO VIBRATORY SCREENS (4.8 cm grate openings)

Screen size (cm)	Maximum mass (g)
+ 2.54	250
- 2.54 + 1.5875	250
- 1.5875 + 0.9525	150
- 0.9525 + 0.5138	150
- 0.5138 + 0.2743	100
- 0.2743 + 0.1295	50

MEASUREMENT OF POWER AND ENERGY CONSUMPTION

The power monitoring equipment consists of a Scientific Columbus watt/watt-hour transducer, a divider, a chart recorder, and a counter (Figure 6). The transducer supplies (with ± 0.10 percent accuracy) an analog current signal directly proportional to the power (watts) and a digital signal directly proportional to energy (watt-hours). Because the transducer is designed to operate from 120-volt, 5-amp inputs, instrument transformers are used to transform the larger primary currents and voltages to these values. The analog dc current signal is passed through a precision 1000-ohm resistor, and the resulting voltage drop is recorded using a chart recorder. Because the transducer is designed to provide exactly 1 milliamp of current for a secondary power of 1500 watts, the instantaneous power in the primary circuit is easily found by

$$P = KI \text{ (1500 watts/milliamp)}$$

where: K = reduction ratio, and
I = dc output current in milliamps.

The voltage drop recorded by the chart recorder is related to the current signal by Ohm's Law, namely V = IR. Since 1 milliamp conducted through 1000 ohms produces a voltage drop of 1 volt, the instantaneous power may be written as

$$P = KV \text{ (1500 watts/volt)}$$

where: P = instantaneous power in watts
K = reduction ration (product of current and potential transformer ratios), and
V = recorded voltage.

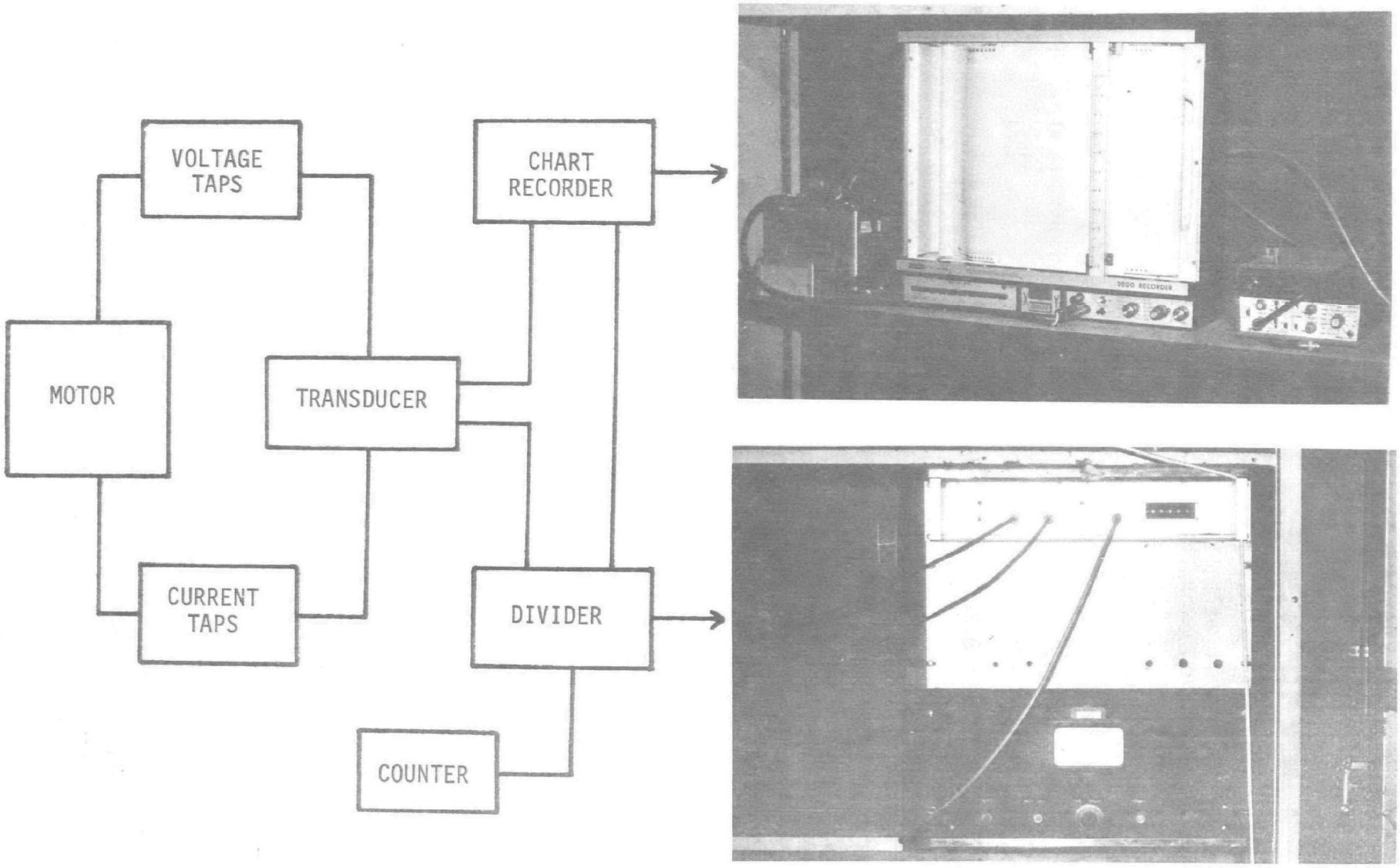

Figure 6. Schematic of power monitoring system.

The digital watt-hour signal is also based on a full load power draw of 1500 watts in such a way that a specified pulse rate is produced for full-load power. In this particular case, 2160 pulses/h for a full load of 1500 watts was chosen. It corresponds to a value of 0.696 watt-hours (Wh) per pulse for the secondary circuit. The numerical value for the primary circuit is found by multiplying 0.696 by the reduction ratio. For the Gruendler grinder, the product of the tranformer ratios is 144; so each digital pulse provided by the transducer represents 100 Wh in the primary circuit. This signal is then passed to a divider, which counts the incoming pulses and for every n pulse (where n is a specified number between 1 and 99,999) provides two output pulses. One of the pulses (representing 100n watts) is passed to the counter, and thereby a record of the total energy (kWh) is kept. The second pulse triggers an event marker on the chart recorder and thus provides a permanent record of the energy consumption.

Specific energy, i.e., energy consumption per unit of dry weight of reduced material, was determined from the energy data provided by the transducer and from measurement of the actual tonnage of material shredded during the energy measurement interval. That is, specific energy (megajoules (MJ)/metric ton or kWh/ton) was calculated as the quotient of energy measured (MJ or kWh) divided by the dry weight of the material reduced during the test period. Net energy was used for specific energy calculations and was determined by subtracting the freewheeling energy from the gross energy that the transducer measured. Freewheeling power was measured and recorded before and after all experimental runs.

DATA COLLECTION PROCEDURE

The shredder and all electronic equipment are turned on at least a half hour before any data are taken to allow steady-state operating conditions to be reached. At this time, the first check on freewheeling power consumption is made. A second check is made at some time during the run, and a third when all the refuse has been shredded, just before shutting down the system. The average of the three then is used as the freewheeling power for the day.

Raw refuse is desposited on the laboratory floor by a packer truck and loaded onto the feed conveyor by a front-end loader. Although it is not essential that the feed rate be held constant, the loader operator tried to maintain an even flow rate once the feed conveyor is turned on. Once loading begins, both feed and product conveyors are started, and shredding is commenced. Refuse is shredded for approximately 10 min before data collection is initiated. This time interval allows sufficient time for material to build up in the shredder and for the shredder to reach steady-state operation.

To obtain a sample of shredded refuse, the output conveyor is stopped at a specified position. At the same time, the chart recorder pen position is noted. Since both chart speed and conveyor speed are known, accurate correlation of energy consumption and particle size is possible. The refuse sample is obtained by removing all of the shredded refuse from the specified conveyor section. From the weight of this sample the flow rate, Q, is found from:

$$Q = cvw$$

where: v = belt speed on m/min
w = sample mass in kg/m section of conveyor, and
c = conversion factor from kg/min to metric tons/h = 0.06.

A portion of the sample taken from the output conveyor is weighed, dried, and reweighed to determine the air-dry moisture content of the sample before being analyzed for size distribution information. Size distributions are obtained with the use of two sets of screens. For particle sizes above 2.5 cm, large, manually vibrated screens having a fixed ratio of 2 between successive screen sizes are used. Material placed on the screens is shaken, stirred, and shaken again until no further material is observed to fall from the screen. For sizes below 2.5 cm, a SWECO Vibro-Energy Rotary Screen is utilized. The SWECO screens make it possible to screen particles as small as 0.02 cm, although for all practical purposes, screening to 0.13 cm is usually the lower limit. Because of the somewhat lower degree of control that could be exerted on the screening action of the SWECO screens, much closer attention was paid to the mass of material originally placed on the screen and to the duration of the screening.

PROCEDURE FOR OBTAINING RESIDENCE TIME

Data on the residence time of material within the grinder was obtained through the introduction of a small amount of tracer into the feed material and subsequent examination of the output. Because the grinder is equipped with a hood that extends slightly more than 2 m down the feed conveyor, it was difficult as well as dangerous to attempt to observe the entrance of the tracer into the grinder itself. To surmount this problem, tracer material was weighed and placed in a small bag to which a length of string was fastened. The bag of tracer was then buried in the feed material. While the tracer was traveling with the conveyor, a steady pull could be felt on the string. The time of the sharp tug (i.e., the signal of entry) was duly noted.

The output was monitored for the appearance of the tracer, which consisted of strips of distinctively colored paper that allowed it to be distinguished from the remainder of the waste stream. As soon as tracer material was observed in the output, its position was marked on the moving bed of shredded refuse. Likewise, the point of depletion of the tracer material was marked on the bed of refuse. After depletion of the tracer, both input and output conveyors were halted. The shredded refuse containing the tracer on the ouput conveyor was then completely removed in 0.9 m segments, and each segment was weighed. Each segment was then thoroughly and completely mixed and divided into 2000-g samples, one of which was retained for analysis. The retained sample was dried and weighed again to ascertain its moisture content before manually sorting tracer material from the refuse. In this manner, the complete time history of tracer material from introduction into the grinder to discharge could be determined.

Mill holdup was determined by stopping both conveyors at the time a steady-state condition was reached in the grinder and collecting the material that then emerged from the grinder. To determine when a steady-state condition had been reached, the chart recording of power consumption was monitored for a period of relatively constant power draw. When such a point of constant power draw was observed, the feed and discharge conveyors were stopped, and a large sheet of plywood was placed under the grinder to catch and retain the mill holdup for weighing. Output flow rate data were then collected as previously described, and if manpower requirements permitted, energy consumption was determined as well.

SECTION 3

SHREDDING STUDIES

Study data were gathered systematically using various forms of single, multiple, and progressive shredding of raw and processed refuse. In the present context, (a) single-stage shredding implies a single pass through the shredder at a specified feed rate, moisture content, grate spacing, speed, etc.; (b) multiple shredding implies that the product becomes the feed for the next stage of shredding, which occurs for the same shredder conditions of grate spacing and speed; and (c) progressive shredding also implies that the product becomes the feed for the next stage of shredding, which in general occurs in a situation where the grate spacing has been reduced. To reflect adequately the various processing configurations that could be used in developing commercial waste processing facilities, three material forms were studied: Raw packer truck MSW, light fraction obtained after air classsification of shredded MSW product (ACLF), and the light fraction obtained after air classification and screening (SLF). The results are presented in terms of material groups for the various machine arrangements.

MUNICIPAL SOLID WASTE STUDIES (GRUENDLER HAMMERMILL)

Single-Stage Shredding With Three Grate Openings

Raw refuse was shredded in a single pass manner in the Gruendler hammermill for three separate grate openings of 4.8, 2.5, and 1.8 cm (1.9, 1.0, and 0.7 in.). Various mass flow rates were shredded at each grate spacing. Energy measurements and product samples for size distribution analysis were gathered for each experimental run.

For these tests, a range of feed rates was tested so that an overall average product size and energy consumption per ton could be established. For the experiments conducted with 1.8-cm (0.7-in.) grate spacings, the maximum hourly feed rate was limited to between 0.7 and 5.3 metric tons (0.8 and 6.0 tons) on a dry-weight basis to avoid overloading the grinder motor. The range of dry and wet feedrates used in these experiments is given in Table 2.

The results of the tests conducted with 4.8-cm (1.9-in.) grate openings showed average characteristic and nominal product sizes of 1.83 and 4.23 cm (0.72 and 1.68 in.) (Table 3). The standard deviation was 0.41 cm (0.16 in.) for the former and 0.89 cm (0.35 in.) for the latter. The average specific energy consumption (E_0) was 54.6 MJ/metric ton (13.8 kWh/ton), with a standard deviation of 13.9 MJ/metric ton (3.5 kWh/ton). The average moisture content (MC) of the shredded material was 29.8 percent, with a standard deviation of 7.6 percent.

TABLE 2. FEEDRATES USED IN THE SIZE REDUCTION OF RAW MSW WITH THE GRUENDLER HAMMERMILL

Grate opening	Minimum feed rate				Maximum feed rate			
	Dry		Wet		Dry		Wet	
cm (in.)	metric tons/h	(tons/h)	metric tons/h	(tons/h)	metric tons/h	(tons/h)	metric tons/h	(tons/h)
4.8 (1.9)	1.0	(1.1)	1.5	(1.7)	5.8	(6.4)	7.4	(8.1)
2.5 (1.0)	0.5	(0.6)	0.9	(1.0)	5.1	(5.6)	7.4	(8.2)
1.8 (0.7)	0.7	(0.8)	1.14	(1.3)	3.7	(4.1)	5.3	(5.8)

Table 3. SIZE REDUCTION OF RAW MSW USING 4.8-CM (1.9-IN) GRATE OPENINGS WITH THE GRUENDLER HAMMERMILL

	Product size						
	X_o		X_{90}		E_o		Air-dry MC*
	cm	(in.)	cm	(in.)	MJ/ metric ton	(kWh/ton)	(percent)
	1.12	(0.44)	2.97	(1.17)	40.4	(10.2)	40.4
	1.60	(0.63)	2.92	(1.15)	58.6	(14.8)	39.1
	1.88	(0.74)	4.70	(1.85)	62.6	(15.8)	36.5
	1.75	(0.69)	3.94	(1.55)	49.5	(12.5)	20.5
	1.57	(0.62)	5.59	(2.20)	69.3	(17.5)	23.1
	2.16	(0.85)	4.95	(1.95)	41.6	(10.5)	21.-
	2.54	(1.00)	4.78	(1.88)	34.1	(8.6)	29.3
	1.55	(0.61)	3.30	(1.30)	64.2	(16.2)	27.3
	2.31	(0.91)	4.57	(1.80)	80.0	(20.2)	22.4
	1.68	(0.66)	4.95	(1.95)	36.4	(9.2)	38.1
Avg.	1.83	(0.72)	4.23	(1.68)	54.6	(13.8)	29.8
Std. Dev.	0.41	(0.16)	0.89	(0.35)	13.9	(3.5)	7.6

*Moisture content of shredded material.

Energy consumption using a grate spacing of 2.5 cm (1.0 in.) averaged 99.4 MJ/metric ton (25.1 kWh/ton), with a standard deviation of 28.1 MJ/metric ton (7.1 kWh/ton) (Table 4). The average characteristic and nominal product sizes were, respectively, 0.74 and 1.52 cm (0.29 and 0.60 in.). The standard deviations were, respectively, 0.18 and 0.25 cm (0.07 nd 0.10 in.). The average moisture content of the shredded material was 28.8 percent, with a standard deviation of 7.9 percent.

Size reduction at the smallest grate openings, namely 1.8 cm (0.7 in.) (Table 5) required an average specific energy of 167.1 MJ/metric ton (42.2 kWh/ton), with a standard deviation of 45.1 MJ/metric ton (11.4 kWh/ton). The average characteristic and nominal product sizes were, respectively, 0.53 and 1.17 cm (0.21 and 0.46 in.), with standard deviations of 0.13 and 0.18 cm (0.05 and 0.07 in.), respectively. The shredded material had an average moisture content of 27.2 percent, with a standard deviation of 9.0 percent.

Size reduction of raw MSW using a Gruendler hammermill has shown the increase in energy consumption and the decrease in product size as a consequence of decreasing the size of the grate openings. There was a significant increase in energy requirement as the grate spacing was decreased from 2.5 to 1.8 cm (1.0 to 0.7 in.) (Figure 7). Grate openings in the range of 1.8 and 2.5 cm (0.7 and 1.0 in.) appear to represent the knee of the curve, with the curve becoming exceedingly steep for values smaller than 1.8 cm (0.7 in.).

The same data from another viewpoint, namely that of characteristic and nominal product sizes (Figures 8 and 9), show the knee of the energy curve to occur in the range of 0.74 and 0.53 (0.29 and 0.21 in.) for the former and in the range of 1.52 and 1.17 cm (0.60 and 0.46 in.) for the latter. The relation of shredded product size to size of grate openings is shown in Figure 10.

In the size reduction of raw MSW, given a specific grate spacing, a considerable variation in sample-to-sample data can be expected, as evidenced by the values of the standard deviation for energy consumption, characteristic product size, and nominal product size. In general, the ratio of standard deviation to average value was approximately 26 percent for energy data, 24 percent for characteristic sizes and 18 percent for nominal sizes. Consequently, to secure representative data with regard to energy consumption and shredded product size, perhaps 8 to 10 samples should be the minimum collected.

Single-Stage Shredding With No Grates

An additional series of tests was performed with the Gruendler hammermill operating without any grate bars at a feed rate of 6.9 metric tons/h (7.6 tons/h) on a wet basis and 5.9 metric tons/h (6.5 tons/h) on a dry basis. As expected, this manner of shredding produces a very coarse product size (Figure 11) when compared to raw refuse. The characteristic and nominal sizes are 15.2 and 25.4 cm (6.0 and 10.0 in.), respectively, because of the relatively small residence time of the material within the mill. The physical character of the material consists of torn grocery bags, plastic

TABLE 4. SIZE REDUCTION OF RAW MSW USING 2.5-CM (1.0-IN.) GRATE OPENINGS WITH THE GRUENDLER HAMMERMILL

	Product size						
	X_o		X_{90}		E_o		Air-dry MC*
	cm	(in.)	cm	(in.)	MJ/metric ton	(kWh/ton)	(percent)
	0.56	(0.22)	1.37	(0.54)	82.0	(20.7)	15.1
	0.76	(0.30)	1.70	(0.67)	85.1	(21.5)	8.8
	0.99	(0.39)	1.80	(0.71)	112.1	(28.3)	11.7
	0.48	(0.19)	1.12	(0.44)	86.3	(21.8)	38.0
	0.71	(0.28)	1.57	(0.62)	67.7	(17.1)	35.8
	0.79	(0.31)	1.63	(0.64)	118.0	(29.8)	36.8
	0.53	(0.21)	1.22	(0.48	137.4	(34.7)	32.4
	0.46	(0.18)	1.02	(0.40)	80.0	(20.2)	35.0
	0.58	(0.23)	1.37	(0.54)	99.4	(25.1)	32.2
	0.38	(0.15)	1.04	(0.41)	108.9	(27.5)	35.1
	0.79	(0.31)	1.73	(0.68)	97.4	(24.6)	35.1
	0.66	(0.26)	1.42	(0.56)	74.8	(18.9)	29.6
	0.84	(0.33)	1.63	(0.64)	115.6	(29.2)	30.6
	0.69	(0.27)	1.35	(0.53)	95.0	(24.0)	35.1
	0.76	(0.30)	1.57	(0.62)	77.6	(19.6)	30.0
	1.04	(0.41)	1.93	(0.76)	99.0	(25.0)	21.3
	0.56	(0.22)	1.42	(0.56)	85.9	(21.7)	37.4
	0.94	(0.37)	1.83	(0.72)	92.7	(23.4)	25.3
	1.60	(0.26)	1.45	(0.57)	116.4	(29.4)	32.3
	0.76	(0.30)	1.70	(0.67)	158.0	(39.9)	28.8
	0.94	(0.37)	1.70	(0.67)	106.1	(26.8)	32.2
	0.86	(0.34)	1.70	(0.67)	168.3	(42.5)	27.8
	1.02	(0.40)	1.80	(0.71)	75.6	(19.1)	22.2
	0.89	(0.35)	1.52	(0.60)	49.9	(12.6)	23.5
Avg.	0.74	(0.29)	1.52	(0.60)	99.4	(25.1	28.8
Std.Dev.	0.18	(0.07)	0.25	(0.10)	28.1	(7.1)	7.9

*Moisture content of shredded material.

TABLE 5. SIZE REDUCTION OF RAW MSW USING 1.8-CM (0.7-IN) GRATE OPENINGS WITH THE GRUENDLER HAMMERMILL

	Product size						
	X_o		X_{90}		E_o		Air-dry MC*
	cm	(in.)	cm	(in.)	MJ/metric ton	(kWh/ton)	(percent)
	0.76	(0.30)	1.37	(0.54)	288.7	(72.9)	37.1
	0.58	(0.23)	1.32	(0.52)	184.5	(46.6)	33.0
	0.84	(0.33)	1.63	(0.64)	131.9	(33.3)	22.5
	0.41	(0.16)	0.97	(0.38)	153.3	(38.7)	30.6
	0.38	(0.15)	1.07	(0.42)	161.2	(40.7)	25.0
	0.46	(0.18)	1.04	(0.41)	163.9	(41.4)	27.6
	0.61	(0.24)	1.27	(0.50)	140.2	(35.4)	15.9
	0.51	(0.20)	1.02	(0.40)	119.6	(30.2)	20.8
	0.53	(0.21)	1.19	(0.47)	230.5	(58.2)	23.0
	0.48	(0.29)	1.02	(0.40)	145.3	(36.7)	23.0
	0.66	(0.26)	1.35	(0.53)	249.1	(62.9)	21.8
	0.53	(0.21)	1.12	(0.44)	157.6	(39.8)	30.9
	0.58	(0.23)	1.22	(0.48)	134.2	(33.9)	29.6
	0.51	(0.20)	1.17	(0.46)	173.4	(43.8)	31.8
	0.43	(0.17)	0.94	(0.37)	144.1	(36.4)	28.7
	0.48	(0.19)	1.14	(0.45)	131.5	(33.2)	33.9
	0.51	(0.20)	1.02	(0.40)	133.5	(33.7)	26.5
Avg.	0.53	(0.21)	1.17	(0.46)	167.1	(42.2)	27.2
Std.Dev.	0.13	(0.05)	0.18	(0.07)	45.1	(11.4)	9.0

*Moisture content of shredded material.

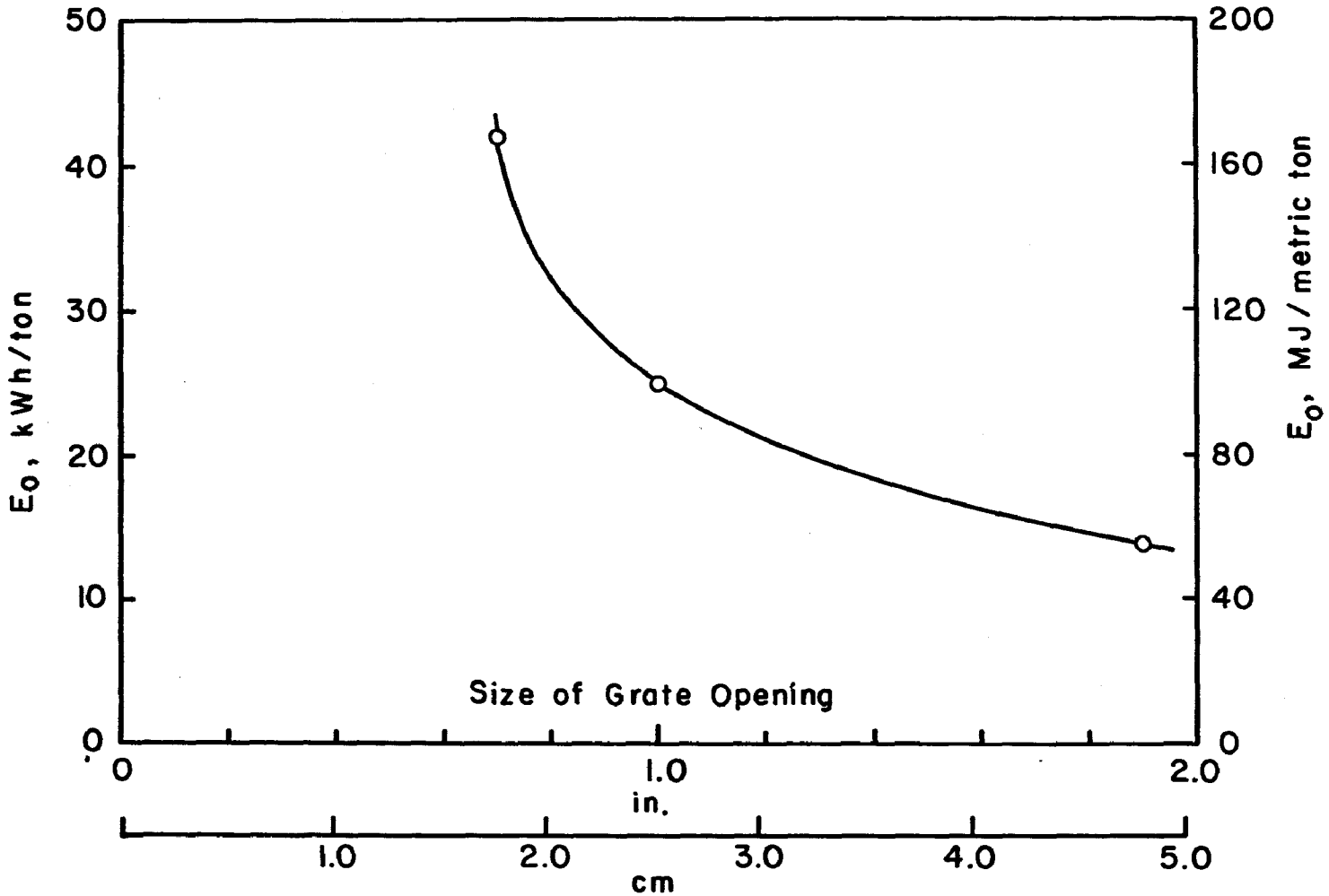

Figure 7. Energy consumption for size reduction of raw MSW as a function of grate opening size (Gruendler hammermill).

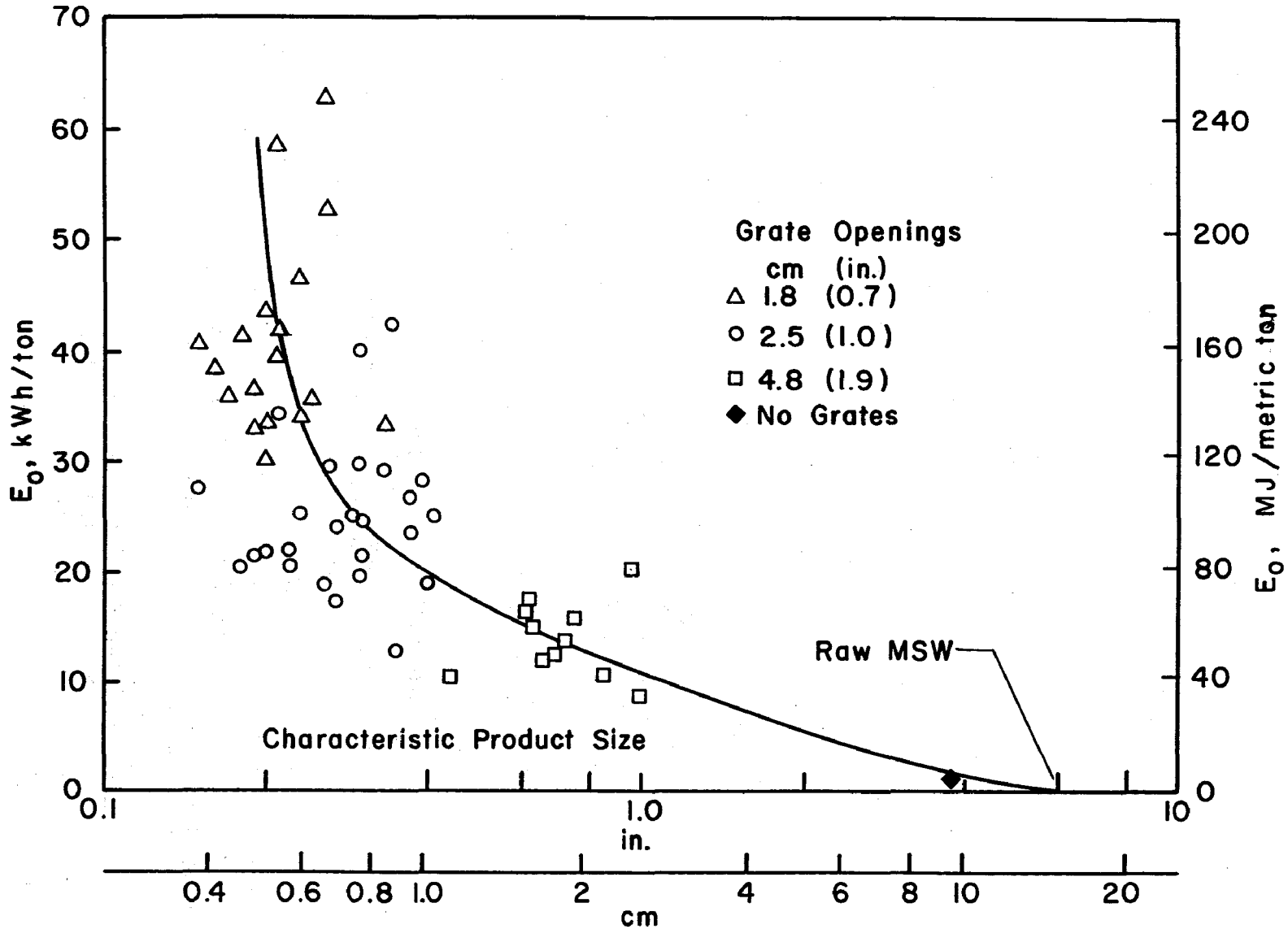

Figure 8. Energy required to reduce raw MSW to a given characteristic product size with a Gruendler hammermill.

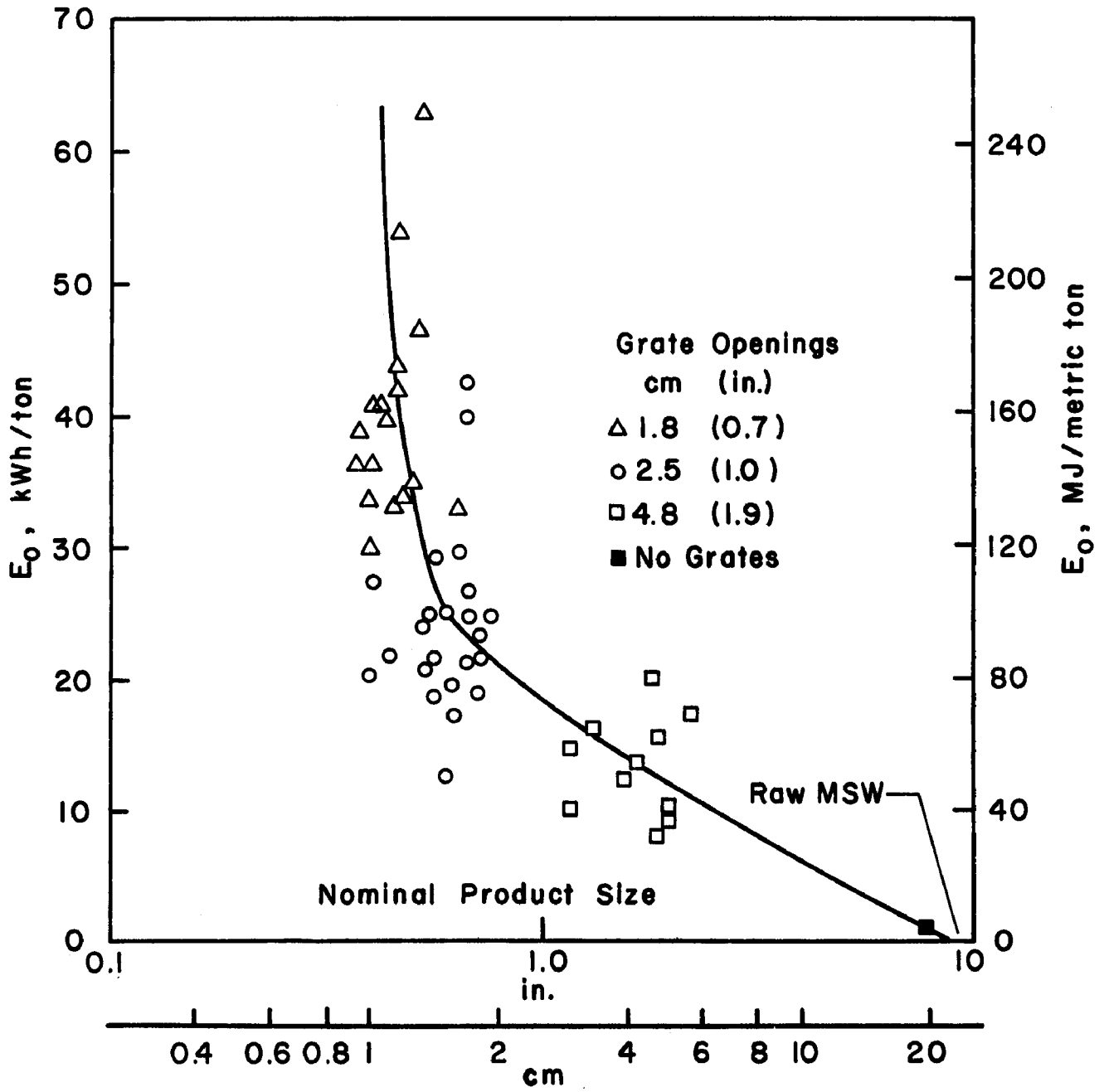

Figure 9. Energy required to reduce raw MSW to a given nominal product size with a Gruendler hammermill.

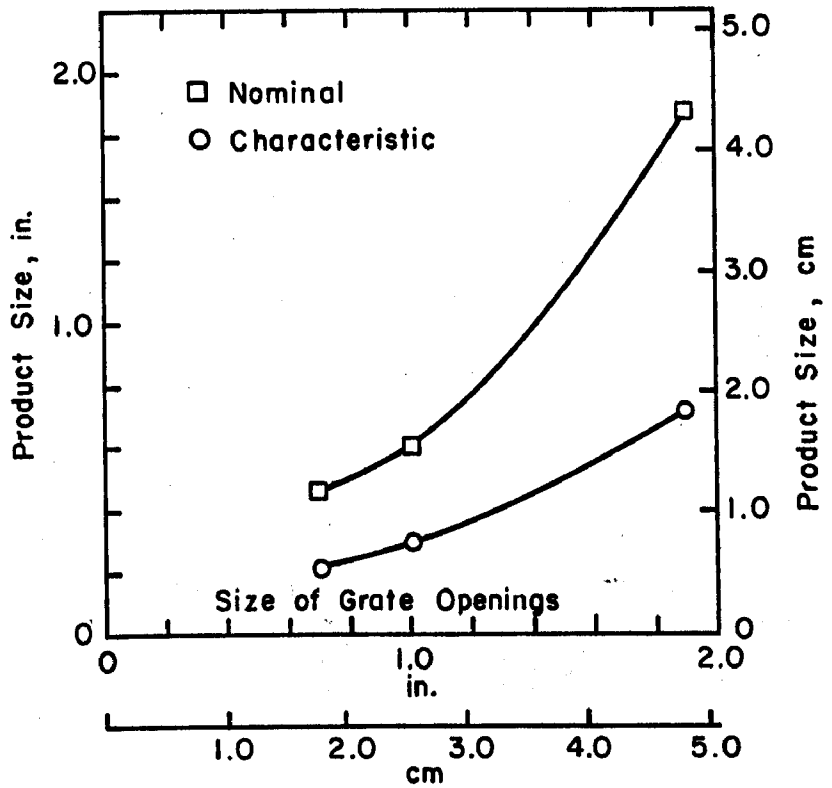

Figure 10. Relation of shredded raw MSW product size to size of grate openings (Gruendler hammermill).

Figure 11. Sample of raw MSW shredded in a Gruendler hammermill without grate bars.

bags, and cardboard containers. Other than glass containers, objects smaller than approximately 30 cm (12 in.) undergo little size reduction. The energy consumption amounted to 4.4 MJ/metric ton (1.1 kW/h/ton), with respective characteristic and nominal product sizes of 9.6 and 19.8 cm (3.8 and 7.8 in.).

Multiple Shredding

In this series of experiments, raw MSW was shredded three consecutive times in the Gruendler hammermill at each of three different grate spacings, namely 4.8, 2.5, and 1.8 cm (1.9, 1.0, and 0.7 in.). Three runs were conducted for primary, secondary, and tertiary size reductions so that average values for energy consumption and product sizes could be developed.

Use of the 4.8-cm (1.9-in.) grate spacing for the multiple shreddings reduced the characteristic and nominal sizes from 15.2 and 25.4 cm (6.0 and 10.0 in.) to 0.53 and 1.12 cm (0.21 and 0.44 in.) respectively (Table 6). The specific energy ranged from 54.6 MJ/metric ton (13.8 kWh/ton) for primary size reduction to 17.4 MJ/metric ton (4.4 kWh/ton) for tertiary size reduction.

Multiple shredding using grate spacings of 2.5 cm (1.0 in.) decreased the characteristic and nominal sizes from 15.2 and 25.4 cm (6.0 and 10.0 in.) to 0.46 and 1.02 cm (0.18 and 0.40 in.) respectively (Table 6). The energy required decreased from 143.7 MJ/metric ton (36.3 kWh/ton) for primary size reduction to 16.2 MJ/metric ton (4.1 kWh/ton) for tertiary size reduction. The shift in the size distribution as a consequence of multiple shredding using grate spacings of 2.5 cm (1.0 in.) is shown in Figure 12.

Last, multiple size reduction at the smallest grate spacing tested, namely 1.8 cm (0.7 in.), decreased the characteristic and nominal sizes from 15.2 and 25.4 cm (6.0 and 10.0 in.) to 0.36 and 0.74 cm (0.14 and 0.29 in.) respectively (Table 6). As in the two previous cases, energy consumption decreased. In this case the decrease was from an initial value of 167.1 MJ/metric ton (42.2 kWh/ton) for primary shredding to 31.3 MJ/metric ton (7.9 kWh/ton) for tertiary shredding. The movement of the size distribution towards the finer end of the size spectrum as the number of size reductions using 1.8 cm (0.7 in.) grate spacings increased is shown in Figure 12.

AIR-CLASSIFIED LIGHT FRACTION STUDIES

The results of tests dealing with the shredding of ACLF, whose characteristics are given in Section 2, are presented first in terms of multiple shredding studies performed using the Gruendler hammermill and then for a sequence of single, multiple, and progressive shredding tests using the W-W machine.

Multiple Shredding (Gruendler Hammermill)

In this test, raw MSW was shredded using the Gruendler hammermill equipped with 2.5-cm (1.00-in.) grate openings and air classified to obtain an ACLF. The ACLF was then shredded using the same mill and grate openings

TABLE 6. MULTIPLE SHREDDING OF RAW MSW WITH THE GRUENDLER HAMMERMILL

D_o		Feed size F_o		Feed size F_{90}		Product size X_o		Product size X_{90}		E_o	
cm	(in.)	cm	(in.)	cm	(in.)	cm	(in.)	cm	(in.)	MJ/ metric ton	kWh/ ton
4.8	(1.9)	15.2	(6.0)	25.4	(10.0)	1.83	(0.72)	4.27	(1.68)	54.6	(13.8)
4.8	(1.9)	1.83	(0.72)	4.27	(1.68)	0.86	(0.34)	1.73	(0.68)	21.8	(5.5)
4.8	(1.9)	0.86	(0.34)	1.73	(0.34)	0.53	(0.21)	1.12	(0.44)	17.4	(4.4)
2.5	(1.0)	15.2	(6.0)	25.4	(10.0)	0.84	(0.33)	1.60	(0.63)	143.7	(36.3)
2.5	(1.0)	0.84	(0.33)	1.60	(0.63)	0.58	(0.23)	1.24	(0.49)	31.7	(8.0)
2.5	(1.0)	0.58	(0.23)	1.24	(0.49)	0.46	(0.18)	1.02	(0.40)	16.2	(4.1)
1.8	(0.7)	15.2	(6.0)	25.4	(10.0)	0.53	(0.21)	1.19	(0.47)	167.1	(42.2)
1.8	(0.7)	0.53	(0.21)	1.19	(0.47)	0.41	(0.16)	0.91	(0.36)	53.1	(13.4)
1.8	(0.7)	0.41	(0.16)	0.91	(0.36)	0.36	(0.14)	0.74	(0.29)	31.3	(7.9)

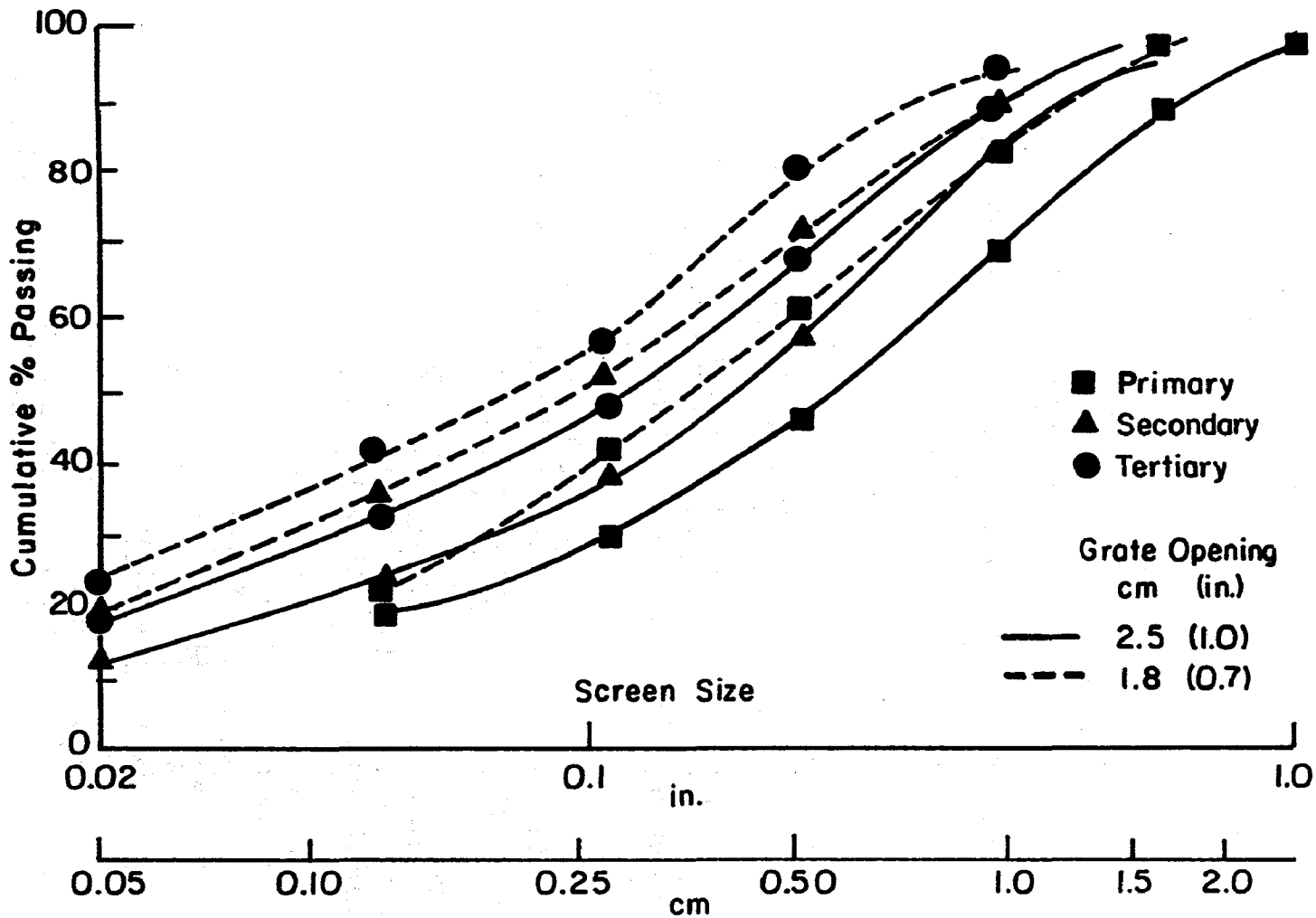

Figure 12. Size distribution of raw MSW after multiple shredding with grate openings of 2.5 and 1.8 cm (1.0 and 0.7 in.) in the Gruendler hammermill.

(primary size reduction of ACLF). An additional shredding of the primary size reduction product was also conducted (secondary size reduction). In essence, this experiment simulates size reduction of ACLF using two hammermills with identical grate openings operating in series. Energy consumption and material flow rates were monitored for each step of size reduction. In addition, samples were collected for size distribution analyses of feed and product materials. The characteristic and nominal feed sizes of the ACLF for this set of tests were 1.22 and 1.93 cm (0.48 and 0.76 in.), respectively.

The characteristic size of the ACLF was reduced to 0.94 and 0.89 cm (0.37 and 0.35 in.) after primary and secondary shredding, respectively (Table 7). The energy consumption as a consequence of these size reductions decreased from 30.1 MJ/metric ton (7.6 kWh/ton) for primary size reduction to 19.4 MJ/metric ton (4.9 kWh/ton) for secondary size reduction. There was only a small decrease in material size as a consequence of secondary shredding: F_0 was 0.94 cm (0.37 in.) and X_0 was 0.89 cm (0.35 in.). The shift in the size distribution toward the finer size ranges is shown in Figure 13.

Single-Stage Shredding (W-W Hammermill)

In this set of experiments, the ACLF with characteristic feed sizes in the W-W hammermill of 1.14 and 1.40 cm (0.45 and 0.55 in.) was reduced in one step using grates with openings of 2.54, 1.91, 1.27, and 0.64 cm (1.00, 0.75, 0.50, and 0.25 in.) to determine the energy required for single-stage size reduction. Energy consumption and the weight of the material shredded were measured so that the specific energy could be calculated. At the same time, samples of feed and product material were collected for size distribution analyses.

The results of this set of experiments show the rapid increase in energy consumption as the size of the grate openings are decreased (Table 8). In Run 1, energy consumption increased more than ninefold -- 44.7 to 407.1 MJ/metric ton (11.3 to 102.8 kWh/ton) -- as the characteristic product size decreased from 1.07 to 0.30 cm (0.42 to 0.12 in.). Similarly, in Run 2 energy consumption increased more than twelvefold -- 26.5 to 324.7 MJ/metric ton (6.7 to 82 kWh/ton) as the characteristic size of the product decreased from 0.89 to 0.28 cm (0.35 to 0.11 in.).

The size distribution of the shredded ACLF shifted toward the finer end of the size spectrum as the size of the grate openings was reduced from 2.54 to 0.64 cm (1.00 to 0.25 in.) (Figure 14). This figure illustrates the test conditions and results of Run 1.

Multiple Shredding (W-W Hammermill)

In this set of experiments, the ACLF of a particular feed size was reduced three times through the same grate openings of the W-W hammermill to study the effect of multiple size reductions. The tests consisted of primary shredding of the ACLF, secondary shredding of the primary product, and tertiary shredding of the secondary product. In all, four separate tests

TABLE 7. MULTIPLE SHREDDING OF ACLF WITH THE GRUENDLER HAMMERMILL

D_o		Feed size				Product size				E_o	
		F_o		F_{90}		X_o		X_{90}			
cm	(in.)	cm	(in.)	cm	(in.)	cm	(in.)	cm	(in.)	MJ/ metric ton	kWh/ ton
2.54	(1.00)	1.22	(0.48)	1.93	(0.76)	0.94	(0.37)	1.42	(0.56)	30.1	(7.6)
2.54	(1.00)	0.94	(0.37)	1.42	(0.56)	0.89	(0.35)	1.40	(0.55)	19.4	(4.9)

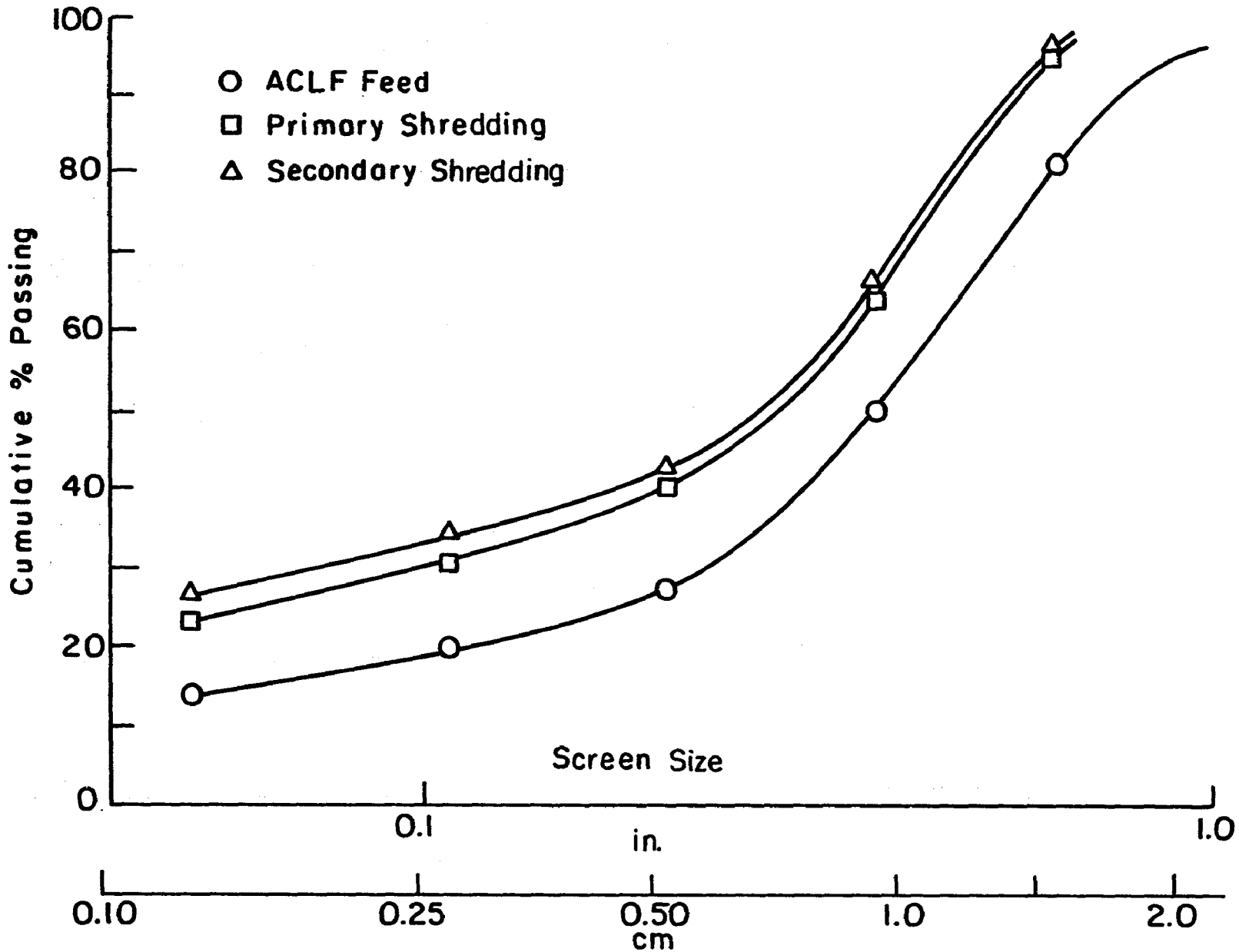

Figure 13. Size distribution for ACLF feed after primary and secondary shredding with the Gruendler hammermill.

TABLE 8. SINGLE-STAGE SHREDDING OF THE ACLF WITH THE W-W HAMMERMILL

Test run	D_o		Feed size F_o		Feed size F_{90}		Product size X_o		Product size X_{90}		E_o	
	cm	(in.)	cm	(in.)	cm	(in.)	cm	(in.)	cm	(in.)	MJ/ metric ton	kWh/ ton
1	2.54	(1.00)	1.14	(0.45)	2.08	(0.82)	1.07	(0.42)	1.98	(0.78)	44.7	(11.3)
	1.91	(0.75)	1.14	(0.45)	2.08	(0.82)	0.79	(0.31)	1.78	(0.70)	78.0	(19.7)
	1.27	(0.50)	1.14	(0.45)	2.08	(0.82)	0.61	(0.24)	1.55	(0.61)	133.1	(33.6)
	0.64	(0.25)	1.14	(0.45)	2.08	(0.82)	0.30	(0.12)	0.91	(0.36)	407.1	(102.8)
2	2.54	(1.00)	1.40	(0.55)	3.68	(1.45)	0.89	(0.35)	1.63	(0.64)	26.5	(6.7)
	1.91	(0.75)	1.40	(0.55)	3.68	(1.45)	0.76	(0.30)	1.37	(0.54)	45.1	(11.4)
	1.27	(0.50)	1.40	(0.55)	3.68	(1.45)	0.61	(0.24)	1.27	(0.50)	77.2	(19.5)
	0.64	(0.25)	1.40	(0.55)	3.68	(1.45)	0.28	(0.11)	1.02	(0.40)	324.7	(82.0)

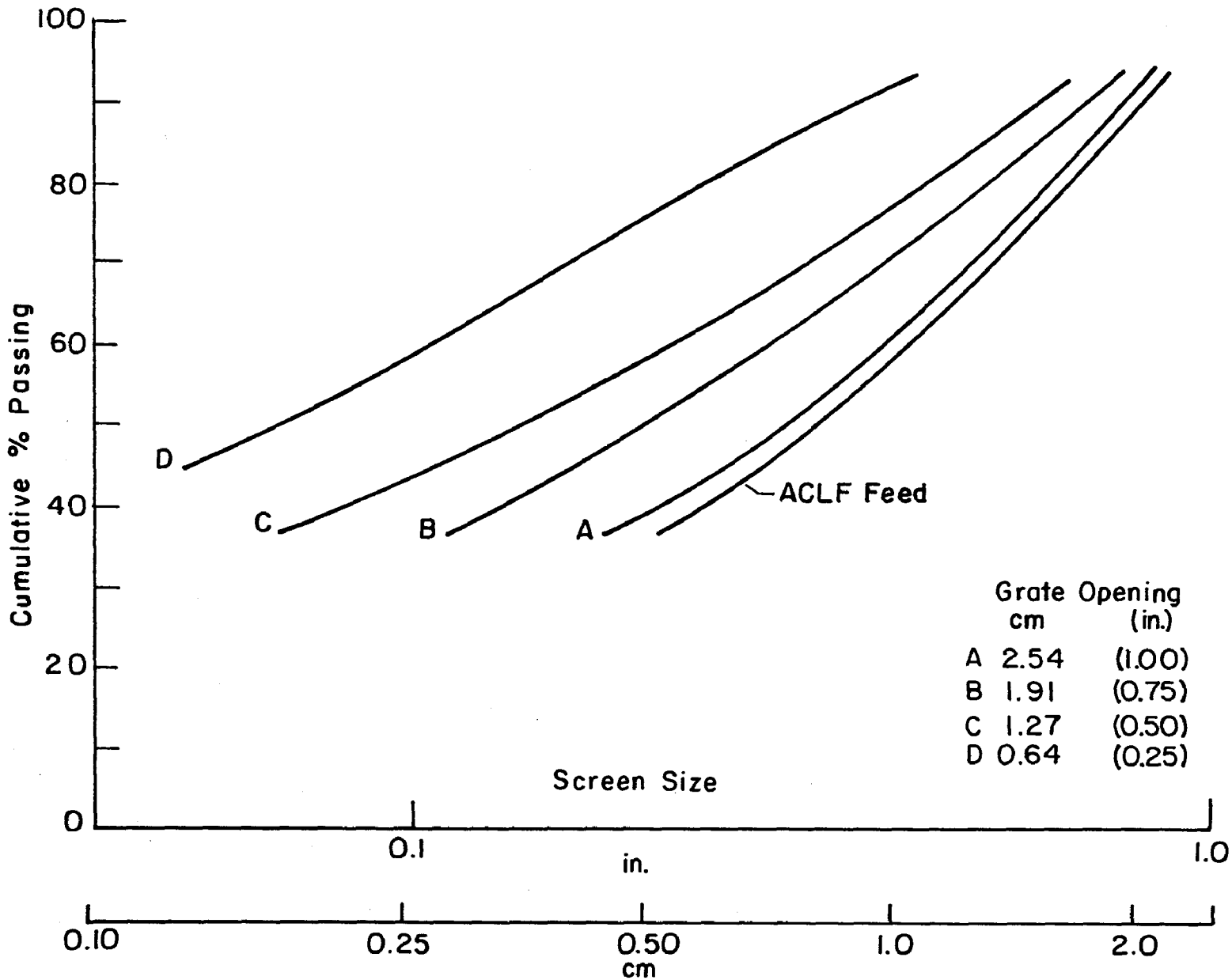

Figure 14. Size distribution of the ACLF after single-stage shredding with the W-W hammermill.

were conducted at grate openings of 2.54, 1.91, 1.27, and 0.64 cm (1.00, 0.75, 0.50, and 0.25 in.). In each case, energy consumption was recorded, and samples for size distribution analysis of feed and product material were gathered. The characteristic and nominal feed sizes of the ACLF were 1.24 and 1.98 cm (0.49 and 0.78 in.), respectively (Table 9).

Within each test run (i.e., all size reductions with a given grate opening) energy consumption decreased as the number of shreddings increased (Table 9). This decrease resulted from the relative decrease in the ratio of feed size to product size as the number of shreddings increased.

This relative decrease in specific energy within each test run was generally smaller as the grate openings became smaller. This observation must be qualified, however, because the data collected for the 0.64-cm (0.25-in.) grate openings are of dubious quality owing to the difficulty of screening such fine, fluffy material. Consequently, the 0.64 cm (0.25 in.) data did not follow the indicated trend. However, for test runs 1, 2, and 3 (Table 9), the trend is apparent. Specific energy decreased 24.5 percent in the first run, 48.9 percent in the second, and 59.0 percent in the third (2.54, 1.91, and 1.27 cm grate openings, respectively).

Progressive Shredding (W-W Hammermill)

In this series of tests, the ACLF with an initial characteristic feed size of 1.02 cm (0.40 in.) and a nominal size of 2.08 cm (0.82 in.) was reduced in the W-W hammermill by consecutive shreddings through sequentially decreasing grate openings. The procedure was as follows:

1) The ACLF was shredded in the W-W hammermill fixed with 2.54-cm (1.00-in.) grate openings.

2) The product from the first shredding was shredded subsequently through 1.91-cm (0.75-in.) grate openings.

3) The product from the second shredding was then shredded through 1.27-cm (0.50-in.) grate openings.

4) Last, the product from the third shredding was shredded through 0.64-cm (0.25-in.) grate openings.

In this manner, there was both a decrease in feed size and a decrease in grate opening for each shredding step. Measurements of energy consumption, quantities of material shredded, and samples for size distribution analyses of feed and product sizes were gathered at each step of size reduction.

Energy consumption increased from 24.2 to 177.4 MJ/metric ton (6.1 to 44.8 kWh/ton) as the size of the grate openings decreased from 2.54 to 0.64 cm (1.00 to 0.25 in.) (Table 10). Over the course of the test, the material decreased in characteristic and nominal size from 1.02 and 2.08 cm (0.40 and 0.82 in.) to 0.15 and 0.46 cm (0.06 and 0.18 in.), respectively.

TABLE 9. MULTIPLE SHREDDING OF THE ACLF WITH THE W-W HAMMERMILL

Test run	D_o		Feed size F_o		Feed size F_{90}		Product size X_o		Product size X_{90}		E_o	
	cm	(in.)	cm	(in.)	cm	(in.)	cm	(in.)	cm	(in.)	MJ/ metric ton	kWh/ ton
1	2.54	(1.00)	1.24	(0.49)	1.98	(0.78)	0.76	(0.30)	1.19	(0.47)	28.9	(7.3)
	2.54	(1.00)	0.76	(0.30)	1.19	(0.47)	0.71	(0.28)	1.09	(0.43)	25.3	(6.4)
	2.54	(1.00)	0.71	(0.28)	1.09	(0.43)		(0.23)		(0.37)	21.8	(5.5)
2	1.91	(0.75)	1.24	(0.49)	1.98	(0.78)	0.76	(0.30)	1.14	(0.45)	52.7	(13.3)
	1.91	(0.75)	0.76	(0.30)	1.14	(0.45)	0.66	(0.26)	1.12	(0.44)	34.1	(8.6)
	1.91	(0.75)	0.66	(0.26)	1.12	(0.44)	0.56	(0.22)	1.09	(0.43)	28.5	(7.2)
3	1.27	(0.50)	1.24	(0.49)	1.98	(0.78)	0.53	(0.21)	1.24	(0.49)	85.9	(21.7)
	1.27	(0.50)	0.53	(0.21)	1.24	(0.49)	0.41	(0.16)	1.14	(0.45)	50.7	(12.8)
	1.27	(0.50)	0.41	(0.16)	1.14	(0.45)	0.36	(0.14)	1.04	(0.41)	35.2	(8.9)
4	0.64	(0.25)	1.24	(0.49)	1.98	(0.78)	0.43	(0.17)	1.19	(0.47)	272.1	(68.7)
	0.64	(0.25)	0.43	(0.17)	1.19	(0.47)	0.15	(0.06)	0.76	(0.30)	147.7	(37.3)

TABLE 10. PROGRESSIVE SHREDDING OF THE ACLF WITH THE W-W HAMMERMILL

D_o		Feed size				Product size				E_o	
		F_o		F_{90}		X_o		X_{90}			
cm	(in.)	cm	(in.)	cm	(in.)	cm	(in.)	cm	(in.)	MJ/ metric ton	kWh/ ton
2.54	(1.00)	1.02	(0.40)	2.08	(0.82)	0.76	(0.30)	1.65	(0.65)	24.2	(6.1)
1.91	(0.75)	0.76	(0.30)	1.65	(0.65)	0.69	(0.27)	1.52	(0.60)	27.2	(9.4)
1.27	(0.50)	0.69	(0.27)	1.52	(0.60)	0.28	(0.11)	0.86	(0.34)	45.1	(11.4)
0.64	(0.25)	0.28	(0.11)	0.86	(0.34)	0.15	(0.06)	0.46	(0.18)	177.4	(44.8)

SCREENED LIGHT FRACTION STUDIES

Single-Stage Shredding (W-W Hammermill)

The SLF was reduced in four separate tests using grate openings of 2.54, 1.91, 1.27, and 0.64 cm (1.00, 0.75, 0.50, and 0.25 in.) in the W-W hammermill. The characteristic and nominal sizes of the SLF before each size reduction were 3.36 and 4.57 cm (1.15 and 1.80 in.), respectively. All tests involved single-stage size reduction -- that is, SLF of the aforementioned size was used as the feed material for each grate opening.

Samples for size distribution analyses of the reduced products and of the SLF feed material were collected for each set of experiments. Energy measurements and quantities of material shredded were recorded to determine the specific energy required for size reduction at each grate opening.

The energy requirements for size reduction of the SLF at each grate opening ranged from 63.8 MJ/metric ton (16.2 kWh/ton) for producing characteristic and nominal sizes of 1.68 and 2.37 cm (0.66 and 0.92 in.), respectively, to 356.4 MJ/metric ton (90.0 kWh/ton) for producing characteristic and nominal sizes of 0.94 and 1.42 cm (0.37 and 0.56 in.), respectively (Table 11). The ratio of characteristic product size to characteristic feed size ranged from 0.57 for the 2.54-cm (1.00-in.) grate opening to 0.32 for the 0.64-cm (0.25-in.) grate opening. As this ratio of product to feed size decreased, the specific energy required for size reduction climbed rather steeply. To illustrate, a ratio of 0.57 resulted in an energy consumption of 63.8 MJ/metric ton (16.2 kWh/ton), whereas a ratio of 0.32 required 356.4 MJ/metric ton (90.0 kWh/ton). The energy requirement increased by a factor of five, and the ratio of product to feed size decreased by approximately 56 percent.

Progressive Shredding (W-W Hammermill)

In this series of size reduction experiments, the SLF was shredded consecutively through grate openings of decreasing size in the W-W hammermill. The characteristic size of the SLF was 3.18 cm (1.25 in.), and the corresponding nominal size was 6.10 cm (2.40 in.). The test consisted of a progressive decrease in feed size and grate opening and consisted of the following procedure:

1) The SLF was shredded using grates with 2.54-cm (1.00-in.) openings.

2) The grate size was then decreased to 1.91 cm (0.75 in.) and the reduced product from the previous run was shredded through it.

3) The grate size was next decreased to 1.27 cm (0.50 in.), and the reduced product from the previous run was shredded through it.

4) Last, the grate openings were changed to 0.64 cm (0.25 in.), and the reduced product from the previous run was shredded through it.

The product from shredding at each larger grate opening consequently became the feed for size reduction at the next smaller grate opening. Samples for

TABLE 11. SINGLE-STAGE SHREDDING OF THE SLF FOR A GIVEN FEED SIZE AND DIFFERENT GRATE OPENINGS WITH THE W-W HAMMERMILL

D_o		Feed size				Product size				E_o	
		F_o		F_{90}		X_o		X_{90}			
cm	(in.)	cm	(in.)	cm	(in.)	cm	(in.)	cm	(in.)	MJ/ metric ton	kWh/ ton
2.54	(1.00)	3.36	(1.15)	4.57	(1.80)	1.68	(0.66)	2.37	(0.92)	63.8	(16.2)
1.91	(0.75)	3.36	(1.15)	4.57	(1.80)	1.37	(0.54)	1.98	(0.78)	115.6	(29.2)
1.27	(0.50)	3.36	(1.15)	4.57	(1.80)	1.12	(0.44)	1.60	(0.63)	226.1	(57.1)
0.64	(0.25)	3.36	(1.15)	4.57	(1.80)	0.94	(0.37)	1.42	(0.56)	356.4	(90.0)

size distribution analyses of feed and product sizes were taken after each size reduction step. Energy measurements and shredded quantities were recorded to determine the specific energy for each step of size reduction.

Results of the progressive shredding of SLF show a relatively small increment in energy requirement for each of the first three steps of size reduction (Table 12). The relatively small increments of size reduction are responsible for this. Typically, the ratios of characteristic product size to characteristic feed size for each shredding step were in the range of 0.50 to 0.80. The gradual movement of the size distribution toward the finer end of the spectrum was a consequence of each incremental step of size reduction (Figure 15). More than a twofold increase in energy consumption was observed in the fourth step of size reduction.

The cumulative energy requirement (sum of each E_0 increment) was 302.0 MJ/metric ton (76.7 kWh/ton) to achieve a characteristic size reduction of 3.18 to 0.58 cm (1.25 to 0.23 in.), or correspondingly, a nominal size reduction of 6.10 to 1.09 cm (2.40 to 0.43 in.). The ratio of final characteristic product size to initial characteristic feed size, 0.58 and 3.18 cm (0.23 and 1.25 in.), respectively, was 0.18.

Multiple Shredding (Hammermill)

The shredding experiments conducted with the Gruendler hammermill involved multiple shredding of SLF previously obtained through processing in our resource recovery facility. The overall scope of the experiment consisted of the following steps:

1) Primary size reduction of raw MSW.

2) Air classification of shredded MSW.

3) Trommel screening of the ACLF to recover the SLF.

4) Storage of the SLF.

5) Shredding of the SLF using the Gruendler hammermill (primary size reduction of the SLF).

6) Collection and storage of the shredded SLF.

7) A final shredding of the previously shredded SLF (secondary size reduction of the SLF).

Consequently, the SLF was actually shredded three times — once during primary size reduction of the MSW and twice as the SLF. The latter two shreddings are the ones of concern here.

To avoid any confusion with primary, secondary, and tertiary size reduction of raw MSW (the terms generally applied to multiple size reduction of raw MSW), one should realize that a previous size reduction as MSW is implicit in the definition of that term, "screened light fraction". In this study, the SLF is taken as the base or feed material.

TABLE 12. PROGRESSIVE SHREDDING OF THE SLF WITH THE W-W HAMMERMILL

D_o		Feed size F_o		Feed size F_{90}		Product size X_o		Product size X_{90}		E_o	
cm	(in.)	cm	(in.)	cm	(in.)	cm	(in.)	cm	(in.)	MJ/ metric ton	kWh/ ton
2.54	(1.00)	3.18	(1.25)	6.10	(2.40)	1.65	(0.66)	2.26	(0.89)	42.1	(10.7)
1.91	(0.75)	1.68	(0.66)	2.26	(0.89)	1.30	(0.51)	1.73	(0.68)	52.0	(13.2)
1.27	(0.50)	1.30	(0.51)	1.73	(0.68)	0.97	(0.38	1.30	(0.51)	62.6	(15.9)
0.64	(0.25)	0.97	(0.38)	1.30	(0.51)	0.58	(0.23)	1.09	(0.43)	145.3	(36.9)

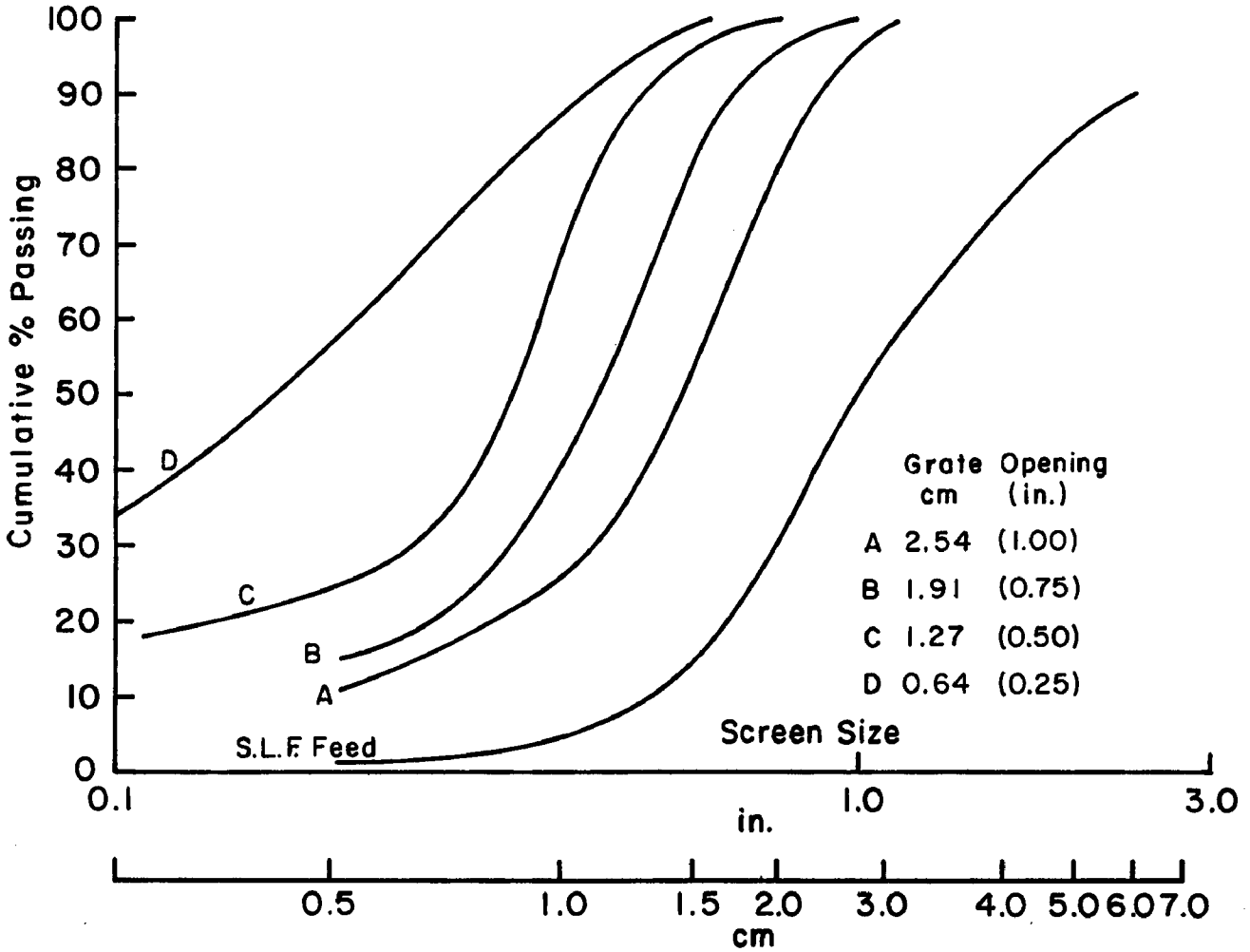

Figure 15. Size distribution of the SLF after progressive shredding with a W-W hammermill.

Primary and secondary size reductions of the SLF were studied for two different conditions of feed size -- namely, the SLF recovered after primary size reduction of raw MSW using 2.5-cm (1.0-in.) grate openings and 1.8-cm (0.7-in.) grate openings. The characteristic sizes of the SLF corresponding to shredding with these grate openings and subsequent air classification and trommel screening were 1.45 and 1.02 cm (0.57 and 0.40 in.), respectively. Feed rates for the primary and secondary size reduction of the SLF were 1.8 and 2.7 metric tons/h (2.0 and 3.0 tons/h) for grate openings of 1.8 and 2.5 cm (0.7 and 1.0 in.), respectively.

Energy recordings and samples for size distribution analyses were taken for each stage of size reduction. The particle size data are reported as the average of three samples each of the SLF feed, the primary shredded product, and the secondary shredded product.

The results of the shredding tests show the degree of size reduction and energy requirement for various feed sizes and grate openings (Table 13). In the shredding experiments using 2.5-cm (1.0-in.) grate openings, the SLF was reduced from a feed with a characteristic particle size of 1.45 cm (0.57 in.) to a product with a characteristic particle size of 1.17 cm (0.46 in.) while undergoing primary size reduction. These characteristic particle sizes correspond to nominal particle sizes of 2.29 and 1.60 cm (0.09 and 0.63 in.), respectively. The energy associated with this degree of size reduction was 49.1 MJ/metric ton (12.4 kWh/ton).

Secondary size reduction of the SLF using 2.5-cm (1.0-in.) grate openings further decreased the characteristic particle size of 1.02 cm (0.40 in.) and the nominal size to 1.5 cm (0.59 in.). This additional degree of size reduction required 28.5 MJ/metric ton (7.2 kWh/ton). The shift in the size distribution toward the finer end of the size spectrum as a consequence of multiple shreddings at a grate opening of 2.5 cm (1.0 in.) is shown in Figure 16.

Results of the experiments conducted with 1.8-cm (0.7-in.) grate openings showed the following degree of size reduction and energy requirement. Primary size reduction decreased the characteristic particle size of the SLF from 1.02 cm (0.40 in.) to 0.99 cm (0.39 in.). These characteristic particle sizes correspond to nominal sizes of 1.55 cm (0.61 in.) and 1.45 cm (0.57 in.), respectively (Table 13). The energy required to achieve this degree of size reduction was 35.2 MJ/metric ton (8.9 kWh/ton).

Secondary size reduction of the SLF using 1.8-cm (0.7-in.) grate openings resulted in a decrease in characteristic size from 0.99 to 0.91 cm (0.39 to 0.36 in.), or alternatively, from 90 percent passing sizes of 1.45 to 1.40 cm (0.57 to 0.55 in.). This degree of size reduction required 49.9 MJ/metric ton (12.6 kWh/ton). The shift in size distributions as a result of multiple shreddings at a grate opening of 1.8 cm (0.7 in.) is shown in Figure 17.

The cumulative energy consumed by the Gruendler hammermill for both primary and secondary size reduction is the total net energy required to shred SLF to the size resulting from two consecutive shreddings with the

TABLE 13. MULTIPLE SHREDDING OF THE SLF WITH THE GRUENDLER HAMMERMILL

D_o		Shredding stage	Feed size F_o		Feed size F_{90}		Product size X_o		Product size X_{90}		E_o	
cm	(in.)		cm	(in.)	cm	(in.)	cm	(in.)	cm	(in.)	MJ/ metric ton	kWh/ ton
2.5	(1.0)	Primary	1.45	(0.57)	2.29	(0.90)	1.17	(0.46)	1.60	(0.63)	49.1	(12.4)
2.5	(1.0)	Secondary	1.17	(0.46)	1.60	(0.63)	1.02	(0.40)	1.50	(0.59	28.5	(7.2)
1.8	(0.7)	Primary	1.02	(0.40)	1.55	(0.61)	0.99	(0.39)	1.45	(0.57)	35.2	(8.9)
1.8	(0.7)	Secondary	0.99	(0.39)	1.45	(0.57)	0.91	(0.36)	1.40	(0.55)	49.9	(12.6)

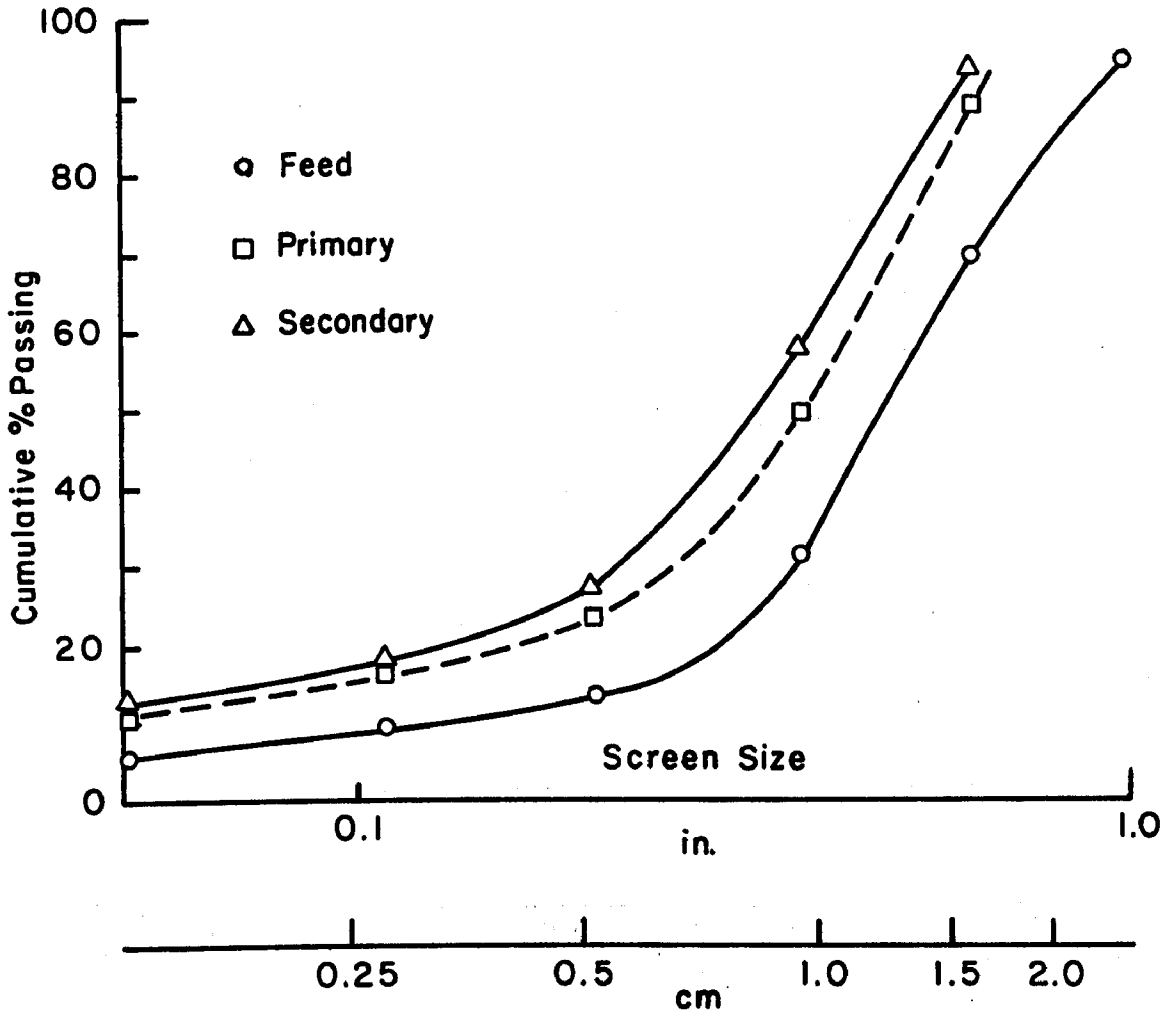

Figure 16. Size distribution of the SLF after multiple shredding with 2.5-cm (0.7-in.) grate openings in the Gruendler hammermill.

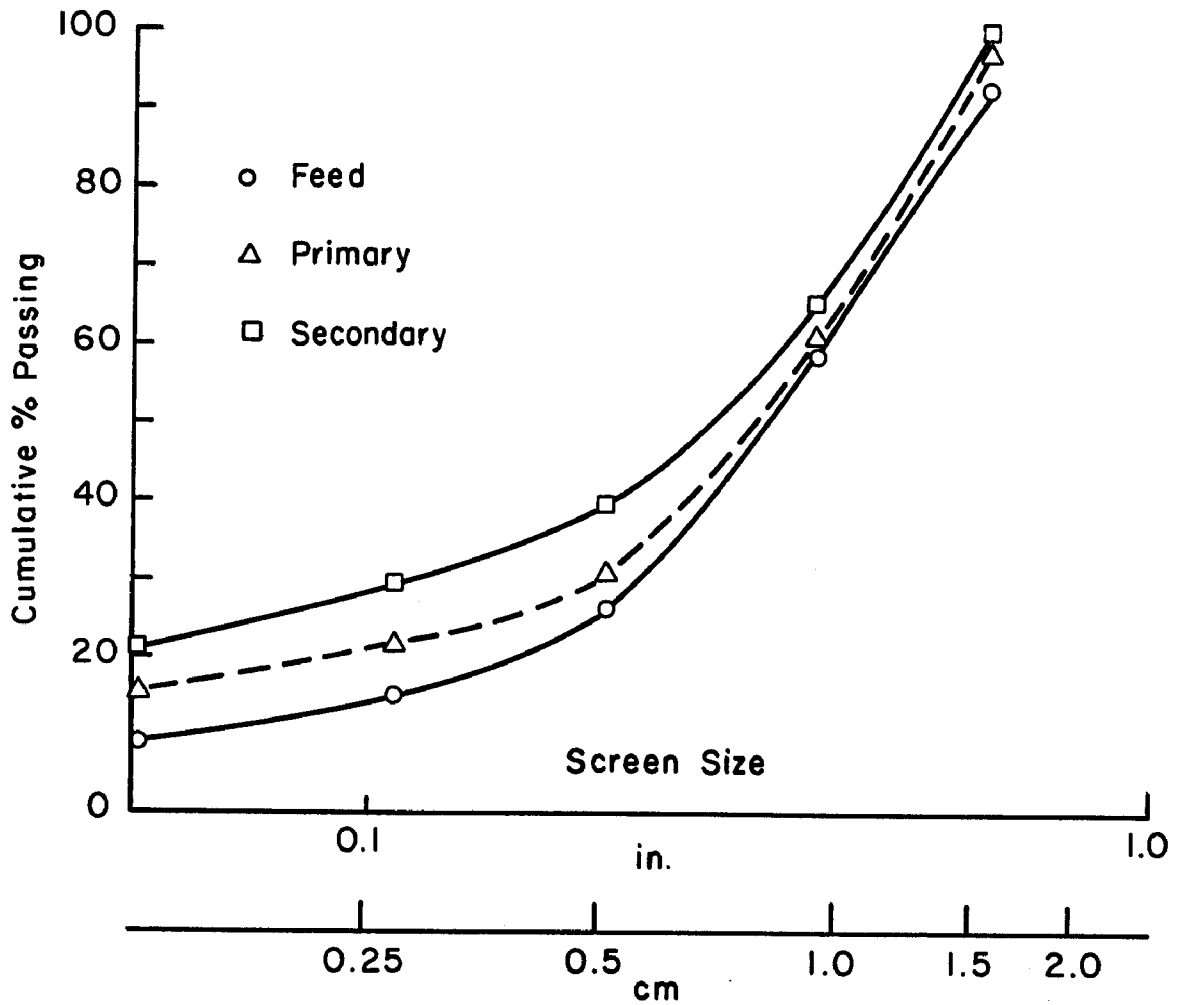

Figure 17. Size distribution of the SLF after multiple shredding with 1.8-cm (0.7-in.) grate openings in the Gruendler hammermill.

same grate openings. For example, in the case of 2.5-cm (1.0-in.) grate openings, a cumulative energy requirement of 77.6 MJ/metric ton (19.6 kWh/ton) was needed to reduce the SLF from a characteristic size of 1.45 to 1.02 cm (0.57 to 0.40 in.). The corresponding reduction in nominal size was 2.29 to 1.50 cm (0.90 to 0.59 in.).

Similarly, the cumulative energy requirement for the 1.8-cm (0.7-in.) grate openings was 85.1 MJ/metric ton (21.5 kWh/ton) for consecutive shredding of the SLF from a characteristic size of 1.02 to 0.91 cm (0.40 to 0.36 in.), or a nominal size of 1.55 to 1.40 cm (0.61 to 0.55 in.).

SECTION 4

WEAR STUDIES

To characterize the size reduction process completely, the hammer wear was evaluated along with other comminution parameters. Detailed investigations were performed of the type and degree of hammer wear resulting from the size reduction of raw MSW and SLF. The raw MSW measurements were conducted with the Gruendler hammermill operating at 1200 rpm using a rotor complement of 44 hammers in conjunction with three different sets of grate bar spacings and five hardfacing materials. A previous raw MSW shredding study [3] considered the effects of rpm on hammer wear. The investigations with SLF were conducted with the W-W hammermill using four different grate sizes and four hardfacing materials. The goals of the wear experiments were to determine the best type of hardfacing alloy to be used and to establish the rate of material loss from the hardfaced hammers as a consequence of size reduction of these particular solid waste forms.

Hammer wear is generally characterized as wear resulting from abrasion or impact. Soft hardfacing materials generally perform well against abrasive materials. Raw municipal solid waste is a composite material containing both abrasive and hard materials; consequently, materials with a full spectrum of hardness values (14 to 56 Rockwell C hardness) were tested to establish the optimum hardfacing material. Because of the abrasive nature of the cellulosic materials in the SLF, relatively hard welding alloys (42 to 63 Rockwell C hardness) were chosen for testing. One point of the research was to test whether or not extremely hard alloys would result in better hammer wear than other softer alloys. In addition, wear rates were examined to quantify the trend in wear as the grate openings were reduced.

HARDFACING MATERIALS AND APPLICATION

Raw MSW Tests

The hardfacing materials tested were alloys in welding electrode form and were readily available from local distributors. The alloys were deposited on the hammer surface using manual electric arc welding. Hardfacing was done in such a manner as to minimize localized heating of the base hammer material (cast manganese steel), which causes embrittling transformations.

In all, five different hardfacing alloys were applied and tested: Stoody 2110, Stoody 31, Coated Tube Stoodite (all manufactured by Stoody Company), Amsco Super 20 (manufactured by Abex Corporation), and Alloy X

(manufacturer unknown, but the composition was determined metallurgically). The hardfacing materials contained various alloy contents and elements (Table 14). The cost of the hardfacing electrodes tested (50-lb lots, 5/32-in. diameter) varied from $123 to $193 (Table 14).

All electrodes tested were easy to apply except for the Coated Tube Stoodite, which had a tendency to drip and splatter. Considerable practice was necessary to obtain a good weld deposition with this electrode. The hammers used are shown in Figures 18 and 19.

Screened Light Fraction

The hardfacing materials chosen were Stoody 31 and Coated Tube Stoodite manufactured by the Stoody Company, Amsco Super 20 manufactured by the Abex Corporation, and Haystellite Tungfine manufactured by the Cabot Corporation. The hardfacing materials contained various alloy contents and elements (Table 15). The approximate costs of the hardfacing materials tested (50-lb lots, 5/32-in. diameter) varied from $123 to $668 (Table 15).

All hardfacing materials (except Haystellite Tungfine) were in welding electrode form and were applied to the hammers by manual electric arc welding. The Haystellite Tungfine was applied to the hammer tips by the hammermill manufacturer using oxy-acetylene welding. The base hammer material was 1045 carbon steel.

EXPERIMENTAL PROCEDURE

Raw MSW Test (Gruendler Hammermill)

The general experimental procedure called for three sets of wear experiments. Each set was accomplished at a specific grate opening, namely 4.8, 2.5, and 1.8 cm (1.9, 1.0, and 0.7 in.). Before each data set commenced, the hammers were hardfaced and weighed to establish the initial weight for that test set. After shredding a specific tonnage of MSW, the hammers were cleaned with a wire brush to remove all electrode slag, dust, and dirt, then weighed again to establish the final weights. The net weight loss was then calculated for each hammer.

The experimental procedure also called for determination of the hardness of each hardfacing material as well as that of the base material (cast manganese steel). Consequently, test beads of each hardfacing alloy were run on a hammer and tested for hardness.

Screened Light Fraction (W-W Hammermill)

The experimental procedure called for wear determinations using: (1) a characteristic feed size of 1.73 cm (0.68 in.) and a nominal feed size of 2.72 cm (1.07 in.), (2) grate openings of 2.54, 1.91, 1.27, and 0.64 cm (1.00, 0.75, 0.50, and 0.25 in.), and (3) the four hardfacing materials described in the preceding section. The as-deposited hardness of each hardfacing material was determined before initiating the wear experiments.

Table 14. COMPARISON OF HAMMER AND HARDFACING MATERIALS USED FOR SHREDDING RAW MSW

Material	Composition	Hardness (R_c)		Approximate cost of electrode[a]
		As deposited	Work-hardened	
Cast manganese steel	C = 1.11 percent Mn = 12.7 percent Si = 0.54 percent	14[b]	38	--
Hardfacing alloy:				
Stoody 2110	Alloy content = 37 percent (Cr, Mn, Nc, Si, C) iron base	21	NA[c]	$123
Alloy X[d]	Alloy content = 20 percent (Cr, Mn, Ni, Mo, C) iron base	38	45	NA
Stoody 31	Alloy content = 35 percent (Cr, Mn, Si, Mo, C) iron base	46	NA	123
Coated Tube Stoodite	Alloy content = 39 percent (Cr, Mn, Si, Mo, Zr, C) iron base	55	NA	129
Amsco Super 20	Alloy content = 40 percent (Cr, Mo, C, W) iron base	56	NA	193

[a] 50-lb lot, 5/32-in. diameter.
[b] As cast.
[c] Not available.
[d] Manufacturer unknown; composition determined by metallurgical analysis.

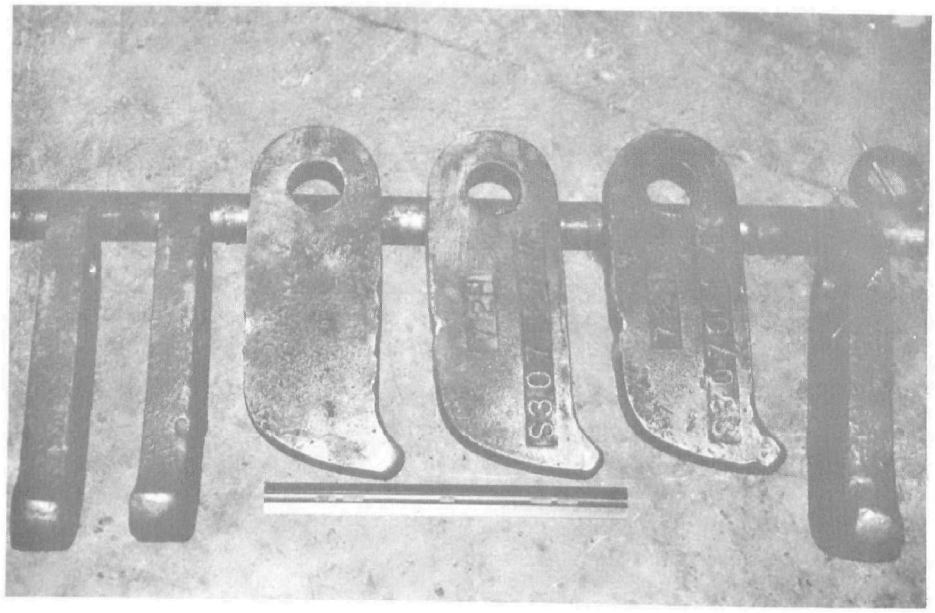

Figure 18. Bare manganese hammers before hardfacing.

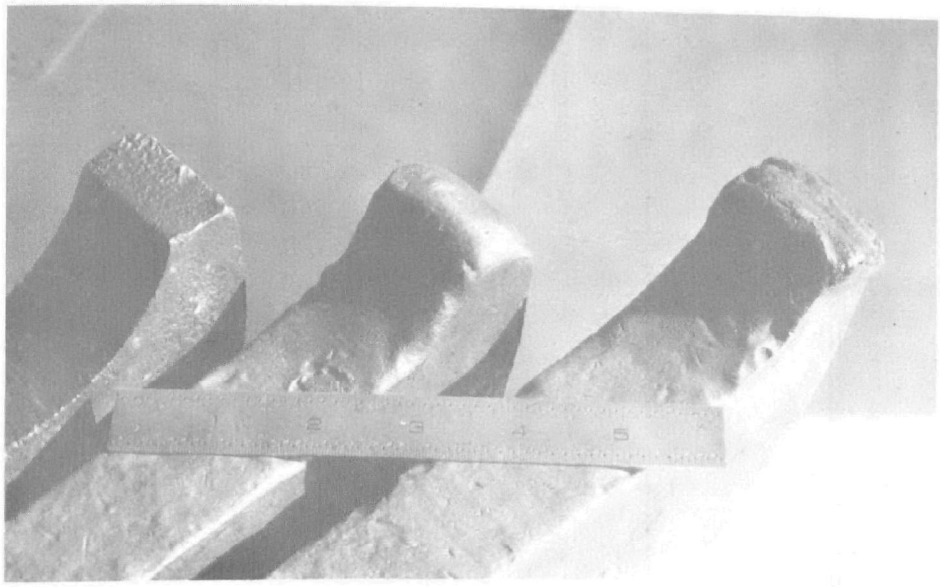

Figure 19. Hammers used for shredding raw MSW: Left, new manganese steel hammer; Center, worn hammer; right, resurfaced hammer.

Table 15. COMPARISON OF HARDFACING MATERIALS USED FOR SHREDDING SLF

Material	Composition	Hardness as deposited	Approximate cost of electrode*
Stoody 31	Alloy content = 35 percent (Cr, Mn, Si, Mo, C), iron base	41.9	$123
Coated Tube Stoodite	Alloy content = 39 percent (Cr, Mn, Si, Mo, Zr, C), iron base	49.5	129
Amsco Super 20	Alloy content = 40 percent (Cr, Mo, C, W), iron base	56.6	193
Haystellite Tungfine	61 percent tungston carbide filler, balance steel tube	63.0	668

* 50-lb lot, 5/32-in. diameter.

Before beginning experiments at each grate opening, all tipped hammers were brushed clean with a wire brush and weighed. After shredding a specific weight of SLF, the hammers were removed from the grinder, brushed clean, and weighed. The difference between the initial and final weights equalled the net weight loss. The wear rate is reported here as kg of hammer weight lost per metric ton of material shredded (kg/metric ton) or as pounds per ton (lb/ton).

HARDENESS MEASUREMENTS

The Rockwell C hardness of each hardfacing material was measured using a standard Rockwell hardness tester. To measure the hardness, a sample bead of each hardfacing material was welded on a hammer and ground to provide a flat testing surface. Care was taken during grinding to minimize localized temperature buildups that could result in low hardness values. During the hardness measurements, the hammers with the sample welds were mounted securely on the tester to insure a valid hardness test.

Raw MSW Test

Four hardness tests were conducted for MSW on each hardfacing alloy as well as on the surface of the cast manganese steel hammer. The average hardness values (Rockwell C) ranged from 14 for the hammer itself to 56 for the hardest alloy tested (Amsco Super 20) (Table 14). These values are reported as deposited, and therefore they do not include any work-hardening. The effect of work-hardening was measured in only two instances, since hardness determinations after work-hardening require sectioning of the hammers to obtain test specimens. In the two cases tested, the base hammer material (manganese steel) increased in hardness from 14 to 38, and Alloy X increased in hardness from 38 to 45 (Table 14).

Screened Light Fraction

Four hardness measurements were conducted on each hardfacing material. The average hardness values (Rockwell C) ranged from 41.9 for the softest material tested (Stoody 31) to 63.0 for the hardest material tested (Haystellite Tungfine (Table 15). These hardness values are as deposited and therefore do not include any work-hardening.

WEAR MEASUREMENTS

MSW Tests

Wear measurements were conducted at three different grate openings -- namely 4.8, 2.5, and 1.8 cm (1.9, 1.0, and 0.7 in.). Experiments at 4.8-cm (1.9-in.) grate openings used bare hammers of cast manganese steel, hammers tipped with Alloy X (manufacturer unknown), and hammers tipped with Amsco Super 20. The alignment of the tipped and untipped hammers consisted of two rows of bare hammers (12 hammers in each row), one row of 10 hammers hardfaced with Alloy X, and one row of 10 hammers hardfaced with Super 20. Consequently, each row encountered exactly the same material and quantities seen by the other rows. This approach eliminated tonnage and composition as factors within each data set.

In the second data set, four materials were tested at a grate spacing of 2.5 cm (1.0 in.). The hammer alignment consisted of one row of bare hammers and one row each of hammers tipped with Stoody 31, Coated Tube Stoodite, and Amsco Super 20.

To test an additional alloy (Stoody 2110) in the wear experiments conducted at a grate spacing of 1.8 cm (0.7 in.), the row normally containing bare hammers was tipped with Stoody 2110, except for two hammers along the center of the rotor. Each of the other three rows consisted of hammers hardfaced with Stoody 31, Coated Tube Stoodite, and Amsco Super 20, respectively. The two bare hammers were needed to maintain a control for the 1.8-cm (0.7-in.) data set and also for later correlation with the data obtained in the 4.8- and 2.5-cm (1.9- and 1.0-in.) data sets. Likewise, Amsco Super 20 was used in each data set as yet another control.

Screened Light Fraction

These wear measurements were conducted with grate opening diameters of 2.54, 1.91, 1.27, and 0.64 cm (1.00, 0.75, 0.50, and 0.25 in.). For each grate opening, there were four rows of hammers. Each row contained five hammers tipped with one of the four alloys -- Stoody 31, Coat Tube Stoodite, Amsco Super 20, or Haystellite Tungfine. Consequently, each row encountered exactly the same material and quantities experienced by the other rows. This technique eliminated tonnage and composition as variables for experiments carried out at each grate opening.

Wear data are reported as kg/metric ton and lb/ton. The data have been normalized for a full complement of 20 hammers.

RESULTS

Raw MSW Tests

The wear experiments conclusively showed that wear increased dramatically as the grate opening was reduced to 1.8 cm (0.7 in.). The two control cases (i.e., bare hammers and hammers hardfaced with Amsco Super 20) used in each data set provide a record of increased wear as the grate spacing was reduced. If the hammer wear found in the experiments is normalized to a full set of hammers (i.e., 44 hammers) and expressed as kilograms of weight lost per metric ton shredded (kg/metric ton), or as pounds per ton (lb/ton), the bare manganese hammers exhibited wear rates of 0.042, 0.057, and 0.140 kg/metric ton (0.084, 0.114, and 0.279 lb/ton) at grate spacings of 4.8, 2.5, and 1.8 cm (1.9, 1.0 and 0.7 in.), respectively. For the same grate openings, the wear rates for hammers hardfaced with Amsco Super 20 were respectively, 0.043, 0.054, and 0.089 kg/metric ton (0.086, 0.107, and 0.178 lb/ton) (Table 16). The rapid increase in wear is particularly apparent in Figure 20. The curve becomes very steep when grate openings are smaller than 2.5 cm (1.0 in.).

Another perspective of the wear rates can be gained by considering wear as a function of the average characteristic shredded product size (Figure 21). The average characteristic product sizes of MSW shredded through grate openings of 4.8, 2.5, and 1.8 cm (1.9, 1.0 and 0.7 in.) were 1.83, 0.74, and

TABLE 16. WEAR DATA FOR VARIOUS HARDFACING MATERIALS USED FOR SHREDDING RAW MSW

Material	Hardness[a] (R_c)	Wear rate, kg/metric ton (lb/ton)		
		4.8-cm grate (1.9-in.)	2.5-cm grate (1.0-in.)	1.8-cm grate (0.7-in.)
Manganese steel base material	14	0.042 (0.084)	0.057 (0.114)	0.140 (0.279)
Stoody 2110	21	b	b	0.144 (0.287)
Alloy X[c]	38	0.031 (0.061)	b	b
Stoody 31	46	b	0.038 (0.076)	0.092 (0.183)
Coated Tube Stoodite	55	b	0.054 (0.108)	0.056 (0.112)
Amsco Super 20	56	0.043 (0.086)	0.054 (0.107)	0.089 (0.178)

[a] Hardness values are initial values as deposited without work-hardening.
[b] Wear not measured.
[c] Manufacturer unknown.

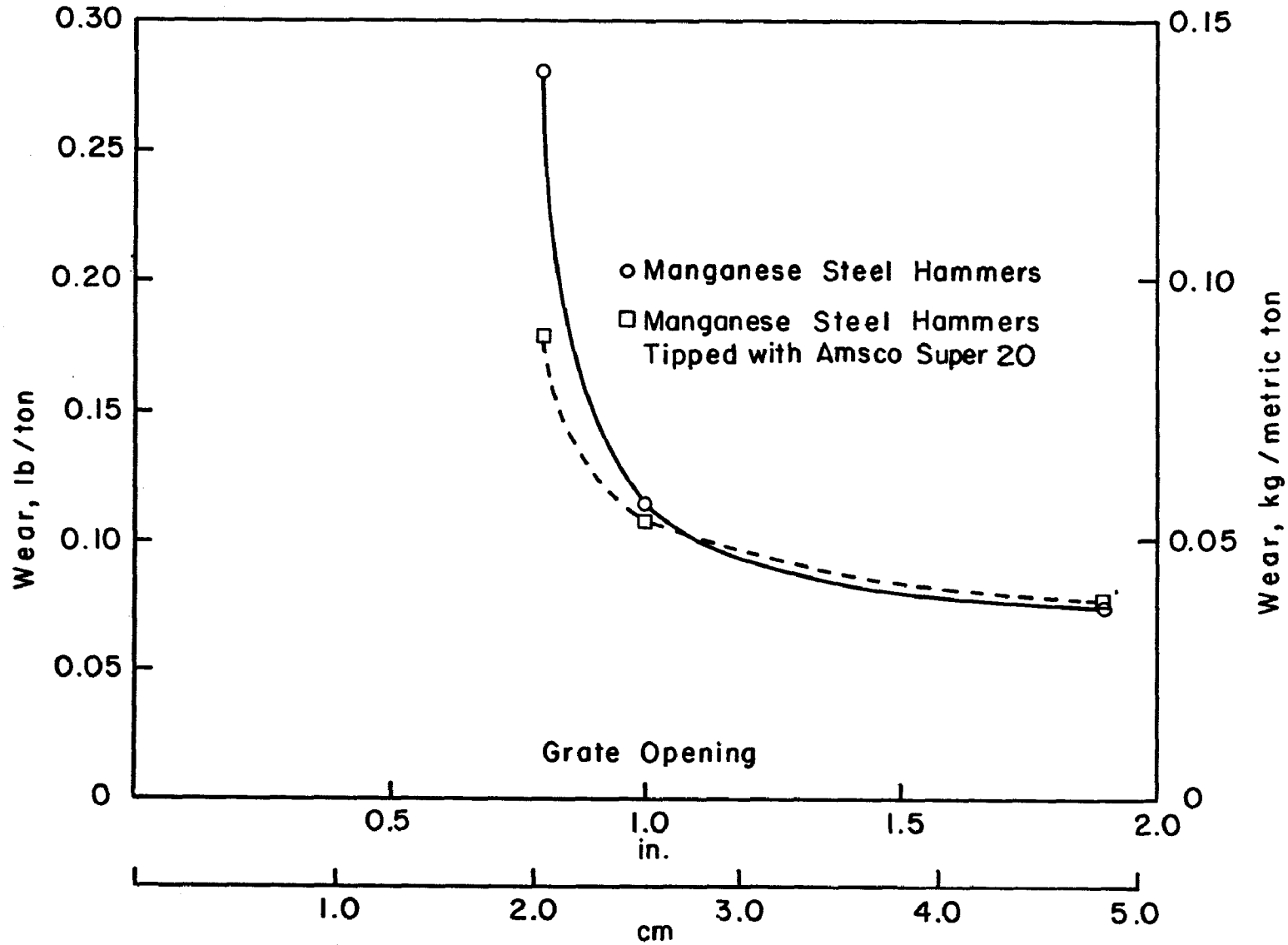

Figure 20. Hammer wear as a function of grate opening: Raw MSW, Gruendler hammermill (characteristic feed size, 15 cm or 6 in., nominal feed size, 33 cm or 13 in.).

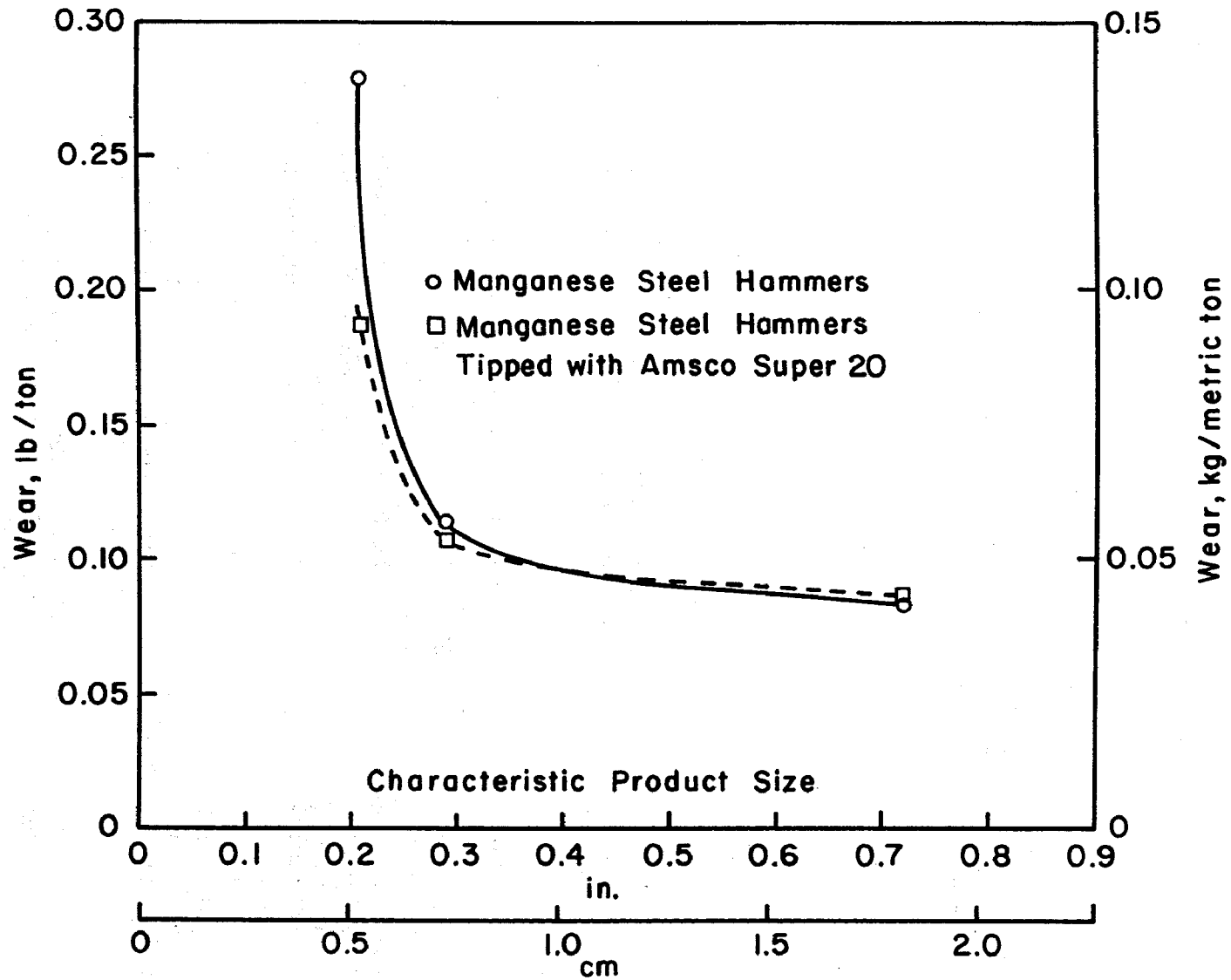

Figure 21. Hammer wear as a function of average characteristic product size: Raw MSW, Gruendler hammermill (characteristic feed size, 15 cm or 6 in.; nominal feed size, 33 cm or 13 in.).

0.53 cm (0.72, 0.29, and 0.21 in.), respectively. Figure 21 shows the wear rates from Table 16 plotted versus the characteristic product size. The steepness of this curve for product sizes smaller than 0.74 cm (0.29 in.) shows the penalty that was paid to produce the finer particle sizes.

These same wear data can also be correlated with the average nominal particle size (Figure 22). These curves are similar to those of Figure 21 and show a rapid increase in wear when nominal sizes are smaller than 1.5 cm (0.6 in.).

Figure 23 shows the relationship between hammer wear and alloy hardness for several grate openings after weld deposition. The fact that hardness can be used as a parameter to characterize hardfacing alloys is noteworthy, since hardness is a quantity that can be easily measured. Despite differences in manufacturer and composition, alloys that exhibited similar hardness values also underwent similar degrees of wear in our tests.

The functional relationship of wear and hardness shows that for certain hardness ranges, a minimum of wear occurs. For instance, in experiments conducted with a grate opening of 4.8 cm (1.9 in.), a minimum of wear occurred in the range $36 \leq R_C \leq 44$. Similarly, in the experiments conducted at a grate spacing of 2.5 cm (1.0 in.), a minimum occurred in the range $40 \leq R_C \leq 46$.

For the harder alloys, Coated Tube Stoodite ($R_C = 55$) and Amsco Super 20 ($R_C = 56$), chipping of the weld deposits represented the primary mode of material wear. For the tests at grate spacings of 4.8 and 2.5 cm (1.9 and 1.0 in.), these harder materials wore no better than the softer bare manganese hammers (Figure 23).

The results of the experiments conducted with a grate spacing of 1.8 cm (0.7 in.) were slightly different from those obtained at the larger grate openings. At grate spacings of 1.8 cm (0.7 in.), wear decreased as the hardness increased to a value of about 46 R_C (Figure 23). Although the hammers tipped with Coated Tube Stoodite (55 R_C) showed considerably less wear than either Stoody 31 (46 R_C) or Amsco Super 20 (56 R_C), this result should be viewed with skepticism. The results for Coated Tube Stoodite should not be viewed as representative of improved wear resistance, but as indicative of the haphazard nature of impact loadings on the hammer tips during shredding of MSW. This point of view is supported by the identical wear exhibited by Coated Tube Stoodite and Amsco Super 20 in experiments carried out at grate openings of 2.5 cm (1.0 in.) (Figure 23). The fact that there was a noticeable lack of hard, difficult material to reduce in the experiments conducted at 1.8-cm (0.7-in.) grate openings lends further support to this viewpoint.

Visual inspection of the weld deposits after shredding showed that chipping was the predominant mode of material loss for the harder alloys, namely Amsco Super 20 and Coated Tube Stoodite (Figures 24 and 25). The softer hardfacing alloys presented a smooth, worn appearance as a result of abrasion and did not show signs of chipping. Consequently, chipping was considered to be the limiting factor regarding the wear characteristics of the harder alloys. Accelerated material loss as a result of chipping occurs when the R_C is greater than 50 (Figure 23).

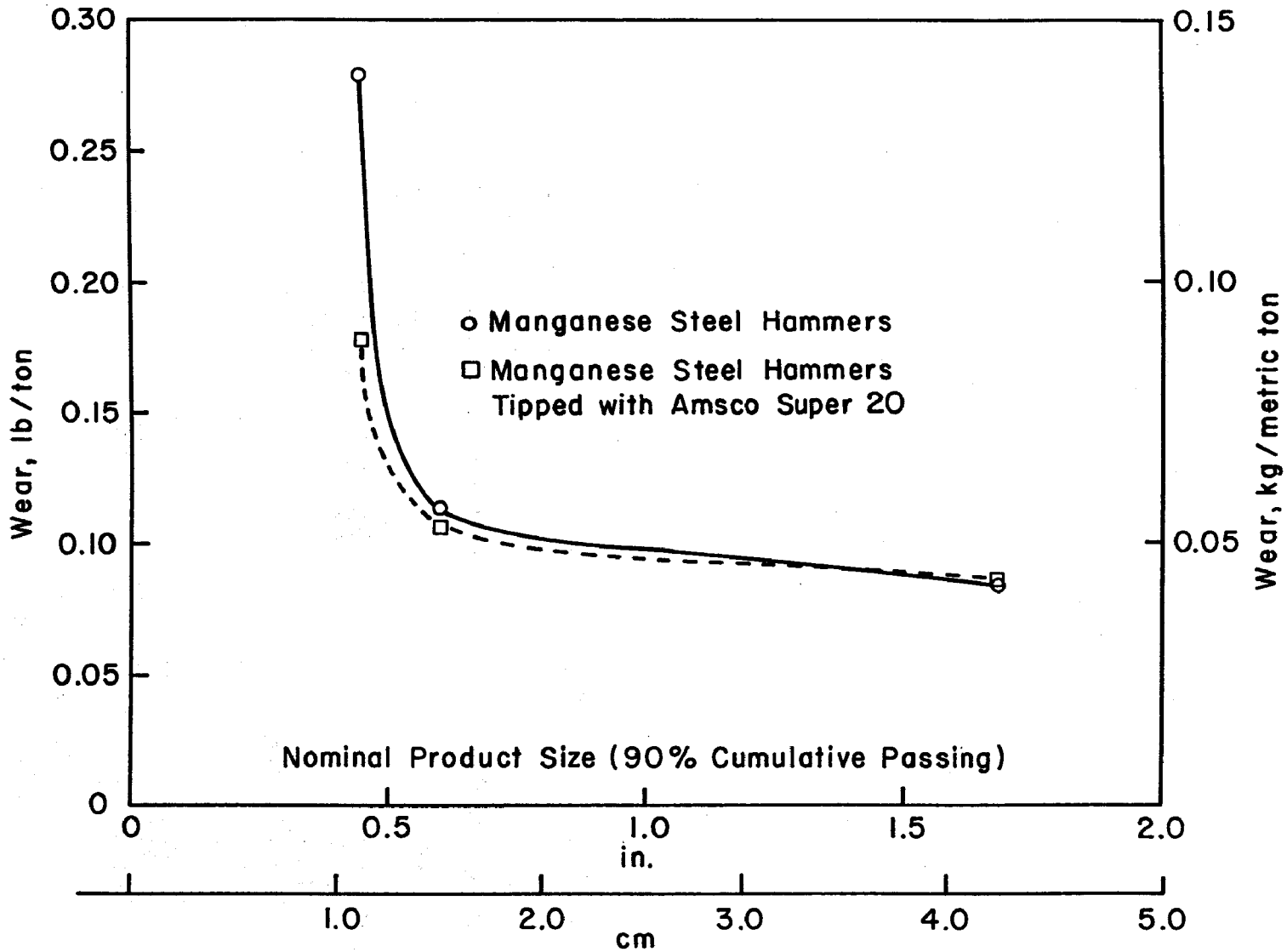

Figure 22. Hammer wear as a function of average nominal product size: Raw MSW, Gruendler hammermill (characteristic feed size, 15 cm or 6 in., nominal feed size, 33 cm or 13 in.).

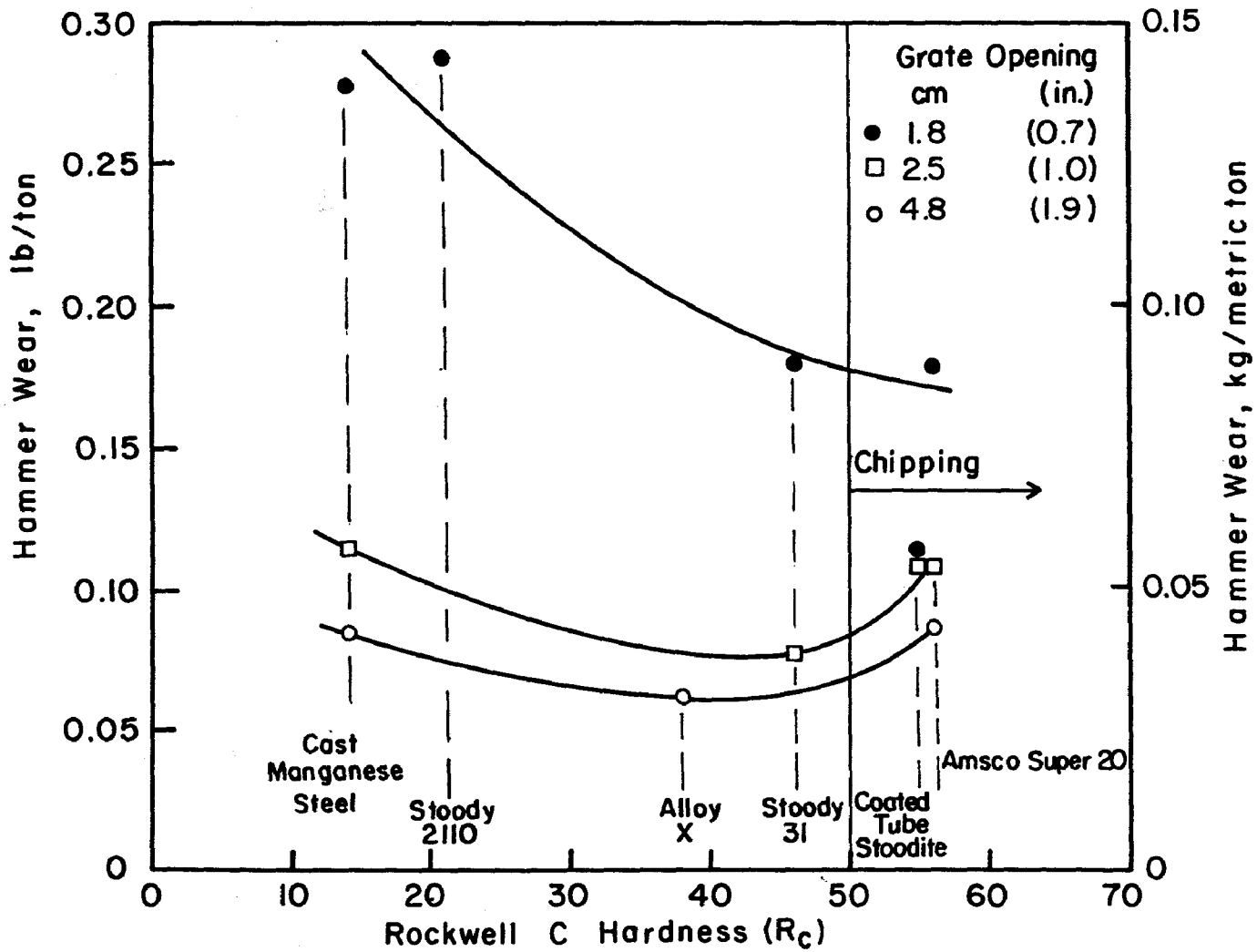

Figure 23. Hammer wear as a function of hardness for several different grate openings: Raw MSW, Gruendler hammermill (characteristic feed size, 15 cm or 6 in., nominal feed size, 33 cm or 13 in.).

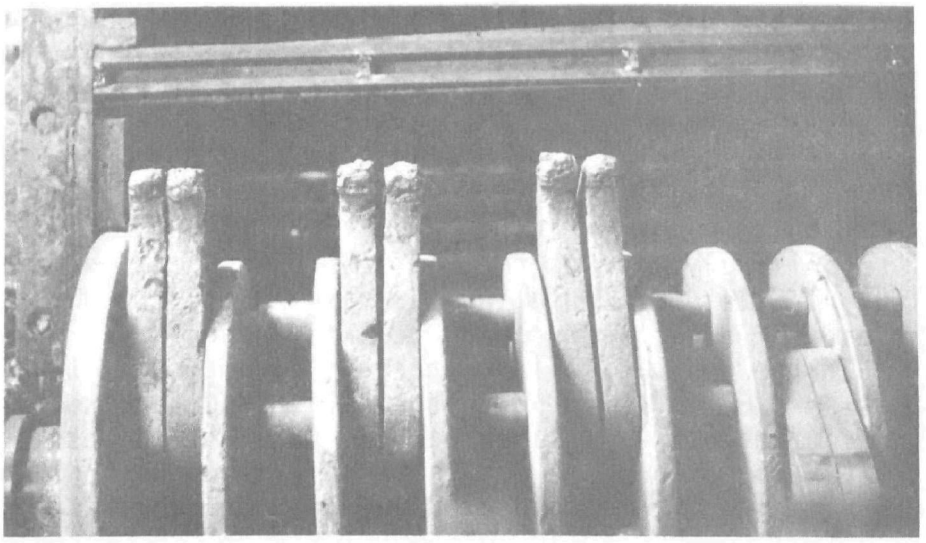

Figure 24. Evidence of chipping on hammers tipped with hardfacing alloys exceeding R_C 50 (before removal for weighing).

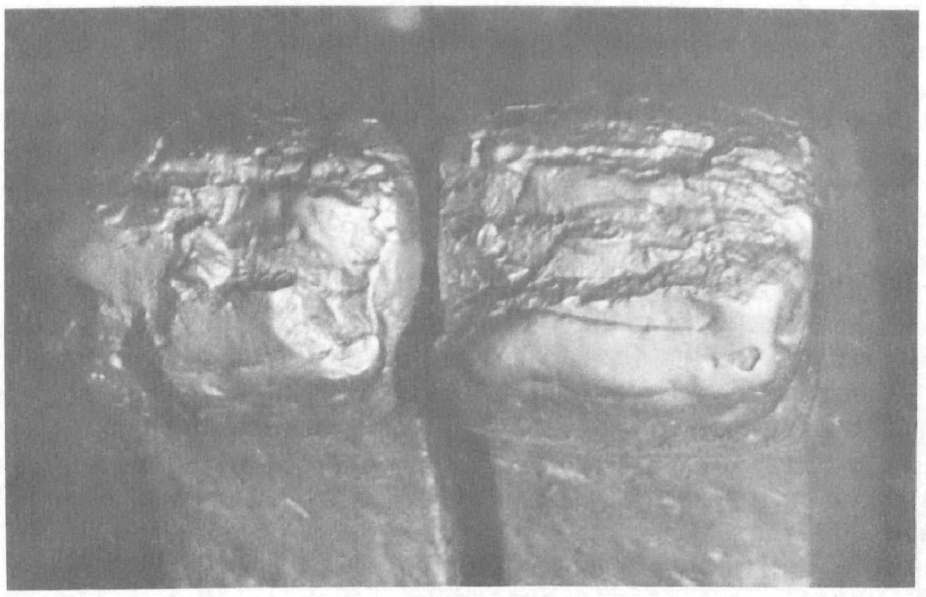

Figure 25. Closeup of hammers (showing chipping of hardfacing weld deposits on hammer tips).

Screened Light Fraction

The wear experiments with SLF for various hardfacing materials show the general trend of increased wear with smaller grate openings (Table 17). As seen from Figure 26, these wear rates increase from an average of approximately 0.003 to 0.007 kg/metric ton (0.005 to 0.014 lb/ton) as the diameters of the grate openings were decreased from 2.54 to 0.64 cm (1.0 to 0.25 in.) (Figure 26).

Rather surprisingly, curves for the best fit of the experimental data show relatively little difference in wear rates among the different hardfacing materials for experiments conducted at various grate opening sizes (Figure 26). If the unusually high wear rate for Haystellite Tungfine at grate openings of 0.64 cm (0.25 in.) is considered unrepresentative of that material, an argument could possibly be made that the softest alloy (Stoody 31) exhibited the highest degree of wear. This argument can be further supported by examining the functional dependence of wear rates on alloy hardness (Figure 27). Here again, discounting the high wear rate of Haystellite Tungfine at a grate opening diameter of 0.64 cm (0.25 in.), a slightly greater degree of wear could be argued for the softest alloy, Stoody 31. Practically, however, given the limitations and uncontrollable variables in the size reduction of SLF, all hardfacing materials tested here were considered to have similar wear characteristics.

The relationship between hammer wear and characteristic product size (Figure 28) is similar to that depicted for hammer wear and grate opening diameter (Figure 27). In general, wear rates increased from approximately 0.003 to 0.007 kg/metric ton (0.005 to 0.014 lb/ton as the characteristic product size decreased from 1.52 to 0.43 cm (0.60 to 0.17 in.).

Visual inspection of the hammers after removal from the hammermill showed the wear to be abrasive in nature, as evidenced by a shiny, smooth appearance of the weld deposits. No signs of chipping were found.

CONCLUSIONS

Several noteworthy findings resulted from the hammer wear research on the shredding of raw MSW. First, hammer wear under optimum conditions of hardfacing selection can be expected to be roughly two to three times as great for grate openings of 1.8 cm (0.7 in.) than for grate openings of 4.8 cm (1.9 in.) in the size reduction of solid waste by hammermill shredding. This fact should be weighed when considering the use of 2.5-cm (1.0 in.) or smaller grate openings for shredding raw MSW.

Second, using a scientific procedure (such as that followed here), an optimum hardfacing alloy can be found that will result in a minimum of wear for specific operating conditions. The tests reported here indicate that hardfacing alloys with as-deposited hardness in the range $36 \leq R_c \leq 46$ should lose a minimum of material during the shredding of MSW (at least in the range of grate spacings tested).

Third, alloys that exhibit an as-deposited hardness in excess of 50 R_c may show high degrees of wear because of chipping of the weld deposits.

TABLE 17. WEAR DATA FOR VARIOUS HARDFACING MATERIALS USED FOR SHREDDING SLF

Material	Hardness*	Wear rate, kg/metric ton (lb/ton)							
		2.54-cm (1.0-in.) grate		1.91-cm (0.75-in.) grate		1.27-cm (0.50-in.) grate		0.64-cm (0.25-in.) grate	
Stoody 31	41.9	0.0039	(0.0078)	0.0030	(0.0061)	0.0066	(0.0132)	0.0060	(0.0120)
Coated Tube Stoodite	49.5	0.0022	(0.0043)	0.0029	(0.0058)	0.0055	(0.0110)	0.0041	(0.0081)
Amsco Super 20	56.6	0.0025	(0.0049)	0.0033	(0.0065)	0.0051	(0.0101)	0.0058	(0.0115)
Haystellite Tungfine	63.0	0.0027	(0.0054)	0.0023	(0.0046)	0.0044	(0.0088)	0.0085	(0.0170)

*H rdness values are initial values as deposited without work-hardening.

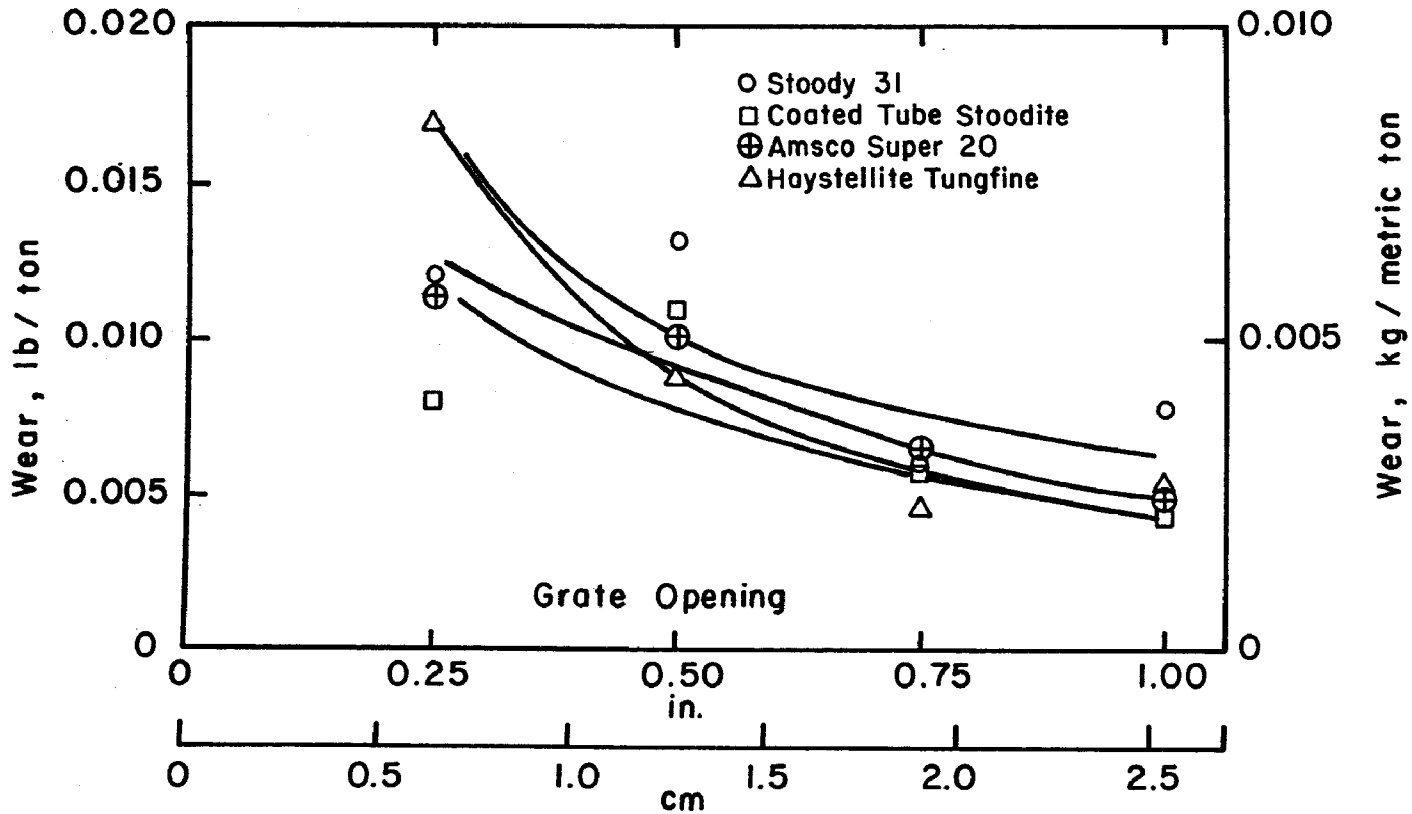

Figure 26. Hammer wear as a function of grate opening: SLF, W-W hammermill (characteristic feed size, 1.73 cm or 0.68 in.; nominal feed size, 2.72 cm or 1.07 in.).

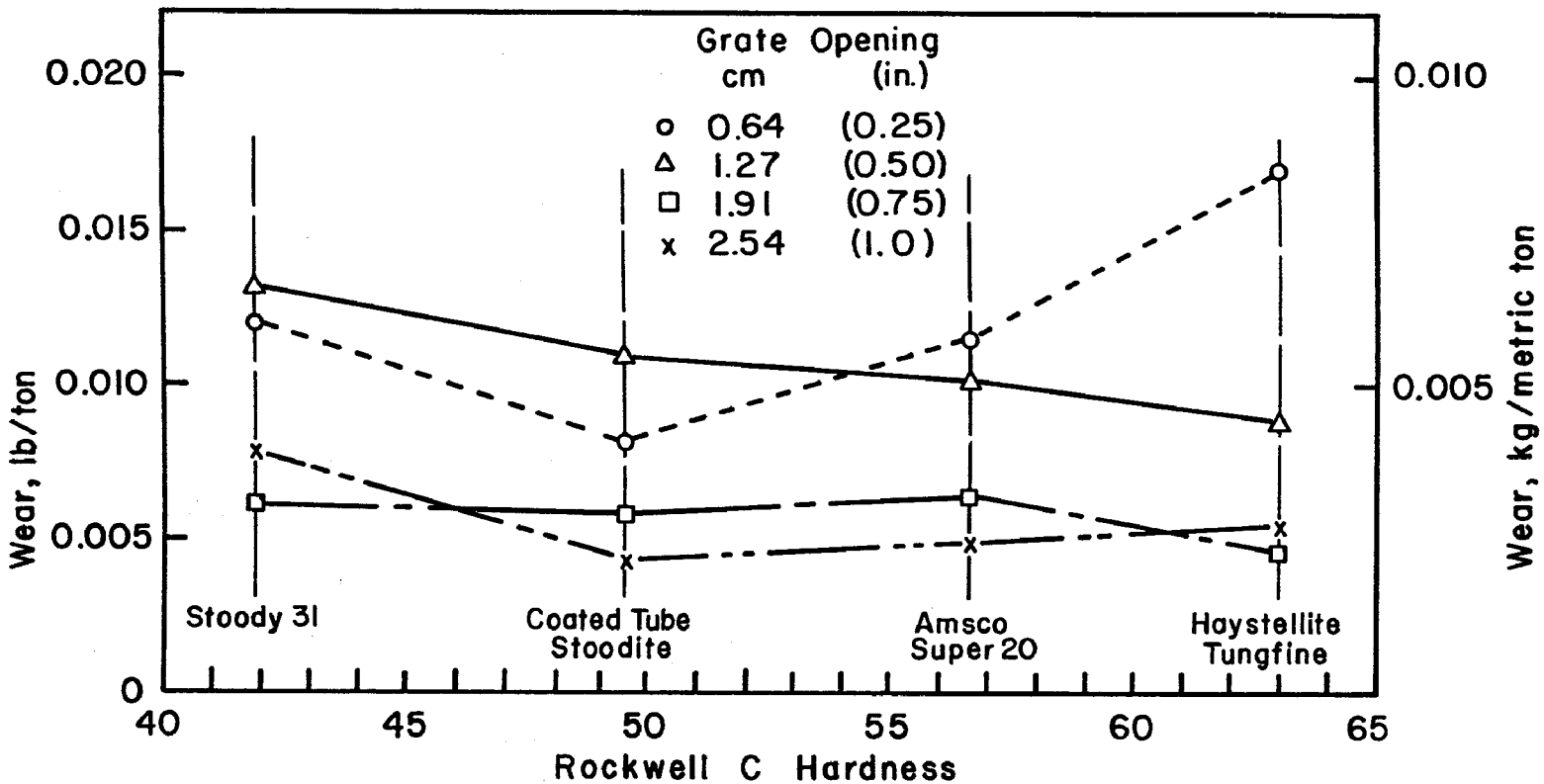

Figure 27. Hammer wear as a function of hardness for several different grate openings: SLF, W-W hammermill (characteristic feed size, 1.73 cm or 0.68 in.; nominal feed size, 2.72 cm or 1.07 in.).

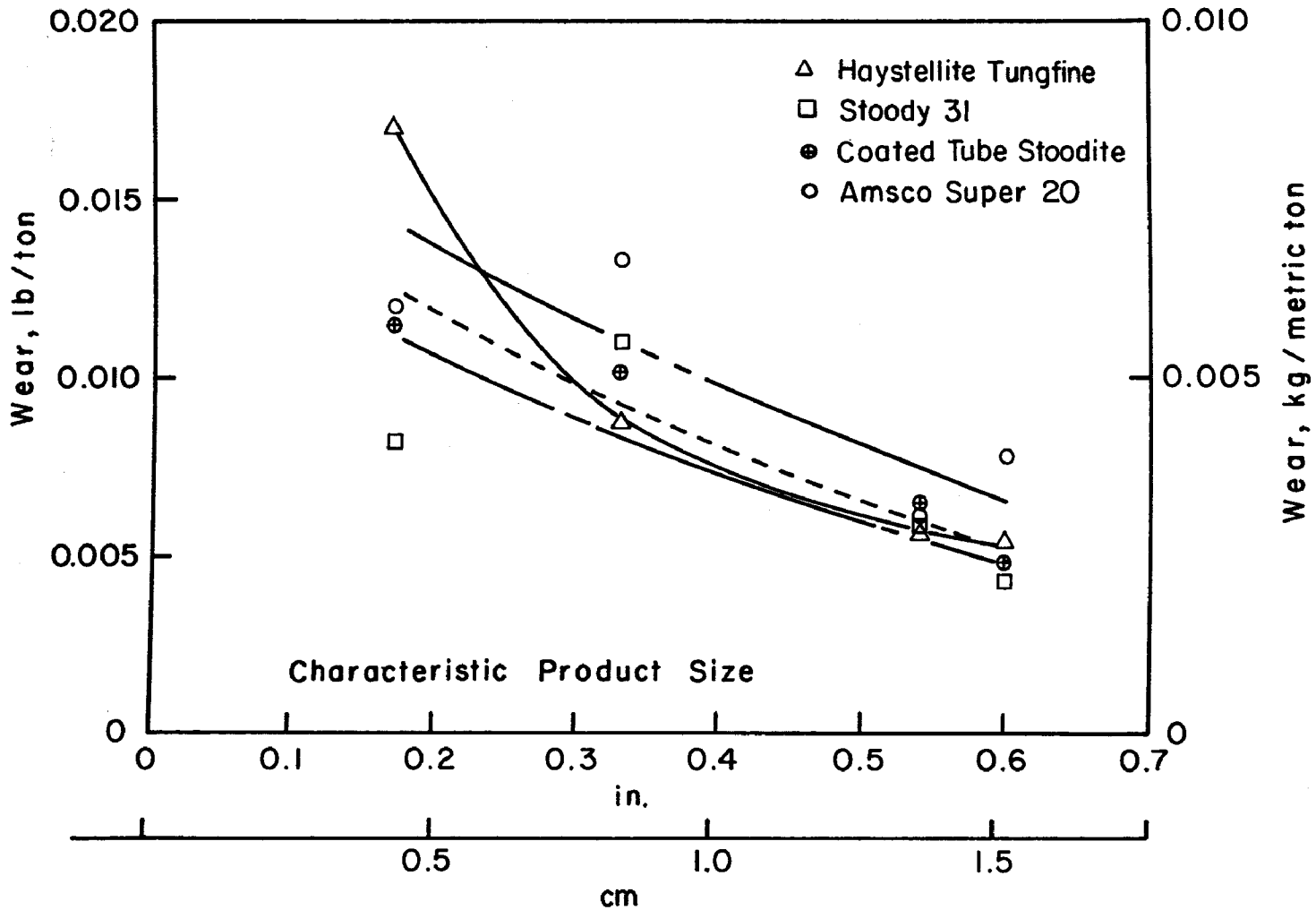

Figure 28. Hammer wear as a function of average characteristic product size: SLF, W-W hammermill (characteristic feed size, 1.73 cm or 0.68 in.; nominal feed size, 2.72 cm or 1.07 in.).

The degree of chipping will depend on the nature of the MSW being shredded. MSW that contains large quantities of hard objects such as white goods, steel bar stock, hardened gears, etc. will cause more severe chipping than will MSW that contains little of such material. In the latter case, alloys in the range of 48 to 52 R_C could provide the optimum hardfacing material.

Screened Light Fraction

This research on hammer wear as a consequence of the size reduction of the SLF has uncovered several important findings. First, hammer wear increased approximately 250 percent as the grate openings were decreased from 2.54 to 0.64 cm (1.0 to 0.25 in.). These results are for SLF with a characteristic feed size of 1.73 cm (0.68 in.) and a nominal size of 2.72 cm (1.07 in.).

Second, hammer wear was found to be independent of the type of hardfacing applied. This is an interesting finding, especially since a relatively wide range of alloy hardness values ($41.9 \leq R \leq 63.0$) was tested. Most hardfacing manufacturers contend that the harder alloys should wear better under abrasive conditions. The results of our tests did not uphold this contention.

Last, the shiny, smooth appearance of the weld deposits after shredding the SLF indicated that this material was abrasive in nature. None of the chipping behavior that characterized the harder alloys ($R_C \geq 50$) during the size reducion of raw MSW was evident during the size reduction of the SLF.

SECTION 5

INTERRELATION OF THE COMMINUTION PARAMETERS

Variables such as flow rate, moisture content, shredder holdup, residence time for material within the mill, degree of size reduction, etc. have been identified as controlling the size reduction process of refuse. For example, product particle size distribution is a function of the feed particle size and the mean residence time, and the power requirements of the shredder are shown to be a function of the mill holdup and the moisture content of the refuse. Also, if the grate opening size and characteristic feed size are specified, the degree of size reduction can be computed. This determination in turn enables the prediction of characteristic product size, specific energy, and hammer wear. Consideration will be given to the quantitative relationship between the governing variables and their use for predictive purposes.

REPRESENTATIVE PARTICLE SIZE

The product resulting from a size reduction or shredding operation typically exhibits a range of sizes that may span three to four orders of magnitude. It has been shown that this size distribution Y(x) can be represented by the Rosin-Rammler equation, as follows:

$$Y(x) = 1 - \exp[-(x/X_0)^n] \tag{1}$$

where n is a numerical constant, x is the screen size, and X_0 is a characteristic particle size. When x is substituted for X_0 in the above equation, namely

$$Y(x) = (1 - 1/e) = 0.632 \tag{2}$$

it follows that the percent passing is 63.2 percent. Thus the characteristic particle size, X_0, is the size that corresponds to 63.2 percent passing. The exponent n may be found from the slope of the line

$$\ln[\ln(1-Y(x))] = n\ (\ln x - \ln X_0) \tag{3}$$

and is a measure of the uniformity of the size distribution. In other words, n is a measure of the width of a size distribution if plotted as in Figure 29, which is a typical size distribution for raw MSW presented in terms of the mass fraction (m_i) within a given class (i) instead of the more commonly used percent passing (Y(x)).

To develop useful predictive relationships, it becomes necessary to correlate the comminution variables in terms of some particle size, since correlations in terms of the entire distribution are usually not tractable.

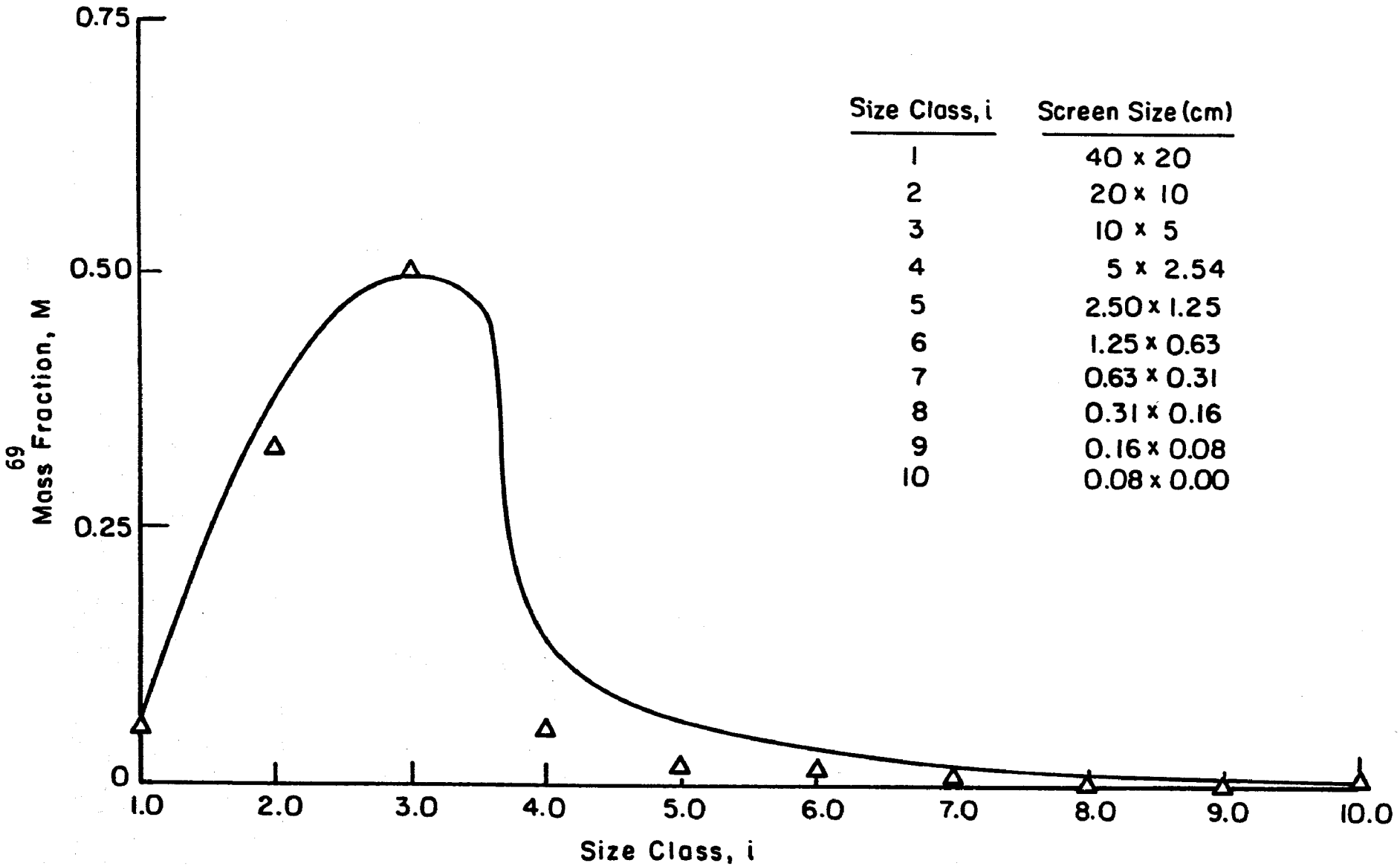

Figure 29. Mass fraction representation of the size distribution for raw MSW.

The two representative particle sizes that are used are: (a) the previously discussed characteristic size corresponding to 63.2 percent passing, and (b) the so-called nominal size, which corresponds to 90 percent passing. The nominal size is the most prevalent parameter used in the industry, particularly in refuse-derived fuel situations. Nonetheless, it should be noted that the characteristic size has proven to be the most useful variable for denoting particle size. Attempts to use nominal size have resulted in significantly more data scatter when studying energy and size relationships. Perhaps one reason for the good correlation of characteristic size and energy consumption is that this size is more representative of the average size than is the nominal size. Furthermore, the characteristic size is derived from a fundamental consideration of the size distribution representing the entire size spectrum of the material. Consequently, the characteristic size is used here as the primary size for correlation purposes. The relationship between these two sizes for shredded raw MSW and for two forms of light fraction are given in Figures 30 and 31, respectively.

DEGREE OF SIZE REDUCTION

The degree of size reduction (Z_0) is introduced as a means of generalizing the size reduction data obtained over a wide range of operating and mill conditions. This term is defined as

$$Z_0 \equiv (F_0 - X_0)/F_0 \tag{4}$$

where F_0 and X_0 are the characteristic feed size and characteristic product size, respectively. Thus the degree of size reduction is a dimensionless quantity approaching unity as X_0 approaches zero, and approaching zero as X_0 approaches F_0. To complete the generalization, an additional non-dimensional parameter is required and can be formed by the ratio of the grate opening size (D_0) to the characteristic feed size (F_0) -- that is, D_0/F_0. The parametric nature of the comminution process with grate opening size is shown in Figure 32 when the degree of size reduction (Z_0) is represented in terms of the D_0/F_0 ratio. Essentially, for a particular value of the ratio D_0/F_0, the value of Z_0 increases as the size of the grate openings increase. In other words, a smaller characteristic particle size is produced as the grate openings increase in size. As shown in Figure 32, this trend holds for the ACLF forms as well as the raw MSW. A full explanation for this seemingly contradictory effect requires the introduction of other parameters affecting the size reduction process.

ENERGY

Another example of the parametric nature of grate opening size is demonstrated by the relationship between specific energy (E_0) and degree of size reduction (Z_0). For the three material forms studied, the E_0 increases as the D_0 decreases for a given value of Z_0 (Figure 33). In the case of raw MSW, E_0 values for the interval $0.88 \leq Z_0 \leq 1.00$ correspond to the average E_0 values for single-stage size reduction using the grate spacings specified. But E_0 values in the region $0.00 \leq Z_0 \leq 0.55$ correspond to the E_0 values experienced during multiple size reductions using the grate spacings indicated. Though each mill has a distinctive family of curves, for the ACLF the

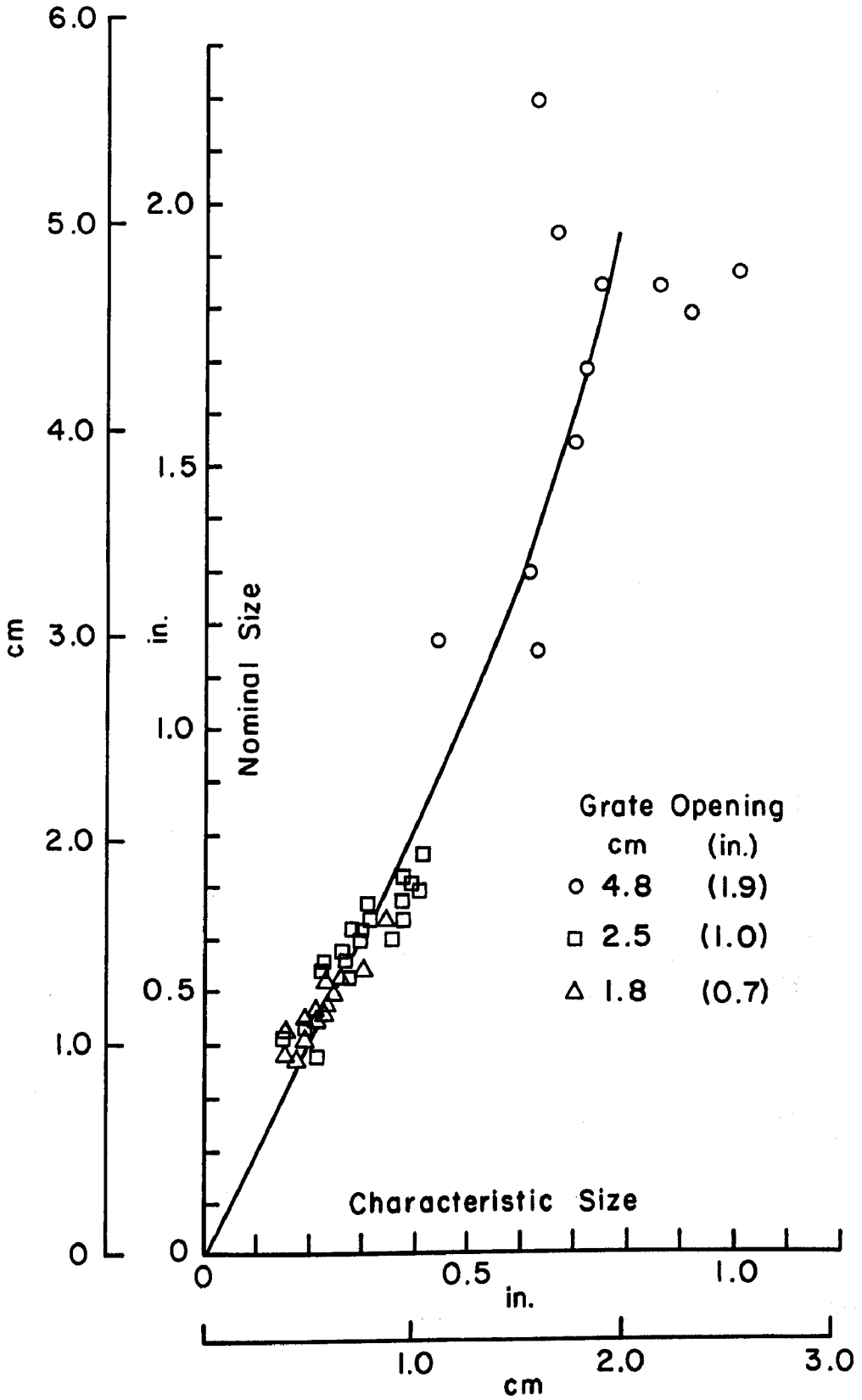

Figure 30. Nominal size as a function of characteristic size for shredded raw MSW, Gruendler hammermill.

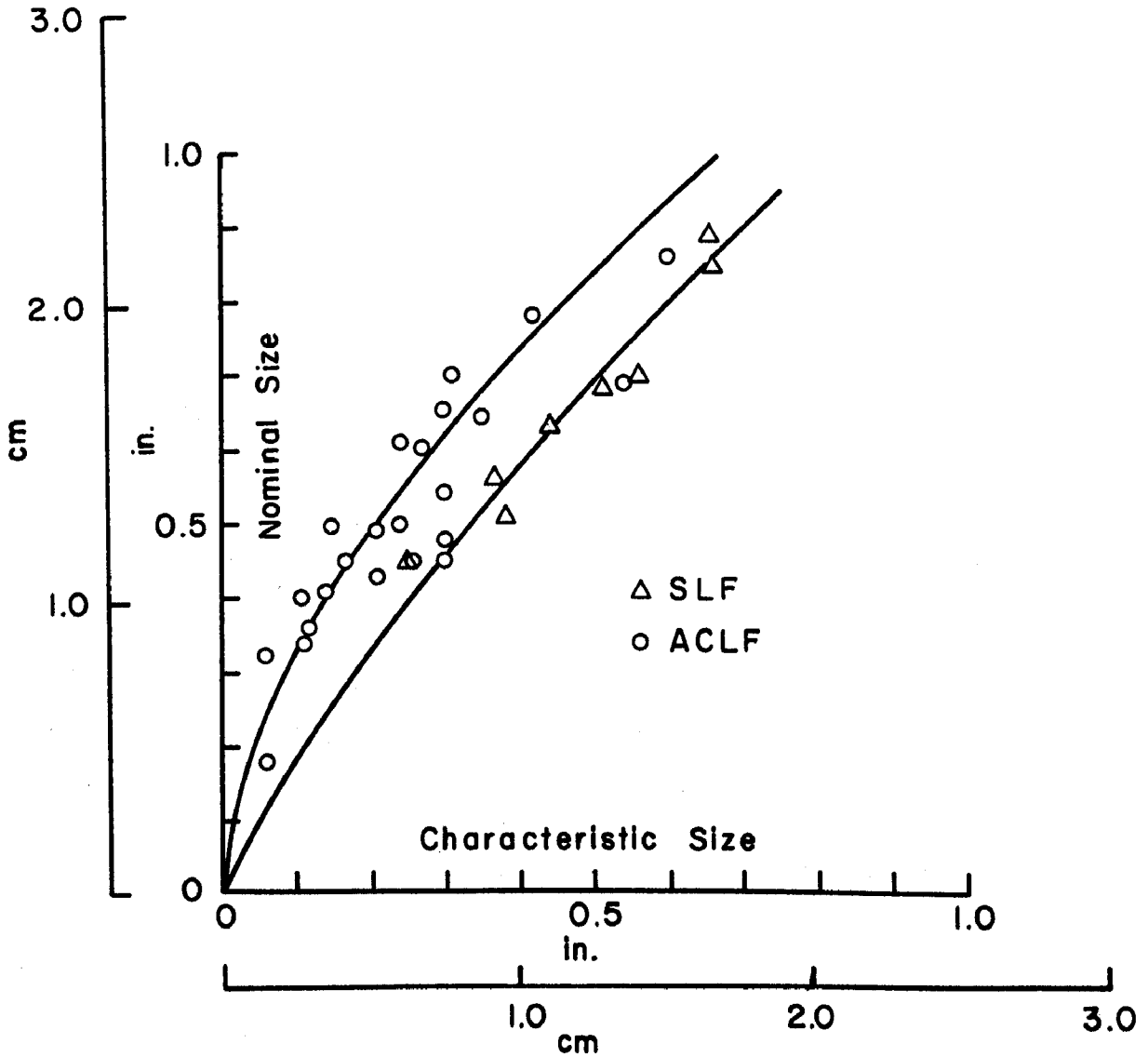

Figure 31. Nominal size as a function of characteristic size for shredded ACLF and SLF, W-W hammermill.

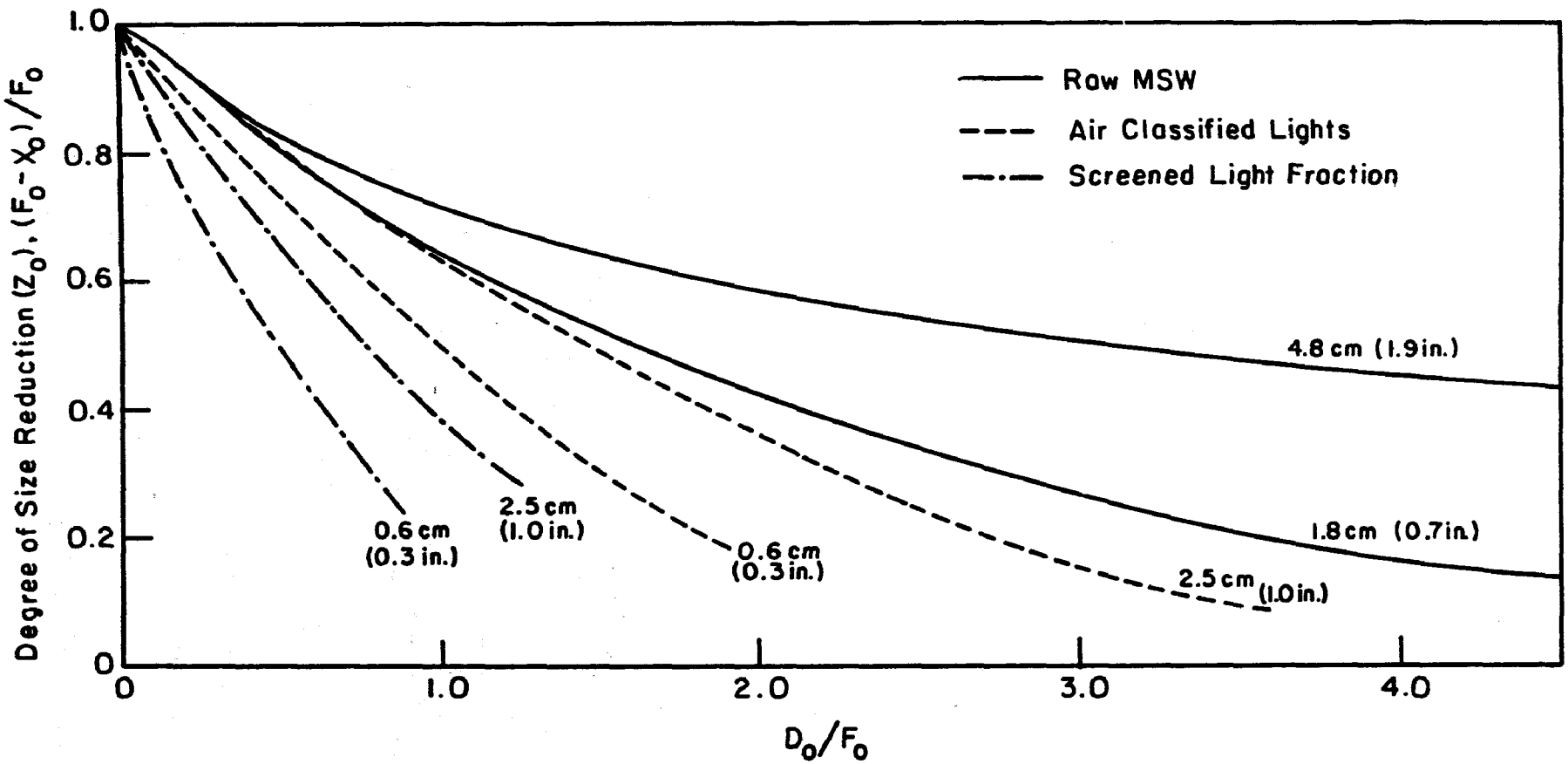

Figure 32. Degree of size reduction as a function of the ratio of grate spacing to characteristic feed size for raw MSW, ACLF, and SLF.

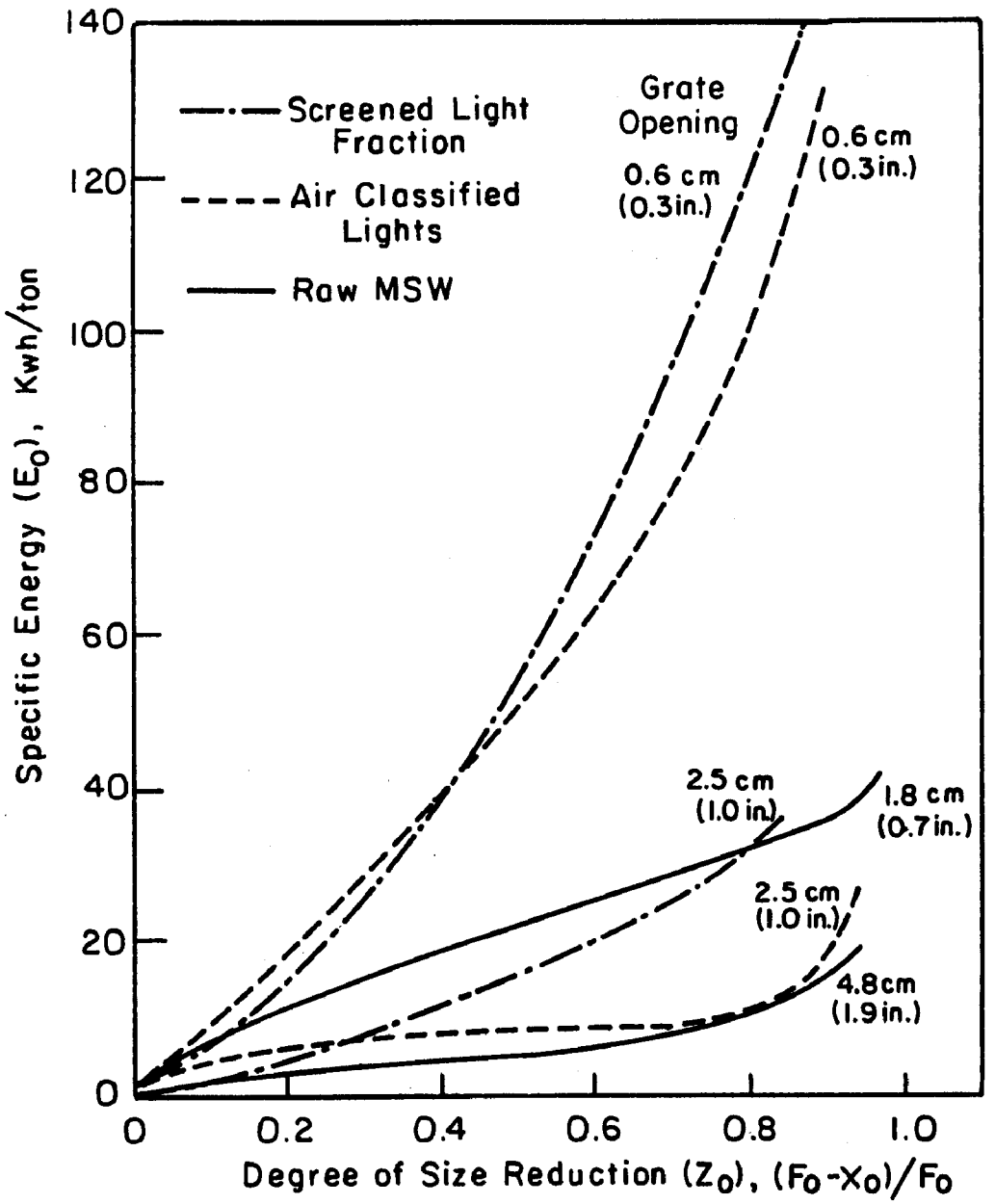

Figure 33. Specific energy as a function of degree of size reduction for raw MSW, ACLF, and SLF.

similarity of energy consumption data obtained from both the Gruendler and W-W mills implies a similarity in comminution mechanism for this material. In the case of SLF, the data indicate that the Gruendler mill requires more energy to attain a given degree of size reduction. For example, at 2.5-cm (1.0-in.) grate openings for both the Gruendler and W-W hammermills, the specific energy required to attain a degree of size reduction of 0.25 would be 72 and 24 MJ/metric ton (18 and 6 kWh/ton), respectively. The difference in the location of the curves for both mills when fitted with the same grate openings represents a departure from the data presented for the size reduction of ACLF, where similar grate openings resulted in approximately the same energy consumption for both hammermills.

To gain a further appreciation of the interrelated nature of the energy and size variables (E_o, Z_o, and D_o/F_o), several diagrams (Figures 34, 35, and 36) were developed for the three fractions of solid waste studied. The motivation for combining these three variables stems from the fact that the ratio of grate opening to characteristic feed size specifies both the degree of size reduction (which characterizes the product size) and the energy consumption. Consequently, one figure provides both the energy required for size reduction and the resulting size of the product when the type of material, feed size, and grate opening size are specified. A comparison of these figures shows that for a given value of D_o/F_o, the steepness of both Z_o and E_o curves is generally the greatest for the SLF, followed by the ACLF and raw MSW. Consequently, from the standpoint of minimum energy consumption and maximum particle size reduction, raw MSW is the least difficult material to grind, followed closely by the ACLF, and more distantly by the SLF. The reason for the relatively high energy requirement and small degree of size reduction for SLF is probably that fiber makes up more than 75 percent of this fraction.

This situation may also be viewed in terms of the following two cases. In the first case, 2.5-cm (1.0-in.) grate openings and a D_o/F_o ratio of 0.2 result in a decrease in the degree of size reduction from 0.93 for raw MSW to 0.86 for SLF (Table 18). In addition, the specific energy increases from

Table 18. COMPARISON OF DEGREE OF SIZE REDUCTION AND SPECIFIC ENERGY FOR DIFFERENT SOLID WASTE FRACTIONS

D_o cm (in.)	D_o/F_o	Material	Z_o	E_o MJ/metric ton	E_o (kWh/ton)
2.5 (1.0)	0.2	Raw MSW	0.93	67	(17)
2.5 (1.0)	0.2	ACLF	0.92	79	(20)
2.5 (1.0)	0.2	SLF	0.86	154	(39)
2.5 (1.0)	0.8	Raw MSW	0.72	37	(9)
2.5 (1.0)	0.8	ACLF	0.71	40	(10)
2.5 (1.0)	0.8	SLF	0.48	59	(15)

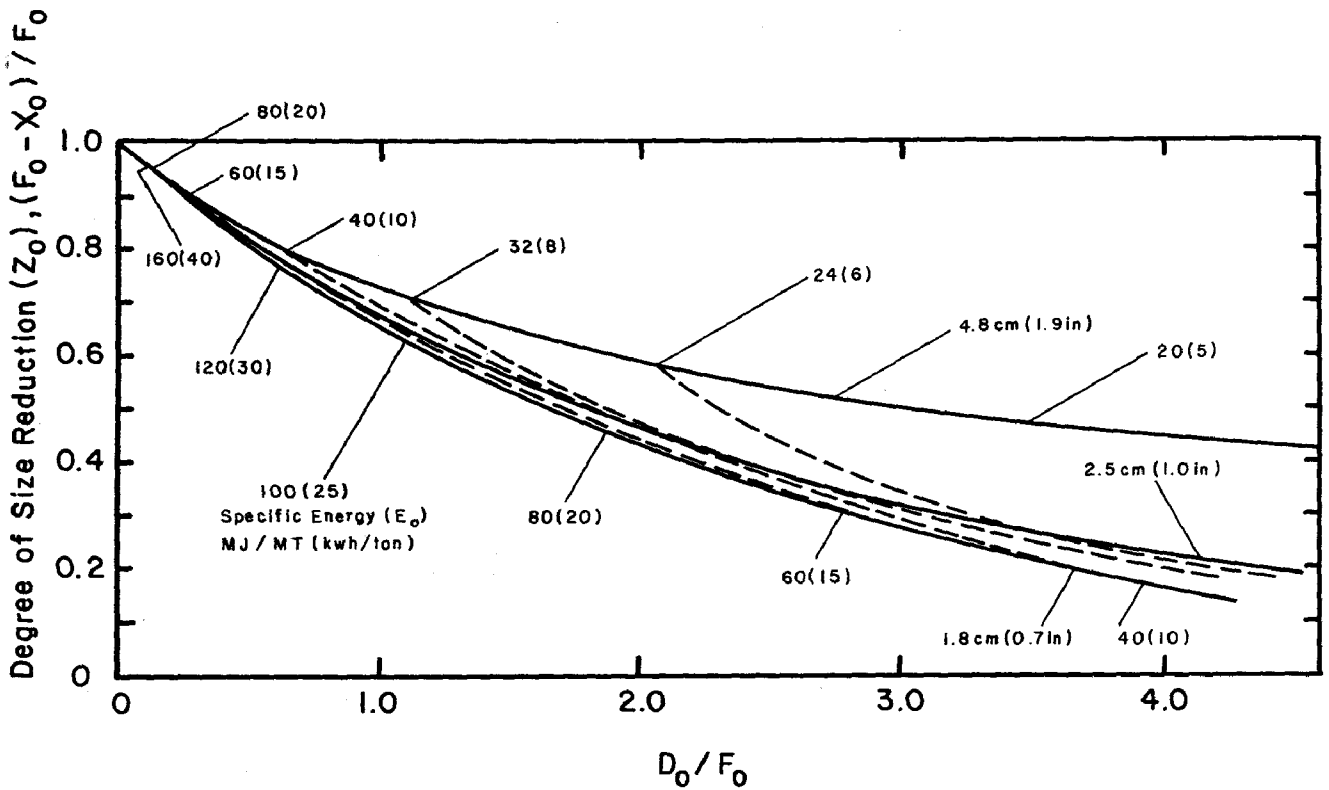

Figure 34. Degree of size reduction as a function of the ratio of grate opening to characteristic feed size for raw MSW.

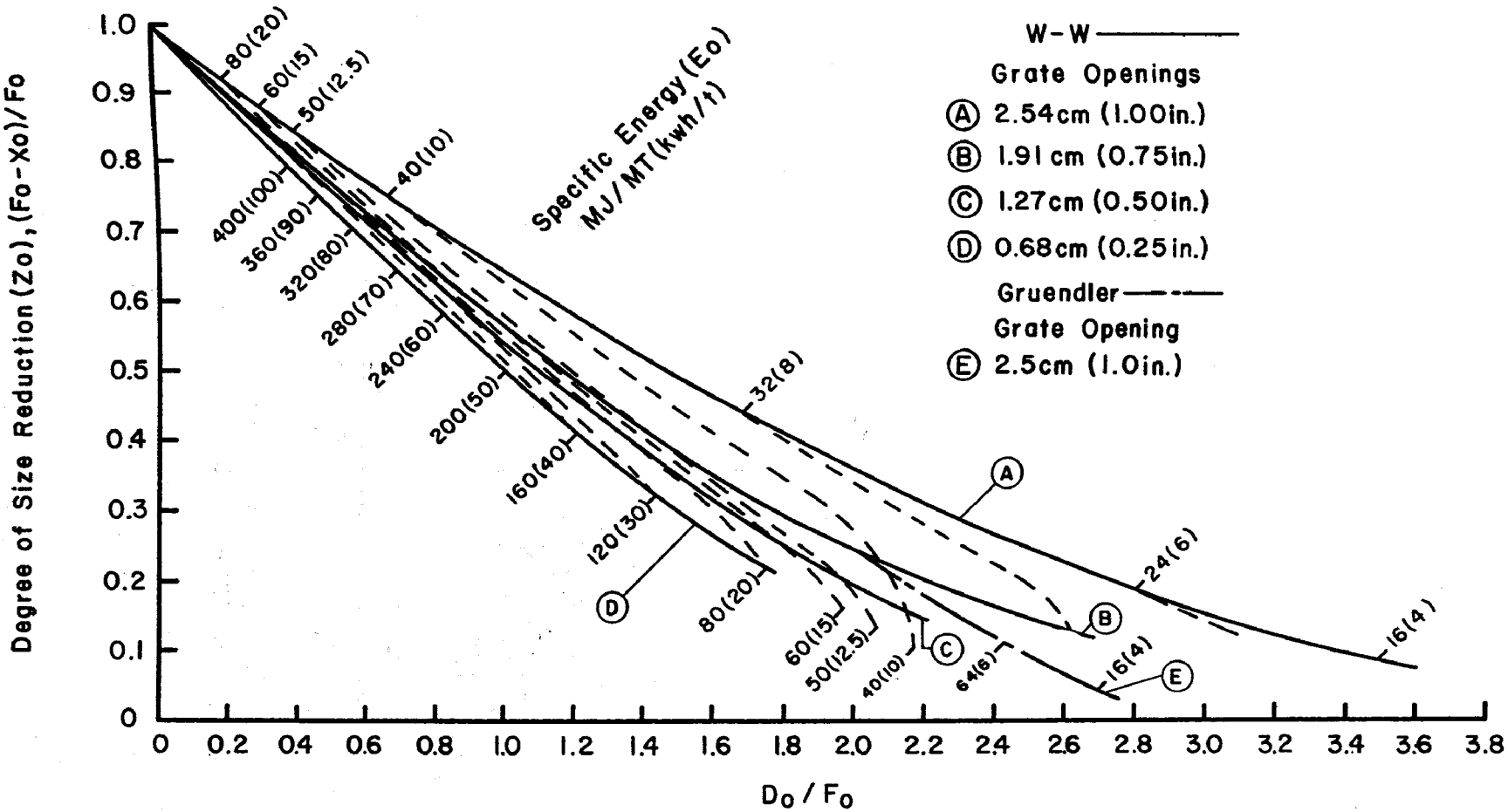

Figure 35. Degree of size reduction as a function of the ratio of grate opening to characteristic feed size for ACLF.

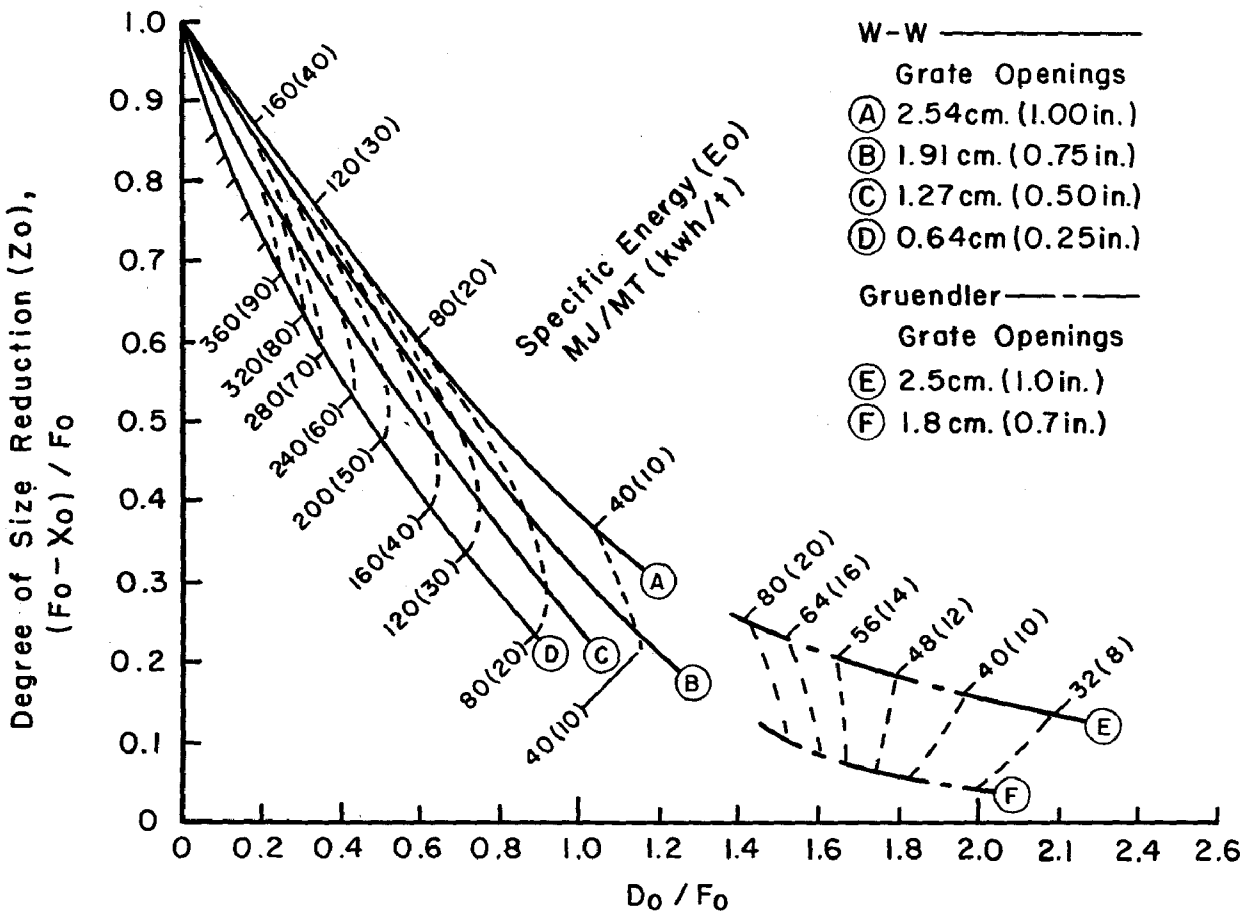

Figure 36. Degree of size reduction as a function of the ratio of grate opening to characteristic feed size for SLF.

67 MJ/metric ton (17 kWh/ton) for raw MSW to 154 MJ/metric ton (39 kWh/ton) for SLF. The second case assumes the same grate spacing, 2.5 cm (1.0 in.), and a D_0/F_0 ratio of 0.8. For these conditions, raw MSW and ACLF yield similar degrees of size reduction and energy requirements (namely, Z_0 values of 0.72 and 0.71 and E_0 values of 37 and 40 MJ/metric ton (9 and 10 kWh/ton), respectively (Table 18). However, the SLF yields considerably lower Z_0 values and considerably higher E_0 values than the other two materials.

RESIDENCE TIME

Although the ability of a refuse shredder to affect size reduction may be partly described by a study of the feed and product size distributions, such a study does not truly characterize the actual process of comminution. One important variable affecting the degree of size reduction is the amount of time a particle resides within the shredder. This residence time may be best expressed as a residence time distribution (i.e., a distribution of the probable time a particle will remain within the comminution device). Most commercial refuse shredders are some form of hammermill with an integral set of grates, the spacing of which may be varied to control the product particle size. It may reasonably be assumed that because of the action of the hammers, the material within the shredder is uniformly mixed and that there is no stratification of particles on the basis of particle size. If this assumption is valid, then the residence time distribution may in turn be assumed to be the same regardless of the size of the particle. The grates thus act as a classifier, passing those particles smaller than the grate spacing and returning the rest to the grinding zone where the same residence time distribution that is applied to the feed is again applied to the recycled material. This process is shown schematically in Figure 37. In this figure, Figure 37, $\underline{f}$ and $\underline{p}$ are the vectors describing the circuit feed and product size distributions, $\underline{r}$ is the recycled material size distribution, and $\underline{m}_f$ and $\underline{m}_p$ are the size distributions of the material entering and exiting the actual grinding zone. Figure 38 shows the form of the residence time distribution R(t), for the test shredder as determined from unit impulse tracer tests. The mean residence time may be determined from either the residence time distribution or the equation

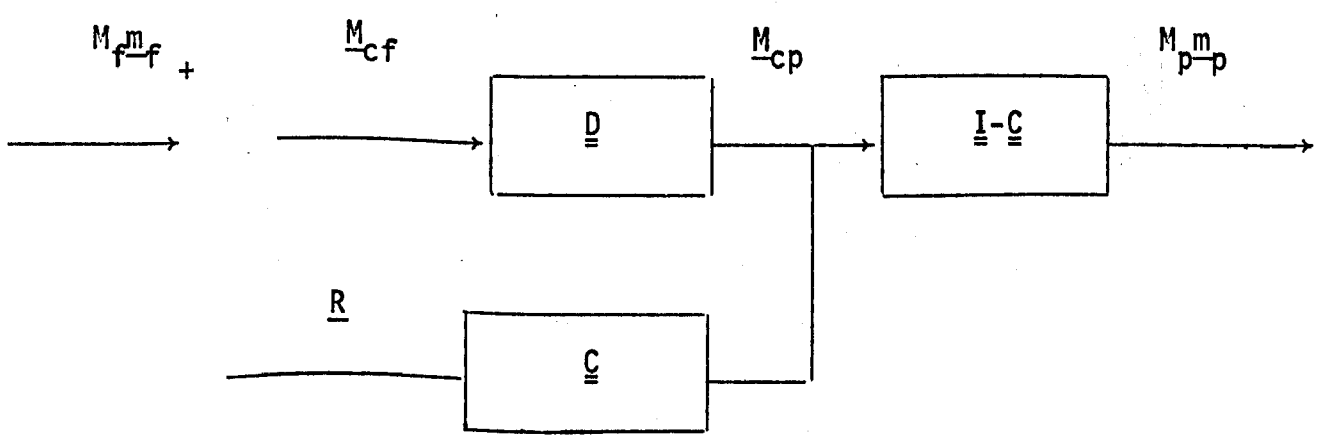

Figure 37. Schematic representation of milling process.

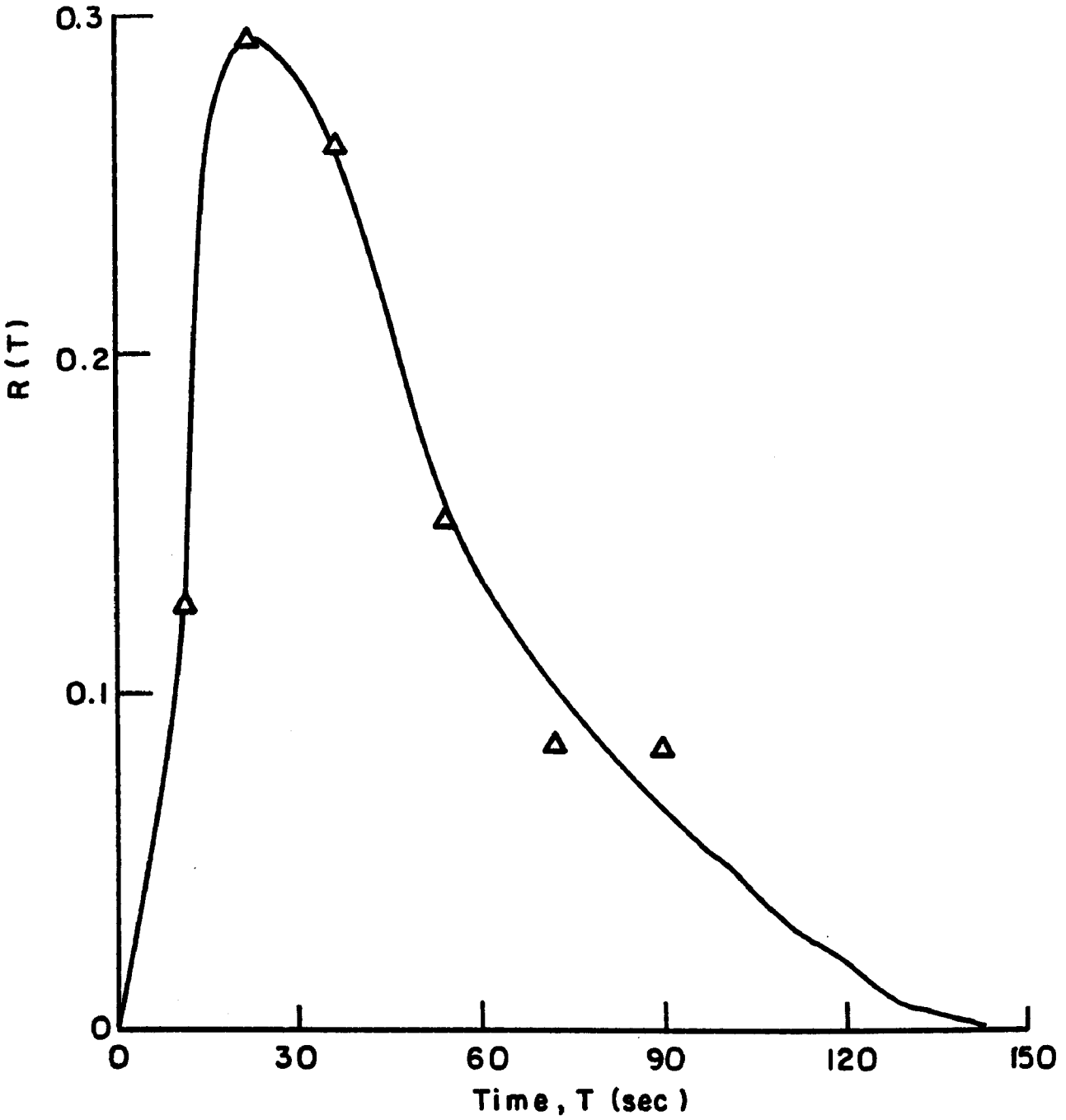

Figure 38. Residence time distribution for size reduction of raw MSW.

$$\tau = \frac{H}{Q} 3.6 \tag{5}$$

where: τ is the mean residence time (sec), H is the mill holdup (kg), which is the instantaneous mass of material within shredder; and Q is the flow rate (tons/hr). There is some evidence that the form of a normalized residence time distribution, $R(\theta)$, is invariant with flow rate where $R(t)$ and $R(\theta)$ are related by

$$R(t) = R(\theta)/\tau \tag{6}$$

where: is the mean residence time (sec) and $\theta = t/\tau$. Figure 39 shows the normalized residence time distribution for the test shredder.

MILL HOLDUP

Both the dynamics of hammermilling and the highly compressible nature of refuse lead to the belief that there may be some relationship between flow rate and holdup. To test for this relationship, the Gruendler hammermill was fitted with 1.3- and 2.5-cm grates, and holdup/flow rate data were collected for a wide range of operating conditions. The results of regression analysis on the data show that for the 1.3-cm grate spacing

$$Q_{1.3} = 0.039\ H^{0.95} \tag{7}$$

and for the 2.5-cm grates

$$Q_{2.5} = 0.086\ H^{0.94} \tag{8}$$

where: Q is the output flow rate (tons/hr) and H is the mill holdup (kg).

Flow rate is shown as a function of holdup because laboratory (as well as most commercial) conditions are such that it is the output rather than the input flow rate that is measured. Of course, under optimum steady state conditions, the converse of Equations 7 and 8 also hold, i.e.,

$$H = 30.4\ Q_{1.3}^{1.05} \tag{9}$$

$$H = 13.6\ Q_{2.5}^{1.06} \tag{10}$$

Figure 40 shows the curves representing Equations 7 and 8 (or 9 and 10).

Since flow rate is more readily measured than holdup, substitution of Equation 9 into Equation 5 and correcting for the different units of Q and H yields:

$$\tau = 109.4\ Q_{1.3}^{0.05} \tag{11}$$

and

$$\tau = 49.0\ Q_{2.5}^{0.05} \tag{12}$$

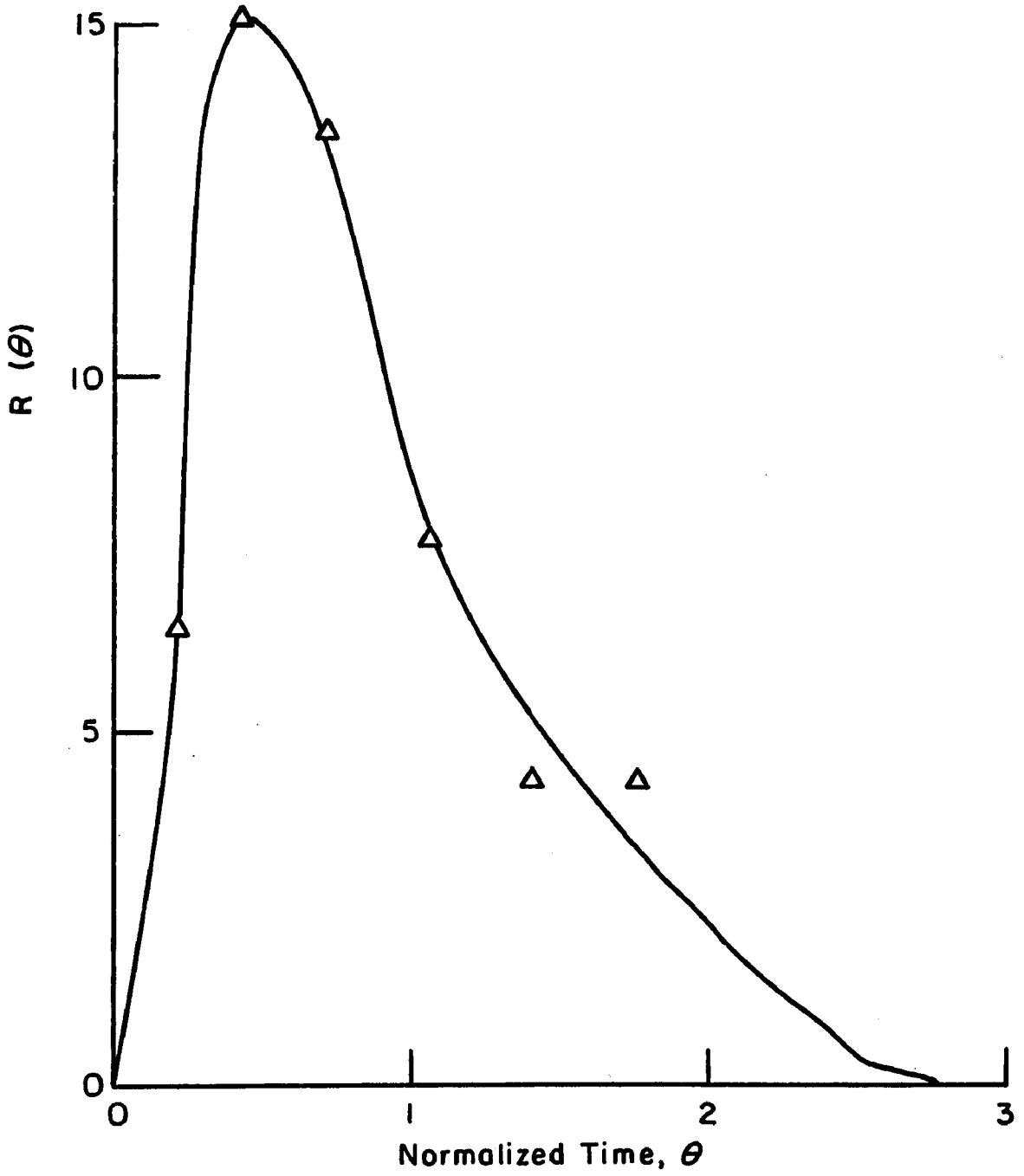

Figure 39. Normalized residence time distribution for size reduction of raw MSW.

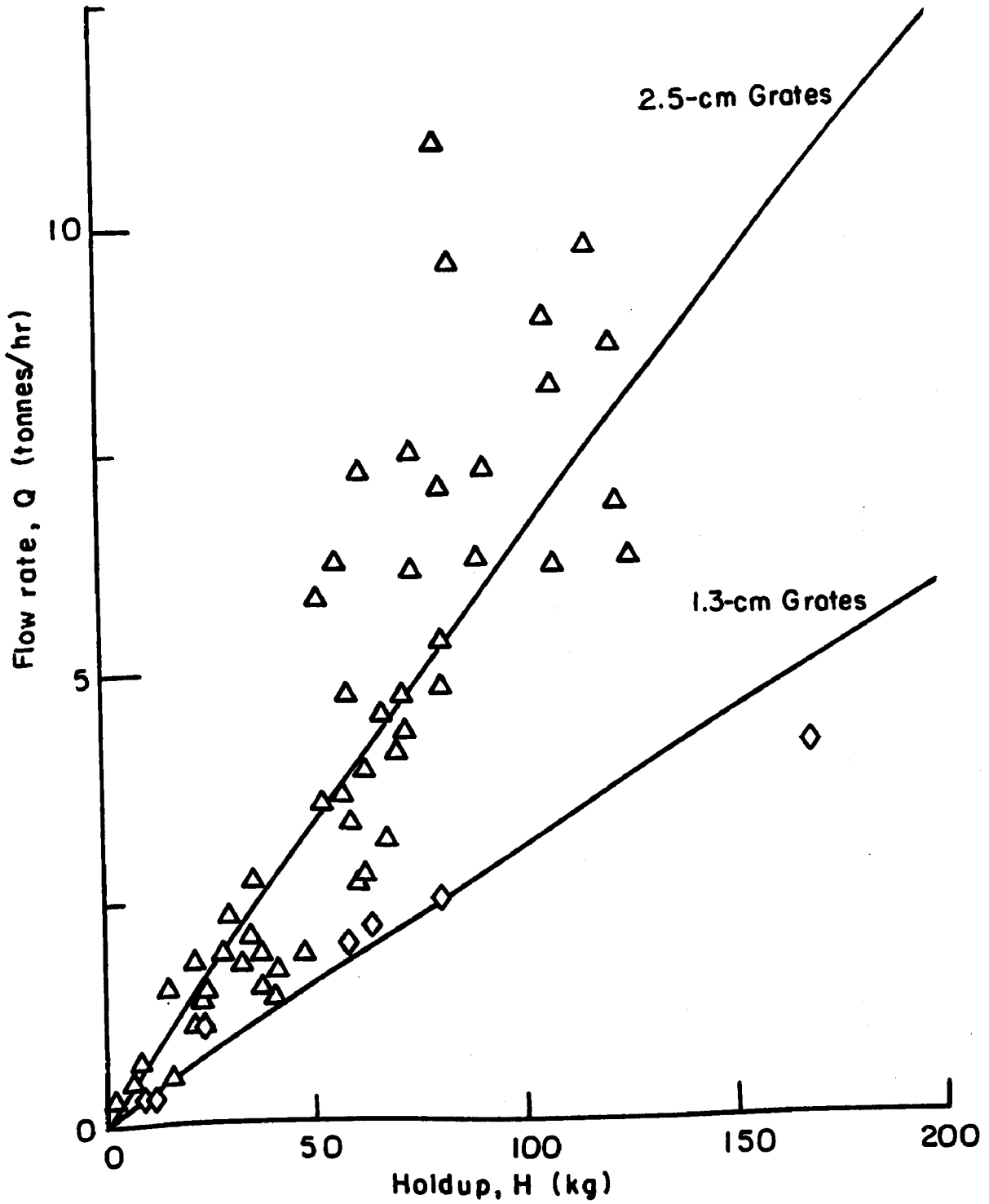

Figure 40. Flow rate as function of mill holdup for raw MSW.

Thus an increase in flow rate leads to increased holdup and a longer mean residence time.

The effect of the grates is twofold. Not only do the grates act as an internal classifier for the mill, but they also act as an impedance to flow of material through the shredder. The resistance to material flow is a function of the actual physical characteristics of the grates; i.e.,

$$Q = \frac{1}{Z(g_s, A, A_{total})} H^{0.95} \tag{13}$$

where: g_s is the grate spacing, A is the space between the grate bars, and A_{tot} = A + total cross sectional area of the grate bars. Examination of Equations 7 and 8 show that for constant holdup, the output flow rate roughly doubles as the grate spacing is doubled.

Calculation of the cross sectional areas of the grate bars and the spaces between the bars show that the area through which material could flow is effectively doubled in the test mill by using the larger grate bars. In other words, changing from the 1.3- to the 2.5-cm grates doubled the effective area through which material could flow, thus leading to the proportional increase in product flow rate.

Through the use of X_0 as a convenient measure of the coarseness of a size distribution, it is possible to demonstrate, as in Figure 41, that as flow rate increases, the shredder product size distribution becomes steadily smaller. This effect is explained by recalling that Equations 11 and 12 indicate that the mean residence time increases with flow rate. Not unexpectedly then, a longer residence time within the mill leads to a smaller characteristic particle size.

It was also found that power requirements increase with holdup (Figure 42). On the other hand, it was noted that increasing the moisture content for constant holdup led to a decrease in power requirements. This effect is shown in Figure 43 and may be explained by the fact that fibrous material (which is the major component of refuse) tears more readily as it becomes wetter. Since the test mill had a known fixed volume, power draw can be related to the actual density of material within the mill. Alternatively, since flow rate is a readily measured quantity and flow rate and holdup are related by Equations 9 and 10, power requirements can also be explained in terms of flow rate. Analysis of data obtained with the 2.5 cm grates shows the data to be fitted by the equation

$$P = 18.6\ Q^{1.1}\ (1-MC)^{0.36} \tag{14}$$

where: P is the instantaneous power draw (kW), MC is the fractional moisture content, and Q is the flow rate (tons/hr).

HAMMER WEAR

The parameters Z_0 and D_0/F_0 were used to present an overall picture of hammer wear as it pertains to the size reduction of raw MSW and SLF using

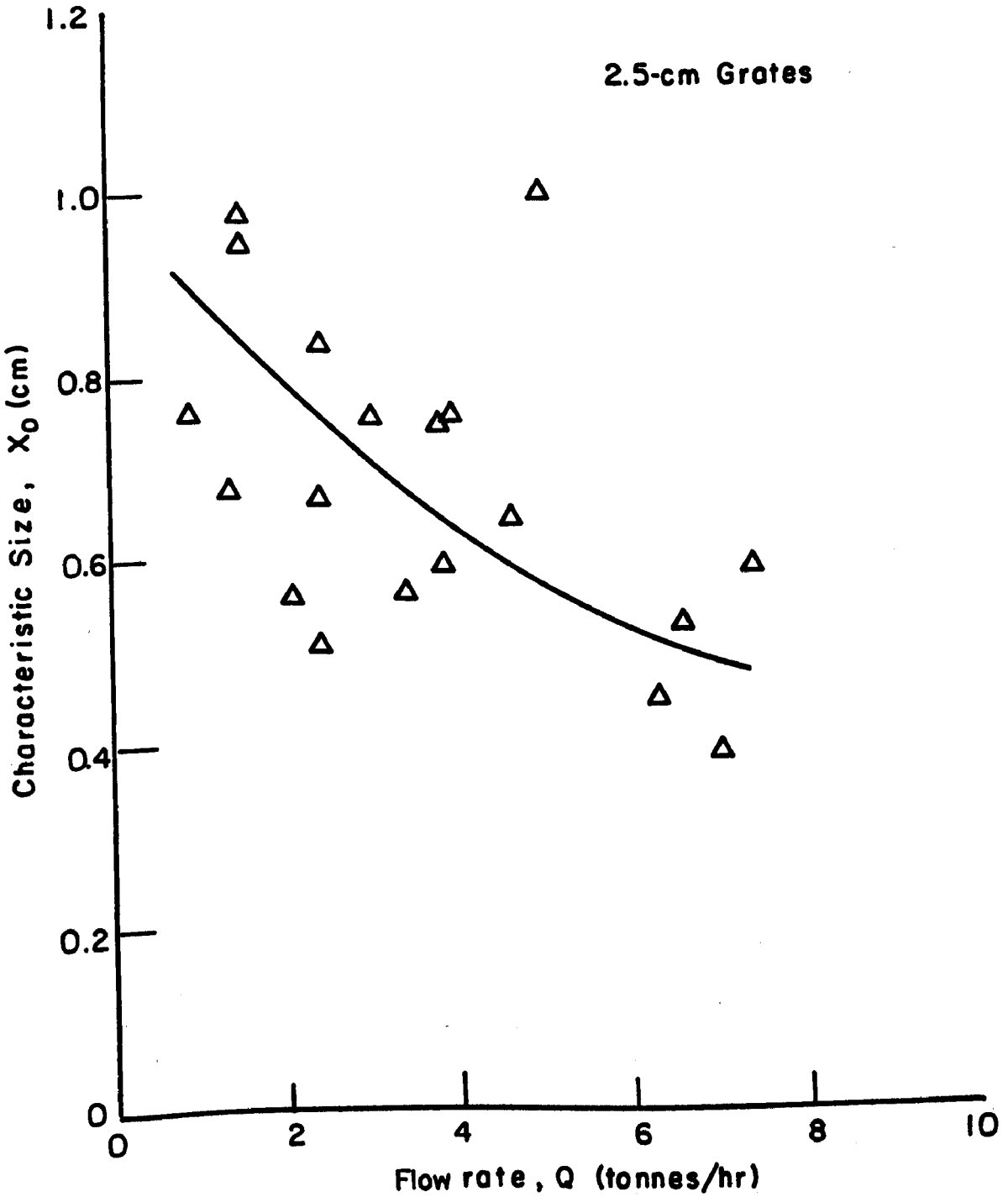

Figure 41. Characteristic particle size as a function of flow rate for raw MSW.

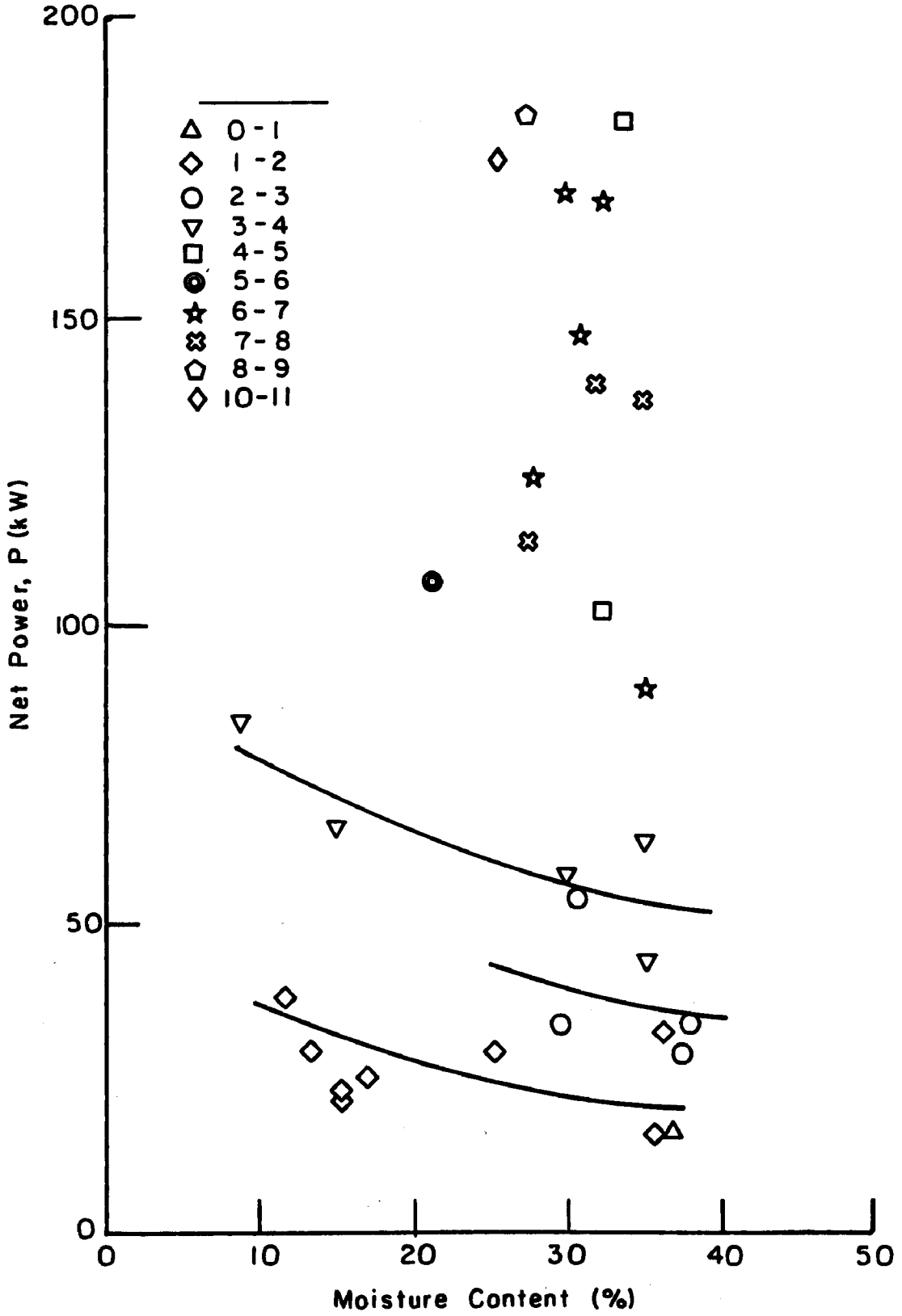

Figure 42. Net power as a function of holdup for raw MSW.

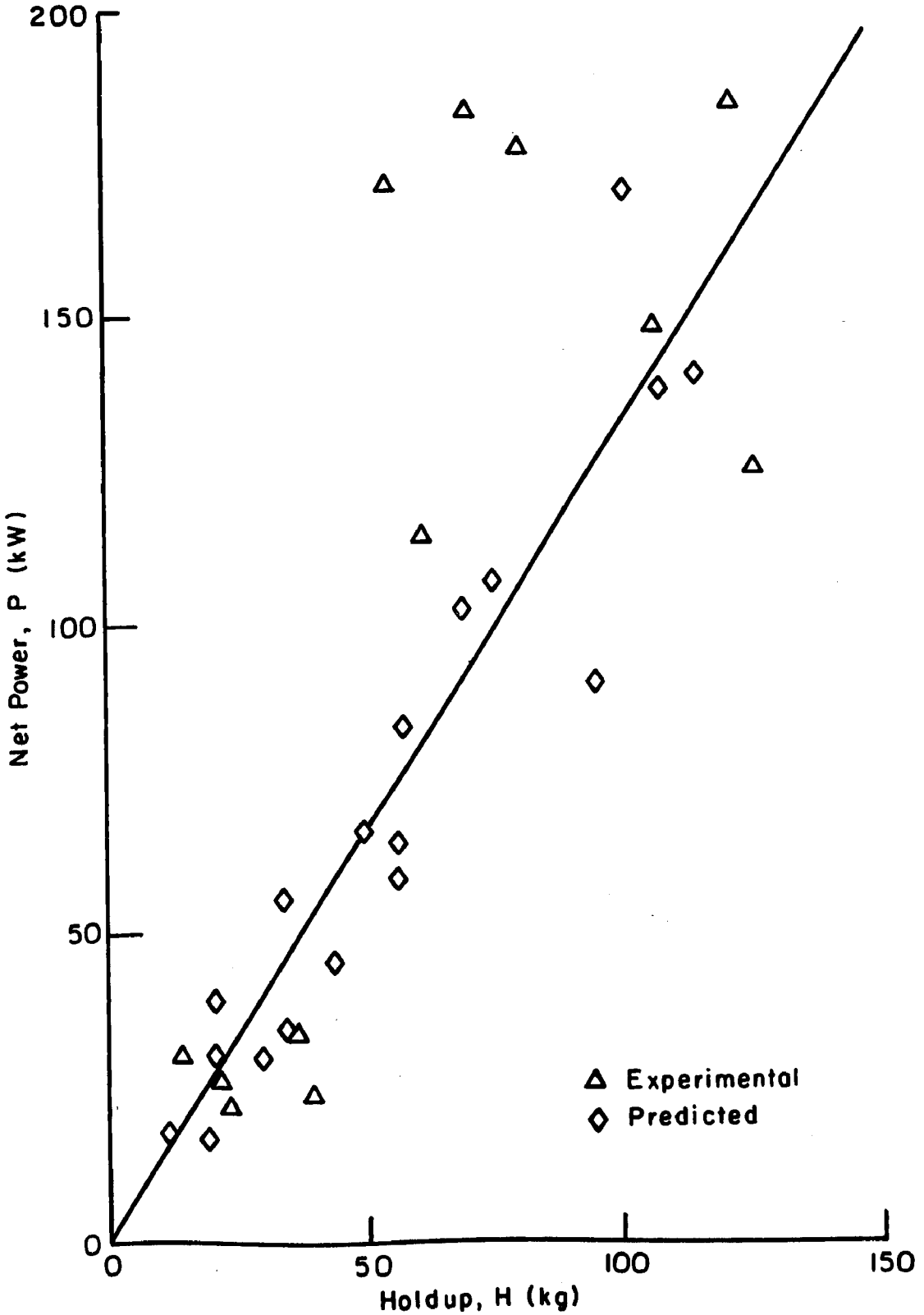

Figure 43. Net power as a function of moisture content for raw MSW.

the Gruendler and W-W hammermills. Each particular material was found to occupy a characteristic region of wear when expressed as a function of degree of size reduction (Z_0) or the ratio D_0/F_0.

The functional dependence of hammer wear on the degree of size reduction shows a greater degree of wear for raw MSW than for SLF (Figure 44). Although the actual data for SLF and raw MSW do not overlap in the same areas of degree of size reduction, extrapolation of the curves does allow some comparison of the wear characteristics of each material. In particular, for a specified value of Z_0, hammer wear resulting from shredding of raw MSW in the Gruendler mill can be seen to be approximately five times as great as that experienced for shredding SLF with the W-W mill.

The smaller degree of wear experienced for SLF is paradoxical when one recalls that from an energy consumption standpoint, SLF required significantly more energy than raw MSW to achieve the same degree of size reduction. This paradox seems to confirm the hypothesis that energy consumption and wear are independent of each other.

The information contained in Figure 44 can be expressed in terms of the ratio of grate opening size (D_0) to feed size (F_0) (Figure 45). This figure indicates wear experienced as a result of size reduction of raw MSW and SLF for particular conditions of grate opening and feed size. The curves occupy distinctive regions of the diagram, and the greater degree of wear for raw MSW compared to that of SLF is again apparent.

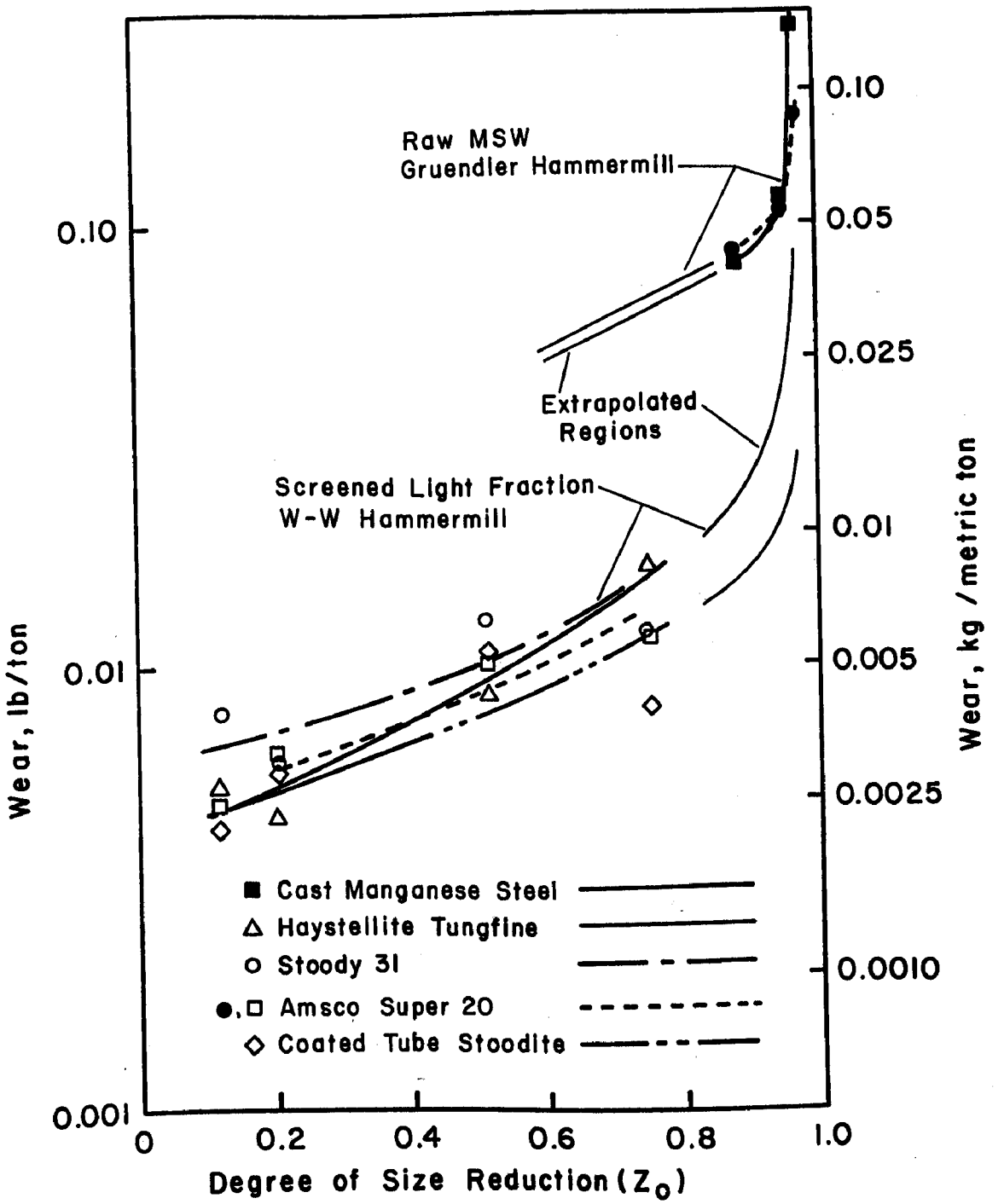

Figure 44. Hammer wear as a function of degree of size reduction for raw MSW and SLF.

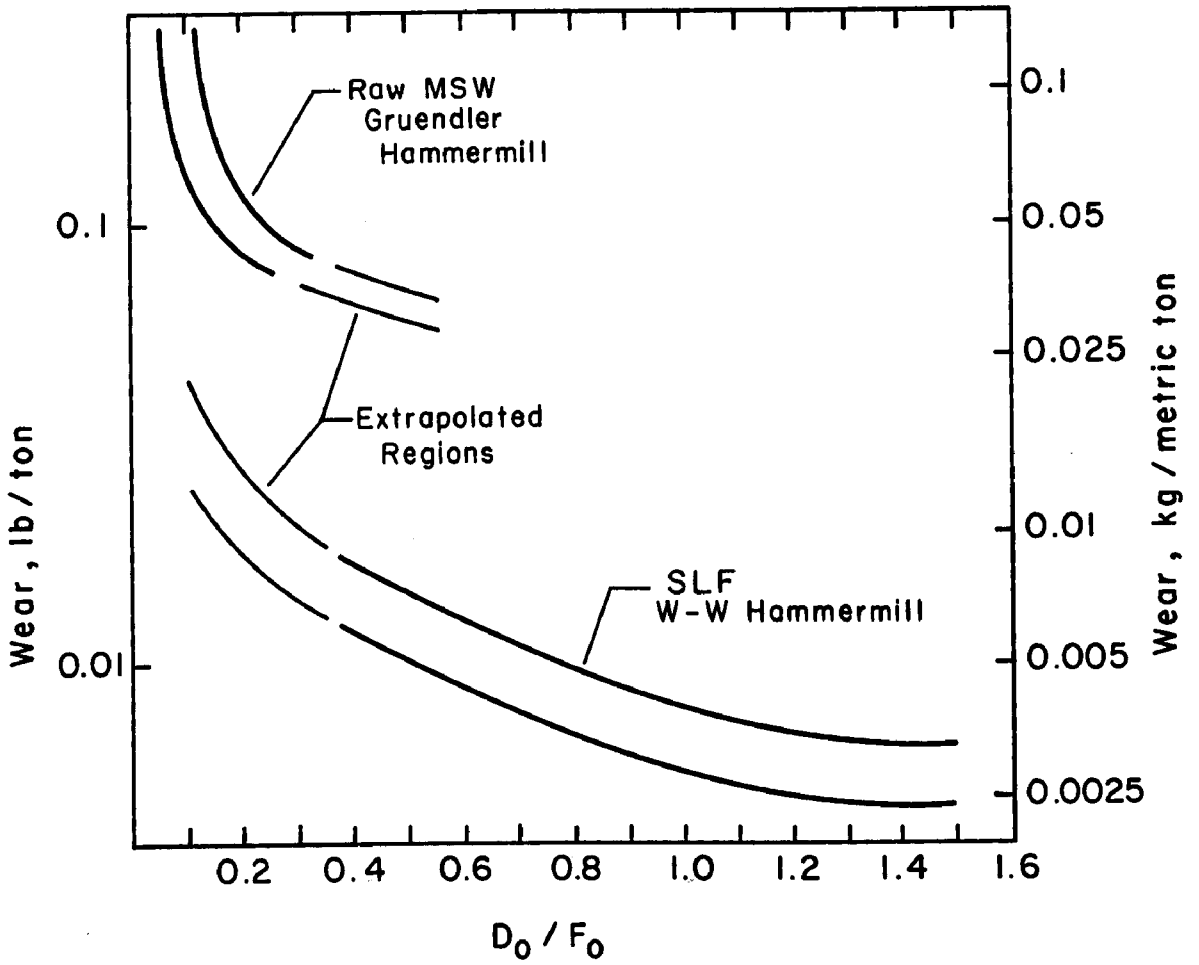

Figure 45. Hammer wear as a function of D_0/F_0 for raw MSW and SLF.

SECTION 6

COMMINUTION MODELS

The concept of employing matrix modeling to simulate the comminution of refuse in a swing hammermill was introduced in previous publications [1,2,3]. In general, matrix models are phenomenological and macroscopic in nature. They have been developed as a means of overcoming the inability of the earlier energy-versus-degree-of-reduction models to provide insight into the nature of the size reduction process. Although some microscopic models that deal with crack formation and propagation are physical in nature, they deal with single events and as such are not suitable for describing complete processes in a mill. The basic feature of the matrix model is its ability to predict product size through the use of the selection and breakage function. In effect, these functions describe what portion of the material will be selected for breakage in each pass, and over what size spectrum the breakage will occur.

Most studies dealing with the application of time-discrete, size-discrete models described by Callcott [4], Callcott and Lynch [5], and Lynch and Draper [6] have been applied to homogeneous brittle materials. Later, this approach was extended by Obeng [1] and Obeng and Trezek [2] to heterogeneous refuse, a solid waste that contains only on the order of 25 percent brittle materials. On the whole, this time-discrete, size-discrete method of modeling the comminution process in a swing hammermill has been only partially successful because these models are essentially black-box representations of the comminution process, in which material transport is implicitly assumed to occur by plug flow. Also, because time is not an explicit variable in the governing equations, a detailed description of mill dynamics is not possible. In these models, the mill matrix coefficients are not easy to interpret physically. Though these models can be used to predict size distributions and illustrate qualitative feed rate and moisture effects, certain basic questions such as why and how the feed rate affects the product size distribution cannot be answered in a fundamental manner.

Motivated by the successful extension of the size-discrete, time-continuous model used for describing mineral batch ball milling to continuous laboratory mills, [7] the matrix approach to the analysis of refuse comminution pursued in the initial studies [1,2,3] was similarly modified to include a residence time distribution. This distribution, the mean value of which is essentially the mill holdup divided by the feed rate, is a major factor in determining the product size distribution. In the case of the overflow discharge ball or rod mills, the mass of holdup is assumed constant so that the mean residence time is solely a function of the feed rate. Unfortunately, this simplification cannot be extended to the hammermilling

of refuse because of its highly compressible nature. Thus the mean residence time will vary with both holdup and feed rate.

The model presented here provides a means of simulating the hammermill size reduction of refuse based on the actual physical variables of the process. It addresses the specific issues of: (a) how the feed rate and moisture content affect the mill holdup, (b) how the mill holdup affects the energy consumption and residence time, and (c) how the selection and breakage functions can be estimated for different operating conditions.

SIZE-DISCRETE, TIME-DISCRETE MODELS

A brief review of the initial application of matrix modeling to refuse comminution is given to aid those readers not familiar with this area and to illustrate the improvement in the method through the use of the size-discrete, time-continuous approach. By representing the particle size range of a particulate assembly by n discrete size intervals

$$x_i \; x_{i+1}; \quad i = 1,2, \ldots n \,, \tag{15}$$

the particulate assembly may be described by a vector $\underline{M}$, i.e.,

$$\underline{M} = H\underline{m} = H \begin{vmatrix} m_1 \\ m_2 \\ \cdot \\ \cdot \\ \cdot \\ m_n \end{vmatrix} \tag{16}$$

where: H = total mass of the assembly, and
m_i = fraction of $\underline{M}$ within the $i^{\underline{th}}$ size class.

Lumping the various breakage mechanisms that may exist in the mill introduces two additional parameters -- the selection function $\underline{S}$ and the breakage function $\underline{B}$. The selection function is a diagonal matrix whose elements represent the fractional rate at which material in each size class is broken, i.e.,

$$S_{ij} = \begin{matrix} 0 \; ; \; i \neq j \\ s_i ; \; i = j \end{matrix} \tag{17}$$

where: s_i = fractional rate at which material in the $i^{\underline{th}}$ size class is broken.

The breakage function is a lower triangular matrix whose elements represent the fraction of material that enters a higher size class after being broken from a lower one. Note that in this case, the term "higher" indicates a particle size that actually is smaller, whereas the converse is

indicated by the term "lower". The assumption also is made that all particles, once broken, leave the original size class and that there is no agglomeration (clumping of particles). The breakage function thus becomes:

$$B_{ij} = \begin{matrix} 0 \; ; \; i = j \\ 0 \; ; \; 1 < j \\ b_{ij} ; i > j \end{matrix} \tag{18}$$

where: b_{ij} = the fraction broken out of the $j^{\underline{th}}$ class, which reports to the $i^{\underline{th}}$ class.

In the time-discrete formulation, the breakage process may be regarded as a series of discrete breakage events in which change of the fractional amount of the particulate assembly within a given size class is the difference between that which is broken out of that class and that which enters from other size classes in the course of a single breakage event. The formulation is:

$$\Delta(Hm_i) = -s_i \, Hm_i + \sum_{j=1}^{i-1} s_j b_{ij} m_j h \tag{19}$$

where: H = total mass of material in the mill at the time of the breakage event.

Under steady-state conditions, H may be factored out, and the result for a single size class is

$$\Delta m_i = - s_i m_i + \sum_{j=1}^{i-1} b_{ij} s_j m_j \tag{20}$$

The n difference equations representing all n size classes may be described by the single matrix expression

$$\underline{\Delta m} = - \underline{\underline{S}} \, \underline{m}_0 + \underline{\underline{B}} \, \underline{\underline{S}} \, \underline{m}_0$$

or

$$\underline{\Delta m} = - (\underline{\underline{I}} - \underline{\underline{B}}) \underline{\underline{S}} \, \underline{m}_0 \tag{21}$$

where I = n x n identity matrix, and
$\underline{m}_0$ = original size distribution.

Since $\underline{\Delta m}$ is the change in size distributions resulting from a single breakage event, Equation 21 may be rewritten as

$$\underline{m}_1 - \underline{m}_0 = -(\underline{\underline{I}}-\underline{\underline{B}})\underline{\underline{S}} \, \underline{m}_0$$

or

$$\underline{m}_1 = [\underline{\underline{I}} - (\underline{\underline{I}}-\underline{\underline{B}})\underline{\underline{S}}]\underline{m}_0 \tag{22}$$

where: $\underline{m}_1$ = size distribution after a single breakage event.

If it is assumed that $\underline{\underline{S}}$ and $\underline{\underline{B}}$ are invariant with respect to the number of breakage events, Equation 22, may be extended to apply to any number of breakage cycles by replacing $\underline{m}_1$ with $\underline{m}_{i+1}$, and $\underline{m}_o$ with $\underline{m}_i$ such that

$$\underline{m}_{i+1} = [\underline{\underline{I}} - (\underline{\underline{I}}-\underline{\underline{B}})\underline{\underline{S}}]\underline{m}_i$$

Multiple use of this equation, replacing $\underline{m}_i$ each time with $\underline{m}_{i+1}$ from the previous cycle, shows that for more than one cycle of breakage, Equation 22 becomes

$$\underline{m}_{N_c} = [\underline{\underline{I}} - (\underline{\underline{I}}-\underline{\underline{B}})\underline{\underline{S}}]^{N_c}\ \underline{m}_o \tag{23}$$

where N_c = the number of cycles of breakage.

The preceding method is the one employed by Obeng [1] in his research in which both single and multiple cycles of breakage were studied. For multiple cycles, N_c was estimated from

$$N_c = m-1 \tag{24}$$

where: $m-1 = n(x_1/x_m)/\ln(x_1/x_2)$,
x_1 = maximum feed size, and
x_m = maximum product size.

Subject to the important restriction that the eigenvalues must be positive [8,9] for

$$\underline{\underline{I}} - (\underline{\underline{I}}-\underline{\underline{B}})\underline{\underline{S}},\ \lambda_i = 1 - (1-b_{ii})s_i,\ i = 1,2,\ \ldots,\ n$$

Equation 23 may be reduced by a similarity transform to [8]

$$\underline{m}_{N_c} = \underline{\underline{T}}\ \underline{\underline{J}}\ (N_c)\ \underline{\underline{T}}^{-1}\ \underline{m}_o \tag{25}$$

in which $\underline{\underline{T}}$ is the n x n lower triangular matrix composed of the column eigenvectors of $\underline{\underline{I}} = (\underline{\underline{I}}-\underline{\underline{B}})\underline{\underline{S}}$, such that:

$$T_{ij} = \begin{cases} 0 & i < j \\ 1 & i = j \\ \sum_{k=1}^{i-1} \dfrac{b_{ik}\ s_k}{\lambda_j-\lambda_i}\ T_{kj} & i > j \end{cases} \tag{26}$$

$\underline{\underline{J}}(N_c)$ is an n x n diagonal matrix with elements

$$J_{ij}(N_c) = \begin{cases} 0 & i \neq j \\ [1 - (1-b_{ij})s_i]^{N_c} & i = j \end{cases} \tag{27}$$

Equation 25 is obviously more amenable to use than is Equation 23 because it eliminates the need to compute the N_c^{th} power of $[\underline{\underline{I}} - (\underline{\underline{I}}-\underline{\underline{B}})\underline{\underline{S}}]$. Implicit in the use of Equations 23 and 25 is the existence of plug flow conditions in

the mill. Such an assumption has not been substantiated by any experimental evidence [10,11,12].

SIZE-DISCRETE, TIME-CONTINUOUS MODEL

In the second approach, the particle size range of any particulate assembly may again be divided into n discrete intervals

$$x_i \; x_{i+1}; \quad i = 1,2, \ldots n$$

where x_i is some size usually associated with a set of standard screen sizes.

A particulate assembly whose individual particle sizes are within this range is then represented by the vector $\underline{M}$ such that

$$\underline{M} = H \, \underline{m} = |H \, m_1 m_2 \ldots m_i \ldots m_n|^T$$

where: H is the total mass of the assembly and m_i is the fraction within the $x_i \; x_{i+1}$ size class.

It follows that if $\underline{M}$ represents the material within the grinder at any particular time, H represents the mass of material held in the mill (the mill holdup).

A mass balance on the $i^{\underline{th}}$ size class at time t yields

$$\frac{d}{dt} [H \, m_i(t)] = -s_i(H \, m_i(t)) + \sum_{j=1}^{i-1} b_{ij} s_j (H m_j(t)) \tag{28}$$

where: H = mill holdup,
m_i = mass fraction in the $i^{\underline{th}}$ interval,
s_i = fractional rate at which material is broken out of the $i^{\underline{th}}$ interval (the $i^{\underline{th}}$ selection function), and
b_{ij} = fraction of material which, once broken, reports to the $i^{\underline{th}}$ interval from the $j^{\underline{th}}$ interval (the breakage function).

If it is assumed that s_i and b_{ij} are independent of both x_i and time, then the model may be linearized and the breakage process represented by n simultaneous differential equations, which may be written in matrix form as

$$\frac{d}{dt} [H \, \underline{m} \, (t)] = -[\underline{\underline{I}} - \underline{\underline{B}}] \, \underline{\underline{S}} \, H \, \underline{m} \, (t) \tag{29}$$

where: $\underline{\underline{I}}$ = n x n identity matrix,
$\underline{\underline{S}}$ = n x n diagonal matrix of selection functions, and
$\underline{\underline{B}}$ = the n x n lower triangular matrix of breakage functions.

For a batch process with an initial size distribution $\underline{m_b}$ (o), H is constant and Equation 29 is reduced to

$$\frac{d}{dt}[\underline{m}_b(t)] = -[\underline{\underline{I}}-\underline{\underline{B}}]\,\underline{\underline{S}}\,\underline{m}_b(t) \tag{30}$$

the solution of which is

$$\underline{m}_b(t) = \exp\,[-(\underline{\underline{I}}-\underline{\underline{B}})\,\underline{\underline{S}}t]\,\underline{m}_b(o) \tag{31}$$

Equation 31 may be evaluated through the iterative solution for the exponential

$$\exp[-(I-B)S\ t] = \sum_{j=0}^{\infty}[-(I-B)\ S\ t]^j/j! \tag{32}$$

However, when $s_i \neq s_j$ for all i and j, a similarity transform leads to an easier solution.

Through the use of a constant n x n matrix $\underline{\underline{T}}$, a linear transformation may be made between $\underline{m}_b$ and a new state vector $\underline{m}_b^*$, such that:

$$\underline{m}_b(t) = \underline{\underline{T}}\,\underline{m}_b^*(t),\ \underline{m}_b^*(t) = \underline{\underline{T}}^{-1}\,\underline{m}_b(t) \tag{33}$$

Replacing $\underline{m}_b$ by $\underline{m}_b^*$ in Equation 30 gives the equation

$$\frac{d}{dt}[\underline{\underline{T}}\,\underline{m}_b^*(t)] = -[\underline{\underline{I}}-\underline{\underline{B}}]\underline{\underline{S}}\ T\ \underline{m}_b^*(t) \tag{34}$$

or

$$\frac{d}{dt}[\underline{m}_b^*(t)] = \underline{\underline{T}}^{-1}[-(\underline{\underline{I}}-\underline{\underline{B}})\underline{\underline{S}}]\underline{\underline{T}}\ \underline{m}_b^*(t) \tag{35}$$

Assume that

$$\underline{\underline{T}}^{-1}\,[-(\underline{\underline{I}}-\underline{\underline{B}})\ \underline{\underline{S}}]\ \underline{\underline{T}} = \underline{\underline{P}} \tag{36}$$

where: $\underline{\underline{P}}$ is an n x n diagonal matrix with diagonal elements $p_1, p_2, \ldots, p_n$.

It follows that the eigenvalues of the left hand side of Equation 36 are equal to the diagonal elements, p_i, i = 1,2, ..., n. Solving for the roots of the characteristic equation shows

$$|\lambda\underline{\underline{I}} - \underline{\underline{T}}^{-1}\,[-\underline{\underline{I}}-\underline{\underline{B}})\ \underline{\underline{S}}]\ \underline{\underline{T}}| = 0 \tag{37}$$

However

$$\lambda\underline{\underline{I}} - \underline{\underline{T}}^{-1}\,[-(\underline{\underline{I}}-\underline{\underline{B}})\ \underline{\underline{S}}]\underline{\underline{T}} = \underline{\underline{T}}^{-1}\,[\lambda\underline{\underline{I}} + (\underline{\underline{I}}-\underline{\underline{B}})\underline{\underline{S}}]\underline{\underline{T}} \tag{38}$$

Hence the characteristic equation may be written as

$$|\underline{\underline{T}}^{-1}\,[\lambda\underline{\underline{I}} + (\underline{\underline{I}}-\underline{\underline{B}})\ \underline{\underline{S}}]\ \underline{\underline{T}}| = 0 \tag{39}$$

from which $\underline{\underline{T}}^{-1}$ and $\underline{\underline{T}}$ may be factored, leaving

$$|\lambda\underline{\underline{I}} + (\underline{\underline{I}}-\underline{\underline{B}})\ \underline{\underline{S}}| = 0 \tag{40}$$

and thus showing that the eigenvalues of $-(\underline{\underline{I}}-\underline{\underline{B}})\ \underline{\underline{S}}$ are equal to the eigen-

values of $\underline{\underline{T}}^{-1}[-(\underline{\underline{I}}-\underline{\underline{B}})\underline{\underline{S}}]\underline{\underline{T}}$, which in turn are the diagonal elements of $\underline{\underline{P}}$. In addition, since $\underline{\underline{I}}$ and $\underline{\underline{S}}$ are diagonal and $\underline{\underline{B}}$ is lower triangular, $-(\underline{\underline{I}}-\underline{\underline{B}})\underline{\underline{S}}$ becomes lower triangular, the main diagonal of which are the elements s_i, $i = 1,2...n$. Standard matrix algebra tells us that the eigenvalues of a lower triangular matrix are simply the elements of the main diagonal. From this it is obvious that

$$\underline{\underline{P}} = -\underline{\underline{S}}. \tag{41}$$

Substituting Equation 41 into Equation 36 shows that

$$\frac{d}{dt}[m_b^*(t)] = -\underline{\underline{S}}\,\underline{m}_b^*(t) \tag{42}$$

which has the solution

$$\underline{m}_b^*(t) = \underline{\underline{J}}\, m_b^*(o) \tag{43}$$

where

$$J = \begin{vmatrix} e^{-s_1 t} & o & \cdot & \cdot & \cdot & o \\ o & e^{-s_2 t} & \cdot & \cdot & \cdot & o \\ \cdot & \cdot & \cdot & & & \\ \cdot & \cdot & & \cdot & & \\ \cdot & \cdot & & & \cdot & \\ o & o & & & & e^{-s_n t} \end{vmatrix}$$

By using Equation 33, Equation 43 may be transformed to give

$$\underline{m}_b(t) = \underline{\underline{T}}\,\underline{\underline{J}}\,\underline{\underline{T}}^{-1}\, m_b(o) \tag{44}$$

Because of the decoupling that occurs when the original differential equation is transformed, the $\underline{\underline{T}}$-matrix is known as the modal matrix. Returning to Equation 36 and premultiplying both sides by $\underline{\underline{T}}$ results in

$$[-(\underline{\underline{I}}-\underline{\underline{B}})\underline{\underline{S}}]\,\underline{\underline{T}} = \underline{\underline{T}}\,\underline{\underline{P}} \tag{45}$$

The right side of this equation becomes

$$\underline{\underline{T}}\,\underline{\underline{P}} = \begin{vmatrix} p_1 T_{11} & p_2 T_{12} & \cdots & p_n T_{1n} \\ p_1 T_{21} & p_2 T_{22} & \cdots & p_n T_{2n} \\ & & & \cdot \\ & & & \cdot \\ & & & \cdot \\ p_1 T_{n1} & p_2 T_{n2} & \cdots & p_n T_{nn} \end{vmatrix} \tag{46}$$

and the left side may be rewritten as

$$[-(\underline{\underline{I}}-\underline{\underline{B}})\underline{\underline{S}}]\,\underline{\underline{T}} = [-(\underline{\underline{I}}-\underline{\underline{B}})\underline{\underline{S}}]\,[\underline{u}_1\ \underline{u}_2 \cdots \underline{u}_n] \tag{47}$$

where: $\underline{u}_i$ = a column vector representing the $i\underline{th}$ column of $\underline{\underline{T}}$.

Equating, column by column, Equations 46 and 47 results in

$$-[I-B]\ \underline{\underline{S}}\ \underline{u}_i = p_i \underline{u}_i \tag{48}$$

or

$$[p_i\ \underline{\underline{I}} + (\underline{\underline{I}}-\underline{\underline{B}})\ \underline{\underline{S}}]\ \underline{u}_i = 0 \tag{49}$$

which establishes a set of n equations for which $\underline{u}_i$ may be solved when s_i is substituted for p_i. Solving for the values of the eigenvectors $\underline{u}_i$ yields the modal matrix $\underline{\underline{T}}$. In this case, a set of eigenvectors that satisfies Equation 49 is such that

$$T_{ij} = \begin{matrix} 0 & & i < j \\ 1 & & i = j \\ \sum_{k=j}^{i-1} & \left(\dfrac{b_{ik}\ s_k}{s_i - s_j}\right) T_{kj} & i > j \end{matrix} \tag{50}$$

Equation 44 is the solution of the linearized, lumped-parameter, size-discrete, time-continuous equation for batch grinding. To extend the equation to continuous grinding, it is necessary to introduce the concept of residence time. Residence time is defined as the length of time a particle within a size interval remains in the mill. Since no single value for the residence time will hold in all cases, a residence time distribution is proposed that is the probable time a particle will remain within the mill. If it is assumed that all size intervals are characterized by a single residence time distribution, then the open circuit mill is the average of the batch response weighted with respect to residence time, i.e.,

$$\underline{m}_{cp} = \int_0^\infty \underline{m}_b(t)\ R(t)dt \tag{51}$$

where: R(t) is the residence time distribution. Substituting the relation given in Equation 44 for $\underline{m}_b$ gives the solution for continuous grinding

$$\underline{m}_{cp} = \underline{\underline{T}}[\int_0^\infty \underline{\underline{J}}(t)\ R(t)dt]\ \underline{\underline{T}}^{-1}\ \underline{m}_{cf} \tag{52}$$

where: $\underline{m}_{cp}$ = continuous product size distribution, and
$\underline{m}_{cf}$ = continuous feed size distribution.

Now, letting

$$\theta = \frac{t}{\tau}$$

where: t = time and
τ = mean residence time = ratio of holdup to feedrate, H/M_{cf}.

The result, by substituting, is:

$$\underline{m}_{cp} = \underline{\underline{T}}\,\underline{\underline{J}}_c(\tau)\,\underline{\underline{T}}^{-1}\,\underline{m}_{cf} \tag{53}$$

where: $\underline{\underline{J}}_c(\tau) = \int_0^\infty \exp[(-s_i\tau)\theta]\,R(\theta)d\theta \qquad \begin{matrix} i = j \\ i \neq j \end{matrix}$

A block diagram of the open circuit mill is shown in Figure 46. $\underline{\underline{D}}$ represents the mill matrix,

$$\underline{\underline{D}} = \underline{\underline{T}}\,\underline{\underline{J}}_c\,(\tau)\,\underline{\underline{T}}^{-1} \tag{54}$$

If, after passing through the mill, the product is classified and a portion recycled to the mill feed, a closed circuit is formed that significantly alters the final product. The closed circuit schematic is shown in Figure 47. The classifier matrix $\underline{\underline{C}}$ of Figure 47 is an n x n diagonal matrix, the entries of which represent the fraction within each size class that is recycled to the mill.

For the closed circuit [13,14]

$$\underline{M}_{cp} = \underline{\underline{D}}\,\underline{\underline{M}}_{cf} \tag{55}$$

$$\underline{M}_{cp} = (\underline{\underline{I}}-\underline{\underline{C}})\underline{M}_{cp} \tag{56}$$

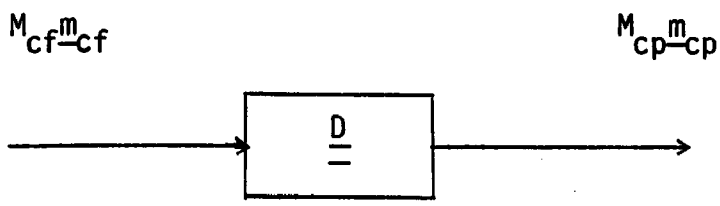

Figure 46. Diagram of open circuit milling.

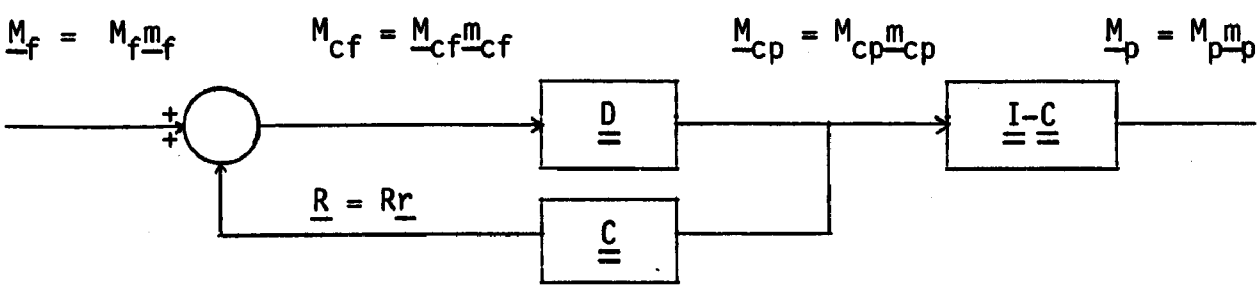

Figure 47. Diagram of closed circuit milling.

$$\underline{R} = \underline{\underline{C}}\,\underline{M}_{cp} \tag{57}$$

$$\underline{M}_{cf} = \underline{M}_f + \underline{R} \tag{58}$$

Substituting Equation 57 into Equation 58 gives

$$\underline{M}_{cf} = \underline{M}_f + \underline{\underline{C}}\,\underline{M}_{cp} \tag{59}$$

which in turn may be substituted into Equation 55 to show that

$$\underline{M}_{cp} = \underline{\underline{D}}(\underline{M}_f + \underline{\underline{C}}\,\underline{M}_{cp})$$

By rearranging terms to get

$$(\underline{\underline{I}}-\underline{\underline{D}}\,\underline{\underline{C}})\,\underline{M}_{cp} = \underline{\underline{D}}\,\underline{M}_f$$

the left side may be premultiplied by $(\underline{\underline{I}}-\underline{\underline{D}}\,\underline{\underline{C}})^{-1}$

$$\underline{M}_{cp} = (\underline{\underline{I}}-\underline{\underline{D}}\,\underline{\underline{C}})^{-1}\ \underline{\underline{D}}\,\underline{M}_f \tag{60}$$

Finally, if Equation 60 is substituted into Equation 56, the result is

$$\underline{M}_p = (\underline{\underline{I}}-\underline{\underline{C}})(\underline{\underline{I}}-\underline{\underline{D}}\,\underline{\underline{C}})^{-1}\ \underline{\underline{D}}\,\underline{M}_f \tag{61}$$

or

$$M_p\underline{m}_p = (\underline{\underline{I}}-\underline{\underline{C}})\ \underline{\underline{D}}\ (\underline{\underline{I}}-\underline{\underline{C}}\,\underline{\underline{D}})^{-1}\ M_f\underline{m}_f$$

Since under steady-state conditions $M_p = M_f$, the solution to the continuous closed circuit mill product equation is:

$$\underline{m}_p = (\underline{\underline{I}}-\underline{\underline{C}})\ \underline{\underline{D}}\ (\underline{\underline{I}}-\underline{\underline{C}}\,\underline{\underline{D}})^{-1}\ \underline{m}_f \tag{62}$$

IMPLEMENTATION OF THE MODEL

In hammermill size reduction of MSW studies, it is virtually impossible to determine selection and breakage functions for even the coarsest size classes by an examination of zero order production relationships as described by Herbst [15], Herbst and Mika [16], and Grandy and Fuerstenau [17]. On the other hand, nonlinear, optimal parameter estimation has been used with some success in the past [18,19] and was chosen in this instance as the technique most likely to prove useful.

Parameter estimation itself is based on two fundamental assumptions:

1) The size reduction process is linear, i.e..,

$$s_i \neq s_i(m(t));\ i=1,\ \ldots,\ n$$

and

$$b_{ij} \neq b_{ij}(m(t));\ j=1,\ \ldots,\ n-1;\ i = j+1,\ \ldots,\ n$$

or, in other words, s_j and b_{ij}, and not functions of the size distribution existing in the mill (under steady-state conditions, $m_i(t)$ is relatively constant).

2) The size-discrete breakage function can be normalized. This implies that for a constant ratio between successive sizes,

$$b_{ij} = b_{i-j+1,\ 1}$$

and

$$B_{ij} = B_{i-j+1,\ 1};\ j=1,\ \ldots,\ n-2;\ i = j+1,\ \ldots,\ n-1$$

where

$$B_{ij} = \sum_{k=i}^{n} b_{kj}$$

The second assumption means that the breakage function depends only on the difference, i-j, and not independently on i and j. It also implies that if B_{ij} is plotted against $(x_i^2/x_j\ x_{j+1})^{1/2}$, a single curve will result for all i,j. Finally, since the $n^{\underline{th}}$ size class contains all material finer than x_n, it is apparent that

$$b_{nj} = \sum_{k=n-j+1}^{n} b_{k1};\ j-2,\ \ldots,\ n-1 \tag{63}$$

With single-size class feed and short grind times, some batch size-reduction systems are characterized by what is known as zero-order kinetics of appearance of material in size classes much smaller than the feed size. If this is true it follows that

$$\frac{d}{dt}\left[Y_i(t)\right] = \sum_{j=1}^{i-1} B_{i-j+1,1}\ s_j m_j(t) \simeq K_i \tag{64}$$

where: $Y_i(t)$ = cumulative fraction finer than x_i, and
K_i = zero order production rate constant.

In the limit as $t \to 0$

$$m_1(t) \gg m_j(t);\ j=2,\ \ldots,\ i-1$$

and therefore Equation 64 reduces to

$$B_{i,1}\ s_1 = K_i \tag{65}$$

It has been experimentally noted [20] that the zero-order production rate constants, K_i, are of the form

$$K_i = K^* \left(\frac{x_i^{\ 2}}{x_1\ x_2}\right)^{\alpha/2};\ i=2,\ \ldots,\ n \tag{66}$$

where: K^* and α are time-invariant constants.

When Equation 66 is applicable and is substituted for K_i in Equation 65, then the feed size cumulative breakage functions may be found from

$$B_{i,1} = \frac{K^*}{s_1} \left(\frac{x_i^2}{x_1 \, x_2} \right)^{\alpha/2} \tag{67}$$

The more general constraint

$$B_{ij} s_j = K_i; \; j=1, \ldots, i-1 \tag{68}$$

shows that

$$\frac{B_{i1}}{B_{k1}} = \frac{B_{ij}}{B_{kj}}$$

which, in light of Equation 67, becomes

$$\frac{B_{ij}}{B_{kj}} = \left(\frac{x_j}{x_k} \right)^{\alpha} \tag{69}$$

If Equation 68 is to be satisfied, the breakage function must be subject to being normalized in the sense of Epstein [21], i.e.,

$$B_{ij} = \frac{K^*}{s_1} \left(\frac{x_i^2}{x_j \, x_{j+1}} \right)^{\alpha/2} \tag{70}$$

The remaining selection functions may be established from Equation 68 with i=n. Rearranging yields

$$s_j = \frac{B_{nj}}{K_n}$$

Substituting the expressions for B_{nj} and K_n in Equations 70 and 66 gives the result

$$s_j = s_1 \left(\frac{x_j x_{j+1}}{x_1 x_2} \right)^{\alpha/2} \tag{71}$$

Finally, the individual breakages may be obtained from the difference

$$b_{i1} = B_{i1} - B_{i+1,1}; \; i-2, \ldots, n, \tag{72}$$

from the normalized equation

$$b_{ij} = b_{i-j+1,1};\ j-1,\ \ldots,\ n-1;\ i = j+1,\ \ldots, n-1 \tag{73}$$

and from Equation 63.

In the actual use of the model, it is necessary to find a means of evaluating the integral of Equation 53. One way to do this is to use a numerical scheme. One of the simplest is Simpson's approximation

$$\int_a^b f(x)dx = \frac{h}{3}[f_0(x) + 4f_1(x) + 2f_2(x) + 4f_3(x) + \ldots + 2f_{n-2}(x) + 4f_{n-1}(x)+f_n(x)] \tag{74}$$

where: $h = (b-a)/n$, and
n = number of intervals, 2,4,6,...

Since six values for the residence time distribution can be obtained experimentally, this approximation to the integral is relatively easy to implement.

The procedure followed for the parameter estimation by means of a nonlinear optimization scheme is shown in Figure 48. The general procedure is as follows:

1. Initial guesses for s_1, K^*, and α are supplied.

2. Equality, inequality, and tolerance constraints are supplied.

3. Experimental values of $\underline{m}_f$, $\underline{m}_p$, $R(\theta)$, τ and $\underline{\underline{C}}$ are entered.

4. A predicted $\underline{m}_p$ is calculated.

5. The percent error between the predicted and experimental values of $\underline{m}_p$ is calculated.

6. s_1, K^*, and α are adjusted to reduce the objective function, and steps 2 through 5 are followed again.

7. If Δs_1, ΔK^*, and $\Delta\alpha$ are less than the tolerance criterion, then exit; otherwise go back to step 6.

The procedure followed for mill simulation uses the results from the parameter estimation to predict the mill product for untested operating conditions. The steps are only slightly different from those employed in parameter estimation. Figure 49 is the flow chart of the steps followed. They are:

1. Enter the maximum size and number of size classes;

2. Enter size distribution, residence time, flow rate, s_1, K^* and α data.

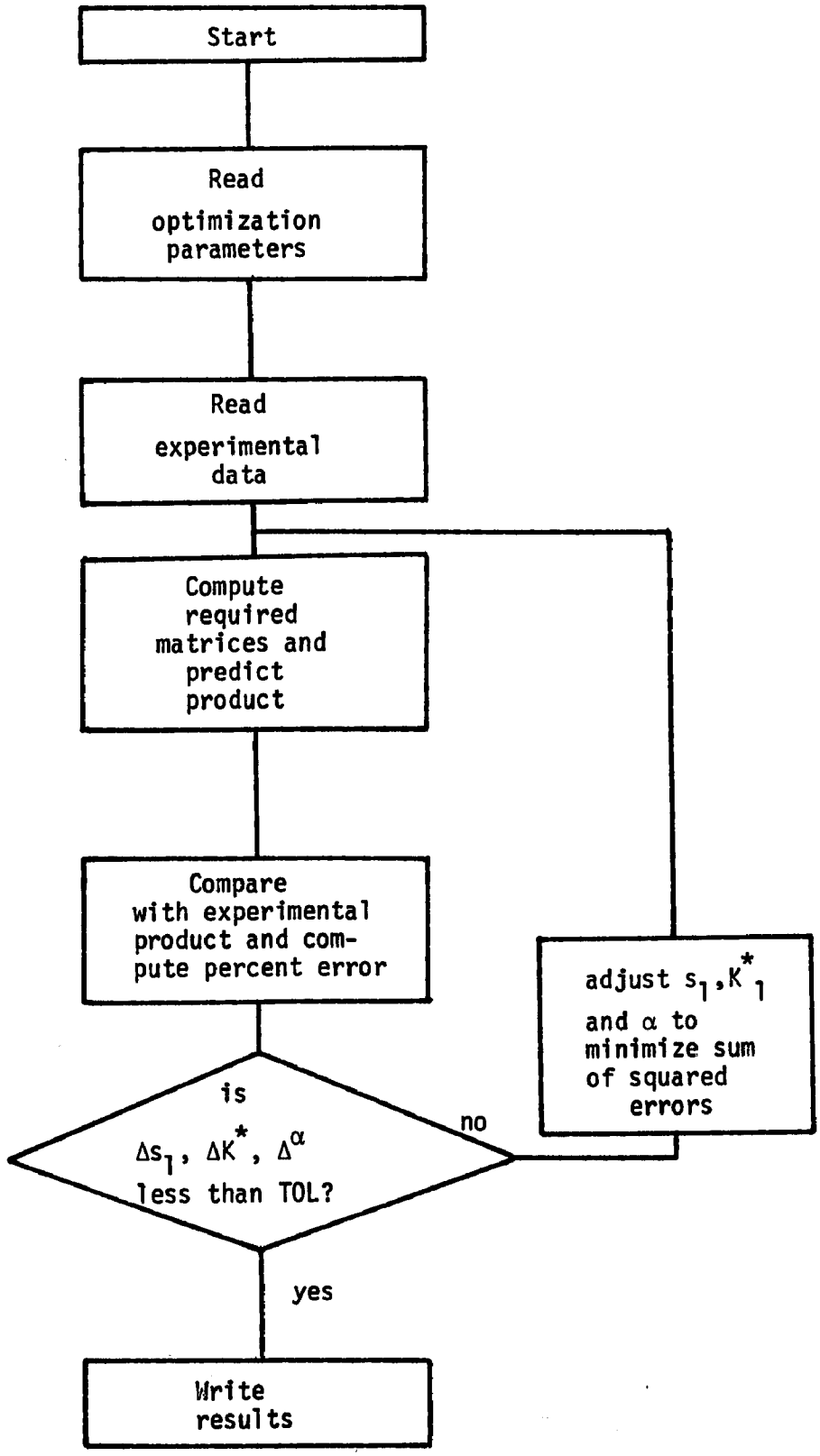

Figure 48. Nonlinear optimization flow chart for parameter estimation.

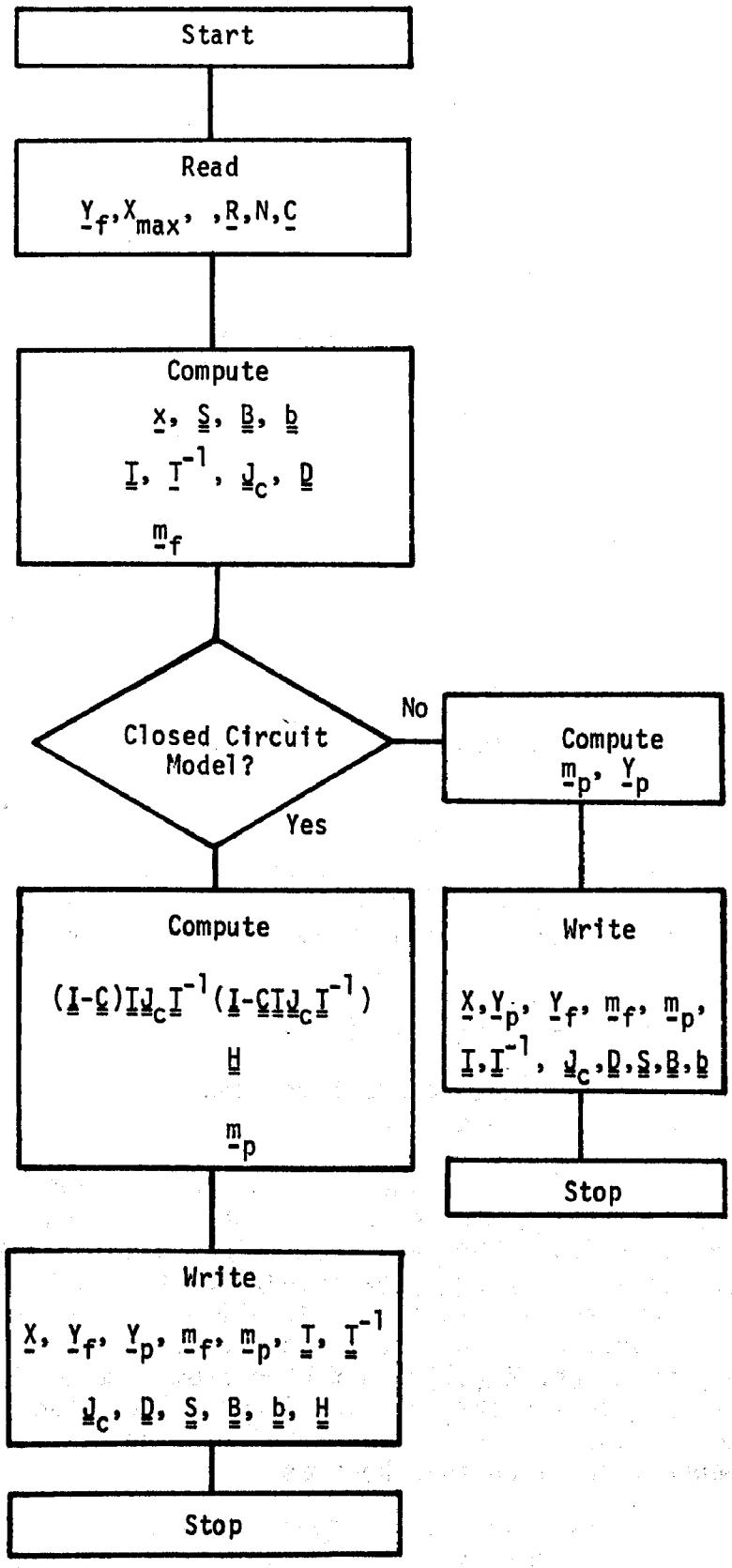

Figure 49. Flow chart for mill simulation calculations.

3. If a closed loop model is to be used, enter the experimental classifier matrix.

4. Calculate the size classes (a fixed ratio $x_i/x_{i+1} = 2$ was used).

5. Calculate the remaining selection functions by Equation 71.

6. Calculate the cumulative and individual breakage functions from Equations 63, 70, 72, and 73.

7. Calculate the modal matrix, $\underline{\underline{T}}$, and its inverse.

8. Calculate the matrix, $\underline{\underline{J}}_c$, by either Simpson's approximation or the use of a functional model for the normalized residence time distribution.

9. Calculate the open circuit mill matrix.

10. If an open circuit model is desired, calculate the product and exit; otherwise, calculate the closed circuit matrix.

11. Calculate the product and exit.

RESIDENCE TIME DISTRIBUTION

The residence time distribution model implies neither a fully mixed nor a plug flow, but rather a system whose product lies somewhere between the two limits. Obviously, two of the major parameters involved are the shape of the normalized residence time distribution curve and the mean residence time. With most systems, it may reasonably be assumed that the form taken by the normalized form of this curve may be easily found from

$$R(t) = R(\theta)/\tau \tag{75}$$

where: $R(\theta)$ = normalized residence time, and
τ = mean residence time.

The experimentally determined form of the residence time distribution as determined from unit impulse tests is shown in Figure 50 and the normalized form in Figure 51. The data from which these graphs were constructed are taken from Shiflett [22]. The results of the tests were plotted at the midpoints of each sample time interval, which in turn was determined by the speed of the product conveyor and the distance between conveyor cleats. A complementary function, $R'(t)$, was formed from Figure 50 by selecting values of $R(t)$ every 10 sec for the interval $0 \leq t \leq 140$, summing the values, and dividing each by the sum (since the total must be no greater than unity). The complementary function thus becomes

$$R'(t) = 1 - \sum_{i=1}^{n} [R_i(t)/ \sum_{j-1}^{n} R_j(t)]$$

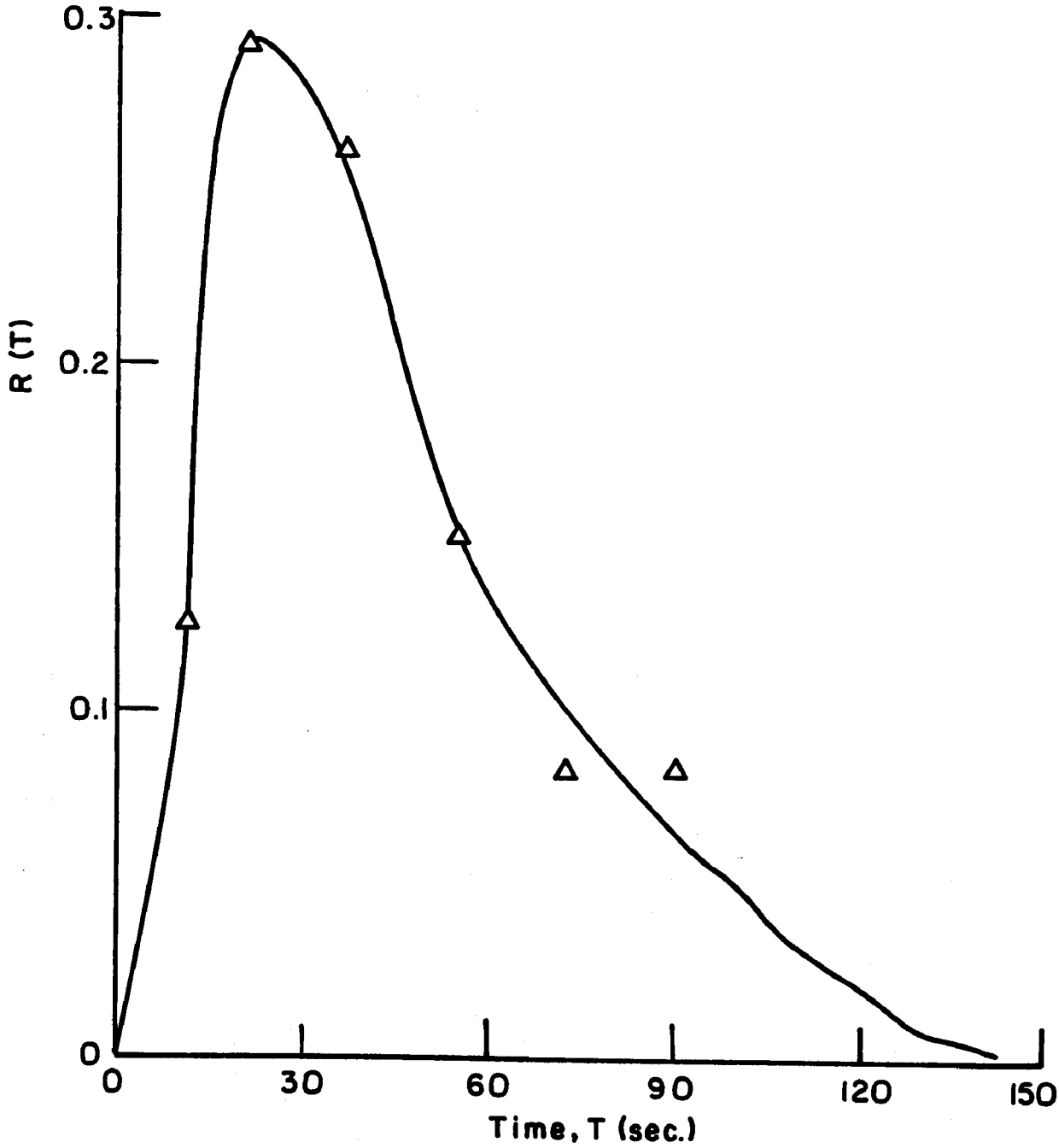

Figure 50. Residence time distribution.
(Data from Shiflett (22))

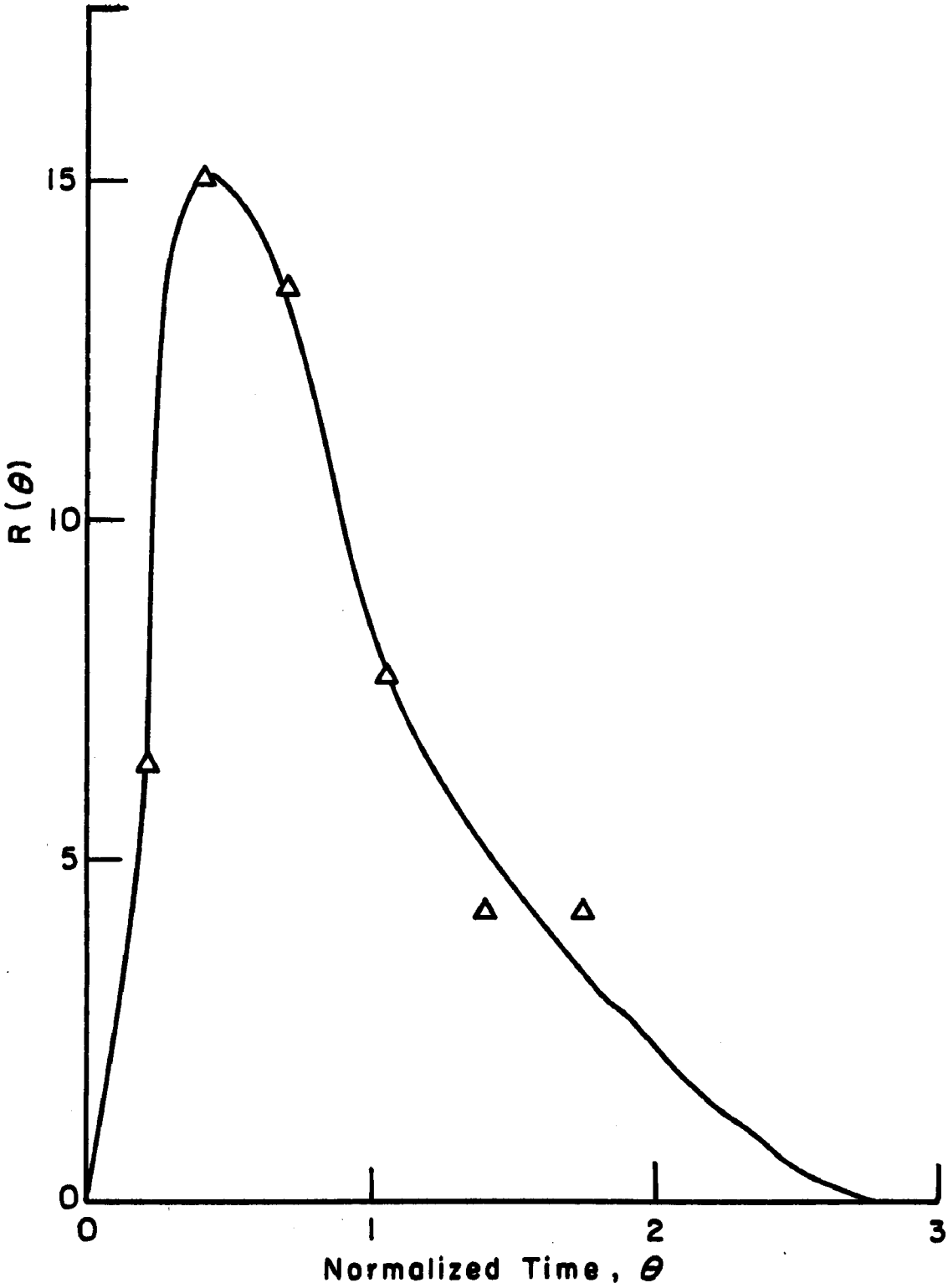

Figure 51. Normalized residence time distribution. (Data from Shiflett (22))

and is plotted in Figure 52. It is interesting to note that this representation shows the grinder to approximate a pure delay and a perfect mixer in series, the time constant for which is found from the slope of the straight portion of the curve.

The mean residence time, τ, may be found in several ways:

1. From flow rate/holdup data

$$\tau = k \frac{H}{Q} \tag{76}$$

where: H = mill holdup (kg),
Q = flow rate (tons/hr), and
k = conversion factor between kg-hr/ton to sec = 3.6

2. From the residence time distribution curve

$$\tau = \sum_{i=1}^{n} R_i(t)t_i / \sum_{i=1}^{n} R(t) \tag{77}$$

3. From the complementary function R'(t)

$$\tau = \text{delay} + \text{time constant} \tag{78}$$

As shown by the data listed below, the mean residence times calculated by each method are all in fairly close agreement:

Method	τ
1	51.4
2	45.7
3	44.7

Figure 53 shows the variation in the characteristic size with the change in mean residence time. As the figure indicates, the charactertistic size shifts toward the finer sizes with an increase in τ. This fact again demonstrates the general validity of the assumptions on which the model is based.

SIMULATION RESULTS

Optimization Technique

To use Equations 55 or 62 for mill simulation, it is first necessary to determine values for the selection and breakage functions. The selection function for large size classes normally is determined by way of batch grinding tests with single-size feed. Examination of the rate of disappearance of the feed (i.e., first order kinetics of disappearance) after incremental amounts of grinding yields sufficient information to determine the initial selection function through the use of

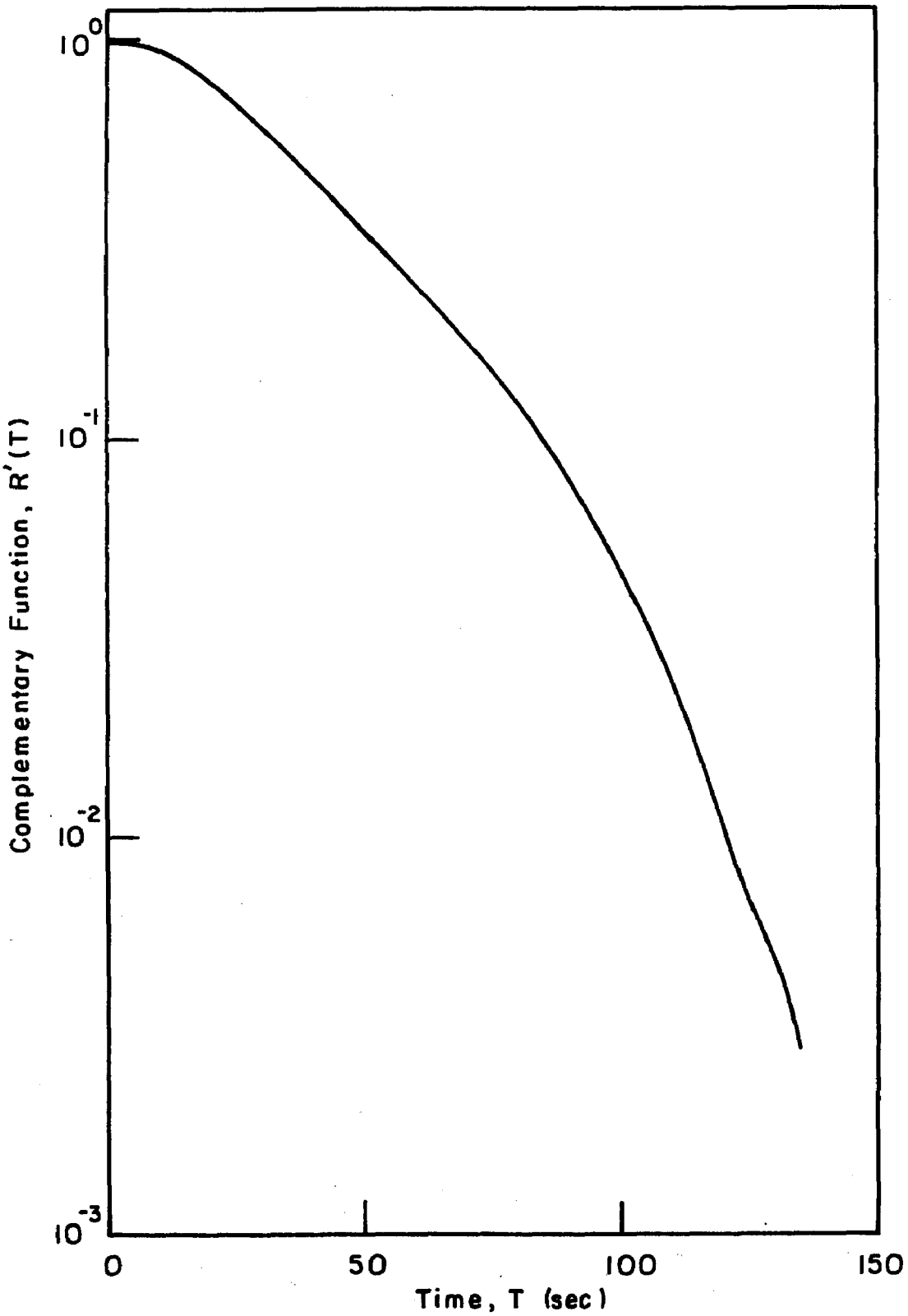

Figure 52. Complementary residence time function.

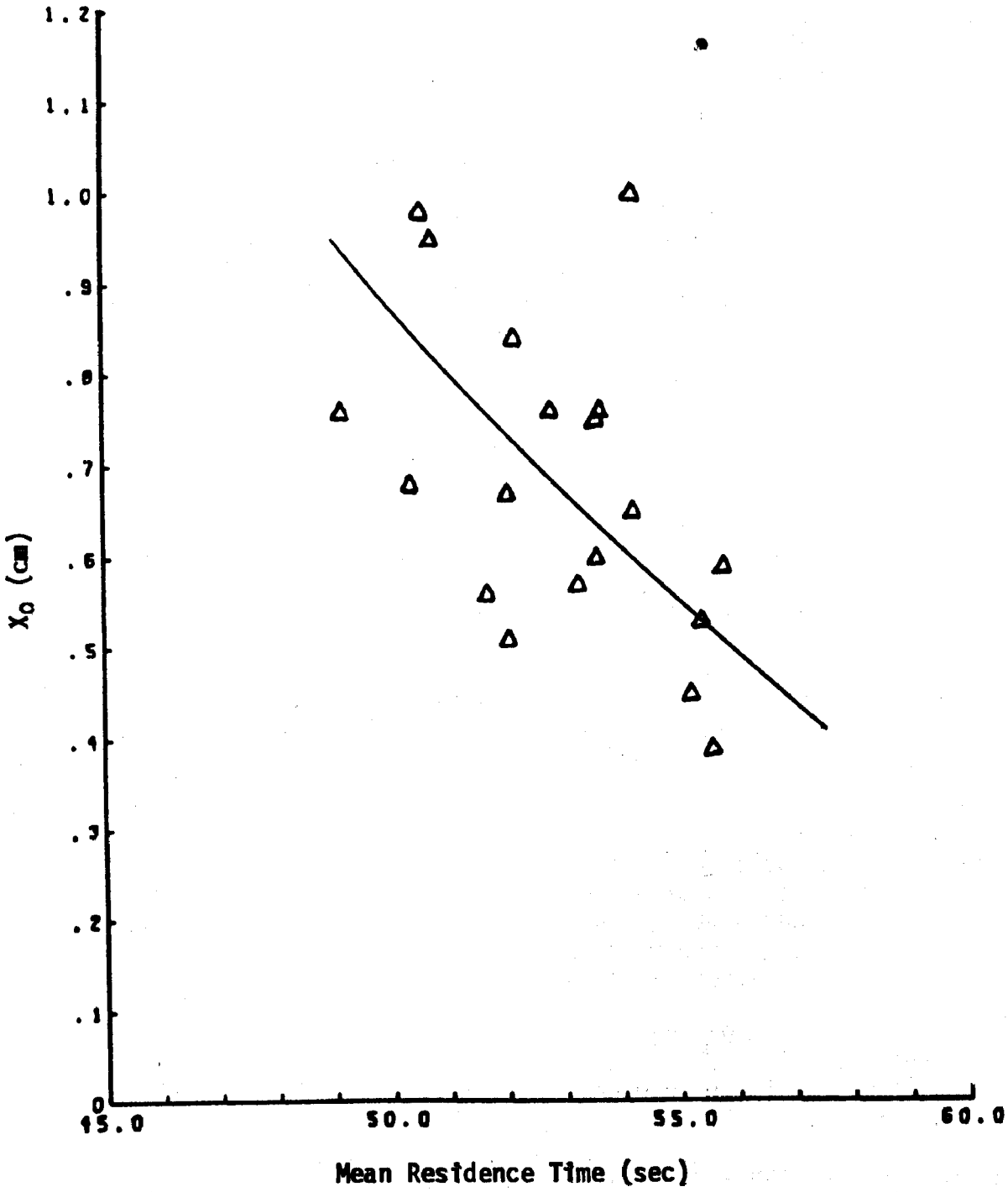

Figure 53. Characteristic size and variation with mean residence time.

$$s_1(t) = \frac{d}{dt}[\ln m_1(t)]$$

The remaining selection functions may be obtained by employing a functional relationship such as Equation 71. Feed-size breakage functions may be obtained through a study of the zero-order production rates of material in size classes that are much smaller than the feed after short grinding times. The remainder of the breakage functions are found through the assumption of "normalizability" of the breakage function.

Because batch tests could not be conducted with the system discussed here, an alternative means of determining selection and breakage functions had to be found. If the techniques described above are followed, the unknown selection and breakage functions are determined from the initial selection function, the particle size under question, and the zero order production constants. A log-log plot of the zero order production rate constants against particle size yields values for K^* and α in Equation 67. Since the particle sizes are known, it follows that once the feed size selection function and K^* and α from Equation 67 are determined, the system is completely described. Therefore, rather than having to determine the n + 1 unknowns (n zero order production constants and the feed size selection function) of the n-size class system, it is necessary only to determine the values of the three parameters s_1, K^*, and α. For systems with which the batch tests cannot be made, a possible technique for determining s_1, K^* and α is the use of a nonlinear optimization approach.

Austin and Klimpel [19] did some work along such lines, though they determined experimentally values for the breakage function and were seeking alternative means of obtaining selection functions. The objective function chosen to show how well the predicted product matched that of the experimental was the sum of the squares of the errors between predicted and experimental values. An alternative objective function included a weighting factor for those size classes for which experimentally determined selection functions were available. The optimization technique employed by the two researchers was the conjugate gradient technique proposed by Goldfarb and Lapidus [23]. The conjugate gradient technique can be used in solving (minimizing) the general nonlinear, n dimensional objective function, subject to certain univariant constraints, i.e.,

$$0 \leq x_i \leq C_i \quad , \quad i = 1, 2{,}000, n \tag{79}$$

where x_i = a principal variable of the objective function, and
C_i = a limiting value.

In the present study, the assumption that Equation 68 holds for all values of i imposes an additional constraint, namely that

$$B_{2,1} = \frac{K^*}{s_1}\left(\frac{x_2^{\,2}}{x_1 x_2}\right)^{\alpha/2} = 1 \tag{80}$$

Further equality constraints that may be placed on the problem are

$$\sum_{i=1}^{n} m_{i\ \text{predicted}} = 1 \tag{81}$$

and

$$m_{i\ \text{experimental}} - m_{i\ \text{predicted}} = 0;\ i = 1,2,\ldots,n \tag{82}$$

It is possible to reduce the number of equality constraints involved by noting that satisfaction of the last set of constraints automatically satisfies the second (although the converse is generally not true). An objective function to be minimized may then be formed through a combination of the first and third equality constraints.

The optimization technique selected for use in the present work is based on Powell's nonderivative search method [24] for unconstrained problems. Powell's basic technique was modified by Fiacco and McCormick [25] to include the use of penalty functions for constraints and was further modified and adapted for use on a CDC 6400 by Radcliffe and Suh [26]. Complete descriptions of the techniques and modifications are available in the source articles and texts and hence are not presented here. The constrained objective function to be minimized took on the exterior penalty function form

$$u(\underline{x}) = F(\underline{x}) + \frac{1}{r_g} \sum_{i=1}^{m_g} [g_i(\underline{x})]^2 + \frac{1}{r_h} \sum_{i=1}^{m_h} [h_i(\underline{x})]^2 \tag{83}$$

where: $F(\underline{x})$ = unconstrained objective function,
$g_i(\underline{x})$ = inequality constraint,
$h_i(\underline{x})$ = equality constraint, and
r_g, r_h = inequality and equality constraint weighting factors that decrease as each suboptimum is found.

While operating in a feasible region, the $g_i(\underline{x})$ are set equal to zero, leaving only the weighted equality constraints and the unconstrained objective function. It is to be expected that the choice of unconstrained objective function and equality constraints would have a bearing on the efficiency of the solution.

For the current problem, it was found that in the initial stages of the search, convergence was facilitated by forming the unconstrained objective function from

$$F(\underline{x}) = \left|1.0 - B_{21}\right| \tag{84}$$

and by allowing the squares of the errors to be added as equality constraints. Once a feasible region was established by this method for the variables s_1, K^*, and α, it was possible to solve the problem as an unconstrained minimization problem using the values of s_1, K^* and α previously found as initial guesses and the sum of the squares of the errors as an objective function.

Results

Several minimizations were made in correspondence with different flow rates and experimental size distributions. The results are presented in Table 19. The sum of the squares of the errors ranged from 0.0614 to 0.0028, with an average of 0.0200. The exponent α from Equation 67 remains relatively constant ($\alpha_{ave} = 0.835$, whereas the constant K* ranges between 0.19 and 0.41. Values of K* are plotted against feed rate in Figure 54. Although K* decreases with flow rate before achieving a constant value, the ratio of K* to s_1, is, in almost all cases, close to unity. The initial selection function is plotted in Figure 55 and shows a trend to decrease with flow rate from 1 to 4 metric tons/hr, and thereafter to maintain a constant value of approximately 0.29. The implication therefore is that for low flow rates, the mass of material within the mill (how densely it is packed) affects the selection function; but as the flow rate increases further, the change in mill holdup has little or no effect.

The model suffers from its failure to give a value for B_{21} equal to one. At the lowest flow rate, B_{21} is equal to 0.35, and at times it even exceeds 1.0 (which, according to the definition, is physically impossible). The difficulty is caused by attempting to apply Equation 68 to all values of i, when in general it has been noted [17] that the zero order production rate constants for the coarse size classes cannot be characterized by the same equation as for the fine sizes. The cumulative breakage function presented in this section must then be taken to be the best compromise between the characteristic equations for both the coarse and fine size ranges.

Figure 56 shows the relationship between the initial cumulative breakage function, B_{21}, and flow rate. As might be expected from the fact that K^*/s_1 generally is close to unity (particularly at higher flow rates) and α is constant, B_{21} remains relatively constant.

A listing of the optimization program is presented in the Appendix. Since the values of s_1, K*, and α tend to remain constant for higher flow rates, a flow rate of 7.4 metric tons/hr was chosen as a test of the ability of the model to predict the output of the mill. With $s_1 = 0.290$, $K^* = 28$, and $\alpha = 0.804$, a product size distribution was predicted and compared to the experimental results. Figure 57 graphically demonstrates differences between the predicted and actual measured size distributions. Except for the first less-than-zero value for m_i, the predicted m_i values follow the experimental values fairly closely. The sum of the squares of the errors in the simulation trial was under 0.02. This fact demonstrates that the compromise breakage functions obtained as a result of parameter estimation permit reasonably good results to be obtained with simulation. A listing of the simulation program is also provided in the Appendix.

CONCLUDING REMARKS

Despite the fact that B_{21} is not predicted to equal unity, the size-discrete, time-continuous model adapted to describe the swing hammermill size reduction of refuse is shown to be a close approximation to the real system. Significant differences between this system and typical ball mill

Table 19. SUMMARY OF OPTIMIZATION RESULTS

s_1	K*	K^*/s_1	α	F(x)	B_{21}	Q (tons/hr)
.405	.190	.469	.826	.0119	.351	.9
.297	.347	1.168	.804	.0271	.884	1.4
2.95	.347	1.176	.804	.0614	.890	1.5
.300	.336	1.120	.804	.0504	.849	1.5
.106	.311	2.934	.809	.00597	2.220	2.1
.407	.411	1.010	.977	.00458	.720	2.4
.336	.253	.753	.805	.0161	.569	2.4
.514	.396	.770	1.057	.00166	.553	2.4
.306	.294	.961	.804	.0215	.726	3.0
.332	.252	.759	.814	.00745	.573	3.4
.071	.292	4.113	.841	.00964	3.090	3.8
.073	.300	4.110	.898	.00277	3.010	3.8
.287	.314	1.094	.804	.0196	.829	3.9
.286	.308	1.077	.804	.0549	.815	4.6
.285	.308	1.081	.804	.0249	.817	5.0
.289	.290	1.003	.804	.0168	.759	6.2
.290	.284	.979	.804	.0135	.742	6.6
.290	.281	.969	.804	.0123	.732	7.0
.291	.276	.948	.804	.0168	.717	7.4

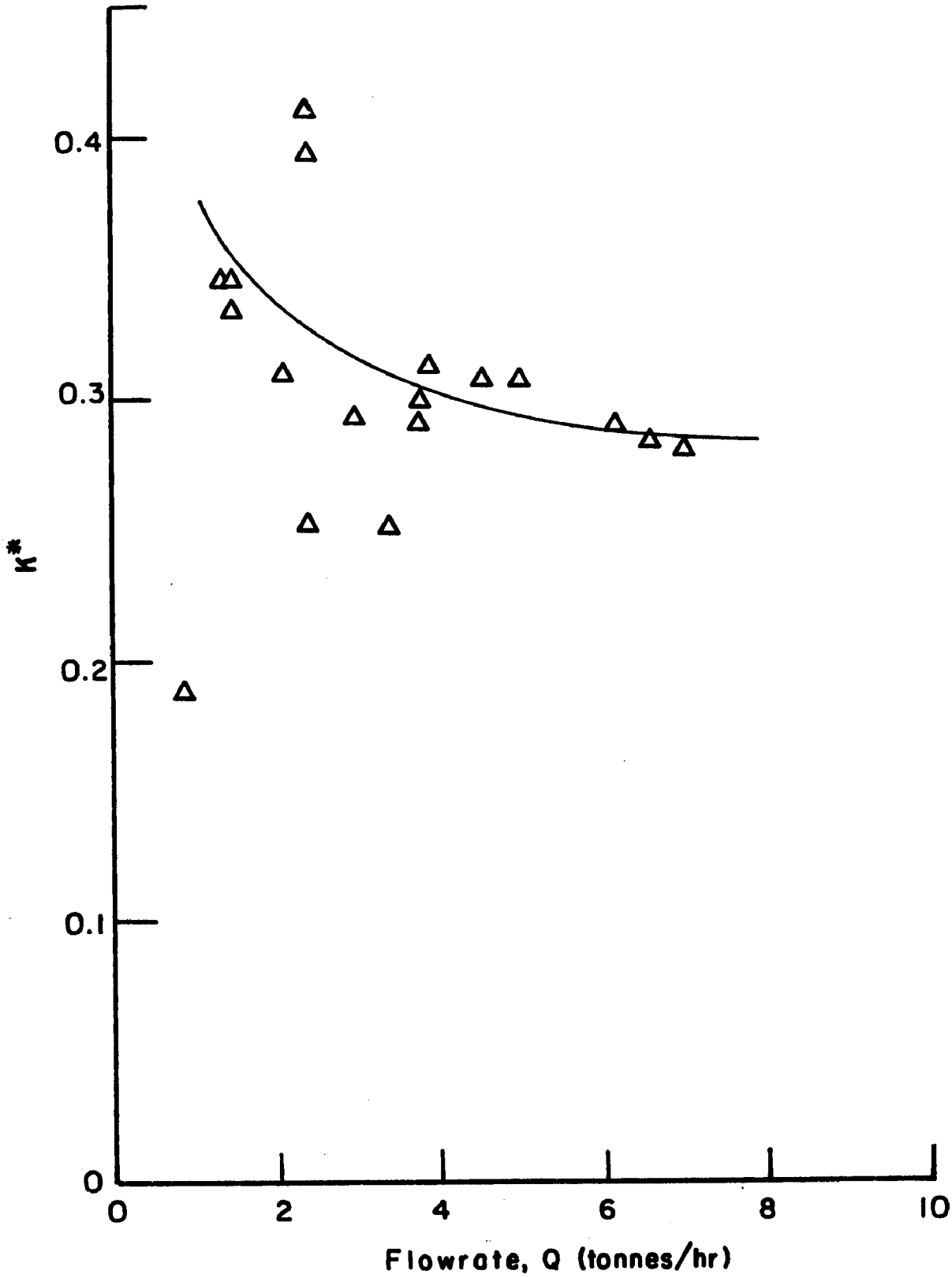

Figure 54. Variation of K* flow rate.

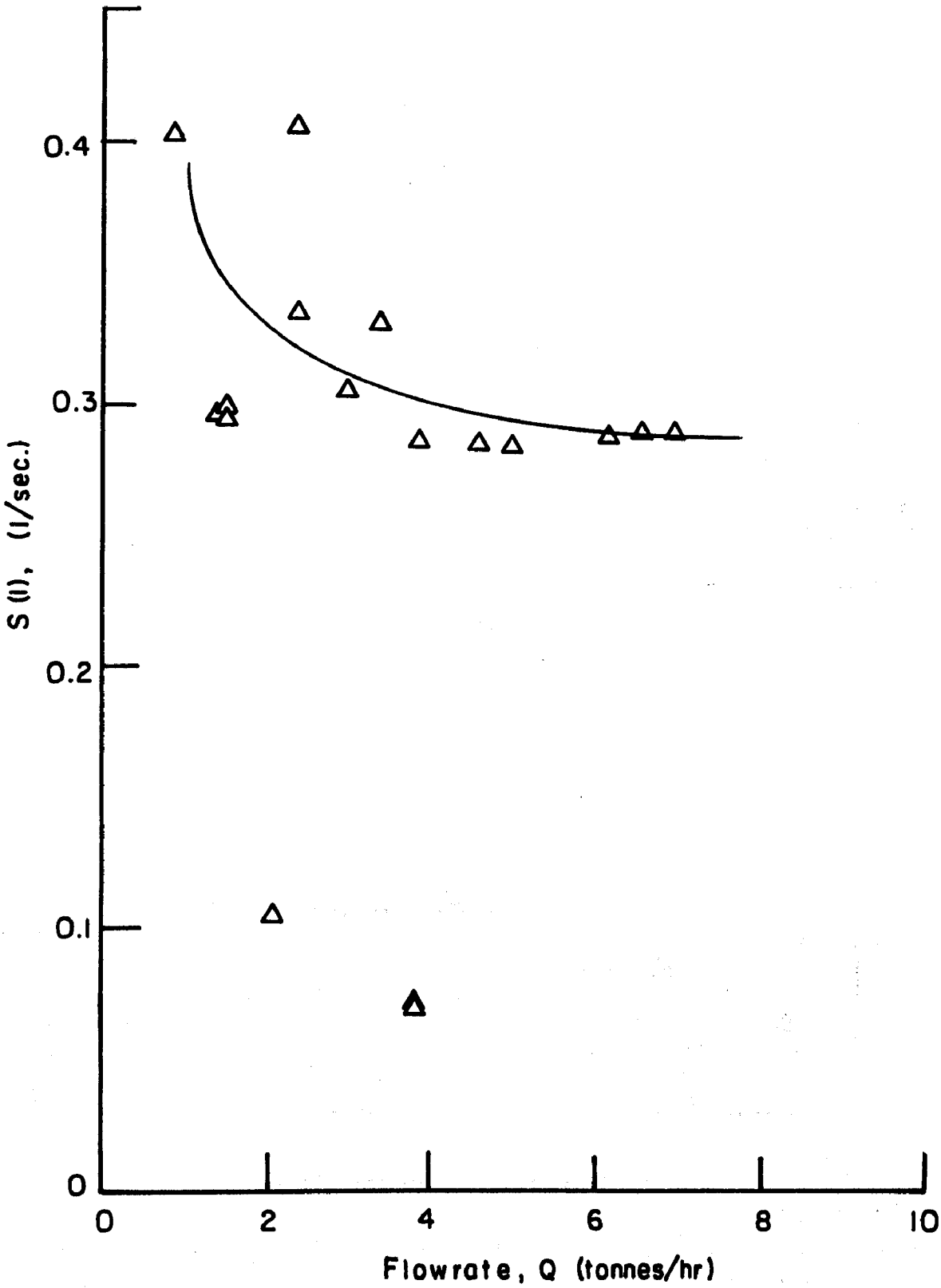

Figure 55. Variation of initial selection function with flow rate.

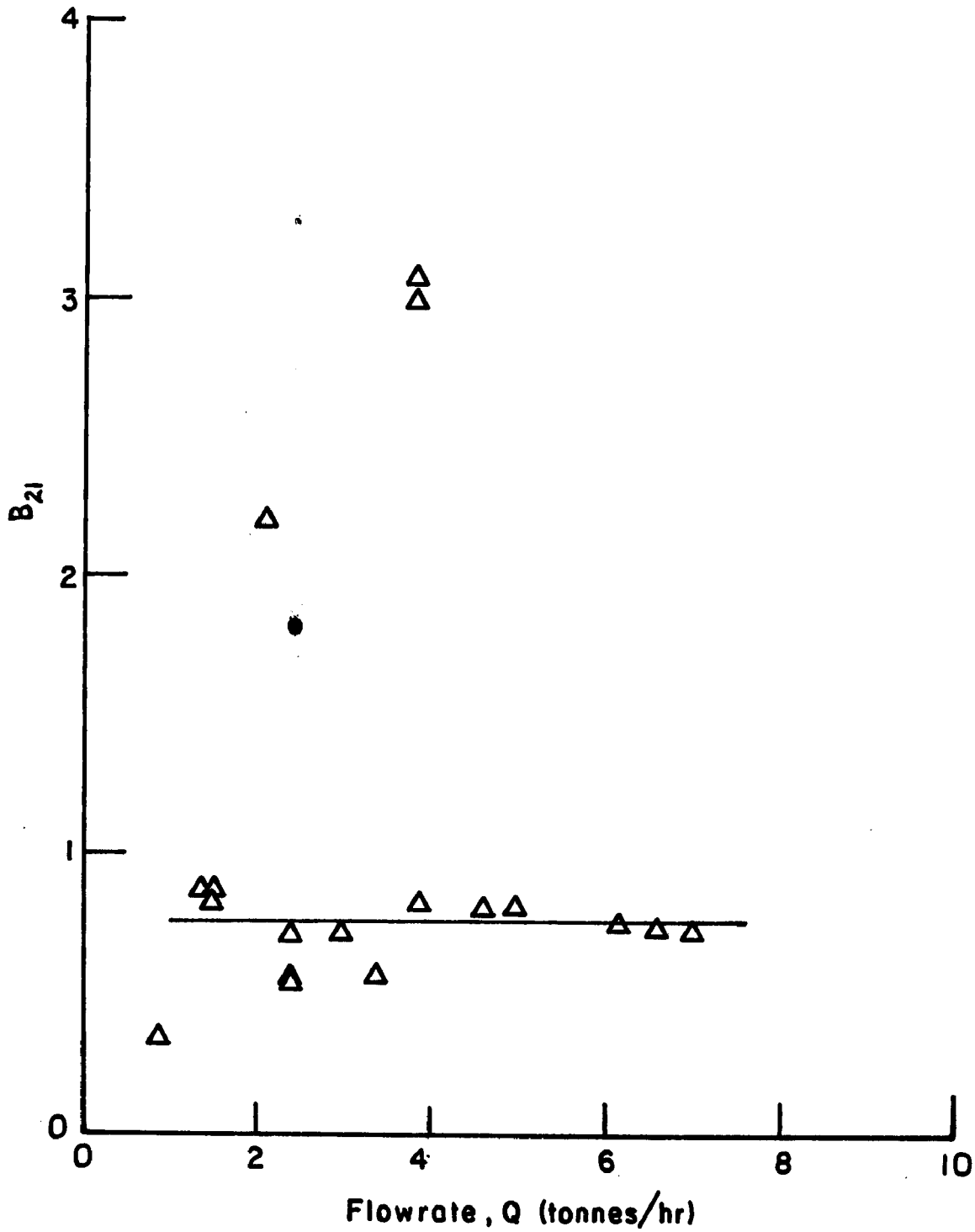

Figure 56. Variation of initial breakage function with flow rate.

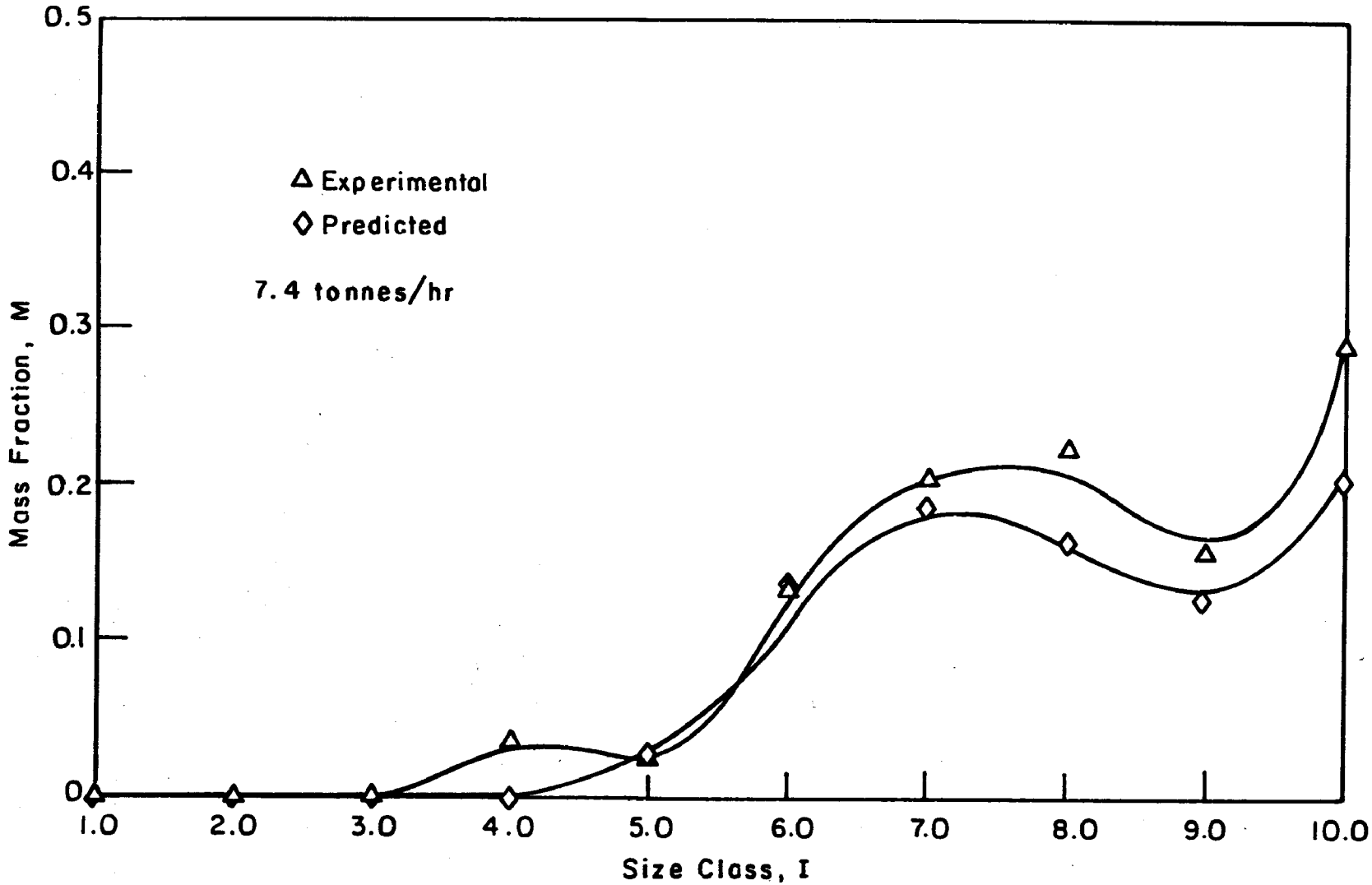

Figure 57. Comparison of predicted and actual measured size distributions.

applications are that (1) the mean residence time increases with refuse flow rate rather than decreasing as in overflow discharge ball mills, and (2) it is not possible to determine experimentally any of the selection or breakage functions. The optimization technique used has been found to be an effective means of finding values for the selection and a compromise breakage function.

The fractional rate of breakage decreases with flow rate, while the zero-order production rate remains constant. Therefore, from a knowledge of the mean residence time and the relation between s_1 and Q, the product size distribution may be predicted for any set of mill operating conditions. An alternative to the single stage of breakage model for predicting size distribution has been found that takes into account the fact that the residence time is appreciable.

SECTION 7

UNIT OPERATION AND SYSTEM DESIGN CONSIDERATIONS

This section deals with the manner in which the size reduction data obtained from the experimental protocol can be used and extended. These generalizations pertain to performance predictions of both unit operations and system configurations.

GRATE SPACING CONSIDERATIONS

To develop the capability of predicting energy requirements and degree of size reduction for various grate spacings, a functional relationship between specific energy (E_0) and degree of size reduction (Z_0) as well as a a relationship between Z_0 and the grate spacing parameter D_0/F_0 was established. These relations assumed the general form of $y = ax^b$, namely

$$E_0 = a_1 z_0^{b_1} = a_1[(F_0 - x_0)/F_0]^{b_1} \tag{85}$$

and

$$Z_0 = a_2(D_0/F_0)^{b_2} \tag{86}$$

Using the raw MSW data with grate openings of 4.8 cm (1.9 in.), 2.5 cm (1.0 in.), and 1.8 cm (0.7 in.), specific energy can be expressed in terms of Z_0 as follows:

$$D_0 = 4.8 \text{ cm } (1.9 \text{ in.}) \quad E_0(\text{MJ/metric ton}) = 61.4\ Z_0^{1.40} \tag{87}$$

$$E_0(\text{kWh/ton}) = 15.5\ Z_0^{1.40} \tag{88}$$

$$D_0 = 2.5 \text{ cm } (1.0 \text{ in.}) \quad E_0(\text{MJ/metric ton}) = 109.3\ Z_0^{1.17} \tag{89}$$

$$E_0(\text{kWh/ton}) = 27.6\ Z_0^{1.17} \tag{90}$$

$$D_0 = 1.8 \text{ cm } (0.7 \text{ in.}) \quad E_0(\text{MJ/metric ton}) = 172.3\ Z_0^{0.82} \tag{91}$$

$$E_0(\text{kWh/ton}) = 43.5\ Z_0^{0.82} \tag{92}$$

The correlation coefficient of each of the above equations exceeded 0.95.

To complete the generalization, the coefficients a_1, a_2, b_1 and b_2 in Equations 85 and 86 can be expressed in terms of D_0 in the form such as

a_1 = (CONST) $D_o^{(CONST)}$ etc. The expressions for these coefficients take the form

$$a_1 = 295.23\ D_o(cm)^{-1.01} \text{ for Equations 87, 89, and 91} \tag{93}$$

$$a_1 = 29.21\ D_o\ (in.)^{-1.01} \text{ for Equations 88, 90, and 92} \tag{94}$$

and

$$b_1 = 0.66\ D_o\ (cm)^{0.50} \text{ for Equations 87, 89, and 91} \tag{95}$$

$$b_1 = 1.05\ D_o\ (in.)^{0.50} \text{ for Equations 88, 90, and 92} \tag{96}$$

with correlation coefficients of each equation exceeding 0.87.

Substitution of Equations 91 and 93 into Equation 85 yields

$$E_o(\text{MJ/metric ton}) = 295.23\ D_o\ (cm)^{-1.01} Z_o^{\ 0.66\ D_o(cm)^{0.50}} \tag{97}$$

Similarly, substitution of Equations 92 and 94 into Equation 85 yields

$$E_o(\text{kWh/ton}) = 29.21\ D_o\ (in.)^{-1.01}\ Z_o^{\ 1.05\ D_o\ (in.)^{0.50}} \tag{98}$$

These relations can be used to predict E_o for any grate spacing in the mill, the highest confidence being within the range of the data.

Applying a similar procedure for expressing Equation 86 yields the following:

$$D_o = 4.8 \text{ cm } (1.0 \text{ in.}):\quad Z_o = 0.65\ (D_o/F_o)^{-0.28} \tag{99}$$

$$D_o = 2.5 \text{ cm } (1.0 \text{ in.}):\quad Z_o = 0.45\ (D_o/F_o)^{-0.43} \tag{100}$$

$$D_o = 1.8 \text{ cm } (0.7 \text{ in.}):\quad Z_o = 0.34\ (D_o/F_o)^{-0.51} \tag{101}$$

The correlation coefficients for these equations were greater than 0.94 in all cases. Likewise, the coefficient a_2 and b_2 can be expressed as

$$a_2 = 0.24\ D_o\ (cm)^{0.65} \tag{102}$$

$$a_2 = 0.43\ D_o\ (in.)^{0.65} \tag{103}$$

and

$$b_2 = -0.72\ D_o\ (cm)^{-0.60} \tag{104}$$

$$b_2 = -0.42\ D_o\ (in.)^{-0.60} \tag{105}$$

with correlation coefficients of each equation exceeding 0.98.

Substitution of Equations 102 and 104 into Equation 86 yields

$$Z_o = 0.24\ D_o\ (cm)^{0.65}\ (D_o/F_o)^{-0.72}\ D_o\ (cm)^{-0.60} \tag{106}$$

Substitution of Equations 103 and 105 into Equation 86 yields

$$Z_o = 0.43\ D_o\ (in.)^{0.65}(D_o/F_o)^{-0.42}\ D_o\ (in.)^{-0.60} \tag{107}$$

Equations 106 and 107 can now be used to predict the characteristic product size (X_o) through the definition of degree of size reduction (Z_o) when F_o and D_o are specified. As is the case with the energy expressions, the empirical nature of the equations limits their useful range.

It is interesting to note that the general form of Equations 97 and 98 is

$$E_o = \alpha D_o^{-1}\ Z_o^{\beta}\ D_o^{0.5} \tag{108}$$

where the parametric influence of D_o enters the equation both as a reciprocal and also as an exponent of Z_o. The parametric influence of D_o is also apparent in the equations expressing Z_o in terms of the ratio D_o/F_o, Equations 106 and 107.

The relationships among E_o, Z_o, and D_o/F_o (ie., Equations 97, 98, 106 and 107) can be used to develop curves that describe size reduction using the Gruendler hammermill (Figure 58). This figure presents analytical results for size reduction of raw refuse as a function of various hypothetical grate spacings.

The data shown in Figure 58 are the result of mathematical calculations based on the manipulative procedure outlined previously in this section as opposed to the actual test data presented in Figure 34. Comparison of the analytical computations (Figure 58) and actual test results (Figure 34) shows good agreement.

The primary purpose and utility of the analytical approach is to allow prediction and evaluation of shredder performance without resorting to actual testing. For example, in the following section on unit process optimization, different processing options will be evaluated analytically to ascertain the optimum processing sequence for size reduction of raw MSW.

TORQUE RELATIONS

In a rotating system subject to drag, the torque necessary to overcome the drag force is given by

$$T = \int_o^{R_2} r dF_d \tag{109}$$

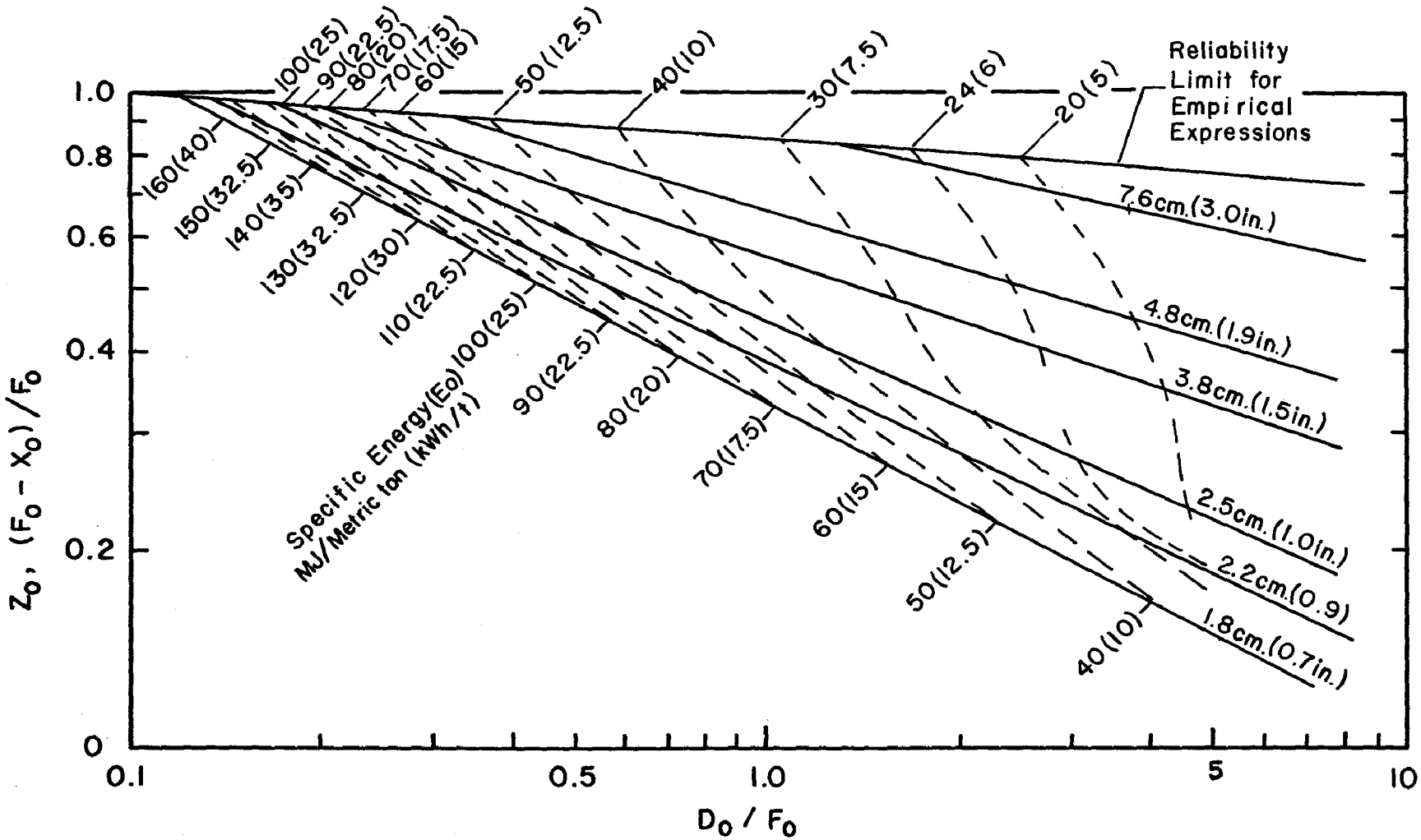

Figure 58. Size reduction of raw MSW extended to several different grate openings.

In addition, it has often been noted that the force of drag on a body of cross-sectional area A_{cs} is given by

$$F_d = C_d \frac{\rho v^2 A_{cs}}{2} \tag{110}$$

Replacing v^2 by $(rw)^2$ in Equation 110, taking the derivative with respect to r, and substituting the resulting expression into Equation 109 gives

$$T = \frac{3}{2} C_d Nh \rho\omega^2 \int_0^{R_2} r^3 dr \tag{111}$$

in which A_{cs} has been replaced by Nhr where N is the number of hammers, h is the hammer width, and r is the total hammer length. Since most hammermills are designed so that hammers are offset from the center of rotation and only a portion of the hammer actually collides with the refuse in the mill, the lower limit of integration in Equation 111 may be changed from zero to R_1, the radius at which the hammer first becomes exposed to refuse. Solving Equation 111 then yields

$$T = \frac{3}{8} C_d Nh \rho \frac{\omega^2}{2}(R_2-R_1)[R_2^3 + R_2^2R_1 + R_2R_1^2 + R_1^3] \tag{112}$$

The effect of varying the physical characteristics of the mill (holding refuse density constant) may be found by taking the ratio of Equation 112 for different sets of operating conditions, i.e.,

$$\frac{T_a}{T_b} = \left(\frac{N_a}{N_b}\right)\left(\frac{h_a}{h_b}\right)\left(\frac{R_{2_a} - R_{1_a}}{R_{2_b} - R_{1_b}}\right)\left(\frac{RPM_a}{RPM_b}\right)\left[\frac{R_{2a}^3 + R_{2a}^2R_{1a} + R_{2a}R_1^2 + R_{1a}^3}{R_{2b}^3 + R_{2b}^2R_{1b} + R_{2b}R_{1b}^2 + R_{1b}^3}\right] \tag{113}$$

UNIT PROCESS OPTIMIZATION

The determination of the optimum processing sequence to minimize energy consumption during size reduction is one of the perplexing problems facing the resource recovery industry. Both single-stage and two-stage shredding of raw MSW have been practiced for a number of years, with the proponents of either camp maintaining that theirs is the optimum method of size reduction. If indeed there is an optimum manner in which to reduce raw MSW as well as other fractions of processed refuse, considerable energy savings could be realized, since the typical resource recovery plant may process as much as 1000 metric tons/day.

The present size reduction data obtained for raw MSW, ACLF, and SLF are applicable to the controversy involving the optimal processing sequence for size reduction. To shed light on this problem, the results of our studies will be extended to hypothetical resource recovery systems to ascertain the optimum processing sequence. Although the actual numerical values for specific energy and product size may be different for some grinders shredding the same material and using identical grate opening sizes, the trends

established here are general enough to apply to most size reduction processes. The hypothetical processes to be studied will involve the size reduction of ACLF as well as raw MSW and will be limited to the consideration of single- and two-stage size reduction.

Raw MSW

To determine the relative merits of single- and two-stage size reduction of raw MSW, two cases are examined. The first case assumes a material with a characteristic feed size of 15.2 cm (6.0 in.) (a typical raw MSW) and a desired characteristic product size of approximately 0.60 cm (0.24 in.). Two different processing sequences for two-stage size reduction can be developed for the preceding conditions with the use of Figure 59. This figure was developed using the analytical approach described in this section under Grate Spacing Considerations. It contains curves for the grate spacings of interest -- namely, 7.6, 4.8, 2.5, and 1.8-cm (3.0, 1.9, 1.0, and 0.7 in.).

To obtain the desired output size, an iterative procedure must be used to determine the appropriate grate opening sizes (Table 20). The first processing sequence requires a grate opening size (D_0) of 2.5 cm (1.0 in.) for both primary and secondary size reduction. Cumulative energy consumption is 107 MJ/metric ton (27 kWh/ton), with 75 and 32 MJ/metric ton (19 and 8 kWh/ton) required for primary and secondary shreddings, respectively.

The second processing sequence requires primary and secondary size reduction utilizing 7.6- and 1.8-cm (3.0- and 0.7-in.) grate openings, respectively (Table 20). The cumulative energy consumption is 124 MJ/metric ton (31 kWh/ton) with 37 and 87 MJ/metric ton (9 and 22 kWh/ton) required for primary and secondary size reduction, respectively.

Single-stage size reduction to the desired product size is affected by utilizing a grate spacing of 1.8 cm (0.7 in.) (Table 20). This method requires 158 MJ/metric ton (40 kWh/ton).

Minimum energy consumption to meet the assumed specifications is realized using two-stage size reduction with both stages having 2.5-cm (1.0-in.) grate spacings. Notice that even though the two-stage size reduction sequences are more energy efficient than the single-stage system, there is also an optimum between the different two-stage systems.

The second case investigated assumes the same feed size as used previously. However, the desired product size is now approximately 0.90 cm (0.35 in.). To arrive at the desired product size, two-stage size reduction using 4.8-cm (1.9-in.) grate openings in each shredder is required (Table 20). The cumulative energy required by this sequence is 75 MJ/metric ton (19 kWh/ton), with 55 MJ/metric ton (14 kWh/ton) required for the first stage and 20 MJ/metric ton (5 kWh/ton) required for the second stage.

Single-stage size reduction to meet the product size specification can be accomplished using a grate spacing of 2.5 cm (1.0 in.). The energy consumption for single-stage size reduction is 91 MJ/metric ton (23 kWh/ton),

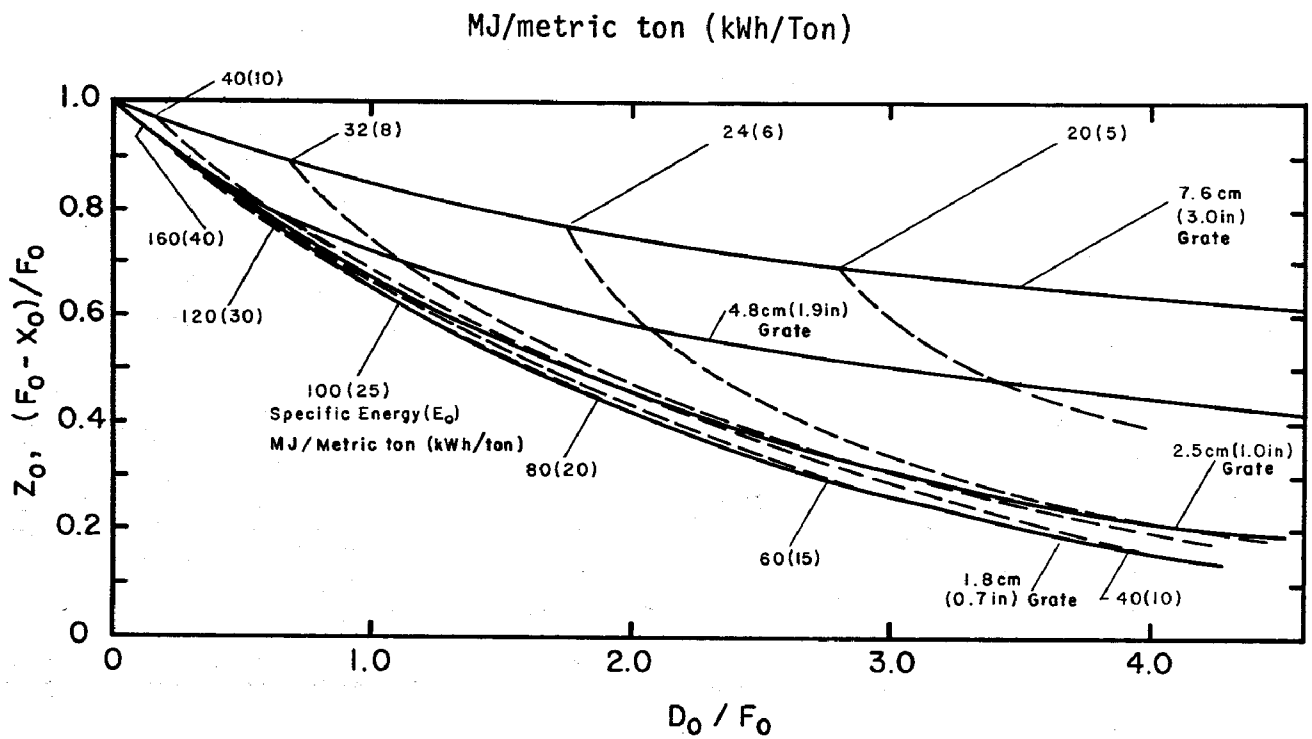

Figure 59. Degree of size reduction and specific energy requirement for shredding raw MSW as a function of D_o/F_o.

Table 20. SINGLE- AND DOUBLE-STAGE SHREDDING OF RAW MSW IN THE GRUENDLER HAMMERMILL

Stages of size reduction	F_o cm	F_o (in.)	D_o cm	D_o (in.)	D_o/F_o	Z_o	X_o/F_o	X_o cm	X_o (in.)	E_o MJ/mt*	E_o (kWh/ton)	Cumulative E_o MJ/mt*	Cumulative E_o (kWh/ton)
Case 1:													
Two	15.2	(6.0)	2.5	(1.0)	0.17	0.94	0.06	0.91	(0.36)	75	(19)	107	(27)
	0.91	(0.36)	2.5	(1.0)	2.78	0.34	0.66	0.61	(0.24)	32	(8)	---	
Two	15.2	(6.0)	7.6	(3.0)	0.50	0.92	0.08	1.22	(0.48)	37	(9)	124	(31)
	1.21	(0.48)	1.8	(0.7)	1.46	0.53	0.47	0.58	(0.23)	87	(22)	---	
One	15.2	(6.0)	1.8	(0.7)	0.12	0.96	0.04	0.64	(0.25)	158	(40)	158	(40)
Case 2:													
Two	15.2	(6.0)	4.8	(1.9)	0.32	0.88	0.12	1.83	(0.72)	55	(14)	75	(19)
	1.83	(0.72)	4.8	(1.9)	2.64	0.52	0.48	0.89	(0.35)	20	(5)	---	
One	15.2	(6.0)	2.5	(1.0)	0.17	0.94	0.06	0.91	(0.36)	91	(23)	91	(23)

*mt = metric ton

or approximately 21 percent greater than that for the two-stage sequence described previously.

The trend evolved here indicates that two-stage size reduction is the preferred mode of processing with regard to raw MSW. However, because of the complicated relationships among E_0, D_0, and F_0, there may also be an optimal sequence among various two-stage alternatives. Consequently, care must be taken to consider a number of possible combinations of grate spacings to achive the desired product size with a minimum expenditure of energy.

Air Classified Light Fraction

Single- and double-stage size reductions of ACLF were investigated to determine if an optimal processing sequence exists for this material. This section examines three different cases with the help of Figure 35 -- namely, reduction of material from 10.16 to 0.71 cm (4.00 to 0.28 in.), from 5.08 to 0.70 cm (2.00 to 0.28 in.), and from 2.54 to 0.35 cm (1.00 to 0.14 in.) (Table 21).

As with raw MSW, double-stage size reduction of the ACLF requires less energy than single-stage reduction for all cases examined. The discrepancy between cumulative energy consumption of single-stage and double-stage sequences in each case diminishes as the initial feed size decreases. The cumulative energy figures in Table 21 show the increases in energy requirements of single-stage processing as opposed to double-stage processing as 124 percent, 54 percent, and 46 percent for feed sizes of 10.16, 5.08, and 2.54 cm (4.00, 2.00, and 1.00 in.), respectively.

The double-stage shredding process thus offers the optimal method for size reduction of the ACLF. The discrepancies in total energy expenditure between single- and double-stage processing sequences are generally larger than those outlined previously for raw MSW.

Screened Light Fraction

The consequences of single- and double-stage size reduction of SLF are evaluated for three different cases (Figure 36) assuming feed sizes of 10.16, 5,08, and 2.54 cm (4.00, 2.00, and 1.00 in.), respectively, and a desired product size of approximately 1.27 cm (0.50 in.) (Table 22).

In each case, double-stage size reduction requires less total energy than single-stage. As with ACLF, the difference between energy required for double- versus single-stage size reduction for each case tends to diminish as the initial feed size decreases.

The information developed here on the relative merits of single- and double-stage size reduction of raw MSW, ACLF, and SLF indicates that double-stage size reduction yields the minimum expenditure of energy. Definite energy savings can result, particularly for large overall degrees of size reduction (i.e., X_0/F_0 approaching zero). The data presented here are especially pertinent to the size reduction of ACLF and SLF.

Table 21. SINGLE- AND DOUBLE-STAGE SHREDDING OF ACLF IN THE W-W HAMMERMILL

Stages of size reduction	F_o cm (in.)	D_o cm (in.)	D_o/F_o	Z_o	X_o/F_o	X_o cm (in.)	E_o MJ/mt*	E_o (kWh/ton)	Cumulative E_o MJ/mt*	Cumulative E_o (kWh/ton)
Case 1:										
Two	10.16 (4.00)	2.54 (1.00)	0.25	0.90	0.10	1.02 (0.40)	71	(18)	115	(29)
	1.02 (0.40)	1.91 (0.75)	1.88	0.28	0.72	0.74 (0.29)	44	(11)	---	
One	10.16 (4.00)	1.27 (0.50)	0.13	0.93	0.07	0.71 (0.28)	257	(65)	257	(65)
Case 2:										
Two	5.08 (2.00)	1.91 (0.75)	0.38	0.82	0.18	0.91 (0.36)	91	(23)	131	(33)
	0.91 (0.36)	1.91 (0.75)	2.08	0.23	0.77	0.71 (0.28)	40	(10)	---	
One	5.08 (2.00)	1.91 (0.50)	0.25	0.87	0.13	0.66 (0.26)	202	(51)	202	(51)
Case 3:										
Two	2.54 (1.00)	1.91 (0.75)	0.75	0.66	0.34	0.86 (0.34)	63	(16)	328	(83)
	0.86 (0.34)	0.64 (0.25)	0.74	0.62	0.38	0.33 (0.13)	265	(67)	---	
One	2.54 (1.00)	0.64 (0.25)	0.25	0.86	0.14	0.36 (0.14)	479	(121)	479	(121)

*mt = metric ton

Table 22. SINGLE- AND DOUBLE-STAGE SHREDDING OF SLF IN THE W-W HAMMERMILL

Stages of size reduction	F_o cm (in.)	D_o cm (in.)	D_o/F_o	Z_o	X_o/F_o	X_o cm (in.)	E_o MJ/mt*	E_o (kWh/ton)	Cumulative E_o MJ/mt*	Cumulative E_o (kWh/ton)
Case 1:										
Two	10.16 (4.00)	1.91 (0.75)	0.19	0.85	0.15	1.52 (0.60)	269	(68)	301	(76)
	1.52 (0.60)	1.91 (0.75)	1.25	0.19	0.81	1.24 (0.49)	32	(8)	---	
One	10.16 (4.00)	0.64 (0.25)	0.06	0.88	0.12	1.22 (0.48)	606	(153)	606	(153)
Case 2:										
Two	5.08 (2.00)	2.54 (1.00)	0.50	0.65	0.35	1.78 (0.70)	91	(23)	139	(35)
	1.78 (0.70)	1.91 (0.75)	1.07	0.27	0.73	1.30 (0.51)	48	(12)	---	
One	5.08 (2.00)	1.27 (0.50)	0.25	0.75	0.25	1.27 (0.50)	297	(75)	297	(75)
Case 3:										
Two	2.54 (1.00)	2.54 (1.00)	1.00	0.38	0.62	1.57 (0.62)	44	(11)	80	(20)
	1.57 (0.62)	1.91 (0.75)	1.21	0.21	0.79	1.24 (0.49)	36	(9)	---	
One	2.54 (1.00)	1.91 (0.75)	0.75	0.51	0.49	1.24 (0.49)	100	(25)	100	(25)

*mt = metric ton

SYSTEM OPTIMIZATION

This section considers extending optimization of the unit operation to a resource recovery processing train to minimize the overall energy expenditure. Through the case study approach, a technique is demonstrated for evaluating different processing configurations with regard to product size and energy consumption. The system chosen for evaluation is a resource recovery process that will recover SLF as fluff refuse-derived fuel (RDF). The fuel specification is assumed to call for a characteristic size of 0.71 cm (0.28 in.). The general processing train is assumed to contain the sequence of shredding, air classification, trommel screening of the light fraction, and subsequent shredding of the SLF to meet the size specification of the RDF. The characteristic size of raw MSW is taken as 15.2 cm (6.0 in.).

Two different processing trains are evaluated (Figure 60). The lower train employs single-stage size reduction for both raw MSW and SLF. Initial shredding of raw MSW is followed by air classification, trommel screening, and final shredding to arrive at the specified product size.

Opposing the above, a train is employed using double-stage size reduction for both raw MSW and SLF. Other than an increase in the number of shredders, the two trains are identical with respect to equipment.

By using Figures 35, 36, and 59 and an iterative procedure, the necessary grate spacings were determined for each train (Figure 60). Note that air classification and screening increase the size of the material after processing with each piece of equipment.

The energy balance on the processing trains is also determined through the use of Figures 35, 36, and 59. The quantity of interest is the total energy required for processing expressed as MJ/metric ton (kWh/ton).

Air classifier and trommel screen splits are assumed to be 70/30 and 71/29, respectively. Since we have previously developed specific energy relationships based on the material being reduced, a mass balance on each train must be calculated to determine the energy contribution of each operation to the total energy requirement (Table 23).

Values for the total energy consumption show that the double-stage train requires 214.6 MJ/metric ton (54.4 kWh/ton) of MSW, whereas the single-stage train requires 244.1 MJ/metric ton (61.9 kWh/ton) of MSW, or 14 percent more than the double-stage train.

An energy pathway diagram (Figure 61) shows each processing sequence, with the interval between letters referring to the various processing operations (primary and secondary shredding, air classification, etc.). The greater energy requirement of the single-stage train is evident in this diagram.

The procedure developed here lends itself to evaluations of other processing sequences. The technique requires that data on energy consumption

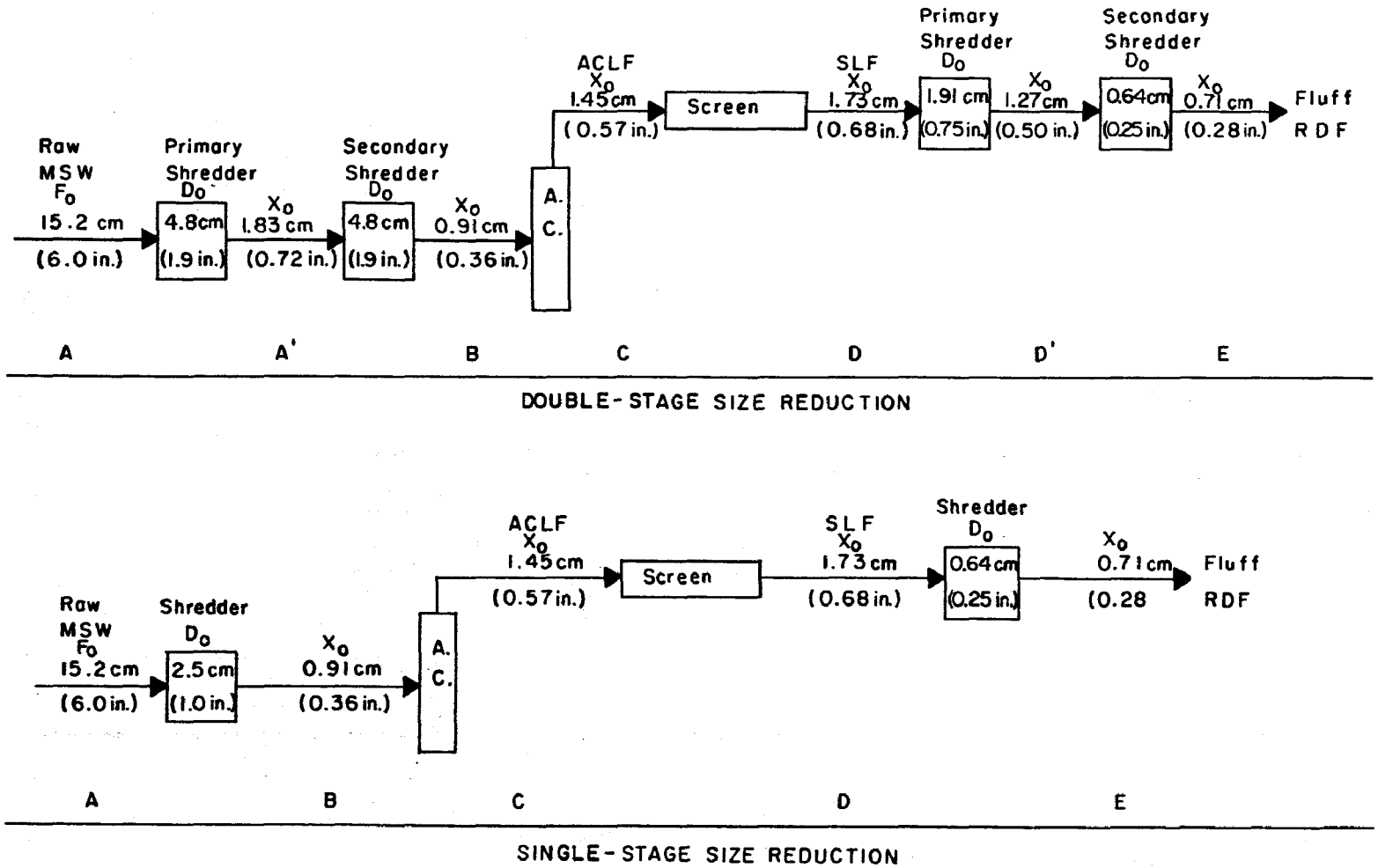

Figure 60. Possible operating configurations for resource recovery units.

Table 23. MASS AND ENERGY BALANCE ON PROCESSING TRAINS FOR RECOVERY OF RDF

Item	Operation	(A) Percent of raw MSW	(B) E_o/operation MJ/mt*	(kWh/ ton)	(A)x(B) E /metric ton (ton) raw MSW MJ	(kWh)	Energy Pathway
Input material for double-stage train:							
Raw MSW	Primary shredding	100	55	(14)	55	(14)	AA'
Raw MSW	Secondary shredding	100	20	(5)	20	(5)	A'B'
Raw MSW	Air classification	100	15	(4)	15	(4)	BC
ACLF	Trommel screening	70	8	(2)	5.6	(1.4)	CD
SLF	Primary shredding	50	44	(11)	22.0	(5.5)	DD'
SLF	Secondary shredding	50	194	(49)	97.0	(24.5)	D'E
Total energy					214.6	(54.4)	
Input material for single-stage train:							
Raw MSW	Single-stage shredding	100	91	(23)	91	(23)	AB
Raw MSW	Air classification	100	15	(4)	15	(4)	BC
ACLF	Trommel screening	70	8	(2)	5.6	(1.4)	CD
SLF	Single-stage shredding	50	265	(67)	132.5	(33.5)	DE
Total energy					244.1	(61.9)	

* mt = metric ton

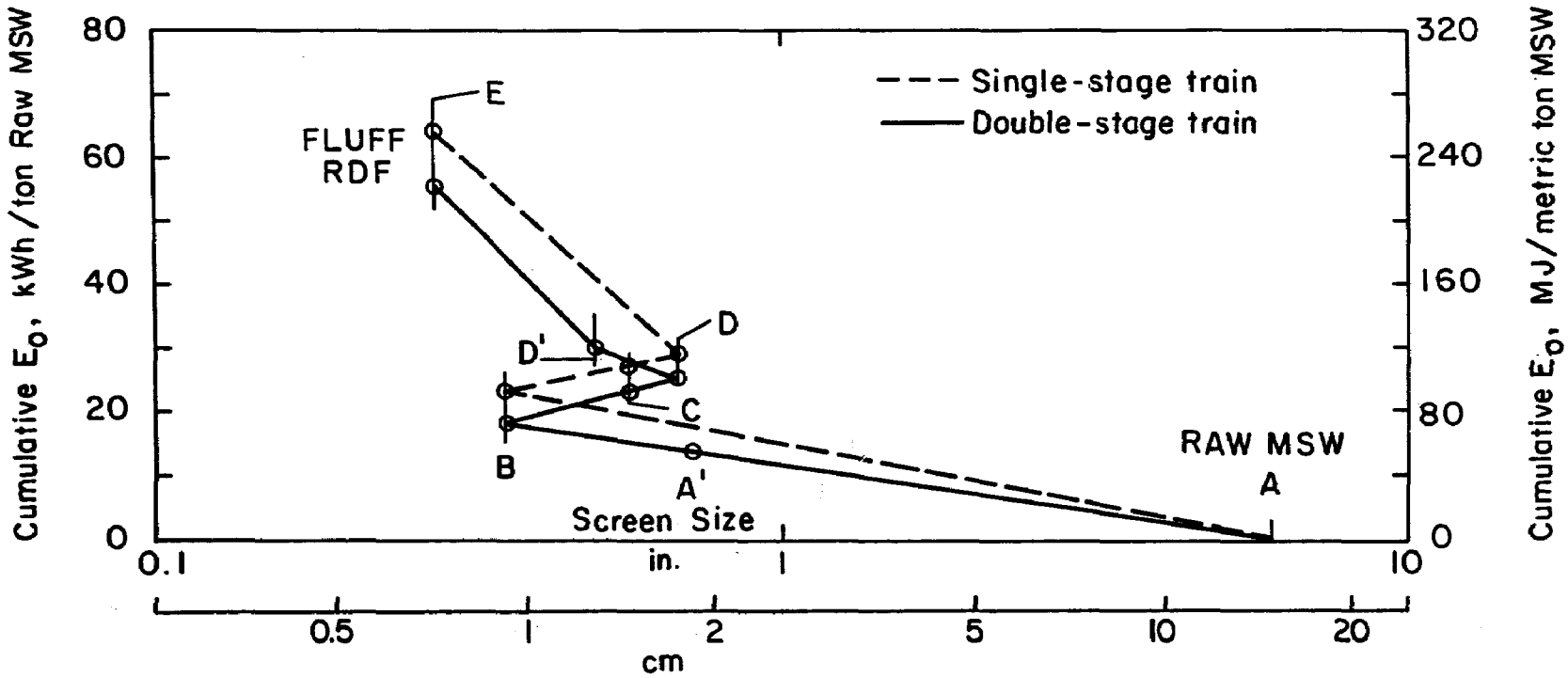

Figure 61. Energy pathway diagram for hypothetical RDF processing trains.

for reducing different fractions of MSW be available as a function of the fundamental parameters Z_0 and D_0/F_0. If such energy consumption information is available in this form, generalizations can be made regarding the optimization of resource recovery processing lines.

REFERENCES

1. Obeng, D.M. Comminution of a Heterogeneous Mixture of Brittle and Non-Brittle Materials. Ph.D. thesis, University of California, Berkeley, Calif., 1974.

2. Obeng, D.M. and Trezek, G.J. Simulation of the Comminution of a Heterogeneous Mixture of Brittle and Non-brittle Materials in a Swing Hammermill. Ind. Eng. Chem. Process Des. Dev., 14, No. 2, 1975.

3. Trezek, G.J. Significance of Size Reduction in Solid Waste Management. EPA-600/2-77-131, U.S. Environmental Protection Agency, July 1977.

4. Calcott, T.G. Solution of Comminution Circuits. Trans. Inst. Min. Metall., Section C, 76, 1967.

5. Calcott, T.G. and Lynch, A.J. An Analysis of Breakage Processes within Rod Mills. Proc. Austral. Inst. Min. and Met. 209, 1964.

6. Lynch, A.J. and Draper, N. An Analysis of the Performance of Multistage Grinding and Cyclone Classification Circuits. Proc. Austral. Inst. Min. and Met. 213, 196.

7. Herbst, J.A., Grandy, G.A., and Mika, T.S. On the Development and Use of Lumped Parameter Models for Continuous Open- and Closed-Circuit Grinding Systems. Trans. Inst. Min. Met., Section C, 80, 1971.

8. Pease, M.C. Methods of Matrix Algebra. Academic Press, New York, N.Y., 1965.

9. Hildebrand, F.B. Advanced Calculus for Applications. Prentice Hall, Englewood Cliffs, N.J., 1962.

10. Stewart, P.S.B. and Restarick, C.J. A Comparison of the Mechanism of Breakage in Full Scale and Laboratory Scale Grinding Mills. Proc. Austr. Inst. Min. Met. 239, 1971.

11. Mori, Y., Jimbo, G. and Yamasaki, M. Residence Time Distribution and Mixing Characteristics of Powders in Open-Circuit Ball Mill. Kagaku-Kogaku (English ed.) 2, 1964.

12. Keinenburg, R., von Seebach, H.M. and Strauss, F. Einfluss von Durchsatz, Mahlkorperfullung und Austragswand aufden Mahlgntfallungsgradund

die Mahlgut Verweilzeitverteilung in Rohrmuhlen, Dechema-Mongraphien 69, 1971, Part 2.

13. Herbst, J.A., Grandy, G.A. and Fuerstenau, D.W. Population Balance Models for the Design of Continuous Grinding Mills. 10th IMPC, London, 1973.

14. Austin, L.G. A Review Introduction to the Mathematical Description of Grinding as a Rate Process. Powder Tech. 5, 1971/72.

15. Herbst, J.A. Batch Ball Mill Simulation: A Method for Estimating Selection and Breakage Functions. M.S. thesis, University of California, Berkeley, Calif., 1968.

16. Herbst, J.A. and Mika, T.S. Mathematical Simulation of Tumbling Mill Grinding: An Improved Method. Proc. IX Int. Min. Proc. Congr. Part III, 1970.

17. Grandy, G.A. and Fuerstenau, D.W. Simulation of Non-Linear Grinding Systems: Rod-Mill Grinding. Trans. Am. Inst. Min. Engrs., 247, 1970.

18. Herbst, J.A. et al. An Approach to the Estimation of the Parameters of Lumped Parameter Grinding Models from On-line Measurements. Zerkleinern, 3rd Europ. Sym. on Comminution, Cannes, 1971. H.C.H. Rumpf and K. Schonert, eds. Dechema-Monographien 69, 1972, Part I.

19. Austin, L.G. and Klimpel, R.R. Determination of Selection-For-Breakage Functions in the Batch Grinding Equation by Nonlinear Optimization. I. and E.C. Fund. 9, 1970.

20. Arbiter, N. and Bhrany, U.N. Correlation of Product Size, Capacity and Power in Tumbling Mills. AIME Trans. 217, 1960.

21. Epstein, B. The Mathematical Description of Certain Breakage Mechanisms Leading to the Logarithmico-Normal Distribution. J. Frank. Inst. 224, 1947.

22. Shiflett, G.R. A Model for the Swing Hammermill Size Reduction of Refuse. D. Eng. Dissertation, Univ. of California, Berkeley, Calif., 1978.

23. Goldfarb, D. and Lapidus, L. Conjugate Gradient Method for Nonlinear Programming Problems with Linear Constraints. Ind. Eng. Chem. Fund. 7, 1968.

24. Powell, M.J.D. An Efficient Method for Finding the Minimum of a Function Without Computing Derivatives. Computer Journal 7, 1964.

25. Fiacco, A.V. and McCormic, G.P. Non-Linear Programming -- Sequential Unconstrained Minimization Technique. John Wiley, New York, N.Y., 1968.

26. Radcliffe, C.W. and Suh, C.H. Kinematic and Mechanism Design. John Wiley, New York, N.Y., 1977.

APPENDIX A

COMMINUTION COMPUTER MODEL

```
LISTING ************************** FUNCTION FFUN ************************** MONDAY
 1...5 6 7.........2.................4.................6.........72
        FUNCTION FFUN(X)
  C
  C OBJECTIVE FUNCTION FOR OPTIMIZATION PROGRAM PCON
  C
        DIMENSION FF(30),GG(30),HH(30),X(30)
        DIMENSION Y(15),XF(15),XP(15),YF(15),YP(15),XPT(15),YPT(15)
        DIMENSION S(15),R(15),THETA(15)
        DIMENSION B(15,15),BB(15,15),D(15,15),JC(15,15),T(15,15),TI(15,15)
        DIMENSION C(15),SIMP(15),ZERO(15)
        DIMENSION F(15,15),G(15,15),GI(15,15),H(15,15)
        REAL JC,KAPPA
        LOGICAL SSE
        COMMON / BLOCK1 / XF,XP,YF,YP,XPT,YPT,R,S,THETA,Y,TAU,N,C,INDEX,NT
        COMMON / BLOCK2 / B,BB,D,F,G,GI,H,JC,T,TI
        COMMON / BLOCK3 / FF,ZERO
        SSE=.TRUE.
  C
  C IF SSE IS TRUE USE THE SUM OF THE SQUARED ERRORS AS THE
  C OBJECTIVE FUNCTION
  C
        IF ( .NOT. SSE ) GO TO 200
        CALL HFUN(HH,X)
        SUM=0.0
        DO 100 I=1,7
        SUM=SUM+HH(I)*HH(I)
  100   CONTINUE
        FFUN=SUM
        RETURN
  200   CONTINUE
        SIZMOD=SQRT(1./2.)
        S1=X(1)
        KAPPA=X(2)
        ALPHA=ABS(X(3))
        BB21=KAPPA*SIZMOD**ALPHA/S1
        FFUN=ABS(1.-BB21)
        RETURN
        END
PILATION.
```

```
 1...5 6 7...........2...................4...................6..........72

          SUBROUTINE GFUN(GG,X)
    C
    C INEQUALITY CONSTRAINTS FOR PROGRAM PCON
    C
          DIMENSION FF(30),GG(30),HH(30),X(30)
          DIMENSION Y(15),XF(15),XP(15),YF(15),YP(15),XPT(15),YPT(15)
          DIMENSION S(15),R(15),THETA(15)
          DIMENSION B(15,15),BB(15,15),D(15,15),JC(15,15),T(15,15),TI(15,15)
          DIMENSION C(15),SIMP(15),ZERO(15)
          DIMENSION F(15,15),G(15,15),GI(15,15),H(15,15)
          REAL JC,KAPPA
          COMMON / BLOCK1 / XF,XP,YF,YP,XPT,YPT,R,S,THETA,Y,TAU,N,C,INDEX,NT
          COMMON / BLOCK2 / B,BB,D,F,G,GI,H,JC,T,TI
          COMMON / BLOCK3 / FF,ZERO
          GG(1)=-X(1)
          GG(2)=X(1)-1.
          GG(3)=-X(2)
          GG(4)=-X(3)
          RETURN
          END

PILATION.
```

```
 1...5 6 7.........2.................4.................6.........72          7

      SUBROUTINE HFUN(HH,X)
C
C EQUALITY CONSTRAINTS FOR PROGRAM PCON
C
C
C CALCULATE VALUES FOR THE SELECTION AND BREAKAGE FUNCTIONS OF A
C CONTINUOS GRINDING MILL
C THE VARIABLE NAMES IN THIS PROGRAM REPRESENT
C     X(I)=THE VARIABLES OF THE OPTIMIZATION ROUTINE
C     FF(I)=THE RESIDUALS TO BE SQUARED BY THE OPTIMIZATION ROUTINE
C     Y(I)=THE SCREEN SIZES
C     XF(I)=THE SIZE DISTRIBUTION OF THE FEED
C     YF(I)=THE CUMULATIVE FRACTION PASSING OF THE FEED
C     XP(I)=THE SIZE DISTRIBUTION OF THE PRODUCT
C     YP(I)=THE CUMULATIVE FRACTION PASSING OF THE PRODUCT
C     XPT(I)=THE PREDICTED SIZE DISTIBUTION FROM THE MODEL
C     YPT(I)=THE PREDICTED CUMULATIVE PASSING
C     R(I)=THE RESIDENCE TIME DISTRIBUTION
C     THETA(I)=NORMALIZED TIME
C     NT=THE NUMBER OF TIME PERIODS
C     S(I)=THE SELECTION FUNCTION
C     C(I)=THE CLASSIFIER FUNCTION
C     B(I,J)=THE BREAKAGE FUNCTION
C     BB(I,J)=THE CUMULATIVE BREAKAGE FUNCTION
C     D(I,J)=THE MILL MATRIX
C     H(I,J)=THE CLOSED LOOP CIRCUIT MATRIX
C     TAU=THE MEAN RESIDENCE TIME
C     N=THE NUMBER OF SIZE CLASSES
C     YMAX=THE MAXIMUM SIZE
C     INDEX=CONTROL TO DETERMINE IF OPEN OR CLOSED LOOP MODEL IS USED
C
      DIMENSION FF(30),X(30),GG(30),HH(30)
      DIMENSION Y(15),XF(15),XP(15),YF(15),YP(15),XPT(15),YPT(15)
      DIMENSION S(15),R(15),THETA(15)
      DIMENSION B(15,15),BB(15,15),D(15,15),JC(15,15),T(15,15),TI(15,15)
      DIMENSION C(15),SIMP(15),ZERO(15)
      DIMENSION F(15,15),G(15,15),GI(15,15),H(15,15)
      REAL JC,KAPPA,MASK
      COMMON / BLOCK1 / XF,XP,YF,YP,XPT,YPT,R,S,THETA,Y,TAU,N,C,INDEX,NT
      COMMON / BLOCK2 / B,BB,D,F,G,GI,H,JC,T,TI
      COMMON / BLOCK3 / FF,ZERO
      LOGICAL ONCE
      DATA ONCE / .FALSE. /
      IF ( ONCE ) GO TO 400
C
C INITIALIZE ALL CONSTANTS TO ZERO
C
      DO 100 I=1,15
      C(I)=0.0
      R(I)=0.0
      THETA(I)=0.0
```

```
 1...5 6 7.........2.................4.................6.........72        7

      Y(I)=0.0
      XF(I)=0.0
      YF(I)=0.0
      XP(I)=0.0
      YP(I)=0.0
100   CONTINUE
C
C READ IN THE NUMBER OF SIZE CLASSES AND THE MAXIMUM SIZE
C
      READ(5,1) N
      INDEX=N
      N=IABS(N)
      READ(5,2) YMAX
C
C READ IN CUMULATIVE PASSING AND RESIDENCE TIME DATA
C
      READ(5,2) (YF(I),I=1,N)
      READ(5,2) (YP(I),I=1,N)
      READ(5,1) NT
      READ(5,2) TAU
      READ(5,3) (R(I),I=1,NT)
      READ(5,3) (THETA(I),I=1,NT)
C
C READ IN THE CLASSIFIER FUNCTION IF A CLOSED LOOP MODEL IS DESIRED
C
      IF ( INDEX.LT.0 ) READ(5,2) (C(I),I=1,N)
C
C SET UP SIZE CLASSES
C
      Y(1)=YMAX
      DO 200 I=2,N
      Y(I)=Y(I-1)/2.
200   CONTINUE
C
C CONVERT CUMULATIVE PASSING TO SIZE DISTRIBUTION
C
      XF(1)=1.0-YF(1)
      XP(1)=1.0-YP(1)
      DO 300 I=2,N
      XF(I)=YF(I-1)-YF(I)
      XP(I)=YP(I-1)-YP(I)
300   CONTINUE
      ONCE=.TRUE.
400   CONTINUE
C
C INITIALIZE ALL WORKING ARRAYS TO ZERO
C
      DO 500 I=1,15
      S(I)=0.0
      SIMP(I)=0.0
      XPT(I)=0.0
```

```
 1...5 6 7.........2.................4.................6.........72        7

      YPT(I)=0.0
      ZERO(I)=0.0
      DO 500 J=1,15
      B(I,J)=0.0
      BB(I,J)=0.0
      D(I,J)=0.0
      F(I,J)=0.0
      G(I,J)=0.0
      GI(I,J)=0.0
      H(I,J)=0.0
      JC(I,J)=0.0
      T(I,J)=0.0
      TI(I,J)=0.0
  500 CONTINUE
      S(1)=X(1)
      KAPPA=X(2)
      ALPHA=ABS(X(3))
C
C CALCULATE THE ZERO ORDER PRODUCTION RATE CONSTANTS
C
      DO 600 I=2,N
      SIZMOD=Y(I)/SQRT(Y(1)*Y(2))
      ZERO(I)=KAPPA*SIZMOD**ALPHA
  600 CONTINUE
C
C CALCULATE BREAKAGE FUNCTIONS
C
      DO 700 I=2,N
      BB(I,1)=ZERO(I)/S(1)
  700 CONTINUE
      DO 800 J=2,N
      DO 800 I=J,N
      BB(I,J)=BB(I-J+1,1)
  800 CONTINUE
      DO 900 J=2,N
      B(J,1)=BB(J,1)-BB(J+1,1)
      DO 900 I=J,N
      MASK=1.0
      IF ( I.EQ.J ) MASK=0.0
      B(I,J)=BB(I,J)-BB(I+1,J)*MASK
  900 CONTINUE
C
C CALCULATE SELECTION FUNCTION
C
      M=N-1
      DO 950 I=2,M
      S(I)=ZERO(N)/BB(N,I)
  950 CONTINUE
C
C CALCULATE THE MATRIX T
C
```

```
 1...5 6 7...........2...................4...................6..........72          7

        DO 1300 J=1,N
        DO 1300 I=J,N
        L=I-1
        IF ( L-J ) 1000,1100,1100
 1000   CONTINUE
        T(I,J)=1.0
        GO TO 1300
 1100   CONTINUE
        DO 1200 K=J,L
        T(I,J)=T(I,J)+((B(I,K)*S(K))/(S(I)-S(J)))*T(K,J)
 1200   CONTINUE
 1300   CONTINUE
  C
  C CALCULATE T INVERSE
  C
        DO 1700 J=1,N
        DO 1700 I=J,N
        L=I-1
        IF ( L-J ) 1400,1500,1500
 1400   CONTINUE
        TI(I,J)=1.0/T(I,I)
        GO TO 1700
 1500   CONTINUE
        DO 1600 K=J,L
        TI(I,J)=TI(I,J)-T(I,K)*TI(K,J)/T(I,I)
 1600   CONTINUE
 1700   CONTINUE
  C
  C CALCULATE THE MATRIX JC USING SIMPSONS APPROXIMATION
  C
        DEL=THETA(2)-THETA(1)
        M=NT-3
        DO 2000 I=1,N
        DO 1800 J=1,NT
        SIMP(J)=EXP(-S(I)*TAU*THETA(J))*R(J)
 1800   CONTINUE
        EVEN=0.0
        ODD=0.0
        DO 1900 K=1,M,2
        ODD=ODD+SIMP(K)
        EVEN=EVEN+SIMP(K+1)
 1900   CONTINUE
        ODD=ODD+SIMP(NT-1)
        JC(I,I)=(DEL/3.)*(4.*ODD+2.*EVEN+SIMP(NT))
 2000   CONTINUE
  C
  C FORM THE MILL MATRIX D BY MULTIPLYING T BY JC BY TT
  C
        DO 2100 J=1,N
        DO 2100 I=J,N
        DO 2100 K=J,I
```

```
1...5 6 7.........2.................4.................6.........72
      D(I,J)=D(I,J)+T(I,K)*JC(K,K)*TI(K,J)
 2100 CONTINUE
 C
 C IF AN OPEN LOOP MODEL IS USED CONTINUE
 C IF A CLOSED LOOP MODEL IS USED GO TO 2300
 C
      IF ( INDEX.LT.0 ) GO TO 2300
 C
 C MULTIPLY D BY THE FEED SIZE DISTRIBUTICN
 C
      DO 2200 I=1,N
      DO 2200 J=1,N
      XPT(I)=XPT(I)+D(I,J)*XF(J)
 2200 CONTINUE
      GO TO 3300
 2300 CONTINUE
 C
 C FORM THE MATRIX F BY MULTIPLYING I-C BY D AND
 C FORM THE MATRIX G BY SUBTRACTING C*D FROM I
 C
      DO 2600 J=1,N
      DO 2600 I=J,N
      F(I,J)=(1.-C(I))*D(I,J)
      L=I-1
      IF ( L-J ) 2400,2500,2500
 2400 CONTINUE
      G(I,J)=1.-C(I)*D(I,J)
      GO TO 2600
 2500 CONTINUE
      G(I,J)=-C(I)*D(I,J)
 2600 CONTINUE
 C
 C CALCULATE G INVERSE
 C
      DO 3000 J=1,N
      DO 3000 I=J,N
      L=I-1
      IF ( L-J ) 2700,2800,2800
 2700 CONTINUE
      GI(I,J)=1.0/G(I,J)
      GO TO 3000
 2800 CONTINUE
      DO 2900 K=J,L
      GI(I,J)=GI(I,J)-G(I,K)*GI(K,J)/G(I,I)
 2900 CONTINUE
 3000 CONTINUE
 C
 C FORM THE CIRCUIT MATRIX H BY MULTIPLYING F BY GI
 C
      DO 3100 J=1,N
      DO 3100 I=J,N
```

```
 1...5 6 7.........2.................4.................6.........72

        DO 3100 K=J,I
        H(I,J)=H(I,J)+F(I,K)*GI(K,J)
 3100   CONTINUE
  C
  C MULTIPLY H BY THE FEED SIZE DISTRIBUTICN
  C
        DO 3200 I=1,N
        DO 3200 J=1,N
        XPT(I)=XPT(I)+H(I,J)*XF(J)
 3200   CONTINUE
 3300   CONTINUE
  C
  C CONVERT THE PREDICTED PRODUCT SIZE DISTRIBUTION TO CUMULATIVE PASSING
  C AND CALCULATE PERCENT ERROR OBJECTIVE FUNCTIONS
  C
        YPT(1)=1.0-XPT(1)
        FF(1)=ABS(XP(1)-XPT(1))
        DO 3400 I=2,N
        YPT(I)=YPT(I-1)-XPT(I)
        FF(I)=ABS(XP(I)-XPT(I))
        IF ( XP(I).NE.0.0 ) FF(I)=(FF(I)/XP(I))*100.
 3400   CONTINUE
        DO 3500 I=4,N
        J=I-3
        HH(J)=XPT(I)-XP(I)
 3500   CONTINUE
        RETURN
    1   FORMAT(I5)
    2   FORMAT(15F5.3)
    3   FORMAT(8F10.3)
        END
```

PILATION.

```
 1...5 6 7.........2.................4.................6.........72        7

      SUBROUTINE MORPRNT(X,FO,FC,GG,HH)
      DIMENSION FF(30),X(30)
      DIMENSION GG(30),HH(30)
      DIMENSION Y(15),XF(15),XP(15),YF(15),YP(15),XPT(15),YPT(15)
      DIMENSION S(15),R(15),THETA(15),ERROR(15)
      DIMENSION B(15,15),BB(15,15),D(15,15),JC(15,15),T(15,15),TI(15,15)
      DIMENSION C(15),SIMP(15),ZERO(15)
      DIMENSION F(15,15),G(15,15),GI(15,15),H(15,15)
      REAL JC,KAPPA
      COMMON / BLOCK1 / XF,XP,YF,YP,XPT,YPT,R,S,THETA,Y,TAU,N,C,INDEX,NT
      COMMON / BLOCK2 / B,BB,D,F,G,GI,H,JC,T,TI
      COMMON / BLOCK3 / FF,ZERO
C
C INITIALIZE THE SIZE DISTRIBUTION ERROR TO ZERO
C
      DO 100 I=1,N
      ERROR(I)=0.0
100   CONTINUE
C
C CALCULATE THE SIZE DISTRIBUTION ERROR
C
      DO 200 I=1,N
      ERROR(I)=XPT(I)-XP(I)
200   CONTINUE
      WRITE(6,1)
      WRITE(6,2) ((I,Y(I),Y(I+1),XF(I),YF(I)),I=1,N)
      WRITE(6,3) TAU
      WRITE(6,4) ((I,R(I),THETA(I)),I=1,NT)
      WRITE(6,5)
      WRITE(6,6) ((I,Y(I),Y(I+1),XP(I),XPT(I),ERROR(I),YP(I),YPT(I),
     $           FF(I)),I=1,N)
      WRITE(6,7)
      WRITE(6,8) ((I,S(I)),I=1,N)
      WRITE(6,9)
      WRITE(6,10) ((B(I,J),J=1,N),I=1,N)
      WRITE(6,11)
      WRITE(6,10) ((BB(I,J),J=1,N),I=1,N)
      WRITE(6,12)
      WRITE(6,10) ((T(I,J),J=1,N),I=1,N)
      WRITE(6,13)
      WRITE(6,10) ((TI(I,J),J=1,N),I=1,N)
      WRITE(6,14)
      WRITE(6,10) ((JC(I,J),J=1,N),I=1,N)
      WRITE(6,15)
      WRITE(6,10) ((D(I,J),J=1,N),I=1,N)
      IF ( INDEX.GT.0 ) GO TO 300
      WRITE(6,16)
      WRITE(6,8) ((I,C(I)),I=1,N)
      WRITE(6,17)
      WRITE(6,10) ((F(I,J),J=1,N),I=1,N)
      WRITE(6,18)
```

```
 1...5 6 7...........2...................4...................6..........72          7

         WRITE(6,10) ((G(I,J),J=1,N),I=1,N)
         WRITE(6,19)
         WRITE(6,10) ((GI(I,J),J=1,N),I=1,N)
         WRITE(6,20)
         WRITE(6,10) ((H(I,J),J=1,N),I=1,N)
   300   CONTINUE
         RETURN
     1   FORMAT(1H1/////10X,11H FEED DATA ////
       $                 15X,32H SIZES ARE GIVEN IN CENTIMETERS /
       $        15X,43H XF(I)=EXPERIMENTAL FEED SIZE DISTRIBUTION /
       $        15X,44H YF(I)=EXPERIMENTAL FEED CUMULATIVE PASSING ////
       $        10X,3H I ,6X,12H SIZE CLASS ,7X,7H XF(I) ,4X,7H YF(I) /)
     2   FORMAT(10X,I2,F10.5,3H  X,F10.5,1X,F10.5,1X,F10.5)
     3   FORMAT(////15X,34H R(I)=RESIDENCE TIME DISTRIBUTION /
       $        15X,36H THETA(I)=NORMALIZED RESIDENCE TIME /
       $        15X,26H TAU=MEAN RESIDENCE TIME= ,F10.5,9H SECONDS ////
       $        10X,3H I ,2X,6H R(I) ,5X,10H THETA(I) /)
     4   FORMAT(10X,I2,1X,F10.5,1X,F10.5/)
     5   FORMAT(1H1/////10X,14H PRODUCT DATA ////
       $        15X,32H SIZES ARE GIVEN IN CENTIMETERS /
       $        15X,46H XP(I)=EXPERIMENTAL PRODUCT SIZE DISTRIBUTION /
       $        15X,47H YP(I)=EXPERIMENTAL PRODUCT CUMULATIVE PASSING /
       $        15X,44H XPT(I)=PREDICTED PRODUCT SIZE DISTRIBUTION /
       $        15X,45H YPT(I)=PREDICTED PRODUCT CUMULATIVE PASSING ////
       $        10X,3H I ,6X,12H SIZE CLASS ,8X,7H XP(I) ,4X,8H XPT(I) ,
       $              3X,7H ERROR ,4X,7H YP(I) ,4X,8H YPT(I) ,3X,
       $              9H PERCENT /
       $              94X,7H ERROR /)
     6   FORMAT(10X,I2,1X,F10.5,3H  X,F10.5,1X,F10.5,1X,F10.5,1X,F10.5,
       $        1X,F10.5,1X,F10.5,1X,F10.5)
     7   FORMAT(1H1,/////15X,27H THE SELECTION FUNCTION IS ////
       $        10X,3H I ,4X,6H S(I) /)
     8   FORMAT(10X,I2,1X,F10.5)
     9   FORMAT(////15X,33H THE BREAKAGE FUNCTION B(I,J) IS ////)
    10   FORMAT(9X,1X,E10.3,1X,E10.3,1X,E10.3,1X,E10.3,1X,E10.3,1X,E10.3,
       $      1X,E10.3,1X,E10.3,1X,E10.3,1X,E10.3)
    11   FORMAT(1H1/////15X,
       $        45H THE CUMULATIVE BREAKAGE FUNCTION BB(I,J) IS ////)
    12   FORMAT(////15X,22H THE MATRIX T(I,J) IS ////)
    13   FORMAT(1H1/////15X,34H THE INVERSE OF T(I,J)=TI(I,J) IS ////)
    14   FORMAT(////15X,23H THE MATRIX JC(I,J) IS ////)
    15   FORMAT(1H1/////15X,27H THE MILL MATRIX D(I,J) IS ////)
    16   FORMAT(////15X,28H THE CLASSIFIER FUNCTION IS ////
       $        10X,3H I ,4X,6H C(I) /)
    17   FORMAT(1H1/////15X,22H THE MATRIX F(I,J) IS ////)
    18   FORMAT(////15X,22H THE MATRIX G(I,J) IS ////)
    19   FORMAT(1H1/////15X,34H THE INVERSE OF G(I,J)=GI(I,J) IS ////)
    20   FORMAT(////15X,37H THE CLOSED CIRCUIT MATRIX H(I,J) IS ////)
         END

PILATION.
```

```
 1...5 6 7...........2...................4...................6.........72        7

        PROGRAM GRIND(INPUT,OUTPUT,TAPE5=INPUT,TAPE6=OUTPUT)
   C
   C IF VALUES FOR FLOWRATE, MOISTURE, S1, KAPPA, AND ALPHA ARE
   C SUPPLIED FROM A KNOWLEDGE OF THE OPERATING CONDITIONS OF THE SHREDDER
   C THAT THE USER WISHES TO EXAMINE THE PROGRAM WILL CALCULATE A
   C PREDICTED PRODUCT SIZE DISTRIBUTION AND COMPARE IT TO AN
   C EXPERIMENTALLY DETERMINED ONE FOR THE SAME OPERATING CONDITIONS
   C AND ESTIMATE THE POWER NECESSARY TO OPERATE THE SHREDDER
   C A GRUENDLER 48-4 SHREDDER WITH 2.5 CM GRATES IS ASSUMED
   C
        REAL KAPPA,MC
        READ(5,1) Q
        READ(5,1) MC
        READ(5,1) S1
        READ(5,1) KAPPA
        READ(5,1) ALPHA
        TIM=3.6*13.61*Q**.064
        P=18.61*Q**1.107*(1.-MC)**.358
        MC=MC*100.
        WRITE(6,2) Q,MC,P
        CALL SHRED(TIM,S1,KAPPA,ALPHA)
        STOP
      1 FORMAT(F10.0)
      2 FORMAT(1H1,5X,18H THE FLOW RATE IS ,F4.1,17H TONNES PER HOUR ///
       $      5X,25H THE MOISTURE CONTENT IS ,F5.1,9H PERCENT ///
       $      5X,33H THE ESTIMATED POWER REQUIRED IS ,F5.1,11H KILOWATTS )
        END
```

PILATION.

```
 1...5 6 7...........2...................4...................6.........72         7

      SUBROUTINE SHRED(TIM,S1,KAPPA,ALPHA)
C
C CALCULATE VALUES FOR THE SELECTION AND BREAKAGE FUNCTIONS OF A
C CONTINUOS GRINDING MILL
C THE VARIABLE NAMES IN THIS PROGRAM REPRESENT
C     X(I)=THE VARIABLES OF THE OPTIMIZATION ROUTINE
C     FF(1)=THE RESIDUALS TO BE SQUARED BY THE OPTIMIZATION ROUTINE
C     Y(I)=THE SCREEN SIZES
C     XF(I)=THE SIZE DISTRIBUTION OF THE FEED
C     YF(I)=THE CUMULATIVE FRACTION PASSING OF THE FEED
C     XP(I)=THE SIZE DISTRIBUTION OF THE PRODUCT
C     YP(I)=THE CUMULATIVE FRACTION PASSING OF THE PRODUCT
C     XPT(I)=THE PREDICTED SIZE DISTIBUTION FROM THE MODEL
C     YPT(I)=THE PREDICTED CUMULATIVE PASSING
C     R(I)=THE RESIDENCE TIME DISTRIBUTICN
C     THETA(I)=NORMALIZED TIME
C     NT=THE NUMBER OF TIME PERIODS
C     S(I)=THE SELECTION FUNCTION
C     C(I)=THE CLASSIFIER FUNCTION
C     B(I,J)=THE BREAKAGE FUNCTION
C     BB(I,J)=THE CUMULATIVE BREAKAGE FUNCTION
C     D(I,J)=THE MILL MATRIX
C     H(I,J)=THE CLOSED LOOP CIRCUIT MATRIX
C     TAU=THE MEAN RESIDENCE TIME
C     N=THE NUMBER OF SIZE CLASSES
C     YMAX=THE MAXIMUM SIZE
C     INDEX=CONTROL TO DETERMINE IF OPEN OR CLOSED LOOP MODEL IS USED
C
      DIMENSION FF(30),X(30),GG(30),HH(30)
      DIMENSION Y(15),XF(15),XP(15),YF(15),YP(15),XPT(15),YPT(15)
      DIMENSION S(15),R(15),THETA(15)
      DIMENSION B(15,15),BB(15,15),D(15,15),JC(15,15),T(15,15),TI(15,15)
      DIMENSION C(15),SIMP(15),ZERO(15)
      DIMENSION F(15,15),G(15,15),GI(15,15),H(15,15)
      REAL JC,KAPPA,MASK
      COMMON / BLOCK1 / XF,XP,YF,YP,XPT,YPT,R,S,THETA,Y,TAU,N,C,INDEX,NT
      COMMON / BLOCK2 / B,BB,D,F,G,GI,H,JC,T,TI
      COMMON / BLOCK3 / FF,ZERO
      LOGICAL ONCE
      DATA ONCE / .FALSE. /
      IF ( ONCE ) GO TO 400
C
C INITIALIZE ALL CONSTANTS TO ZERO
C
      DO 100 I=1,15
      C(I)=0.0
      R(I)=0.0
      THETA(I)=0.0
      Y(I)=0.0
      XF(I)=0.0
      YF(I)=0.0
```

```
 1...5 6 7.........2.................4.................6.........72        7

      XP(I)=0.0
      YP(I)=0.0
  100 CONTINUE
C
C READ IN THE NUMBER OF SIZE CLASSES AND THE MAXIMUM SIZE
C
      READ(5,1) N
      INDEX=N
      N=IABS(N)
      READ(5,2) YMAX
C
C READ IN CUMULATIVE PASSING AND RESIDENCE TIME DATA
C
      READ(5,2) (YF(I),I=1,N)
      READ(5,2) (YP(I),I=1,N)
      READ(5,1) NT
      TAU=TIM
      READ(5,3) (R(I),I=1,NT)
      READ(5,3) (THETA(I),I=1,NT)
C
C READ IN THE CLASSIFIER FUNCTION IF A CLOSED LOOP MODEL IS DESIRED
C
      IF ( INDEX.LT.0 ) READ(5,2) (C(I),I=1,N)
C
C SET UP SIZE CLASSES
C
      Y(1)=YMAX
      DO 200 I=2,N
      Y(I)=Y(I-1)/2.
  200 CONTINUE
C
C CONVERT CUMULATIVE PASSING TO SIZE DISTRIBUTION
C
      XF(1)=1.0-YF(1)
      XP(1)=1.0-YP(1)
      DO 300 I=2,N
      XF(I)=YF(I-1)-YF(I)
      XP(I)=YP(I-1)-YP(I)
  300 CONTINUE
      ONCE=.TRUE.
  400 CONTINUE
C
C INITIALIZE ALL WORKING ARRAYS TO ZERO
C
      DO 500 I=1,15
      S(I)=0.0
      SIMP(I)=0.0
      XPT(I)=0.0
      YPT(I)=0.0
      ZERO(I)=0.0
      DO 500 J=1,15
```

```
1...5 6 7...........2...................4...................6.........72        7

      B(I,J)=0.0
      BB(I,J)=0.0
      D(I,J)=0.0
      F(I,J)=0.0
      G(I,J)=0.0
      GI(I,J)=0.0
      H(I,J)=0.0
      JC(I,J)=0.0
      T(I,J)=0.0
      TI(I,J)=0.0
 500  CONTINUE
      S(1)=S1
C
C CALCULATE THE ZERO ORDER PRODUCTION RATE CONSTANTS
C
      DO 600 I=2,N
      SIZMOD=Y(I)/SQRT(Y(1)*Y(2))
      ZERO(I)=KAPPA*SIZMOD**ALPHA
 600  CONTINUE
C
C CALCULATE BREAKAGE FUNCTIONS
C
      DO 700 I=2,N
      BB(I,1)=ZERO(I)/S(1)
 700  CONTINUE
      DO 800 J=2,N
      DO 800 I=J,N
      BB(I,J)=BB(I-J+1,1)
 800  CONTINUE
      DO 900 J=2,N
      B(J,1)=BB(J,1)-BB(J+1,1)
      DO 900 I=J,N
      MASK=1.0
      IF ( I.EQ.J ) MASK=0.0
      B(I,J)=BB(I,J)-BB(I+1,J)*MASK
 900  CONTINUE
C
C CALCULATE SELECTION FUNCTION
C
      M=N-1
      DO 950 I=2,M
      S(I)=ZERO(N)/BB(N,I)
 950  CONTINUE
C
C CALCULATE THE MATRIX T
C
      DO 1300 J=1,N
      DO 1300 I=J,N
      L=I-1
      IF ( L-J ) 1000,1100,1100
1000  CONTINUE
```

```
 1...5 6 7.........2.................4.................6.........72          7

        T(I,J)=1.0
        GO TO 1300
 1100   CONTINUE
        DO 1200 K=J,L
        T(I,J)=T(I,J)+((B(I,K)*S(K))/(S(I)-S(J)))*T(K,J)
 1200   CONTINUE
 1300   CONTINUE
  C
  C CALCULATE T INVERSE
  C
        DO 1700 J=1,N
        DO 1700 I=J,N
        L=I-1
        IF ( L-J ) 1400,1500,1500
 1400   CONTINUE
        TI(I,J)=1.0/T(I,I)
        GO TO 1700
 1500   CONTINUE
        DO 1600 K=J,L
        TI(I,J)=TI(I,J)-T(I,K)*TI(K,J)/T(I,I)
 1600   CONTINUE
 1700   CONTINUE
  C
  C CALCULATE THE MATRIX JC USING SIMPSONS APPROXIMATION
  C
        DEL=THETA(2)-THETA(1)
        M=NT-3
        DO 2000 I=1,N
        DO 1800 J=1,NT
        SIMP(J)=EXP(-S(I)*TAU*THETA(J))*R(J)
 1800   CONTINUE
        EVEN=0.0
        ODD=0.0
        DO 1900 K=1,M,2
        ODD=ODD+SIMP(K)
        EVEN=EVEN+SIMP(K+1)
 1900   CONTINUE
        ODD=ODD+SIMP(NT-1)
        JC(I,I)=(DEL/3.)*(4.*ODD+2.*EVEN+SIMP(NT))
 2000   CONTINUE
  C
  C FORM THE MILL MATRIX D BY MULTIPLYING T BY JC BY TI
  C
        DO 2100 J=1,N
        DO 2100 I=J,N
        DO 2100 K=J,I
        D(I,J)=D(I,J)+T(I,K)*JC(K,K)*TI(K,J)
 2100   CONTINUE
  C
  C IF AN OPEN LOOP MODEL IS USED CONTINUE
  C IF A CLOSED LOOP MODEL IS USED GO TO 2300
```

```
1...5 6 7.........2.................4.................6.........72        7

  C
        IF ( INDEX.LT.0 ) GO TO 2300
  C
  C MULTIPLY D BY THE FEED SIZE DISTRIBUTICN
  C
        DO 2200 I=1,N
        DO 2200 J=1,N
        XPT(I)=XPT(I)+D(I,J)*XF(J)
 2200   CONTINUE
        GO TO 3300
 2300   CONTINUE
  C
  C FORM THE MATRIX F BY MULTIPLYING I-C BY D AND
  C FORM THE MATRIX G BY SUBTRACTING C*D FROM I
  C
        DO 2600 J=1,N
        DO 2600 I=J,N
        F(I,J)=(1.-C(I))*D(I,J)
        L=I-1
        IF ( L-J ) 2400,2500,2500
 2400   CONTINUE
        G(I,J)=1.-C(I)*D(I,J)
        GO TO 2600
 2500   CONTINUE
        G(I,J)=-C(I)*D(I,J)
 2600   CONTINUE
  C
  C CALCULATE G INVERSE
  C
        DO 3000 J=1,N
        DO 3000 I=J,N
        L=I-1
        IF ( L-J ) 2700,2800,2800
 2700   CONTINUE
        GI(I,J)=1.0/G(I,J)
        GO TO 3000
 2800   CONTINUE
        DO 2900 K=J,L
        GI(I,J)=GI(I,J)-G(I,K)*GI(K,J)/G(I,I)
 2900   CONTINUE
 3000   CONTINUE
  C
  C FORM THE CIRCUIT MATRIX H BY MULTIPLYING F BY GI
  C
        DO 3100 J=1,N
        DO 3100 I=J,N
        DO 3100 K=J,I
        H(I,J)=H(I,J)+F(I,K)*GI(K,J)
 3100   CONTINUE
  C
  C MULTIPLY H BY THE FEED SIZE DISTRIBUTICN
```

```
 1...5 6 7.........2.................4.................6.........72        7

  C
        DO 3200 I=1,N
        DO 3200 J=1,N
        XPT(I)=XPT(I)+H(I,J)*XF(J)
 3200   CONTINUE
 3300   CONTINUE
  C
  C CONVERT THE PREDICTED PRODUCT SIZE DISTRIBUTION TO CUMULATIVE PASSING
  C AND CALCULATE PERCENT ERROR OBJECTIVE FUNCTIONS
  C
        YPT(1)=1.0-XPT(1)
        FF(1)=ABS(XP(1)-XPT(1))
        DO 3400 I=2,N
        YPT(I)=YPT(I-1)-XPT(I)
        FF(I)=ABS(XP(I)-XPT(I))
        IF ( XP(I).NE.0.0 ) FF(I)=(FF(I)/XP(I))*100.
 3400   CONTINUE
        DO 3500 I=4,N
        J=I-3
        HH(J)=XPT(I)-XP(I)
 3500   CONTINUE
        CALL MORPRNT(X,FO,FC,GG,HH)
        RETURN
    1   FORMAT(I5)
    2   FORMAT(15F5.3)
    3   FORMAT(8F10.3)
        END

PILATION.
```

```
 1...5 6 7.........2.................4.................6.........72        7

      WRITE(6,10) ((G(I,J),J=1,N),I=1,N)
      WRITE(6,19)
      WRITE(6,10) ((GI(I,J),J=1,N),I=1,N)
      WRITE(6,20)
      WRITE(6,10) ((H(I,J),J=1,N),I=1,N)
  300 CONTINUE
      RETURN
    1 FORMAT(1H1/////10X,11H FEED DATA ////
     $                15X,32H SIZES ARE GIVEN IN CENTIMETERS /
     $        15X,43H XF(I)=EXPERIMENTAL FEED SIZE DISTRIBUTION /
     $        15X,44H YF(I)=EXPERIMENTAL FEED CUMULATIVE PASSING ////
     $        10X,3H I ,6X,12H SIZE CLASS ,7X,7H XF(I) ,4X,7H YF(I) /)
    2 FORMAT(10X,I2,F10.5,3H  X,F10.5,1X,F10.5,1X,F10.5)
    3 FORMAT(////15X,34H R(I)=RESIDENCE TIME DISTRIBUTION /
     $        15X,36H THETA(I)=NORMALIZED RESIDENCE TIME /
     $        15X,26H TAU=MEAN RESIDENCE TIME= ,F10.5,9H SECONDS ////
     $        10X,3H I ,2X,6H R(I) ,5X,10H THETA(I) /)
    4 FORMAT(10X,I2,1X,F10.5,1X,F10.5/)
    5 FORMAT(1H1/////10X,14H PRODUCT DATA ////
     $        15X,32H SIZES ARE GIVEN IN CENTIMETERS /
     $        15X,46H XP(I)=EXPERIMENTAL PRODUCT SIZE DISTRIBUTION /
     $        15X,47H YP(I)=EXPERIMENTAL PRODUCT CUMULATIVE PASSING /
     $        15X,44H XPT(I)=PREDICTED PRODUCT SIZE DISTRIBUTION /
     $        15X,45H YPT(I)=PREDICTED PRODUCT CUMULATIVE PASSING ////
     $        10X,3H I ,6X,12H SIZE CLASS ,8X,7H XP(I) ,4X,8H XPT(I) ,
     $              3X,7H ERROR ,4X,7H YP(I) ,4X,8H YPT(I) ,3X,
     $              3H PERCENT /
     $              94X,7H ERROR /)
    6 FORMAT(10X,I2,1X,F10.5,3H  X,F10.5,1X,F10.5,1X,F10.5,1X,F10.5,
     $        1X,F10.5,1X,F10.5,1X,F10.5)
    7 FORMAT(1H1,/////15X,27H THE SELECTION FUNCTION IS ////
     $        10X,3H I ,4X,6H S(I) /)
    8 FORMAT(10X,I2,1X,F10.5)
    9 FORMAT(////15X,33H THE BREAKAGE FUNCTION B(I,J) IS ////)
   10 FORMAT(9X,1X,E10.3,1X,E10.3,1X,E10.3,1X,E10.3,1X,E10.3,1X,E10.3,
     $       1X,E10.3,1X,E10.3,1X,E10.3,1X,E10.3)
   11 FORMAT(1H1/////15X,
     $        45H THE CUMULATIVE BREAKAGE FUNCTION BB(I,J) IS ////)
   12 FORMAT(////15X,22H THE MATRIX T(I,J) IS ////)
   13 FORMAT(1H1/////15X,34H THE INVERSE OF T(I,J)=TI(I,J) IS ////)
   14 FORMAT(////15X,23H THE MATRIX JC(I,J) IS ////)
   15 FORMAT(1H1/////15X,27H THE MILL MATRIX D(I,J) IS ////)
   16 FORMAT(////15X,28H THE CLASSIFIER FUNCTION IS ////
     $        10X,3H I ,4X,6H C(I) /)
   17 FORMAT(1H1/////15X,22H THE MATRIX F(I,J) IS ////)
   18 FORMAT(////15X,22H THE MATRIX G(I,J) IS ////)
   19 FORMAT(1H1/////15X,34H THE INVERSE OF G(I,J)=GI(I,J) IS ////)
   20 FORMAT(////15X,37H THE CLOSED CIRCUIT MATRIX H(I,J) IS ////)
      END

PILATION.
```

THE FLOW RATE IS 7.4 TONNES PER HOUR

THE MOISTURE CONTENT IS 30.0 PERCENT

THE ESTIMATED POWER REQUIRED IS 150.2 KILOWATTS

FEED DATA

SIZES ARE GIVEN IN CENTIMETERS
XF(I)=EXPERIMENTAL FEED SIZE DISTRIBUTION
YF(I)=EXPERIMENTAL FEED CUMULATIVE PASSING

I	SIZE CLASS			XF(I)	YF(I)
1	40.00000	X	20.00000	.05400	.94600
2	20.00000	X	10.00000	.32800	.61800
3	10.00000	X	5.00000	.50100	.11700
4	5.00000	X	2.50000	.05500	.06200
5	2.50000	X	1.25000	.01800	.04400
6	1.25000	X	.62500	.01400	.03000
7	.62500	X	.31250	.01000	.02000
8	.31250	X	.15625	.00600	.01400
9	.15625	X	.07813	.00400	.01000
10	.07813	X	0.	.01000	0.

R(I)=RESIDENCE TIME DISTRIBUTION
THETA(I)=NORMALIZED RESIDENCE TIME
TAU=MEAN RESIDENCE TIME= 55.69183 SECONDS

I	R(I)	THETA(I)
1	.25700	.01000
2	14.80300	.36000
3	13.36400	.71000
4	7.76100	1.06000
5	5.14000	1.41100
6	3.34100	1.76100
7	1.74800	2.11100
8	.51400	2.46100

PRODUCT DATA

SIZES ARE GIVEN IN CENTIMETERS
XP(I)=EXPERIMENTAL PRODUCT SIZE DISTRIBUTION
YP(I)=EXPERIMENTAL PRODUCT CUMULATIVE PASSING
XPT(I)=PREDICTED PRODUCT SIZE DISTRIBUTION
YPT(I)=PREDICTED PRODUCT CUMULATIVE PASSING

I	SIZE CLASS			XP(I)	XPT(I)	ERROR	YP(I)	YPT(I)	PERCENT ERROR
1	40.00000	X	20.00000	0.	0.	0.	1.00000	1.00000	0.
2	20.00000	X	10.00000	0.	0.	0.	1.00000	1.00000	0.
3	10.00000	X	5.00000	0.	0.	0.	1.00000	1.00000	0.
4	5.00000	X	2.50000	.03700	-.03143	-.06843	.96300	1.03143	184.93586
5	2.50000	X	1.25000	.03100	.04048	.00948	.93200	.99095	30.57773
6	1.25000	X	.62500	.13500	.15284	.01784	.79700	.83811	13.21530
7	.62500	X	.31250	.20600	.20074	-.00526	.59100	.63737	2.55545
8	.31250	X	.15625	.22400	.17749	-.04651	.36700	.45588	20.76469
9	.15625	X	.07813	.16100	.13716	-.02384	.20600	.32272	14.80564
10	.07813	X	0.	.20600	.30436	.09836	0.	.01836	47.74987

THE SELECTION FUNCTION IS

I	S(I)
1	.29145
2	.16695
3	.09563
4	.05476
5	.03138
6	.01797
7	.01030
8	.00590
9	.00338
10	0.

THE BREAKAGE FUNCTION B(I,J) IS

0.	0.	0.	0.	0.	0.	0.	0.	0.	0.
.306E+00	0.	0.	0.	0.	0.	0.	0.	0.	0.
.175E+00	.306E+00	0.	0.	0.	0.	0.	0.	0.	0.
.101E+00	.175E+00	.306E+00	0.	0.	0.	0.	0.	0.	0.
.576E-01	.101E+00	.175E+00	.306E+00	0.	0.	0.	0.	0.	0.
.330E-01	.576E-01	.101E+00	.175E+00	.306E+00	0.	0.	0.	0.	0.
.189E-01	.330E-01	.576E-01	.101E+00	.175E+00	.306E+00	0.	0.	0.	0.
.108E-01	.189E-01	.330E-01	.576E-01	.101E+00	.175E+00	.306E+00	0.	0.	0.
.620E-02	.108E-01	.189E-01	.330E-01	.576E-01	.101E+00	.175E+00	.306E+00	0.	0.
.831E-02	.145E-01	.253E-01	.442E-01	.772E-01	.135E+00	.235E+00	.411E+00	.717E+00	0.

THE CUMULATIVE BREAKAGE FUNCTION BB(I,J) IS

0.	0.	0.	0.	0.	0.	0.	0.	0.	0.
.717E+00	0.	0.	0.	0.	0.	0.	0.	0.	0.
.411E+00	.717E+00	0.	0.	0.	0.	0.	0.	0.	0.
.235E+00	.411E+00	.717E+00	0.	0.	0.	0.	0.	0.	0.
.135E+00	.235E+00	.411E+00	.717E+00	0.	0.	0.	0.	0.	0.
.772E-01	.135E+00	.235E+00	.411E+00	.717E+00	0.	0.	0.	0.	0.
.442E-01	.772E-01	.135E+00	.235E+00	.411E+00	.717E+00	0.	0.	0.	0.
.253E-01	.442E-01	.772E-01	.135E+00	.235E+00	.411E+00	.717E+00	0.	0.	0.
.145E-01	.253E-01	.442E-01	.772E-01	.135E+00	.235E+00	.411E+00	.717E+00	0.	0.
.831E-02	.145E-01	.253E-01	.442E-01	.772E-01	.135E+00	.235E+00	.411E+00	.717E+00	0.

THE MATRIX T(I,J) IS

.100E+01	0.	0.	0.	0.	0.	0.	0.	0.	0.
-.717E+00	.100E+01	0.	0.	0.	0.	0.	0.	0.	0.
-.739E-01	-.717E+00	.100E+01	0.	0.	0.	0.	0.	0.	0.
-.259E-01	-.739E-01	-.717E+00	.100E+01	0.	0.	0.	0.	0.	0.
-.118E-01	-.259E-01	-.739E-01	-.717E+00	.100E+01	0.	0.	0.	0.	0.
-.602E-02	-.118E-01	-.259E-01	-.739E-01	-.717E+00	.100E+01	0.	0.	0.	0.
-.324E-02	-.602E-02	-.118E-01	-.259E-01	-.739E-01	-.717E+00	.100E+01	0.	0.	0.
-.179E-02	-.324E-02	-.602E-02	-.118E-01	-.259E-01	-.739E-01	-.717E+00	.100E+01	0.	0.
-.101E-02	-.179E-02	-.324E-02	-.602E-02	-.118E-01	-.259E-01	-.739E-01	-.717E+00	.100E+01	0.
-.132E-02	-.233E-02	-.411E-02	-.731E-02	-.132E-01	-.247E-01	-.492E-01	-.116E+00	-.717E+00	.100E+01

THE INVERSE OF T(I,J)=TI(I,J) IS

.100E+01	0.	0.	0.	0.	0.	0.	0.	0.	0.
.717E+00	.100E+01	0.	0.	0.	0.	0.	0.	0.	0.
.588E+00	.717E+00	.100E+01	0.	0.	0.	0.	0.	0.	0.
.501E+00	.588E+00	.717E+00	.100E+01	0.	0.	0.	0.	0.	0.
.433E+00	.501E+00	.588E+00	.717E+00	.100E+01	0.	0.	0.	0.	0.
.377E+00	.433E+00	.501E+00	.588E+00	.717E+00	.100E+01	0.	0.	0.	0.
.330E+00	.377E+00	.433E+00	.501E+00	.588E+00	.717E+00	.100E+01	0.	0.	0.
.289E+00	.330E+00	.377E+00	.433E+00	.501E+00	.588E+00	.717E+03	.100E+01	0.	0.
.254E+00	.289E+00	.330E+00	.377E+00	.433E+00	.501E+00	.588E+00	.717E+00	.100E+01	0.
.256E+00	.291E+00	.331E+00	.377E+00	.428E+00	.487E+00	.554E+00	.630E+00	.717E+00	.100E+01

THE MATRIX JC(I,J) IS

.112E+00	0.	0.	0.	0.	0.	0.	0.	0.	0.
0.	.239E+00	0.	0.	0.	0.	0.	0.	0.	0.
0.	0.	.771E+00	0.	0.	0.	0.	0.	0.	0.
0.	0.	0.	.209E+01	0.	0.	0.	0.	0.	0.
0.	0.	0.	0.	.431E+01	0.	0.	0.	0.	0.
0.	0.	0.	0.	0.	.704E+01	0.	0.	0.	0.
0.	0.	0.	0.	0.	0.	.968E+01	0.	0.	0.
0.	0.	0.	0.	0.	0.	0.	.118E+02	0.	0.
0.	0.	0.	0.	0.	0.	0.	0.	.133E+02	0.
0.	0.	0.	0.	0.	0.	0.	0.	0.	.157E+02

THE MILL MATRIX D(I,J) IS

.112E+00	0.	0.	0.	0.	0.	0.	0.	0.	0.
.913E-01	.239E+00	0.	0.	0.	0.	0.	0.	0.	0.
.322E+00	.382E+00	.771E+00	0.	0.	0.	0.	0.	0.	0.
.706E+00	.816E+00	.947E+00	.209E+01	0.	0.	0.	0.	0.	0.
.107E+01	.123E+01	.140E+01	.159E+01	.431E+01	0.	0.	0.	0.	0.
.123E+01	.139E+01	.158E+01	.177E+01	.196E+01	.734E+01	0.	0.	0.	0.
.112E+01	.126E+01	.143E+01	.159E+01	.175E+01	.189E+01	.968E+01	0.	0.	0.
.859E+00	.972E+00	.109E+01	.122E+01	.134E+01	.144E+01	.151E+01	.118E+02	0.	0.
.598E+00	.666E+00	.749E+00	.832E+00	.911E+00	.979E+00	.103E+01	.107E+01	.133E+02	0.
.943E+00	.106E+01	.119E+01	.133E+01	.145E+01	.155E+01	.163E+01	.169E+01	.172E+01	.157E+02

THE CLASSIFIER FUNCTION IS

I	C(I)
1	1.00000
2	1.00000
3	1.00000
4	.99000
5	0.
6	0.
7	0.
8	0.
9	0.
10	0.

THE MATRIX F(I,J) IS

0.	0.	0.	0.	0.	0.	0.	0.	0.	0.
0.	0.	0.	0.	0.	0.	0.	0.	0.	0.
0.	0.	0.	0.	0.	0.	0.	0.	0.	0.
.706E-02	.816E-02	.947E-02	.209E-01	0.	0.	0.	0.	0.	0.
.107E+01	.123E+01	.140E+01	.159E+01	.431E+01	0.	0.	0.	0.	0.
.123E+01	.139E+01	.158E+01	.177E+01	.196E+01	.704E+01	0.	0.	0.	0.
.112E+01	.126E+01	.143E+01	.159E+01	.175E+01	.189E+01	.968E+01	0.	0.	0.
.859E+00	.972E+00	.109E+01	.122E+01	.134E+01	.144E+01	.151E+01	.118E+02	0.	0.
.590E+00	.666E+00	.749E+00	.832E+00	.911E+00	.979E+00	.103E+01	.107E+01	.133E+02	0.
.943E+00	.106E+01	.119E+01	.133E+01	.145E+01	.155E+01	.163E+01	.169E+01	.172E+01	.157E+02

THE MATRIX G(I,J) IS

.888E+00	0.	0.	0.	0.	0.	0.	0.	0.	0.
-.913E-01	.761E+00	0.	0.	0.	0.	0.	0.	0.	0.
-.322E+00	-.382E+00	.229E+00	0.	0.	0.	0.	0.	0.	0.
-.699E+00	-.888E+00	-.937E+00	-.107E+01	0.	0.	0.	0.	0.	0.
0.	0.	0.	0.	.100E+01	0.	0.	0.	0.	0.
0.	0.	0.	0.	0.	.100E+01	0.	0.	0.	0.
0.	0.	0.	0.	0.	0.	.100E+01	0.	0.	0.
0.	0.	0.	0.	0.	0.	0.	.100E+01	0.	0.
0.	0.	0.	0.	0.	0.	0.	0.	.100E+01	0.
0.	0.	0.	0.	0.	0.	0.	0.	0.	.100E+01

THE INVERSE OF G(I,J)=GI(I,J) IS

.113E+01	0.	0.	0.	0.	0.	0.	0.	0.	0.
.135E+00	.131E+01	0.	0.	0.	0.	0.	0.	0.	0.
.181E+01	.219E+01	.438E+01	0.	0.	0.	0.	0.	0.	0.
-.242E+01	-.291E+01	-.383E+01	-.934E+00	0.	0.	0.	0.	0.	0.
0.	0.	0.	0.	.100E+01	0.	0.	0.	0.	0.
0.	0.	0.	0.	0.	.100E+01	0.	0.	0.	0.
0.	0.	0.	0.	0.	0.	.100E+01	0.	0.	0.
0.	0.	0.	0.	0.	0.	0.	.100E+01	0.	0.
0.	0.	0.	0.	0.	0.	0.	0.	.100E+01	0.
0.	0.	0.	0.	0.	0.	0.	0.	0.	.100E+01

THE CLOSED CIRCUIT MATRIX H(I,J) IS

0.	0.	0.	0.	0.	0.	0.	0.	0.	0.
0.	0.	0.	0.	0.	0.	0.	0.	0.	0.
0.	0.	0.	0.	0.	0.	0.	0.	0.	0.
-.245E-01	-.294E-01	-.387E-01	-.195E-01	0.	0.	0.	0.	0.	0.
.632E-01	.594E-01	.432E-01	-.148E+01	.431E+01	0.	0.	0.	0.	0.
.135E+00	.134E+00	.117E+00	-.165E+01	.196E+01	.704E+01	0.	0.	0.	0.
.152E+00	.153E+00	.139E+00	-.149E+01	.175E+01	.189E+01	.968E+01	0.	0.	0.
.130E+00	.131E+00	.120E+00	-.114E+01	.134E+01	.144E+01	.151E+01	.118E+02	0.	0.
.938E-01	.948E-01	.876E-01	-.777E+00	.911E+00	.979E+00	.103E+01	.107E+01	.133E+02	0.
.157E+00	.159E+00	.148E+00	-.124E+01	.145E+01	.155E+01	.163E+01	.169E+01	.172E+01	.157E+02

TECHNICAL REPORT DATA
(Please read Instructions on the reverse before completing)

1. REPORT NO. EPA-600/2-80-115	2.	3. RECIPIENT'S ACCESSION NO.
4. TITLE AND SUBTITLE SIGNIFICANCE OF SIZE REDUCTION IN SOLID WASTE MANAGEMENT Volume 2		5. REPORT DATE August 1980 (Issuing Date)
		6. PERFORMING ORGANIZATION CODE
7. AUTHOR(S) George M. Savage, George J. Trezek		8. PERFORMING ORGANIZATION REPORT NO.
9. PERFORMING ORGANIZATION NAME AND ADDRESS University of California, Berkeley, California 94607		10. PROGRAM ELEMENT NO. C73D1C
		11. CONTRACT/GRANT NO. R805414
12. SPONSORING AGENCY NAME AND ADDRESS Municipal Environmental Research Laboratory--Cin.,OH, Office of Research and Development, U.S. Environmental Protection Agency, Cincinnati, Ohio 45268		13. TYPE OF REPORT AND PERIOD COVERED Final 7/25/78 - 7/25/79
		14. SPONSORING AGENCY CODE EPA-600/14

15. SUPPLEMENTARY NOTES
See also Volume 1, EPA-600/2-77-131, NTIS PB 272096, and Volume 3 (in preparation)
Project Officer: Carlton C. Wiles 513/684-7871

16. ABSTRACT
This report presents results of shredder tests using raw municipal solid waste, air-classified light fraction, and screened light fraction. The tests simulated single- and multiple-stage size reduction, using a 10-ton per hour swing hammermill and a small, high-speed fixed hammer shredder. The tests are generalized so that the characteristic particle size and energy consumption can be predicted. Various hardfacing materials and their ability to perform with different solid waste materials were also tested. A computerized comminution model of a size-discrete, time-continuous nature has been developed to predict size distribution and energy consumption.

17. KEY WORDS AND DOCUMENT ANALYSIS

a. DESCRIPTORS	b. IDENTIFIERS/OPEN ENDED TERMS	c. COSATI Field/Group
comminution waste treatment refuse resource recovery	size reduction solid waste shredder design	13B

18. DISTRIBUTION STATEMENT Release to public	19. SECURITY CLASS (This Report) unclassified	21. NO. OF PAGES 180
	20. SECURITY CLASS (This page) unclassified	22. PRICE

EPA Form 2220-1 (9-73)

☆ U.S. GOVERNMENT PRINTING OFFICE: 1980-657-165/0115